University of Pretoria

Faculty of Health Science

School of Medicine

**CREATING A STATISTICAL SHAPE MODEL TO AID IN THE ESTIMATION OF INCOMPLETE SOFT TISSUE SEGMENTS OF THE SURFACE OF SOUTH AFRICAN FACES**

Author: Heléne Francia Swanepoel

Student number: 27089691

Submitted to comply with the requirements for the degree in the

Faculty of Health Sciences, University of Pretoria

(Doctor of Philosophy in Anatomy)

This thesis is presented in publication format

**Supervisor:**

Professor Anna Catharina Oettlé

**Co-supervisors:**

Professor Ericka Noelle L'Abbé

Doctor Harold Matthews

**14 February 2024**

# Acknowledgements

This journey would not have been the same without my dear friend Soné van der Walt. From our days in the dissection hall and micro lab, through to our PhD, your friendship, wisdom, and support have been a blessing. Your advice sparked my interest in facial prosthetics, and for that, I am eternally grateful.

My brothers, parents-in-law, and friends, especially Roger and Paola in Australia, your friendship, love and support have carried me through many dark hours.

To my parents, your unwavering support and love have been my stronghold. Thank you for always being interested, for listening, and giving advice and assistance in all ways possible. You have always helped me to be better, do more, and enjoy life. I love you!

To my Ouma Ziena, I am honoured to carry your name and miss you dearly every day. You taught me so many invaluable lessons – from English to baking, and how to be strong, determined, and resilient – all of which I needed to complete this journey.

And to my husband Deon, my favourite human, biggest supporter, and best friend. Thank you for being my anchor and safe place. Your belief in me, along with your constant encouragement, infuriating rationality and humour, have made this journey incredible. Sharing this accomplishment with you is a joy beyond words. And I only beat you by a little bit! I love you.

Finally, what would I be without my Creator and Saviour, Jesus? Your mercy and wondrous gifts have brought me to this point in my life, and Your grace is indeed sufficient.

# Declaration

I declare that the thesis that I am hereby submitting to the University of Pretoria for the degree Doctor in Philosophy in Anatomy, is my own work and that I have never before submitted it to any other tertiary institution for any degree.
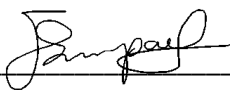
_____                                    14 February 2024
                                                          _____
Heléne Francia Swanepoel                                  Date

# Executive Summary

**Introduction:** A critical gap exists in population-specific data for facial morphology of black South Africans which are essential for the accurate reconstruction of facial features in fields such as aesthetic and reconstructive surgery, prosthodontics and extra-oral facial prosthetics, as well as forensic facial approximations. The objectives of this research were to generate normative reference values of black South African faces for various inter-landmark distances, and to derive a statistical shape model (SSM) of 3D facial shape variation which can be applied to estimate missing soft tissue segments on simulated defective faces.

**Methods:** The study included of 235 computed tomography (CT) and cone-beam computed tomography (CBCT) scans from black South African individuals between the ages of 18 and 87 years. The scans were collected from retrospective records of three medical institutions and excluded individuals that showed conditions potentially affecting facial morphology, including orthodontic treatments, pathological conditions, facial asymmetry, or any history of facial reconstructive surgery. The scans were processed to obtain 3D facial meshes and landmarks were placed at anatomically important loci. For the first objective, inter-landmark distances were calculated, statistically analysed, and compared to published literature on other populations. For the second objective, correspondence of the 3D meshes utilising the landmarks were achieved, and generalised Procrustes analysis and principal component analysis conducted. These steps are crucial in obtaining an SSM comprising the modes of variation and the normal range variance along each mode, which together defines multinormal parameterisation of shape variation. Defect estimations were done by using the SSM to estimate the linear combination of the modes of variation that most closely approximates the intact regions of each face, and estimate the missing regions using a weighted projection onto the modes of variation.

**Results:** Chapter 3 reports on normative facial capulometric measurements specific to the black South African population. It highlights significant differences in facial parameters between sexes and between different populations. The data reveal notable similarities with other African populations, especially in oral features, but significant disparities with non-African groups. Chapter 4 introduces the innovative SSM for extra-oral prosthetic design. This model accurately estimates missing soft tissues, demonstrating a high degree of precision with root mean square errors consistently below 2.58 mm for various facial defects.

**Conclusion:** The normative measurements highlight the unique facial characteristics of the black South African population, demonstrating the necessity of population-specific data in clinical and forensic applications. The development of the SSM represents a novel advancement in digital reconstruction methodologies. It offers a more objective and patient-specific approach in prosthetic design, especially in addressing complex facial defects such as bi-orbital defects or those crossing the facial midline in a demographic that has been largely overlooked in previous research. This model, by reducing the subjectivity and artistic skill previously required in prosthetic design, aligns with the evolving digital trends in medical technology and aims to address specific local needs and challenges in South Africa, and also have potential for global application.

**Keywords:** Facial morphology, Black South African population, normative capulometric measurements extra-oral prosthetics, forensic facial approximations, aesthetic and reconstructive surgery

# Table of Contents

# List of acronyms and abbreviations

| | |
|---|---|
| 2D | Two dimensional |
| 3D | Three dimensional |
| ANOVA | Analysis of variance |
| BF | Bayes Factor |
| CAD | Computer aided design |
| CAM | Computer aided manufacturing |
| CBCT | Cone beam computed tomography |
| CFA | Craniofacial approximation |
| CT | Computed tomography |
| GPA | Generalised Procrustes Analysis |
| HIV | Human immunodeficiency virus |
| ICC | Intraclass correlation coefficient |
| PCA | Principal Component Analysis |
| RMS | Root mean square |
| RMSE | Root mean square error |
| SSM | Statistical shape model |

# Chapter 1: General introduction

Chapter 1 presents the introduction to the thesis with a concise background that explains the rationale behind this research study. A clear problem statement, research aims and thesis layout, and a general methodology section, which gives a brief overview of the study population and methods, are included.

## Background and rationale

The human face, with its intricate details and variations, not only serves as a canvas of expression and communication, (Callahan, 2005; Little, Jones and DeBruine, 2011) but over the years, has garnered attention across various disciplines, from art to anthropology and medicine. In the context of this thesis, inter-population variation noted in facial features (Arslan, Genç, Odabaş and Kama, 2008; Choe, Sclafani, Litner, Yu and Romo, 2004; Liu, Lee, Naqvi, Hoskens, Liu, White et al., 2021; Ngeow and Aljunid, 2009; Porter and Olson, 2001; Xing, Gibbon, Clarke and Liu, 2013), is important to consider in the rehabilitation of facial defects and is the basis for forensic facial approximations of unknown persons.

Facial disfigurement, even seemingly minor or insignificant differences such as acne scars or lesions, may result in social anxiety, body-image issues, depression and poor self-esteem, ultimately affecting quality of life. (Bradbury, 2012; Callahan, 2005; Clarke, 1998; De Sousa, 2010) Facial disfigurement may be caused by several conditions, such as: congenital deformities, cancerous and infectious lesions, trauma, and conditions with unidentified pathology such as cancrum oris (noma). (Feller, Altini, Chandran, Khammissa, Masipa, Mohamed et al., 2014; Sykes and Essop, 2000; Zwane, Mohangi and Shangase, 2018) Cancrum oris predominantly affects individuals with compromised immune systems, especially in areas of extreme poverty such as Sub-Saharan Africa, (Sykes et al., 2000). Another significant cause of facial deformity are cancerous lesions of the head and neck, like Kaposi Sarcoma and non-Hodgkin's Lymphoma (Zwane et al., 2018), which is strongly associated with human immunodeficiency virus (HIV), a widely recognised immuno-suppressive infection and carcinogen. (IARC, 1996; Sengayi, Babb, Egger and Urban, 2015) In South Africa, head and neck cancers (including oesophageal cancers) account for approximately 18% of all cancer diagnoses. (Adeola, Afrogheh and Hille, 2018)

Despite the advances in surgical techniques contributing to the rehabilitation of patients with head and neck defects, many patients are not suitable candidates for surgical intervention. Cost-benefit analyses of each patient's desires, surgical needs, and expected outcomes should determine if surgical

or non-surgical interventions will result in better functional and cosmetic results. Cosmetic prostheses may thus provide viable alternatives for some patient populations, especially elderly patients, or those with significant comorbidities. (Klimczak, Helman, Kadakia, Sawhney, Abraham, Vest et al., 2018) The goal of a cosmetic prosthesis is not only to restore damaged or lost facial structures but also to enhance the patient's quality of life. To achieve successful rehabilitation, the patient's demographics, functional status and psychological well-being must be considered. (Klimczak et al., 2018) Current guidelines for the prosthetic rehabilitation of facial defects in South Africa involve a blend of artistic techniques that are both laborious and time-consuming, requiring substantial artistic expertise. Some techniques incorporate advanced digital methods for designing and manufacturing, such as mirroring of intact contra-lateral features and rapid prototyping using computer-aided manufacturing (CAM). However, the estimations of features crossing the midline of the face, like the nose and mouth, are still problematic. Regrettably, South Africa faces a scarcity of both educational institutions offering training in these skills and skilled technicians who can execute these intricate tasks (Tsĭtã and Owen, 2017). As of 2021, the entire country had only 83 practicing prosthodontists (Tiwari, Bhayat and Chikte, 2021) and only a few of them are involved in extra-oral prostheses. This shortage, coupled with the unequal distribution of services across the nation (Bhayat and Chikte, 2019; Tsĭtã et al., 2017), leads to delays in the production of facial prostheses. Consequently, this can result in long waiting lists for patients urgently requiring rehabilitation, further exacerbating the challenges in this field. The exploration of novel technologies is necessitated. A more robust and semi-automated approach could substantially reduce the cost and waiting times.

Another aspect affected by the importance of population-specific facial morphological data is identification of unknown individuals in forensic anthropology. In cases where there is a strong suspicion regarding the identity of the unknown individual and a close relative is implied, methods such as DNA comparison are utilised to make a personal identification. However, in the South African context, unidentified individuals for which no information is available are commonplace. Many factors are responsible for this including the high crime rates and high incidence of migrant labour, which is associated with the South African socio-political and mining history (L'Abbé, Loots and Meiring, 2005). In these circumstances, the unknown individual cannot be identified with primary identifiers and therefore craniofacial approximations (CFA) is often used (Cavanagh and Steyn, 2011; Stephan, 2015). In CFA, the facial appearance from an unknown individual's skull is estimated and is used to reach out to the public for information that could lead to identification (Ubelaker, Wu and Cordero, 2019). As CFA has become a vital tool in scenarios where traditional identification methods fall short, the method is seen as a form of criminal intelligence when it comes to the investigation of a crime (De

Greef and Willems, 2005; Stephan, 2015; Stephan and Henneberg, 2001). By understanding and applying population-specific data, forensic experts can create more accurate and representative facial approximations, increasing the likelihood of successful identification.

Statistical Shape Models (SSMs) represent the shape variations within a group of similar objects, such as a particular anatomical structure. In essence, SSMs comprise the mean shape of the sample and the principal modes of variation from this mean (Ambellan, Lamecker, von Tycowicz and Zachow, 2019; Audenaert, Pattyn, Steenackers, De Roeck, Vandermeulen and Claes, 2019)(Matthews, 2022). Statistical shape modelling serves as a computational extension of classical anthropometric techniques for modelling anatomical variability within populations by utilising landmarks to capture information about the structure in question. By providing a model of normal variations, SSMs often serve as a basis for inferring and reconstructing missing parts of a structure, including pelvic (Meynen, Matthews, Nauwelaers, Claes, Mulier and Scheys, 2020), mandibular (Raith, Wolff, Steiner, Modabber, Weber, Hölzle et al., 2017), orbital floor (Gass, Füßinger, Metzger, Schwarz, Bähr, Brandenburg et al., 2022), cranial vault and midfacial (skeletal) (Fuessinger, Metzger, Rothweiler, Brandenburg and Schlager, 2022; Fuessinger, Schwarz, Metzger, Semper-Hogg, Gass, Schlager et al., 2017; Fuessinger, Schwarz, Neubauer, Cornelius, Gass, Poxleitner et al., 2019) defects. The goal in such reconstructions is to determine the best linear combination of the modes of variation that accurately reconstructs the structure's landmark coordinates. This process is constrained by the coefficients of the linear combination, which are based on the fitted multinormal probability density (Matthews 2022 Static and Motion facial analysis). Despite a wealth of research on the various applications of SSMs, notable gaps persist, especially within the context of South Africa, as outlined in the subsequent problem statement.

## Problem statement

Facial reconstruction in medical and forensic applications can be benefitted by population specific norms representing facial soft tissue variation. There is a dearth of such population-specific information concerning black South Africans despite being the majority demographic in the country and the predominant demographic represented in forensic cases (L'Abbé, Van Rooyen, Nawrocki and Becker, 2011) and instances of head and neck cancer (Zwane et al., 2018) that may result in facial disfigurement. Furthermore, the existing research on facial prosthetics in South Africa is mainly confined to case studies, with an absence of focused investigations into the precision or effectiveness of facial restoration methods, or potential alternative digital methods. Therefore, this thesis focused

3

on analysing and quantifying the shape variation of South African faces with a view towards improving facial reconstructions.

## Aims and thesis layout

Chapter 2 provides a more in-depth review of the literature as a review paper titled "Recent developments in methodologies for extra-oral facial prosthetics in the South African context" submitted at the *South African Dental Journal*. This literature review provides information relating to facial morphology, facial defects and facial prosthetics, as well as information on various digital technologies used in the design and fabrication of facial prosthetics.

The specific aims of this research were as follow:

1. To use a CT and CBCT scan database of a population of black South Africans to generate normative reference values for various inter-landmark distances that may be used in a wide spectrum of applications related to approximations and reconstructions of the face.
   a. The findings of this aim are reported in Chapter 3, by presenting a manuscript submitted to the *Journal of plastic reconstructive and aesthetic surgery* titled "Normative Facial Capulometric Measurements in a Black South African Population".
2. To derive a statistical shape model of 3D shape variation of black South Africans from the same CT and CBCT scan database and apply it to estimating missing soft tissue segments on simulated defective faces. The accuracy of these estimations was assessed by comparing the estimations to the original unaltered faces.
   a. Chapter 4 presents the findings of this aim in the paper titled "A statistical shape model for estimating missing soft tissues of the face in a black South African population" published in *Journal of Prosthodontics.*

## General methodology

A total sample of 235 retrospectively collected computed tomography (CT) and cone-beam computed tomography (CBCT) scans were included in this study. A sample of 119 CT scans of black South African individuals between the ages of 18 and 85 years were collected from the Cintocare Hospital using the Toshiba Aquilion ONE 640 slice CT scanner. A sample of 118 CBCT scans of black South African individuals between 18 to 87 years old were collected from the University of Pretoria Oral and Dental Hospital and the Life Groenkloof Hospital using the Planmeca ProMax 3D machine. All scan data were anonymised with only age, sex and ancestry recorded for further analysis. Scans showing any

conditions that affected the morphology of the face (e.g., orthodontic treatment, pathological conditions, facial asymmetry, or any facial reconstructive surgery) were excluded.

Further specifics on the sample demographics and methodology are detailed in the Methods sections of Chapter 3 and Chapter 4.

## References

Adeola, H., Afrogheh, A., Hille, J. 2018. The burden of head and neck cancer in Africa: the status quo and research prospects. SADJ. 73:(8):477-88.

Ambellan, F., Lamecker, H., von Tycowicz, C., Zachow, S. 2019. Statistical shape models: understanding and mastering variation in anatomy. Adv Exp Med Biol. 1156:67-84.

Arslan, S.G., Genç, C., Odabaş, B., Kama, J.D. 2008. Comparison of facial proportions and anthropometric norms among Turkish young adults with different face types. Aesthetic Plastic Surgery. 32:(2):234-42.

Audenaert, E.A., Pattyn, C., Steenackers, G., De Roeck, J., Vandermeulen, D., Claes, P. 2019. Statistical shape modeling of skeletal anatomy for sex discrimination: their training size, sexual dimorphism, and asymmetry. Front Bioeng Biotechnol. 7::302.

Bhayat, A., Chikte, U. 2019. Human resources for oral health care in south africa: A 2018 update. Int J Environ Res Public Health. 16:(10):1668.

Bradbury, E. 2012. Meeting the psychological needs of patients with facial disfigurement. Br J Oral Maxillofac Surg. 50:(3):193-6.

Callahan, C. 2005. Facial disfigurement and sense of self in head and neck cancer. Soc Work Health Care. 40:(2):73-87.

Cavanagh, D., Steyn, M. 2011. Facial reconstruction: soft tissue thickness values for South African black females. Forensic Sci Int. 206:(1-3):215. e1-. e7.

Choe, K.S., Sclafani, A.P., Litner, J.A., Yu, G.-P., Romo, T. 2004. The Korean American woman's face: anthropometric measurements and quantitative analysis of facial aesthetics. Arch Facial Plast Surg. 6:(4):244-52.

Clarke, A. 1998. 'What happened to your face?'Managing facial disfigurement. Br J Community Nurs. 3:(1):13-6.

De Greef, S., Willems, G. 2005. Three-dimensional Cranio-Facial Reconstruction in Forensic Identification. J Forensic Sci. 50:(1):JFS2004117.

De Sousa, A. 2010. Psychological issues in acquired facial trauma. Indian J Plast Surg. 43:(2):200-5.

Feller, L., Altini, M., Chandran, R., Khammissa, R., Masipa, J., Mohamed, A., et al. 2014. Noma (cancrum oris) in the South African context. J Oral Pathol Med. 43:(1):1-6.

Fuessinger, M.A., Metzger, M.C., Rothweiler, R., Brandenburg, L.S., Schlager, S. 2022. Cranial reconstruction evaluation-comparison of European statistical shape model performance on Chinese dataset. Bone Reports. 17:101611.

Fuessinger, M.A., Schwarz, S., Metzger, M.C., Semper-Hogg, W., Gass, M., Schlager, S., et al. 2017. Planning of skull reconstruction based on a statistical shape model combined with geometric morphometrics. Int J Comput Assist Radiol Surg. 13::519-29.

Fuessinger, M.A., Schwarz, S., Neubauer, J., Cornelius, C.-P., Gass, M., Poxleitner, P., et al. 2019. Virtual reconstruction of bilateral midfacial defects by using statistical shape modeling. J Craniomaxillofac Surg. 47:(7):1054-9.

Gass, M., Füßinger, M.A., Metzger, M.C., Schwarz, S., Bähr, J.D., Brandenburg, L.S., et al. 2022. Virtual reconstruction of orbital floor defects using a statistical shape model. J Anat. 240:(2):323-9.

IARC. 1996. Human immunodeficiency viruses and human T-cell lymphotropic viruses. IARC monographs on the evaluation of carcinogenic risks to humans.

Klimczak, J., Helman, S., Kadakia, S., Sawhney, R., Abraham, M., Vest, A.K., et al. 2018. Prosthetics in facial reconstruction. Craniomaxillofac Trauma Reconstr. 11:(1):6-14.

L'Abbé, E.N., Loots, M., Meiring, J.H. 2005. The Pretoria Bone Collection: A modern South African skeletal sample. Homo. 56:(2):197-205.

L'Abbé, E.N., Van Rooyen, C., Nawrocki, S.P., Becker, P.J. 2011. An evaluation of non-metric cranial traits used to estimate ancestry in a South African sample. Forensic Sci Int. 209:(1-3):195. e1-.e7.

Little, A.C., Jones, B.C., DeBruine, L.M. 2011. The many faces of research on face perception. Philos Trans R Soc Lond B Biol Sci. 366:(1571):1634-7.

Liu, C., Lee, M.K., Naqvi, S., Hoskens, H., Liu, D., White, J.D., et al. 2021. Genome scans of facial features in East Africans and cross-population comparisons reveal novel associations. PLOS Genetics. 17:(8):e1009695.

Meynen, A., Matthews, H., Nauwelaers, N., Claes, P., Mulier, M., Scheys, L. 2020. Accurate reconstructions of pelvic defects and discontinuities using statistical shape models. Comput Methods Biomech Biomed Engin. 23:(13):1026-33.

Ngeow, W., Aljunid, S. 2009. Craniofacial anthropometric norms of Malaysian Indians. Indian J Dent Res. 20:(3):313.

Porter, J.P., Olson, K.L. 2001. Anthropometric facial analysis of the African American woman. Arch Facial Plast Surg. 3:(3):191-7.

Raith, S., Wolff, S., Steiner, T., Modabber, A., Weber, M., Hölzle, F., et al. 2017. Planning of mandibular reconstructions based on statistical shape models. Int J Comput Assist Radiol Surg. 12:(1):99-112.

Sengayi, M., Babb, C., Egger, M., Urban, M.I. 2015. HIV testing and burden of HIV infection in black cancer patients in Johannesburg, South Africa: a cross-sectional study. BMC Cancer. 15:(1):144.

Stephan, C.N. 2015. Facial Approximation—From Facial Reconstruction Synonym to Face Prediction Paradigm. J Forensic Sci. 60:(3)**:**566-71.

Stephan, C.N., Henneberg, M. 2001. Building faces from dry skulls: are they recognized above chance rates? J Forensic Sci. 46:(3)**:**432-40.

Sykes, L.M., Essop, R.M. 2000. Combination intraoral and extraoral prosthesis used for rehabilitation of a patient treated for cancrum oris: a clinical report. J Prosthet Dent. 83:(6)**:**613-6.

Tiwari, R., Bhayat, A., Chikte, U. 2021. Forecasting for the need of dentists and specialists in South Africa until 2030. PloS one. 16:(5)**:**e0251238.

Tsĭtã, K.P.M., Owen, C.P. 2017. Analysis of the need for, and scope of training in, maxillo-facial prosthodontics in the South African dental technology programme. SADJ. 72:(1)**:**16-21.

Ubelaker, D.H., Wu, Y., Cordero, Q.R. 2019. Craniofacial photographic superimposition: New developments. Forensic Sci Int Synerg. 1:271-4.

Xing, S., Gibbon, V., Clarke, R., Liu, W. 2013. Geometric morphometric analyses of orbit shape in Asian, African, and European human populations. Anthropol Sci. 121:(1)**:**1-11.

Zwane, N.B., Mohangi, G.U., Shangase, S.L. 2018. Head and neck cancers among HIV-positive patients: A five year retrospective study from a Johannesburg hospital, South Africa. SADJ. 73:(3)**:**121-6.

# Chapter 2: Literature review

Chapter 2 presents the literature review as a manuscript of a narrative literature overview submitted to the South African Dental Journal titled: "Recent developments in methodologies for extra-oral facial prostheses in South Africa."

**Title: Recent developments in methodologies for extra-oral facial prostheses in South Africa**

**Authors' information:**

Heléne F Swanepoel: *BSc (Hons), MSc*, Department of Anatomy, University of Pretoria, Pretoria, South Africa (35 years old)

Harold Matthews, *BA, PhD,* Medical Imaging Research Center, Universitair Ziekenhuis, Leuven, Belgium

Ericka N L'Abbé, *BA, MA, PhD,* Department of Anatomy, University of Pretoria, Pretoria, South Africa

Anna C Oettlé, *MBChB, MSc, PhD, DTE*, Anatomy and Histology Department, Sefako Makgatho Health Sciences University, Pretoria, South Africa

**Authors' contributions:**

Heléne F Swanepoel: Principal researcher and primary author 50%

Harold Matthews: Student supervision, article writing 20%

Ericka N L'Abbé: Student supervision, article writing 10%

Anna C Oettlé: Conceptualisation, student supervision, article writing 20%

**Corresponding author:**

Helene F Swanepoel.

646 18th Avenue, Rietfontein, Pretoria, 0084.

Telephone number: +61 493 408 140

Email: franci.dorfling@gmail.com

**Abstract**

The importance of comprehensive rehabilitation approaches to facial disfigurement in South Africa, with a focus on facial prosthetics, is examined in this review. The paper explores the range of surgical and non-surgical interventions available, including the pivotal role of facial prosthetics in improving patient outcomes.

The historical evolution of facial prosthetics is outlined, tracing advancements from early techniques to modern digital methods. The review recognises that while traditional methods remain prevalent in South Africa, there is a growing need for more modern technologies and population-specific approaches due to variations in facial features among different ethnic groups. The use of digital technologies, such as 3D scanning and printing, and digital mirroring and sculpting, is discussed as a means to enhance the design and manufacturing of prosthetics. Particularly, the development and application of a statistical shape model for black South Africans is highlighted for its potential in estimating missing facial tissue segments.

The review argues for the integration of digital technologies in the design and production of facial prosthetics in South Africa and emphasises the need for further research and development in this area to overcome the current limitations and improve accessibility and effectiveness of facial rehabilitation for South African populations.

**Keywords:** facial disfigurement, digital technologies in healthcare, statistical shape model, prosthetic design, facial rehabilitation

**Introduction**

This review considers the importance of facial rehabilitation and examines the treatment options available to South Africans, with a particular emphasis on facial prosthetics and their limitations within the South African context. I argue for the necessity of population-specific criteria and introduce the newly developed statistical shape model (SSM) as a method for estimating missing soft tissue segments on the surface of the face.

Facial disfigurement, whether congenital or acquired, profoundly impacts an individual's psychological and social well-being, often resulting in significant psychological distress, including low self-esteem, anxiety, and most notably, a distorted sense of self. [1] Acquired defects tend to have a more significant impact, as the individual did not have the opportunity to grow, adjust and accept their condition early on in life, but is affected later on by a drastic change in appearance. [2] The face, as a central aspect of human identity, plays a significant role in how an individual is perceived and interacts with the world. [3] Many patients perceive their deformity as visible and conspicuous, which can lead to a reduced frequency of visits to public places and a heightened sense of self-consciousness. [4] This visibility often results in patients feeling that they are subject to prejudice due to their appearance, affecting their self-esteem and overall mental health. [5] Furthermore, societal reactions to facial disfigurement, such as staring, avoidance, and discrimination, exacerbate this psychological distress and can lead to social withdrawal. [6]

The challenges of bodily disfigurement highlight the critical need for comprehensive approaches to facial rehabilitation that address not only the physical aspects of disfigurement but also the associated psychological and social challenges.

**Classification of facial defects**

Various classification systems for defects of the different regions of the face (e.g., maxillary, midface or mandibular) are discussed in the literature, and an overview of these classification systems are presented by Gupta, Verma, Islam and Agarwal [7].

12

In general, facial defects may be divided into congenital and acquired defects. Congenital defects primarily arises either from harmful behaviours engaged in by the mother during pregnancy, where certain harmful substances can cross the placental barrier and lead to abnormal development of foetal structures; or from obstructions that occur during the developmental phase of the foetus, which impede the normal development of tissues. [7]

On the other hand, acquired defects are primarily caused by cancer, as well as infectious lesions (both fungal [8] and bacterial [9]), trauma, and complex conditions like noma (cancrum oris) [10-12]. Additionally, the surgical resection of both cancerous and non-cancerous tumours often results in disfigurement. [13]

Facial defects are further classified according to location as intra-oral, extra-oral or complex (comprising both intra -and extra-oral components) defects. [14, 15] Intra-oral defects mostly require devices such as implants or obturators which fall outside the scope of this review. Extra-oral defects typically relate to the various facial features, including auricular, ocular, orbital, nasal as well as lip and cheek defects [14, 15] and may be rehabilitated by surgical and/or prosthetic reconstruction. Some defects may include more than one feature, for example, the mouth, nose and cheek. Lastly, complex defects involve both intra-oral aspects as well as extra-oral features and typically require surgical and prosthetic intervention.

**Surgical and Non-Surgical Interventions for Facial Disfigurement**

Facial rehabilitation options are influenced by a variety of factors, ranging from the nature of the defect or injury to patient-specific considerations like comorbidities, prior surgeries, the defect's severity, and any previous radiation therapy. The effects of radiation therapy of head and neck cancer patients should especially be considered and appropriately managed. [16] Additionally, resource constraints, such as the availability of specialist materials and expertise, play a significant role. When reconstructing a head and neck defect, it's crucial to consider multiple aspects, including the defect's size, location, the patient's age, and the amount of supportive tissue surrounding it. [17] Typical procedures might encompass the removal or ablation of pathological tissue, reconstruction of underlying bony structures, reshaping of soft facial features like the nose, and ensuring proper skin coverage.

The "reconstructive ladder", a systematic approach to selecting the best soft tissue coverage for a wound defect, was first introduced by Gillies during World War I. This ladder has since continually been modified and updated, however the fundamental principle of reconstructive procedures being graded by difficulty has been maintained. It indicates that reconstructive options are arranged in order of increasing complexity [18], and includes techniques such as primary closure, secondary intention, skin graft, tissue expansion, local flap, regional flap, and free tissue transfer [19]. For smaller defects where there's ample mobile tissue, direct suturing is generally the preferred method. However, for more substantial defects or when direct suturing isn't feasible, options range from free grafts, local skin flaps, pedicled flaps, to free tissue transfers. [20] As medical advancements continue, facial transplantation has emerged as a potential solution for severe, irreparable facial defects, however, is still not commonplace, and has stringent qualifying criteria before consideration. [21]

When none of these options are viable, non-surgical alternatives like facial prosthetics may be a useful alternative to address some functional and cosmetic concerns. Facial prosthetics have been found to play a critical role in the rehabilitation of patients, significantly improving their quality of life and social integration. [4, 5] These prostheses are designed to restore the outward appearance of normality, a crucial aspect of social acceptability, thereby aiding patients in reintegrating into society and functioning more comfortably in social contexts. Furthermore, the use of a facial prosthesis has been correlated with an increase in patients' self-esteem, with the functionality and aesthetics offered by the prosthesis contributing to this improvement. Patients have reported feeling less conspicuous and more at ease in social situations when wearing a prosthesis. [4]

### *History and development of facial prosthetics*

One of the first recorded cases of a person wearing a facial prosthesis is that of Tycho Brahe (1546 – 1601), a Danish scientist who lost his nose in a duel. Brahe shaped wax to remodel the missing part of his nose, created a mould of the wax and cast it in gold or copper. The prosthesis was painted to match his skin and attached with a glutinous adhesive. Since then, the field of maxillofacial rehabilitation has greatly expanded, in part due to the severe impacts of war resulting in advances in reconstructive surgery, prosthetics and plastic surgery, as well as the advent of technology. The 1950's welcomed the

14

first formalised training programs for the design and manufacturing of maxillofacial prostheses as a specialist field in prosthodontics, a branch of dentistry dedicated to designing, producing, and fitting artificial replacements for teeth and other oral structures. [22] Most advances in the past few decades relate to new materials such as silicone elastomers [23-26], as well as new and refined retention methods like osseointegrated implants [26-28].

Traditionally, most design techniques follow a similar pattern of construction. Firstly, a mould of the defect is obtained, and a cast is created from the mould. [29-32] The missing parts are then sculpted on the cast using wax. The sculpting is mostly an artistic process guided by previous photographs, comparisons to relatives' features, mirror images of the patient's own features or even using a donor model [30-32]. The wax model is then fitted to the patient, adjusted as necessary and finally processed into a silicone prosthesis. [29] This is achieved by making a multipart plaster mould of the wax model, melting away the wax and packing the negative plaster mould with silicone elastomer. The final colouring of the prosthesis is either mixed into the silicone during processing [12, 29, 31, 32] or painted on afterwards to match the skin colour of the patient [30].

More recently, digital techniques have emerged to aid in the planning and design of extra-oral prosthetics with the purpose of improving the current conventional methods. [33, 34] These technological advancements have paved the way for non-medical professionals to engage in the production of external maxillofacial prostheses. [34] Various techniques have been proposed as adjuncts or even replacements of certain steps during the fabrication process. These include digital data acquisition (MRI, CT, three-dimensional (3D) photogrammetry, laser scanning or ultrasound) as opposed to the conventional moulding process; computer aided design (CAD) using various software modalities instead of using wax; the use of digital libraries of specific features (most notably noses and ears) as opposed to sculpting from photographs or comparing to relatives; digital mirroring techniques for unilateral defects; and rapid prototyping and additive layer manufacturing methods for creating either the wax model or final prosthesis, as well as applying texture as opposed to manual sculpting and curing. [26, 31, 33, 35-38]

*Extra-oral facial prosthetics in the South African context*

Personal communication with a prominent South African prosthodontist (CP Owen, personal e-mail communication, 4 April 2020) indicated that newer techniques, such as digitally mirroring facial features are being used more often in clinical practice, however very little recent information was found in the literature on the design and manufacturing of maxillofacial prosthetics in South Africa. One South African study did demonstrate the use of rapid prototyping technology and additive manufacturing for the implanted retention frame of a midline facial prosthesis, however no information was given on the design or manufacturing of the silicone prosthesis, itself. [39] Reports on a digital workflow for manufacturing an auricular prosthesis indicated the use of an intra-oral scanner for digital data acquisition and digital mirroring of the intact ear. [40] Another report on auricular prostheses applied digital technologies to aid the positioning of implant placement, and digital mirroring techniques for unilateral defects or scanning of donor ears from a family member for bilateral defects. [41] Other case studies published in South Africa [42, 43] and an appraisal of the websites of private South African facial prosthetics practitioners indicated the use of the traditional methods outlined before for obtaining casts and sculpting of facial features, especially of midline features, are still the norm. A review of the scope of maxillofacial prosthodontics in South Africa [44] similarly stated that the wax models of facial prostheses are "carved *de nova* using casts, old photographs and a general knowledge of anatomy and facial dimensions as a guide".

The traditional method for designing and manufacturing extra-oral prosthetics is very time consuming, energy intensive, and relies heavily on the artistic skills of the clinician or technician to ensure optimal aesthetic outcome. As discussed by Mothopi, Owen, Howes and Naidoo [45], not all maxillo-facial defects can be satisfactorily treated and rehabilitated by conventional methods, which then requires the use of more invasive and expensive methods for effective rehabilitation. The lack of trained technicians [46], concrete population specific guidelines or digital techniques in the South African setting necessitate the exploration of novel and more cost-effective technologies to assist in the design and manufacturing of extra-oral facial prosthetics.

16

**Variations in facial features**

When comparing populations, distinct facial features are reflected as craniometric differences. Cranial variations among populations are likely shaped by evolutionary processes [47]. For instance, vertically long faces are typically associated with Europeans, whereas vertically shorter faces with projecting alveolar regions are more common among non-Europeans (East Asians and Africans). East Asian faces generally exhibit a flatter profile, while African faces tend to project more anteriorly [48].

The orthognathic mandible, which is shorter antero-posteriorly and wider medio-laterally, is predominantly found in populations from temperate and cold climates. In contrast, prognathic mandibles—longer antero-posteriorly and narrower medio-laterally—are common in populations from tropical and subtropical regions [49].

One of the most notable differences, for example, between North American Europeans and African Americans, lies in the midfacial region [50, 51]. Variations in midfacial features, such as the nose, inter-orbital breadth, and alveolar prognathism [52], have been shown to correlate significantly with ancestry, as demonstrated specifically among populations in South Africa [53, 54]. Other examples of interpopulation variation is demonstrated in the soft tissue of the eye, where reports on the position of the canthi indicate that the endocanthion is situated lower than the exocanthion in Australian and Korean populations [55, 56], as opposed to the inverse being found in previous research by the authors on a black South African population [57]. Furthermore, the width of the mouth from cheilion to cheilion is greater in a black South African population as compared to European, East Asian, and North and South American populations.

Inter-population variations in the overall face, as well as nasal and midfacial complexes are critical considerations in the manufacturing of maxillofacial prostheses, as they can significantly impact the visual outcome of the final approximation of the prosthesis.

*Population-specific information for black South Africans*

Scant literature concerning facial norms for black South Africans exists with limited reports on the morphology of the nasal and orbital regions. Several research questions have been addressed on confined areas of the face for black South Africans, for example: the positions of the canthi and eyeball [57],

17

facial profiles [58] and various facial features [59]. Reports on the nose include investigations into the external soft tissue of the female nose [60] and nasal cartilage variations [61]. Recently, significant contributions on lip height and mouth width in black South Africans have been made by Tobias Houlton and colleagues [62-64]. However, most of these studies had relatively small sample sizes and restricted age ranges, which may not be representative of the broader population. Furthermore, a significant portion of these studies used only 2D images [58-60] which may not capture the full complexity of three-dimensional facial features, and is not directly comparable to soft tissue or osteological 3D analysis of facial morphology [65].

In summary, while some strides have been made in understanding the facial norms of black South Africans, the existing body of literature is marked by significant gaps and limitations. A clear need exists for more extensive, representative, and detailed research in this area, ideally employing modern 3D analysis techniques to capture the rich complexity of facial morphology in this population.

### *Digital technologies for designing and manufacturing extra-oral prostheses*

Global advancements in digital technologies have significantly transformed the production of facial prostheses. Enhanced facial scanning capabilities, refined computer sculpting techniques, and the precision of 3D printing have collectively revolutionised the process, allowing it to be conducted in a versatile and multi-faceted manner. Many advantages associated with these techniques, include reduced production times, higher percentage of anatomical accuracy and digital storage of the prosthetic model for future adjustments or manufacturing of prosthetic replacements, [40, 66, 67] as well as improved patient comfort and outcomes.[66] Below are examples of such innovative digital techniques that are gaining traction globally, including in the South African context.

### Digital mirror-imaging of intact parts

To address unilateral defects, both the affected and unaffected side of the face is digitally captured by 3D photogrammetry, laser scanning or other 3D imaging techniques. Subsequent processing to model the prosthesis is achieved using sophisticated software like Meshmixer (Autodesk Inc, San Fransisco CA) or Zbrush (Maxon, Los Angeles CA). The anterior surface of the prosthesis is based on a mirror

image of the intact or healthy side of the face while the diseased side is used to define the posterior surface. Boolean functions are applied to create solid volumes and subtract overlapping areas to finalise the prosthesis model, which can then be 3D printed.

A South African case report presented an innovative workflow for the fabrication of an auricular prosthesis. [40] The process involved the use of an intraoral scanner, the 3 Shape TRIOS 3 Basic, to capture digital impressions of the affected and intact ears in STL format, which were enhanced by placing artificial markers on the tragus for accurate reference during scanning. The captured data was then processed with Autodesk Meshmixer software to invert the normal ear's digital model into a mirror image and merged with mesh of the affected side to create the prosthetic model. The model was 3D printed with a Phrozen LCD resin 3D printer and fitted to the patient to check for any necessary modifications. The final design of the prosthesis was completed digitally, and moulds were designed for the fabrication of the silicone prosthesis which was done manually. The design phase of this prosthesis was markedly reduced to approximately 30 minutes.

A Taiwanese case study reported on the fabrication of an orbital prosthesis for a young patient using a handheld 3D scanner to capture the facial contours, followed by the use of 3D modelling software to design the prosthesis based on a mirrored image of the healthy side of the face. [67] The process also included scanning and integrating a custom-made ocular prosthesis into the digital design. A trial prosthesis was produced to refine the fit, which was followed by the final printing, post-processing, and manual detailing, including painting and hair implantation. The prosthesis was ultimately fitted using a water-based adhesive, offering a non-invasive, cost-effective solution that enhanced comfort and aesthetic outcomes.

**Digital sculpting of missing parts**

Digital sculpting of a prosthesis may be done using specialised software. A case report from Poland meticulously outlined the process for designing and manufacturing a nasal prosthesis. [66] The suggested workflow incorporated a blend of digital techniques including data acquisition using CBCT, digital modelling with Zbrush software, and 3D printing for the prosthetic moulds. Initially, a CBCT scan of the patient's face was captured utilising a CS 9600 CBCT Scanner and subsequently imported into

Zbrush software as a 3D mesh. The region necessitating the prosthesis was marked, with a segment of the mesh extracted and moulded into the prosthesis model employing Zbrush's masking and polygroup tools. To enable detailed free-hand sculpting, the mesh density was augmented using the dynamesh tool. The design process was informed by overlaying a pre-treatment photograph of the patient within Zbrush, calibrating for scale and employing the software's transparency function to discern the absent nasal sections. Following the refinement of the prosthesis's shape and size, the digital model's resolution was increased to facilitate the application of a lifelike skin texture via the alpha spray tool.

The patient was then presented with a computer visualisation of the prospective prosthesis for approval. A trial version of the prosthesis was 3D printed in resin, enabling the patient to evaluate the restoration's form. The trial fitting concentrated on the prosthesis's edge-to-skin interface, with the patient's spectacles providing the principal support. Any requisite adjustments identified at this stage were reincorporated into the Zbrush software to enhance the digital model. The ultimate moulds for the prosthesis were crafted through reverse engineering in Zbrush, utilising tools such as Boolean, Zremesher, Qmesh, and Polygroup island to create a digital negative. The moulds were then fabricated using an SLA printer and injected with a base-coloured silicone to produce the final prosthesis. The cured silicone prosthesis was manually coloured to match with the adjacent tissues.

This combination method allows for an improved workflow that reduces time and is beneficial to the patient. While similar reports have not been found in the South African literature, all the tools and software are readily available and may be easily incorporated into clinical practice.

**The use of SSMs for designing facial prosthetics**

An SSM establishes the boundaries of normal shape (e.g., the face) variation according to the modes of variation [68]. These models are landmark based, using a training set of data, i.e., similarly shaped structures, to describe the mean shape as well as variation in shape. [69]. The mean shape provides knowledge about the general shape of a specific structure, while variation offers knowledge about how much the shape can vary among subjects within the data or population.

New complete shapes (e.g., faces) can be synthesised by defining some linear combination of the modes of variation (**Error! Reference source not found.**). In general, reconstructing missing parts of an out-o f-sample face involves estimating the linear combination that best approximates the intact parts of the face. Metaphorically this can be thought of as moving along the axes of a shape space until an optimal fit is found.
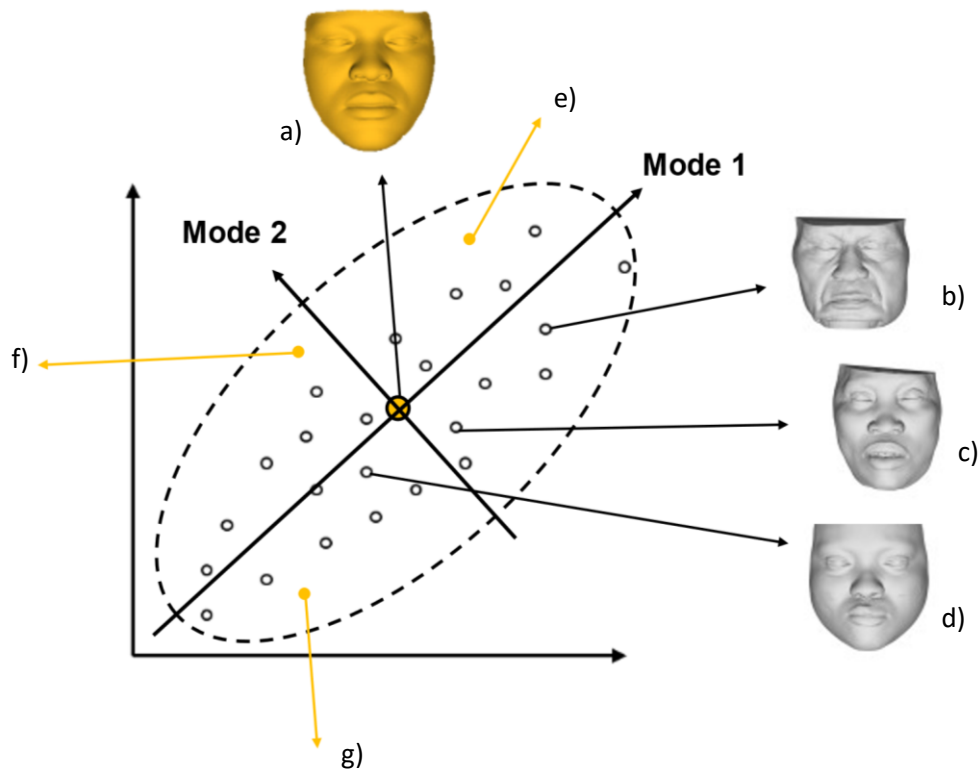


*Figure 1: A shape-space visualising a statistical shape model with each point representing a face. The mean face is illustrated by a) while b) c) and d) are faces in the training sample. The modes of variation (Mode 1 and Mode 2) represent the modes responsible for the greatest amount of variation in the population, while the dotted line illustrates the boundaries of normal variation. By moving along a mode of variation, new realistic and synthetic faces e) f) and g) can be generated.*

To develop a SMM, traditional geometric morphometric techniques are employed in the following three steps: (1) manually or automatically labelling homologous landmarks on a training set to ensure

correspondence between structures in the data set; (2) aligning the data into a common coordinate system by means of generalised Procrustes analysis (GPA); and (3) defining the parameters (i.e., a probability model) of normal variation by utilising principal component analysis (PCA). The SSM can then be used to synthesise shapes similar to those in the training set by mimicking its variation, [69] or to estimate an entire, anatomically sound shape from partial or unclear target shape information.[70]

An SSM of black South African faces was developed to estimate missing facial soft tissue segments. [71] The model was constructed using meshes from computed tomography and cone beam computed tomography images of a black South African sample without facial disfigurement. Simulated facial defects were addressed using the SSM to automatically estimate missing parts. Quantitative evaluations revealed root mean squared errors (RMSE) values below 1.71 mm for defects like one orbit, partial nose, cheek, and lip. However, larger defects like the full nose, bi-orbital, and composite defects showed RMSEs between 2.10 and 2.58 mm. Qualitative assessments highlighted some limitations, mainly the non-smooth blending of estimated parts with surrounding tissues. These issues were linked to sub-optimal region selection, failed non-rigid registration, or defects extending beyond the facial template's coverage. While the model marks a significant step in digital design for facial prosthetics tailored for South African black adults, it has some limitations. The model currently excludes the forehead, ears, and occipital regions, as these are often missing in CBCT scans and focuses solely on the face's outer surface. Despite these constraints, the model provides a realistic depiction of missing areas, as evidenced by the acceptable RMSEs.

## Conclusions and future directions

The digital techniques discussed above aim to streamline the prosthetic design process, minimising the dependence on artistic skills and addressing healthcare resource limitations. The development of a population specific SSM marks a preliminary step towards user-friendly software for 3D printing prosthetics, with the growing feasibility of directly printing silicone prosthetics due to technological advancements. Swanepoel *et al.,* are actively exploring the development of this software, which is envisioned

to feature fundamental medical image processing capabilities such as segmentation, 3D mesh triangulation, and landmark indication. Advanced functionalities, including facial mapping and region of interest selection, are also anticipated to be integrated. The software is expected to support the importation and utilisation of existing, population specific SSMs to facilitate the estimation of missing regions, and smooth transitions between estimated and existing tissues. Ultimately, the software aims to offer comprehensive solutions – including the design and fitting of the estimated region to the internal surface and final modifications for 3D printing, with the aspiration of becoming a valuable tool for clinicians worldwide in creating cost-effective facial prosthetics.

In this literature review, we delved into the complexities of facial morphology and disfigurement and the history and development of facial prosthetics, with a specific focus on the South African population. The intricacies of various advanced digital technologies were presented, emphasising their foundational methodologies, their particular applications in defect reconstruction and future projects for addressing facial disfigurement in a resource limited context like South Africa.

**Conflict of interest:** None

23

**References**

1. Bradbury E. Meeting the psychological needs of patients with facial disfigurement. Br J Oral Maxillofac Surg 2012: 50: 193-6.

2. Poonam P, Rahul B, Bhandari SK. Maxillofacial Defects: Impact on Psychology and Esthetics. In Levine MP, Santos JS, ed. Beauty - Cosmetic Science, Cultural Issues and Creative Developments. IntechOpen, 2021.

3. Callahan C. Facial disfigurement and sense of self in head and neck cancer. Soc Work Health Care 2005: 40: 73-87.

4. Rangel Goulart D, Sigua-Rodriguez EA, Alvarez-Pinzón N, Rocha Fernandez AÚ, Queiroz E. Quality of life of patients with facial prosthesis. Rev Fac Odontol Univ Antioq 2017: 29: 131-47.

5. Johnson FP. The impact of ablative facial cancer surgery and the affect of post-operative facial prostheses. 2010: PhD.

6. Cooke Macgregor F. Facial disfigurement: problems and management of social interaction and implications for mental health. Aesthetic Plast Surg 1990: 14: 249-57.

7. Gupta A, Verma A, Islam J, Agarwal S. Maxillofacial defects and their classification: a review. Int J Adv Res (Indore) 2016: 4: 109-14.

8. Jundt JS, Wong MEK, Tatara AM, Demian NM. Invasive cutaneous facial mucormycosis in a trauma patient. J Oral Maxillofac Surg 2018: 76: 1930.e1–30.e5.

9. Abdul Rahman N, Rajaratnam V, Burchell GL, Peters RMH, Zweekhorst MBM. Experiences of living with leprosy: A systematic review and qualitative evidence synthesis. PLoS Negl Trop Dis 2022: 16: e0010761.

10. Feller L, Altini M, Chandran R, et al. Noma (cancrum oris) in the South African context. J Oral Pathol Med 2014: 43: 1-6.

11. Pham KT, Hotez PJ, Hamilton KL. Reconstructive surgery for the neglected tropical diseases: global gaps and future directions. Plast Reconstr Surg Glob Open 2023: 11: e4987.

12. Sykes LM, Essop RM. Combination intraoral and extraoral prosthesis used for rehabilitation of a patient treated for cancrum oris: a clinical report. J Prosthet Dent 2000: 83: 613-6.

13. Nogueira T, Adorno M, Mendonça E, Leles C. Factors associated with the quality of life of subjects with facial disfigurement due to surgical treatment of head and neck cancer. Med Oral Patol Oral Cir Bucal 2018: 23: e1698-6946.

14. Cristache CM, Tudor I, Moraru L, et al. Digital Workflow in Maxillofacial Prosthodontics—An Update on Defect Data Acquisition, Editing and Design Using Open-Source and Commercial Available Software. Appl Sci (Basel) 2021: 11: 973.

15. Hovhannisyan SR, Mashinyan KA, Zopunyan VR. Maxillofacial defects. 2009.

16. Mmutlana T, Sykes L, Naidu K. An update on the effects of radiation therapy and dental management of head and neck cancer patients. SADJ 2023: 78: 211-16.

17. Klimczak J, Helman S, Kadakia S, et al. Prosthetics in facial reconstruction. Craniomaxillofac Trauma Reconstr 2018: 11: 6-14.

18. De Francesco F, Zingaretti N, Parodi PC, Riccio M. The evolution of current concept of the reconstructive ladder in plastic surgery: the emerging role of translational medicine. Cells 2023: 12: 2567.

19. Mathes SJ, Nahai F. Clinical applications for muscle and musculocutaneous flaps. St. Louis: Mosby, 1982.

20. Gujrathi A, Gandrati S, Gadpayale N, et al. Reconstruction of facial skin defects by various local flaps in rural India. Indian J Appl Res 2021: 1-4.

21. Kantar RS, Alfonso AR, Diep GK, et al. Facial transplantation: principles and evolving concepts. Plast Reconstr Surg 2021: 147: 1022e-38e.

22. Gupta AD, Verma A, Dubey T, Thakur S. Maxillofacial Prosthetics Part 1: A Review. Int J Adv Res (Indore) 2017: 5: 31-40.

23. Waters M, Jagger R, Polyzois G, Williams K. Dynamic mechanical thermal analysis of maxillofacial elastomers. J Prosthet Dent 1997: 78: 501-5.

24. Hatamleh MM, Watts DC. Mechanical properties and bonding of maxillofacial silicone elastomers. Dent Mater 2010: 26: 185-91.

25. Polyzois GL, Eleni PN, Krokida MK. Effect of Time Passage on Some Physical Properties of Silicone Maxillofacial Elastomers. J Craniofac Surg 2011: 22: 1617-21.

25

26. Ariani N, Visser A, Van Oort RP, et al. Current state of craniofacial prosthetic rehabilitation. Int J Prosthodont 2013: 26: 57-67.

27. Khamis MM, Medra A, Gauld J. Clinical evaluation of a newly designed single-stage craniofacial implant: a pilot study. J Prosthet Dent 2008: 100: 375-83.

28. Goiato MC, Delben JA, Monteiro DR, dos Santos DM. Retention systems to implant-supported craniofacial prostheses. J Craniofac Surg 2009: 20: 889-91.

29. Nandini V, Nair KC. A method of fabrication of an extensive facial prosthesis. Trends Biomater Artif Organs 2003: 16: 81-82.

30. Guttal S, Patil N, Shetye A. Prosthetic rehabilitation of a midfacial defect resulting from lethal midline granuloma–a clinical report. J Oral Rehabil 2006: 33: 863-67.

31. Subburaj K, Nair C, Rajesh S, Meshram S, Ravi B. Rapid development of auricular prosthesis using CAD and rapid prototyping technologies. Int J Oral Maxillofac Surg 2007: 36: 938-43.

32. Bhandari A, Manvi P, Mehrotra A, Rao Y. A Simplified and Easy Approach for the Fabrication of Nasal Prosthesis: A Clinical Report. J Indian Prosthodont Soc 2014: 14: 313-8.

33. Farook T, Jamayet N, Abdullah J, Rajion Z, Alam M. A systematic review of the computerized tools and digital techniques applied to fabricate nasal, auricular, orbital and ocular prostheses for facial defect rehabilitation. J Stomatol Oral Maxillofac Surg 2019.

34. Van Heerden I, Fossay A. Changing world of external maxillofacial prosthesis manufacturing. 2019: 362-70.

35. Runte C, Dirksen D, Delere H, et al. Optical data acquisition for computer-assisted design of facial prostheses. Int J Prosthodont 2002: 15: 129-32.

36. Eggbeer D, Evans PL, Bibb R. A pilot study in the application of texture relief for digitally designed facial prostheses. Proc Inst Mech Eng H 2006: 220: 705-14.

37. Mohammed MI, Cadd B, Peart G, Gibson I. Augmented patient-specific facial prosthesis production using medical imaging modelling and 3D printing technologies for improved patient outcomes. Virtual Phys Prototyp 2018: 13: 164-76.

38. Artioli BO, Kunkel ME, Mestanza SN. Feasibility Study of a Methodology Using Additive Manufacture to Produce Silicone Ear Prostheses. 2018: 3: 211-15.

39. Fernandes N, van den Heever J, Hoogendijk C, et al. Reconstruction of an Extensive Midfacial Defect Using Additive Manufacturing Techniques. J Prosthodont 2016: 25: 589-94.

40. Netshilindi NE, Michaels A, Maart RD. An innovative digital workfl ow for the fabrication of a prosthetic ear: A case report. SADJ 2023: 78: 92-96.

41. Heydenrych A, van der Walt JG, van den Heever HJ. Auricular prosthesis positioning using virtual planning in combination with additive manufacturing. J Stomatol Oral Maxillofac Surg 2023: 124: 101258.

42. Jagathpal AJ, Harryparsad A, Doolabh R, Calitz BF. Mechanically-retained facial prosthesis for a large defect following Cancrum Oris: a clinical report. 2017: 7: 44-51.

43. Van den Heever J, Sykes L, Nethononda P, Naidu K. Immediately loaded zygomatic implants used for a functional and aesthetic rehabilitation following a combined maxillectomy and rhinectomy. SADJ 2022: 77: 489-94.

44. Van den Heever J, Sykes LM, Du Plessis F. The scope of maxillofacial prosthodontics: clinical review. SADJ 2012: 67: 593-95.

45. Mothopi M, Owen C, Howes D, Naidoo L. The need for versatility in the prosthodontic treatment of maxillofacial defects: clinical. SADJ 2012: 67: 420-23.

46. Tsĭtã KPM, Owen CP. Analysis of the need for, and scope of training in, maxillo-facial prosthodontics in the South African dental technology programme. SADJ 2017: 72: 16-21.

47. İşcan MY, Steyn M. Craniometric determination of population affinity in South Africans. Int J Legal Med 1999: 112: 91-97.

48. Bastir M, Rosas A. Correlated variation between the lateral basicranium and the face: A geometric morphometric study in different human groups. Arch Oral Biol 2006: 51: 814-24.

49. Novotný V, İşcan MY, Loth S. Morphologic and Osteometric Assessment of age, Sex and Race from the Skull. In İşcan MY, Helmer H, ed. Forensic Analysis of the Skull: Craniofacial Analysis, Reconstruction, and Identification. New York: Wiley-Liss, 1993: 71-88.

50. Farkas LG. Anthropometry of the Head and Face. 2nd ed. New York: Raven Press, 1994.

51. Porter JP. The average African American male face: an anthropometric analysis. Arch Facial Plast Surg 2004: 6: 78-81.

52. Proffit WR, White RP, Sarver DM. Contemporary treatment of dentofacial deformity. St. Louis: Mosby 2003.

53. McDowell JL, Kenyhercz MW, L'Abbé EN. An evaluation of nasal bone and aperture shape among three South African populations. Forensic Sci Int 2015: 252: 189.e1-89.e7.

54. Steyn M, L'Abbé EN, Myburgh J. Forensic anthropology as practiced in South Africa. In Blau S, Ubelaker D, ed. Handbook of Forensic Anthropology and Archaeology. 2nd ed. New York: Routledge, 2016: 151-64.

55. Stephan CN, Davidson PL. The placement of the human eyeball and canthi in craniofacial identification. J Forensic Sci 2008: 53: 612-19.

56. Kim S-R, Lee K-M, Cho J-H, Hwang H-S. Three-dimensional prediction of the human eyeball and canthi for craniofacial reconstruction using cone-beam computed tomography. Forensic Sci Int 2016: 261: 164. e1-64. e8.

57. Dorfling HF, Lockhat Z, Pretorius S, Steyn M, Oettlé AC. Facial approximations: Characteristics of the eye in a South African sample. Forensic Sci Int 2018: 286: 46-53.

58. Beukes S, Dawjee S, Hlongwa P. Soft tissue profile analysis in a sample of South African Blacks with bimaxillary protrusion : scientific. SADJ 2007: 62: 206-12.

59. Roelofse MM, Steyn M, Becker PJ. Photo identification: facial metrical and morphological features in South African males. Forensic Sci Int 2008: 177: 168-75.

60. Wilson SP, Medapati V, Segwapa K. Facial Anthropometric Norms of the Young Black South African Woman. Plast Reconstr Surg Glob Open 2023: 11.

61. McIntosh CND, van Wyk FC, Joubert G, Seedat RY. Lower Lateral Cartilages: An Anatomic and Morphological Study in Noses of Black Southern Africans. Aesthet Surg J 2016: 37: 276-82.

62. Houlton TMR, Jooste N, Steyn M. Mouth Width and Cupid's Bow Estimation in a Southern African Population. J Forensic Sci 2019: 65: 372-79.

63. Houlton TM, Jooste N, Uys A, Steyn M. Lip height estimation in a southern African sample. SADJ 2020: 75: 415-24.

64. Houlton TM, Jooste N, Steyn M, Hemingway J. Visualising trends in dentition to lip mouth morphology using geometric morphometrics. Plos one 2022: 17: e0274127.

65. Van Vlijmen OJ, Maal TJ, Bergé SJ, et al. A comparison between two-dimensional and three-dimensional cephalometry on frontal radiographs and on cone beam computed tomography scans of human skulls. Eur J Oral Sci 2009: 117: 300-05.

66. Egelhoff K, Idzi P, Bargiel J, et al. Implementation of Cone Beam Computed Tomography, Digital Sculpting and Three-Dimensional Printing in Facial Epithesis—A Technical Note. Appl Sci (Basel) 2022: 12: 11974.

67. Sun M-H, Yen C-H, Tsai Y-J, Liao Y-L, Wu S-Y. Fabrication of a facial prosthesis for a 13-year-old child by using a point-and-shoot three-dimensional scanner and CAD/CAM technology. Taiwan J Ophthalmol 2022: 12: 219-22.

68. Claes P, Walters M, Gillett D, et al. The normal-equivalent: a patient-specific assessment of facial harmony. Int J Oral Maxillofac Surg 2013: 42: 1150-58.

69. Cootes TF, Taylor CJ. Statistical models of appearance for computer vision. 2004.

70. Bindernagel M. Articulated Statistical Shape Models. 2013: Master's Degree.

71. Swanepoel HF, Matthews HS, Claes P, Vandermeulen D, Oettlé AC. A statistical shape model for estimating missing soft tissues of the face in a black South African population. J Prosthodont 2023: 1-9.

29

**Continuing Professional Development Questions:**

1. Which of the following is a non-surgical intervention for facial disfigurement?

    A) Skin grafting

    B) Facial prosthetics

    C) Tissue expansion

    D) Local flap

2. Question: What does SSM stand for in the context of designing facial prosthetics?

    A) Soft Surface Modelling

    B) Statistical Shape Model

    C) Standard Surgical Method

    D) Synthetic Skin Mesh

3. In the review, what future direction is mentioned for the development of facial prosthetics?

    A) Decreasing reliance on 3D printing

    B) Focusing solely on surgical interventions

    C) Development of user-friendly software for 3D printing prosthetics

    D) Abandoning digital technologies in favour of traditional methods

4. In the South African context, what is a primary reason for the continued use of traditional methods in manufacturing facial prosthetics?

    A) Preference for older techniques

    B) Higher accuracy of traditional methods

    C) Lack of access to digital technologies

    D) Lower costs associated with traditional methods

5. What is the main purpose of developing population-specific SSMs in facial prosthetics?

    A) To standardize prosthetic designs globally

    B) To accommodate unique facial features of different populations

    C) To reduce the need for surgical interventions

    D) To focus solely on cosmetic improvements

# Chapter 3: Aim 1

This chapter presents the findings of the first aim of this thesis as a manuscript submitted to the *Journal of Plastic, Aesthetic and Reconstructive Surgery* titled "Normative Facial Capulometric Measurements in a Black South African Population".

**Title: Normative Facial Capulometric Measurements in a Black South African Population**

Heléne Francia Swanepoel [1]

Harold Matthews [2,3,4]

Peter Claes [2,3,4,5]

Dirk Vandermeulen [3,5]

Ericka N L'Abbé [1,7]

Anna C Oettlé [1,6]


[1] Department of Anatomy, University of Pretoria, Pretoria, South Africa

[2] Laboratory for Imaging Genetics, Department of Human Genetics, Katholieke Universiteit, Leuven, Belgium

[3] Medical Imaging Research Center, Universitair Ziekenhuis, Leuven, Belgium

[4] Facial Sciences, Murdoch Children's Research Institute, Parkville, Australia

[5] Department of Electrical Engineering, Katholieke Universiteit, Leuven, Belgium

[6] Anatomy and Histology Department, Sefako Makgatho Health Sciences University, Pretoria, South Africa

[7] Forensic Anthropology Research Center, University of Pretoria, Pretoria, South Africa


Corresponding author:

Helene Francia Swanepoel, 11 Northfields Avenue, Gwynneville, NSW, 2500, Australia. Telephone number: +61 493 408 140

Email: franci.dorfling@gmail.com

## Summary

Facial analysis serves as the foundation for surgical planning and is vital for devising suitable treatment strategies in cosmetic and reconstructive surgeries. The aim of this study was to establish normative capulometric values for facial measurements specific to the black South African population. This study reports normative capulometric values of 22 clinically relevant inter-landmark distances for the black South African population. These were derived from 235 computed tomography (CT) and cone beam computed tomography (CBCT) scans of adults aged 18-87 years.

32

Significant sex-differences were found in nasal parameters, with males generally having larger measurements. Few significant differences were found between sexes for ocular parameters, challenging existing literature that suggests sexual dimorphism in these features. Oral parameters showed significant sex differences, with no notable disparities between modalities (CT and CBCT), except for lower lip and vermillion heights.

The study's results were benchmarked against similar studies of different populations, revealing that while the black South African population is in general similar to other African population groups, particularly in oral features, significant differences exist across all facial parameters when compared to non-African populations. The research highlights the unique facial characteristics of the black South African population, providing valuable data for forensic anthropology, prosthodontics, and reconstructive and aesthetic surgery. It emphasises the importance of recognising population-specific features to ensure optimal clinical interventions and contributes to the broader understanding of human facial diversity.

**Keywords**: anthropometry, facial analysis, 3D imaging, forensic anthropology, reconstructive surgery

## Introduction

The human face plays an essential role in normal functioning and social interaction, including recognition, and is of interest in fields as diverse as art, anthropology and medicine. Facial analysis serves as the foundation for surgical planning and is vital for devising suitable treatment strategies in cosmetic and reconstructive surgeries. [1] Beyond the surgical applications, facial measurements are important in dentistry, orthodontics, forensic sciences, maxillofacial prosthetics and other fields. [2]

Facial anthropometry includes both osteological analysis, or craniometry, and soft tissue analysis, or capulometry. Normative capulometric reference values refer to the angular and linear measurements between soft tissue facial landmarks derived from population-specific data of a large sample of the population. [3] The measurements can be taken directly on the subject, or indirectly from two-dimensional (2D) photographs, three-dimensional (3D) stereophotographs and laser surface scans, or computed tomography (CT) and cone beam computed tomography (CBCT) volumetric images. While 2D modalities inherently do not capture variation in the third dimension, lowering the accuracy of associated measurements [4], 3D techniques, in contrast, are similar in accuracy and repeatability to direct anthropometric measures. [5]

Facial features vary greatly between and among populations. Europeans, for instance, typically possess vertically longer faces, while non-European populations such as East Asians and Africans exhibit vertically shorter faces with projecting alveolar regions and different profile characteristics. [6] Variations among these broad, geographic populations are also noted in the mandible [7], midfacial features such as nose shape and inter-orbital breadth [8], and the positioning of orbital soft tissues [9].

Literature on facial norms for black South Africans is sparse. Previous studies have focused on specific facial areas, such as canthi and eyeball positions [9] and external nasal soft tissue [10]. Recently, notable contributions on oral dimensions have been made by Houlton *et. al.* [11, 12]. Yet, many of these studies had small samples sizes, limited age ranges, or relied on 2D imaging. Hence, there is an evident need for comprehensive data that captures the 3D intricacies of the black South African population's facial features.

The aim of this study was to establish normative capulometric values for facial measurements specific to the black South African population.

## Materials and Methods

A sample of 235 retrospective CT and CBCT scans was collected from the University of Pretoria Oral and Dental Hospital, Life Groenkloof Hospital and Cintocare Hospital. Data were anonymised with only age, sex and ancestry recorded for further analysis. Exclusion criteria included any condition that could affect the morphology of the face (e.g., orthodontic treatment, pathological conditions, excessive facial asymmetry, or any facial reconstructive surgery). The study sample comprised 118 CBCT scans of black South African adults with an age range of 18 to 87 years and 119 CT scans of black South African adults between the ages of 18 and 85 years. Ethical approval for this study was obtained from the Faculty of Health Sciences Ethics Committee at the University of Pretoria (Ref# 58/2020).

### *Image segmentation, landmarking and inter-landmark distance computation*

Threshold segmentation of all scans was performed using MeVisLab © 3.0.2 to segment the soft tissue of the face from the surrounding structures and tesselate into a 3D mesh.

MeVisLab was used to manually record the 3D coordinates of 24 capulometric landmarks on the 235 meshes. In the literature, ambiguity exists regarding the definition of the nasolabial angle. Some sources define the nasolabial angle as the angle between the line tangential to the columella and the

line tangential to the upper lip [13] while others used a landmark based method by measuring the angle between the pronasale, subnasale and labiale superius. [14] As this study used capulometric landmarks, the latter method was adopted. Two independent observers performed the landmarking on a subset of 40 meshes in three separate sessions, with at least a 24-hour interval between each session.

Twenty-two clinically relevant inter-landmark distances were computed and analysed. All analyses for ocular parameters were conducted on a smaller subset sample of the CBCTs and CTs with open eyes (n = 126) to ensure accuracy, as ambiguity exists in the placement of the exocanthion when the eyes are closed. Relevant landmarks and inter-landmark distances are listed and defined in Table 1 and illustrated in Figure 1. Outliers in the distribution of each measurement were defined as those more than 3 median absolute deviations from the median and were excluded. The distributions were evaluated for normality through the skewness and kurtosis statistics. All analyses were performed using R Statistical Software (v4.2.2). [15]

### Intra- and inter-observer repeatability

For intra-observer repeatability assessment, intra-class correlation coefficients (ICCs) were calculated for each inter-landmark distance. The variance was partitioned according to a two-way mixed-effects model, and the ICC (2,1) measuring absolute agreement from a single measurement and its 95% confidence interval was calculated using the *irr* package [16]. The general criteria for this assessment are: values below 0.50 signify poor reliability, values between 0.50 to 0.75 correspond to moderate reliability, values spanning 0.75 to 0.90 represent good reliability, and values exceeding 0.90 are indicative of excellent reliability. [17]

For each inter-landmark distance, inter-observer agreement was evaluated by partitioning the variance in the mean of the 6 (k) measurements for each observer according to a two-way random-effects model. The ICC (2, *k*) for assessing absolute agreement between mean measurements was calculated using the *irr* package [16], and a modified repeated-measures Bland Altman analysis conducted via the *SimplyAgree* package [18]. The Bland Altman model included proportional bias, modelling change in bias (mean difference between the two measurements) as a function of the mean of paired measurements. A 95% agreement level was set, and the limits of agreement were determined using the Method of Variance Estimates Recovery (MOVER method).

35

## Univariate statistical analysis

Descriptive statistics were employed to summarise the data and grouped according to sex and modality. A linear regression model was fitted using the base R package, incorporating fixed effects for sex, modality, and age, as well as their two-way and three-way interactions. None of the interactions were significant and the models were re-fitted without the interaction terms. The outcome variable was a single measurement based on the landmark indications of one observer. To facilitate a comprehensive evaluation of the model, the results were subsequently represented through an Analysis of Variance (ANOVA) table. This approach not only aided in assessing the significance of each predictor within the model but also in quantifying their effect sizes, which were calculated using partial eta squared values.

## Comparative analysis with the literature

To contextualize our findings, we performed a targeted literature search and comparative analyses. We searched the MEDLINE; Health Source: Nursing/Academic Edition; Dentistry & Oral Sciences; Academic Search Complete; and CINAHL databases using the terms "anthropometry" AND "face" AND "population". After removing duplicates, 557 abstracts were screened, resulting in 26 articles fitting our criteria: English language full-texts, 3D measurement of soft tissue facial features in adults, with clearly defined parameters. Additionally, 11 articles were identified through examining reference lists. Comparative analyses were conducted using two-sample t-tests (*BSDA* package in R [19]) and Bayes Factor (BF) calculations (*BayesFactor* package in R [20]), comparing sample sizes, means, and variances to our data. The BF is the ratio of the evidence supporting the alternative hypothesis, which posits that there is a difference between population means, to the evidence supporting the null hypothesis. In our statistical analysis, we adopted Jeffreys's [21] scale for interpreting the base 10 logarithm of BFs. On this scale, values below 0 favour the null hypothesis, and above 0 favour the alternative. Values from -0.5 to 0.5 indicate weak evidence. For the alternative hypothesis, evidence strength is categorised as substantial (0.5 to 1), strong (1 to 1.5), very strong (1.5 to 2), and decisive (>2). For the null hypothesis, negative values in these ranges reflect similar evidence strengths, with < -2 being decisive.

## Results

### Intra -and inter-observer repeatability

The results of the intra-class correlation for intra- and inter-observer repeatability are presented in Figure 2. For intra-observer repeatability, most of the facial parameters have good to excellent and excellent repeatability, except for columella width and right eye fissure length which achieved

moderate to excellent ratings, and philtrum width which performed moderately to good. Inter-observer agreement for all facial parameters achieved excellent or good to excellent ratings, except columella width which performed moderately to excellent. Bland Altman plots showing acceptable agreement levels for interobserver agreement are presented in the supplementary materials.

*Univariate statistical analysis for all facial parameters*

Descriptive statistics are presented in Table 2 for all measurements stratified by sex and modality. Absolute measurements of all facial parameters across both modalities are consistently larger for males than for females, except for columella width and length where CBCT female measurements are slightly larger than the CBCT male measurements, and intercanthal distance which is consistent across sexes.

The results of the linear model are presented in Supplementary table 1 and summarised in Figure 3 as a heatmap. Of the total 22 variables, 12, 13 and 9 were significantly associated with sex, age and modality, respectively. The influence of age is evident in the eyes, nose, and mouth. Sex and modality predominantly affect the features of the nose and mouth. The highest partial eta squared values were noted in the effect of sex on the left and right alar length and alar base width, and the effect of age on the upper vermillion height.

## Discussion

The measurement of facial features has practical application for areas like surgical planning and forensic sciences. Accurate and reliable data for these measurements are particularly vital for the black South African population who are underrepresented in the literature. Our study meets this need by providing capulometric values for this population, demonstrating robust methodology through high ICC scores indicating reliable intra- and inter-observer assessments. Most of the parameters showed good to excellent repeatability, affirming our methods' accuracy and the applicability of our findings. This study not only contributes valuable data to a relatively unexplored area but also underscores the importance of including diverse populations in scientific research, particularly in fields where such data have valuable applications in medicine.

Most of the nasal characteristics in our study showed statistically significant differences between sexes. In general, the nasal parameters of males are larger than females. Previous research showed that this difference may be caused by variations in the nose growth process between the sexes, reporting that males have a higher nasal growth velocity for a longer period of time than females. [22] Significant differences between modalities were observed in nasal length, left and right columella

lengths and columella width, with nasal length presenting 1.43 mm shorter in CTs and columella lengths and width approximately 0.6 mm longer. The gravitational effects, which manifest differently between patients in an upright and supine position, [23] as seen in CBCT and CT respectively, could be particularly accentuated here.

Our study identified significant sex-based differences in the right eye fissure length and outer-canthal width, and modality-based differences only in the outer-canthal width. This contrasts with existing literature, which commonly reports significant sexual dimorphism in these facial features across various populations. Our findings align with recent findings indicating less dimorphism in orbital morphology among black South Africans compared to white South Africans [24]. However, cautious interpretation and generalisation are advised due to slightly lower, although still acceptable, ICC repeatability in these parameters, Similar trends of lesser sexual dimorphism in African populations compared to European and South American groups have also been noted in other studies. [25]

Sex differences in mouth width, philtrum width, and lower lip height were noted. Differences between modalities were also notable for mouth width, lower lip, and vermillion heights. These pronounced variations in the mouth region could be due to its fleshy nature and susceptibility to gravitational effects in different modalities, similar to observations in the nose region. Furthermore, the use of supportive struts in the CBCT sample may have impacted these measurements.

The findings of our study were compared to existing literature reporting normative values from diverse populations. The studies employed either direct anthropometry or 3D techniques, including 3D stereophotogrammetry, light scanning and CBCT, to capture inter-landmark facial measurements. A significant majority of these comparisons (415 out of 502) revealed significant disparities between populations (Supplementary table 3). Details of this analysis is presented in Supplementary Tables 2 to 4. Supplementary table 2 provides a comprehensive summary of results from the literature, along with BFs and the corresponding interpretation for each comparison.

Firstly, when we investigated the data by facial features, grouping the individual measurements together as nasal, ocular, or oral parameters, a few patterns became evident (Supplementary table 3). Ocular parameters displayed the most variability across populations. Our study's findings showed differences in 92% of cases when compared to other African groups, and 76% differences when compared against non-African groups. However, the outer-canthal width presented a unique pattern in the ocular data. The outer-canthal width differed from non-African groups in only half of the

comparisons, contrasting with the other ocular parameters where 86% of comparisons were different from non-African groups and 93% when compared to other African groups. This suggests a distinct variability pattern for outer-canthal width compared to other ocular features. Nasal features also displayed significant variability across populations. Our study's findings diverged from 79% of studies on other African populations, including African-Americans, Sudanese, Nigerians, Kenyans, and other black South Africans. This contrast was even starker, at 92%, when compared to non-African populations.

Oral parameters, however, showed a different trend. Comparisons of oral features with other African populations yielded significant differences in 49% of cases. In contrast, 86% of oral parameter comparisons with non-African populations were significantly different. Evidently, while significant differences are widespread across all groups, our black South African cohort shares more similarities with other African groups, particularly concerning oral features, than with non-African groups.

Building on our general analysis of grouped facial features across diverse populations, we delved deeper into specific measurements, comparing the individual parameters with established literature.

Our study's absolute measurements for alar base width are consistent with previous studies on black South Africans, Kenyan, and Nigerian groups, [26-28] supported by strong to very strong BF evidence. Notably, the alar base width in black South Africans is wider than in other populations, including African- American, Iranian, Kenyan, white South African, Turkish, Spanish, and North American white groups [26, 29-33]. Among females, nasal height matches Iranian and African-American groups (strong to very strong BF evidence). [30, 34] Nasal length aligns with black and white South Africans (weak to strong BF), and nasal protrusion is similar to Chinese, Mexican American, and African-Americans (strong to very strong BF). [26, 29-31, 35] For males, nasal length is comparable with black and white South Africans and Chinese (substantial to strong BF), and nasal protrusion resembles Mexican American and African-Americans (strong BF). [26, 29, 35]

Eye fissure lengths in our population are shorter than in most compared groups, with a notable nearly 10 mm difference from a Nigerian group (decisive BF evidence). [36] Both sexes show substantial to very strong similarity to Chinese and Japanese groups. [27, 37] Intercanthal widths are broader compared to all other populations, with a range of 4 to 12 mm difference for females and 1 to 9 mm for males. Outer-canthal widths in our sample are average, with narrower measurements in North American white and European populations, and broader in African-American, Maori, Nigerian, and Kenyan

groups. Both sexes show substantial to very strong similarity with New Zealand European and Iranian groups. [38, 39]

Mouth width findings showed substantial to very strong evidence of similarity to earlier studies on Kenyan, African-American and black South African populations, and philtrum widths are consistent with measurements from both black and white South Africans. [12, 29, 31]

This study was based on a sample population from the Tshwane Metropolitan area in the Gauteng province of South Africa. Although Gauteng is the country's smallest province by land area, it hosts its largest population, with 75% of the Tshwane Metropolitan population self-identifying as black South African. Within this demographic, the prevalent Bantu-speakers' languages noted in the 2011 Census – Sepedi, and Setswana – may be indicative of specific ethnicities present in the Tshwane Metropolitan region. [40] Therefore the findings of this study may not fully represent other South African ethnic groups, such as Xhosa, Venda, or Swazi. As the black South African population is heterogenous, future research may benefit from a more refined approach, by considering the distinct ethnicities comprising the black South African population. Despite this, the value of utilising the broadly classified black South African data for population specific applications are underscored by the significant disparities with other populations.

Although this study reported that age has a significant effect on the findings (13 of the 22 variables were significantly affected by age), this was not further explored as the sample was skewed, with the majority being of younger individuals (147 out of 235 below the age of 40). Future research investigating the effects of age in more distinct terms would be a valuable contribution.

The normative values reported can serve as invaluable guides for clinicians in prosthodontics, reconstructive and aesthetic surgery, ensuring optimal interventions. Our findings also contribute significantly to a more comprehensive understanding of human facial diversity. The nuanced differences and similarities identified between our sample norms and those from around the world, underscore the unique facial characteristics of the black South African population. Recognising these distinct features is paramount, not only for enriching anthropological databases but also for refining practices in forensic anthropology.

40

## Conflict of Interest Statement:

None

## Acknowledgements:

## Declaration of generative AI and AI-assisted technologies in the writing process

During the preparation of this work the author(s) used GPT-4 in order to improve language and readability and reduce word count. After using this tool/service, the author(s) reviewed and edited the content as needed and take(s) full responsibility for the content of the publication.

## References

1. Shahbazi Z, Ardalani H, Maleki M. Aesthetics of Numerical Proportions in Human Cosmetic Surgery. World J Plast Surg 2019: 8: 2228-7914 (Print).

2. Sforza C, de Menezes M, Ferrario V. Soft- and hard-tissue facial anthropometry in three dimensions: what's new. J Anthropol Sci 2013: 91: 159-84.

3. Caple J, Stephan CN. A standardized nomenclature for craniofacial and facial anthropometry. Int J Legal Med 2016: 130: 863-79.

4. Weinberg SM, Raffensperger ZD, Kesterke MJ, et al. The 3D Facial Norms Database: Part 1. A web-based craniofacial anthropometric and image repository for the clinical and research community. Cleft Palate Craniofac J 2016: 53: 185-97.

5. Kook M-S, Jung S, Park H-J, et al. A comparison study of different facial soft tissue analysis methods. J Craniomaxillofac Surg 2014: 42: 648-56.

6. Bastir M, Rosas A. Correlated variation between the lateral basicranium and the face: A geometric morphometric study in different human groups. Arch Oral Biol 2006: 51: 814-24.

7. Novotný V, İşcan MY, Loth S. Morphologic and Osteometric Assessment of age, Sex and Race from the Skull. In İşcan MY, Helmer H, ed. Forensic Analysis of the Skull: Craniofacial Analysis, Reconstruction, and Identification. New York: Wiley-Liss, 1993: 71-88.

8. Porter JP. The average African American male face: an anthropometric analysis. Arch Facial Plast Surg 2004: 6: 78-81.

9. Dorfling HF, Lockhat Z, Pretorius S, Steyn M, Oettlé AC. Facial approximations: Characteristics of the eye in a South African sample. Forensic Sci Int 2018: 286: 46-53.

10. Wilson SP, Medapati V, Segwapa K. Facial Anthropometric Norms of the Young Black South African Woman. Plast Reconstr Surg Glob Open 2023: 11.

11. Houlton TM, Jooste N, Uys A, Steyn M. Lip height estimation in a southern African sample. SADJ 2020: 75: 415-24.

12. Houlton TMR, Jooste N, Steyn M. Mouth Width and Cupid's Bow Estimation in a Southern African Population. J Forensic Sci 2019: 65: 372-79.

13. Quinzi V, Paskay LC, D'Andrea N, et al. Evaluation of the Nasolabial Angle in Orthodontic Diagnosis: A Systematic Review. Appl Sci (Basel) 2021: 11: 2531.

14. Uzun A, Ozdemir F. Morphometric analysis of nasal shapes and angles in young adults. Braz J Otorhinolaryngol 2014: 80: 397-402.

15. R Core Team. 2022 R: A language and environment for statistical computing.

16. Gamer M, Lemon J, Fellows I, Singh P. 2022 irr: Various Coefficients of Interrater Reliability and Agreement. 0.84.1. https://CRAN.R-project.org/package=irr.

17. Koo TK, Li MY. A guideline of selecting and reporting intraclass correlation coefficients for reliability research. J Chiropr Med 2016: 15: 155-63.

18. Caldwell AR. SimplyAgree: an R package and jamovi module for simplifying agreement and reliability analyses. Journal of Open Source Software 2022: 7: 4148.

19. Arnholt A, Evans B. 2023 BSDA: Basic Statistics and Data Analysis. R package version 1.2.2 https://CRAN.R-project.org/package=BSDA

20. Morey R, Rouder J. 2023 BayesFactor: Computation of Bayes Factors for Common Designs. R package version 0.9.12-4.5,

https://CRAN.R-project.org/package=BayesFactor.

21. Jeffreys H. Theory of probability. 3rd ed. Oxford: Claredon Press, 1961.

22. Prahl-Andersen B, Ligthelm-Bakker A, Wattel E, Nanda R. Adolescent growth changes in soft tissue profile. Am J Orthod Dentofacial Orthop 1995: 107: 476-83.

23. Iblher N, Gladilin E, Stark BG. Soft-Tissue Mobility of the Lower Face Depending on Positional Changes and Age: A Three-Dimensional Morphometric Surface Analysis. Plast Reconstr Surg 2013: 131: 372-81.

24. Van der Walt S, Ridel A, L'Abbé E, Oettlé A. Dimensions of the orbital region for biological profiling in a South African sample. 2023.

25. Kleisner K, Tureček P, Roberts SC, et al. How and why patterns of sexual dimorphism in human faces vary across the world. Sci Rep 2021: 11: 5978.

26. Ridel AF, Demeter F, Liebenberg J, et al. Skeletal dimensions as predictors for the shape of the nose in a South African sample: A cone-beam computed tomography (CBCT) study. Forensic Sci Int 2018: 289: 18-26.

27. Sarna K, Sonigra KJ, Ngeow WC. A Cross-Sectional Study to Determine and Compare the Craniofacial Anthropometric Norms in a Selected Kenyan and Chinese Population. Plast Surg (Oakv) 2023: 31: 84-90.

28. Olusanya AA, Aladelusi TO, Adedokun B. Anthropometric Analysis of the Nigerian Face: Any Conformity to the Neoclassical Canons? J Craniofac Surg 2018: 29: 1978-82.

29. Farkas LG, Katic MJ, Forrest CR. Comparison of craniofacial measurements of young adult African-American and North American white males and females. Ann Plast Surg 2007: 59: 692-8.

30. Heidari Z, Mahmoudzadeh-Sagheb H, Khammar T, Khammar M. Anthropometric measurements of the external nose in 18–25-year-old Sistani and Baluch aborigine women in the southeast of Iran. Folia morphologica 2009: 68: 88-92.

31. Virdi SS, Wertheim D, Naini FB. Normative anthropometry and proportions of the Kenyan-African face and comparative anthropometry in relation to African Americans and North American Whites. Maxillofac Plast Reconstr Surg 2019: 41: 9.

32. Ozdemir F, Uzun A. Anthropometric analysis of the nose in young Turkish men and women. J Craniomaxillofac Surg 2015: 43: 1244-47.

33. Menéndez López-Mateos ML, Carreño-Carreño J, Palma JC, et al. Three-dimensional photographic analysis of the face in European adults from southern Spain with normal occlusion: reference anthropometric measurements. BMC Oral Health 2019: 19: 1-8.

34. Liu Y, Kau CH, Talbert L, Pan F. Three-dimensional analysis of facial morphology. J Craniofac Surg 2014: 25: 1890-94.

35. He Z-j, Jian X-c, Wu X-s, et al. Anthropometric measurement and analysis of the external nasal soft tissue in 119 young Han Chinese adults. J Craniofac Surg 2009: 20: 1347-51.

36. Oladipo G, Okoh P, Hart J. Anthropometric study of ocular dimensions in adult ijaws of Nigeria. Res J Med Med Sci 2010: 5: 121-4.

37. Ogawa Y, Wada B, Taniguchi K, Miyasaka S, Imaizumi K. Photo anthropometric variations in Japanese facial features: Establishment of large-sample standard reference data for personal identification using a three-dimensional capture system. Forensic Sci Int 2015: 257: 511.e1-11.e9.

38. Amini F, Mashayekhi Z, Rahimi H, Morad G. Craniofacial morphologic parameters in a Persian population: an anthropometric study. J Craniofac Surg 2014: 25: 1874-81.

39. Antoun JS, Lawrence C, Leow A, et al. A three-dimensional evaluation of Māori and New Zealand European faces. Australasian Orthodontic Journal 2014: 30: 169-75.

40. Frith A. City of Tshwane Metropolitan Municipality 799 from Census 2011.  [14 November 2023]. Available from: https://census2011.adrianfrith.com/place/799.

| Variable | Predictors | Standardised Coefficient (Estimate) in mm | SE of Coefficient | t value | Significance of individual predictors (p-) | Effect size (Partial Eta Squared) | Conclusion |
|---|---|---|---|---|---|---|---|
| **Supplementary table 1: Detailed results of the linear model significance levels and effect sizes** | | | | | | | |
| *General* | | | | | | | |
| Midfacial height (MH) | Sex | 0,43 | 0,59 | 0,72 | 0,471 | 0,003 | Not significant; negligible effect size; no substantial difference in MH between sexes. |
| | Age | -0,16 | 0,30 | -0,55 | 0,585 | 0,001 | Not significant; small effect size; minimal change in MH associated with each additional year of age. |
| | Modality | 1,68 | 0,59 | 2,86 | **0,005** | 0,037 | Significant; explains 3.82% of residual variance; CT modality shows a 1.68 mm increase in MH compared to CBCT. |
| Nasofrontal angle (degrees) (NFA) | Sex | -3,07 | 1,01 | -3,05 | 0,003 | 0,041 | Significant; explains 4.13% of residual variance; males have a 3.07 degrees smaller NFA than females. |
| | Age | -0,11 | 0,50 | -0,22 | 0,825 | 0,000 | Not significant; negligible effect size; minimal change in NFA associated with each additional year of age. |
| | Modality | -0,03 | 0,99 | -0,03 | **0,976** | 0,000 | Not significant; negligible effect size; minimal change in NFA associated with CT modality compared to CBCT. |
| Nasolabial angle (degrees) (NLA) | Sex | 0,09 | 1,66 | 0,05 | 0,956 | 0,001 | Not significant; negligible effect size; no substantial difference in NLA between sexes. |
| | Age | 2,17 | 0,83 | 2,62 | 0,010 | 0,030 | Significant; explains 3.00% of residual variance; each additional year of age is associated with a 2.17 degrees increase in NLA. |
| | Modality | 1,94 | 1,64 | 1,18 | **0,237** | 0,004 | Not significant; small effect size; CT modality shows a 1.94 degrees increase in NSA compared to CBCT. |
| *Nasal parameters* | | | | | | | |
| Nasal length (NL) | Sex | 2,19 | 0,52 | 4,24 | < 0,001 | 0,078 | Significant; explains 7.80% of residual variance; males have a 2.19 mm longer NL than females. |
| | Age | 0,03 | 0,26 | 0,13 | 0,899 | 0,000 | Not significant; negligible effect size; no substantial change in NL associated with each additional year of age. |
| | Modality | -1,43 | 0,51 | -2,80 | **0,006** | 0,035 | Significant; explains 3.50% of residual variance; CT modality shows a 1.43 mm decrease in NL compared to CBCT. |
| Nasal height (NH) | Sex | 1,89 | 0,48 | 3,92 | < 0,001 | 0,064 | Significant; explains 6.50% of residual variance; males have a 1.89 mm longer NH than females. |
| | Age | 0,17 | 0,24 | 0,70 | 0,482 | 0,002 | Not significant; small effect size; minimal change in NH associated with each additional year of age. |
| | Modality | -0,54 | 0,48 | -1,14 | **0,255** | 0,006 | Not significant; small effect size; CT modality shows a 0.54 mm decrease in NH compared to CBCT. |
| Nasal protrusion (depth) (NP) | Sex | 0,51 | 0,26 | 1,98 | 0,049 | 0,011 | Significant; explains 1.12% of residual variance; males have a 0.51 mm longer NP than females. |
| | Age | 0,33 | 0,13 | 2,59 | 0,010 | 0,030 | Significant; explains 3.00% of residual variance; each additional year of age is associated with a 0.33 mm increase in NP. |
| | Modality | 0,01 | 0,25 | 0,05 | **0,963** | 0,000 | Not significant; negligible effect size; no substantial change in NP associated with CT modality compared to CBCT. |
| Alar base width (nasal width) (ABW) | Sex | 4,04 | 0,51 | 7,99 | < 0,001 | 0,195 | Significant; explains 19.50% of residual variance; males have a 4.04 mm wider ABW than females. |
| | Age | 1,22 | 0,25 | 4,82 | < 0,001 | 0,095 | Significant; explains 9.50% of residual variance; each additional year of age is associated with a 1.22 mm increase in ABW . |
| | Modality | 0,42 | 0,50 | 0,85 | **0,397** | 0,001 | Not significant; small effect size; CT modality shows a 0.42 mm increase in ABW compared to CBCT. |
| Alar length Lt (AL Lt) | Sex | 2,70 | 0,33 | 8,26 | < 0,001 | 0,229 | Significant; explains 22.90% of residual variance; males have a 2.70 mm longer AL Lt than females. |
| | Age | 0,31 | 0,16 | 1,87 | 0,062 | 0,016 | Not significant; small effect size; each additional year of age is associated with a 0.31 mm increase in AL Lt. |
| | Modality | 0,41 | 0,32 | 1,27 | **0,204** | 0,006 | Not significant; small effect size; CT modality shows a 0.41 mm increase in AL Lt compared to CBCT |

| Variable | Predictors | Standardised Coefficient (Estimate) in mm | SE of Coefficient | t value | Significance of individual predictors (p-value) | Effect size (Partial Eta Squared) | Conclusion |
|---|---|---|---|---|---|---|---|
| **Supplementary table 1: Detailed results of the linear model significance levels and effect sizes** | | | | | | | |
| *Nasal parameters (continued)* | | | | | | | |
| Alar length Rt (AL Rt) | Sex | 2,99 | 0,34 | 8,73 | **< 0,001** | 0,251 | Significant; explains 25.10% of residual variance; males have a 2.99 mm longer AL Rt than females. |
| | Age | 0,30 | 0,17 | 1,74 | 0,083 | 0,014 | Not significant; small effect size; each additional year of age is associated with a 0.30 mm increase in AL Rt. |
| | Modality | -0,21 | 0,34 | -0,64 | 0,525 | 0,003 | Not significant; negligible effect size; CT modality shows a 0.21 mm decrease in AL Rt compared to CBCT |
| Columella width (CW) | Sex | -0,02 | 0,19 | -0,09 | 0,929 | 0,001 | Not significant; negligible effect size; no substantial difference in CW between sexes. |
| | Age | 0,18 | 0,10 | 1,93 | 0,055 | 0,017 | Not significant; small effect size; each additional year of age is associated with a 0.18 mm increase in CW. |
| | Modality | 0,61 | 0,19 | 3,27 | **0,001** | 0,043 | Significant; explains 4.30% of residual variance; CT modality shows a 0.61 mm increase in CW compared to CBCT |
| Columella length Lt (CL Lt) | Sex | 0,10 | 0,20 | 0,49 | 0,627 | 0,000 | Not significant; negligible effect size; no substantial difference in CL Lt between sexes. |
| | Age | 0,28 | 0,10 | 2,82 | **0,005** | 0,035 | Significant; explains 3.50% of residual variance; each additional year of age is associated with a 0.28 mm increase in CL Lt. |
| | Modality | 0,59 | 0,20 | 2,96 | **0,003** | 0,034 | Significant; explains 3.40% of residual variance; CT modality shows a 0.59 mm increase in CL Lt compared to CBCT |
| Columella length Rt (CL Rt) | Sex | -0,16 | 0,21 | -0,77 | 0,441 | 0,007 | Not significant; small effect size; no substantial difference in CL Rt between sexes. |
| | Age | 0,26 | 0,10 | 2,56 | **0,011** | 0,029 | Significant; explains 2.90% of residual variance; each additional year of age is associated with a 0.26 mm increase in CL Rt. |
| | Modality | 0,47 | 0,20 | 2,29 | **0,023** | 0,020 | Significant; explains 2.00% of residual variance; CT modality shows a 0.47 mm increase in CL Rt compared to CBCT. |
| *Ocular parameters* | | | | | | | |
| Eye fissure length Lt (EFL Lt) | Sex | 0,37 | 0,46 | 0,80 | 0,425 | 0,007 | Not significant; small effect size; no substantial difference in EFL Lt between sexes. |
| | Age | -1,12 | 0,23 | -4,86 | **< 0,001** | 0,168 | Significant; explains 16.80% of residual variance; each additional year of age is associated with a 1.12 mm decrease in EFL Lt. |
| | Modality | 0,68 | 0,46 | 1,48 | 0,143 | 0,006 | Not significant; small effect size; CT modality shows a 0.68 mm increase in EFL Lt compared to CBCT. |
| Eye fissure length Rt (EFL Rt) | Sex | 1,16 | 0,46 | 2,53 | **0,013** | 0,057 | Significant; explains 5.70% of residual variance; males have a 1.16 mm longer EFL Rt than females. |
| | Age | -0,89 | 0,23 | -3,84 | **< 0,001** | 0,113 | Significant; explains 11.30% of residual variance; each additional year of age is associated with an 0.89 mm decrease in EFL Rt. |
| | Modality | 0,46 | 0,46 | 1,00 | 0,319 | 0,003 | Not significant; negligible effect size; CT modality shows a 0.46 mm increase in EFL Rt compared to CBCT. |
| Intercanthal distance (ICD) | Sex | 0,41 | 0,77 | 0,54 | 0,593 | 0,002 | Not significant; negligible effect size; no substantial difference in ICD between sexes. |
| | Age | 1,26 | 0,39 | 3,27 | **0,001** | 0,084 | Significant; explains 8.40% of residual variance; each additional year of age is associated with a 1.26 mm increase in ICD. |
| | Modality | 0,38 | 0,77 | 0,49 | 0,623 | 0,007 | Not significant; negligible effect size; minimal change in ICD associated with CT modality compared to CBCT. |
| Outer-canthal distance (OCD) | Sex | 2,08 | 0,87 | 2,38 | **0,019** | 0,048 | Significant; explains 4.80% of residual variance; males have a 2.08 mm wider OCD than females. |
| | Age | -0,69 | 0,44 | -1,57 | 0,120 | 0,021 | Not significant; small effect size; each additional year of age is associated with a 0.69 mm decrease in OCD. |
| | Modality | 1,92 | 0,87 | 2,20 | **0,030** | 0,034 | Significant; explains 3.40% of residual variance; CT modality shows a 1.92 mm increase in OCD compared to CBCT. |

| Supplementary table 1: Detailed results of the linear model significance levels and effect sizes | | | | | | | |
|---|---|---|---|---|---|---|---|
| Variable | Predictors | Standardised Coefficient (Estimate) in mm | SE of Coefficient | t value | Significance of individual predictors (p-) | Effect size (Partial Eta Squared) | Conclusion |
| *Oral parameters* | | | | | | | |
| Mouth width (MW) | Sex | 3,59 | 0,54 | 6,71 | **< 0,001** | 0,150 | Significant; explains 15.00% of residual variance; males have a 3.59 mm wider MW than females. |
| | Age | 0,96 | 0,27 | 3,59 | **< 0,001** | 0,056 | Significant; explains 5.60% of residual variance; each additional year of age is associated with a 0.96 mm increase in MW. |
| | Modality | 1,24 | 0,53 | 2,34 | **0,020** | 0,019 | Significant; explains 1.90% of residual variance; CT modality shows a 1.24 mm increase in MW compared to CBCT. |
| Philtrum width (PW) | Sex | 1,53 | 0,28 | 5,46 | **< 0,001** | 0,102 | Significant; explains 10.20% of residual variance; males have a 1.53 mm wider PW than females. |
| | Age | 0,48 | 0,14 | 3,41 | **0,001** | 0,051 | Significant; explains 5.10% of residual variance; each additional year of age is associated with a 0.48 mm increase in PW. |
| | Modality | -0,42 | 0,28 | -1,51 | 0,131 | 0,015 | Not significant; small effect size; CT modality shows a 0.42 mm decrease in PW compared to CBCT. |
| Upper lip height (ULH) | Sex | 0,75 | 0,40 | 1,89 | 0,060 | 0,012 | Not significant; small effect size; no substantial difference in ULH between sexes. |
| | Age | 0,42 | 0,20 | 2,11 | **0,036** | 0,020 | Significant; explains 2.00% of residual variance; each additional year of age is associated with a 0.42 mm increase in ULH. |
| | Modality | -0,69 | 0,39 | -1,76 | 0,080 | 0,017 | Not significant; small effect size; CT modality shows a 0.69 mm decrease in ULH compared to CBCT. |
| Upper vermillion height (UVH) | Sex | -0,03 | 0,32 | -0,09 | 0,927 | 0,005 | Not significant; negligible effect size; no substantial difference in UVH between sexes. |
| | Age | -1,23 | 0,16 | -7,57 | **< 0,001** | 0,211 | Significant; explains 21.10% of residual variance; each additional year of age is associated with a 1.23 mm decrease in UVH. |
| | Modality | 0,15 | 0,32 | 0,46 | 0,647 | 0,003 | Not significant; negligible effect size; minimal change in UVH associated with CT modality compared to CBCT. |
| Lower lip height (LLH) | Sex | 2,11 | 0,41 | 5,20 | **< 0,001** | 0,118 | Significant; explains 11.80% of residual variance; males have a 2.161 mm longer LLH than females. |
| | Age | -0,29 | 0,20 | -1,45 | 0,150 | 0,010 | Not significant; small effect size; each additional year of age is associated with a 0.29 mm decrease in LLH. |
| | Modality | 2,38 | 0,40 | 5,93 | **< 0,001** | 0,146 | Significant; explains 14.60% of residual variance; CT modality shows a 2.38 mm increase in LLH compared to CBCT. |
| Lower vermillion height (LVH) | Sex | 0,40 | 0,31 | 1,27 | 0,205 | 0,020 | Not significant; small effect size; no substantial difference in LVH between sexes. |
| | Age | -0,84 | 0,16 | -5,33 | **< 0,001** | 0,119 | Significant; explains 11.90% of residual variance; each additional year of age is associated with a 0.84 mm decrease in LVH. |
| | Modality | 0,90 | 0,31 | 2,90 | **0,004** | 0,051 | Significant; explains 5.10% of residual variance; CT modality shows a 0.90 mm increase in LVH compared to CBCT. |
| Note: The reference categories for sex and modality is Female and CBCT, respectively. Significant values for the predictors are shown in bold. | | | | | | | |

| | This study | | Other studies | | | | | Bayes Factor |
|---|---|---|---|---|---|---|---|---|
| Facial Parameter | Sex (sample size) | Mean ± SD | Author | Sex (sample size) | Population | Modality | Mean ± SD | log10 value* |
| Midfacial Height | F (n = 54) | 62,89 ± 4,00 | (Amini et al., 2014) | F (n = 50) | Iranian | Direct | 64,90 ± 4,50 | 0,957 |
| | | | (Bhandari et al., 2021) | F (n = 113) | Indian | Direct | 60,85 ± 4,53 | 2,206 |
| | | | (Virdi et al., 2019) | F (n = 36) | Kenyan | Direct | 65,30 ± 5,70 | 0,601 |
| | M (n = 64) | 63,75 ± 4,47 | (Amini et al., 2014) | M (n = 50) | Iranian | Direct | 67,10 ± 4,20 | 5,628 |
| | | | (Bhandari et al., 2021) | M (n = 387) | Indian | Direct | 64,44 ± 4,48 | -1,301 |
| | | | (Virdi et al., 2019) | M (n = 36) | Kenyan | Direct | 64,80 ± 6,50 | -1,194 |
| Nasofrontal Angle | F (n = 54) | 141,26 ± 7,39 | (Bayat et al., 2018) | F (n = 100) | Iranian | Direct | 156,16 ± 10,99 | 35,152 |
| | | | (Borman et al., 1999) | F (n = 525) | Turkish | Direct | 137,02 ± 5,37 | 5,988 |
| | | | (Farkas et al., 2007) | F (n = 50) | African-American | Direct | 127,60 ± 8,10 | 26,460 |
| | | | (He et al., 2009) | F (n = 63) | Chinese | Direct | 147,71 ± 5,48 | 10,024 |
| | | | (Virdi et al., 2019) | F (n = 36) | Kenyan | Direct | 127,90 ± 3,00 | 38,624 |
| | M (n = 64) | 137,09 ± 7,8 | (Bayat et al., 2018) | M (n = 100) | Iranian | Direct | 153,52 ± 14,00 | 33,455 |
| | | | (Borman et al., 1999) | M (n = 525) | Turkish | Direct | 136,49 ± 5,80 | -1,767 |
| | | | (Farkas et al., 2007) | M (n = 50) | African-American | Direct | 126,50 ± 12,00 | 10,487 |
| | | | (He et al., 2009) | M (n = 56) | Chinese | Direct | 138,15 ± 8,43 | -1,407 |
| | | | (Virdi et al., 2019) | M (n = 34) | Kenyan | Direct | 127,30 ± 9,00 | 10,050 |
| Nasolabial Angle | F (n = 54) | 105,88 ± 12,38 | (Amini et al., 2014) | F (n = 50) | Iranian | Direct | 94,60 ± 10,50 | 8,839 |
| | | | (Bayat et al., 2018) | F (n = 100) | Iranian | Direct | 78,32 ± 14,14 | 50,340 |
| | | | (Borman et al., 1999) | F (n = 525) | Turkish | Direct | 95,07 ± 10,42 | 15,864 |
| | | | (Farkas et al., 2007) | F (n = 50) | African-American | Direct | 73,90 ± 14,50 | 41,608 |
| | | | (He et al., 2009) | F (n = 63) | Chinese | Direct | 100,05 ± 11,33 | 1,463 |
| | | | (Liu et al., 2013) | F (n = 40) | Chinese | Direct | 119,04 ± 7,31 | 14,380 |
| | | | (Liu et al., 2013) | F (n = 82) | Greek | Direct | 128,77 ± 8,11 | 45,358 |
| | | | (Virdi et al., 2019) | F (n = 36) | Kenyan | Direct | 85,20 ± 13,80 | 17,715 |
| | M (n = 64) | 103,55 ± 11,24 | (Amini et al., 2014) | M (n = 50) | Iranian | Direct | 97,00 ± 8,90 | 3,636 |
| | | | (Bayat et al., 2018) | M (n = 100) | Iranian | Direct | 87,30 ± 14,27 | 24,637 |
| | | | (Borman et al., 1999) | M (n = 525) | Turkish | Direct | 97,79 ± 9,13 | 5,361 |
| | | | (Farkas et al., 2007) | M (n = 50) | African-American | Direct | 71,40 ± 14,50 | 47,542 |
| | | | (He et al., 2009) | M (n = 56) | Chinese | Direct | 98,50 ± 10,54 | 1,229 |
| | | | (Virdi et al., 2019) | M (n = 34) | Kenyan | Direct | 85,50 ± 10,10 | 21,905 |

| Supplementary table 2: Comparative analysis with the literature comparisons | | | | | | | |
|---|---|---|---|---|---|---|---|
| | **This study** | | **Other studies** | | | | **Bayes Factor** |
| **Facial Parameter** | **Sex (sample size)** | **Mean ± SD** | **Author** | **Sex (sample size)** | **Population** | **Modality** | **Mean ± SD** | **log10 value\*** |
| Nasal Length | F (n = 54) | 39,71 ± 4,12 | (Bhandari et al., 2021) | F (n = 113) | Indian | Direct | 44,19 ± 3,40 | 18,322 |
| | | | (Celebi et al., 2017) | F (n = 68) | Columbian | 3D Stereophotogrammetry | 44,14 ± 3,01 | 15,933 |
| | | | (Celebi et al., 2017) | F (n = 48) | Mexican-American | 3D Stereophotogrammetry | 45,17 ± 3,72 | 17,252 |
| | | | (Farkas et al., 2007) | F (n = 50) | African-American | Direct | 42,60 ± 3,70 | 4,501 |
| | | | (Farkas et al., 2007) | F (n = 200) | North American White | Direct | 44,70 ± 3,40 | 26,637 |
| | | | (Galantucci et al., 2016) | F (n = 66) | Italian | 3D Stereophotogrammetry | 43,35 ± 2,55 | 11,626 |
| | | | (He et al., 2009) | F (n = 63) | Chinese | Direct | 50,54 ± 3,87 | 56,399 |
| | | | (Heidari et al., 2009) | F (n = 200) | Iranian Sistani | Direct | 44,00 ± 2,20 | 21,714 |
| | | | (Heidari et al., 2009) | F (n = 200) | Iranian Baluch | Direct | 49,50 ± 2,00 | 91,683 |
| | | | (Jayaratne et al., 2014) | F (n = 52) | Chinese | 3D Stereophotogrammetry | 44,65 ± 4,06 | 13,750 |
| | | | (Liu et al., 2013) | F (n = 40) | Chinese | 3D Stereophotogrammetry | 43,82 ± 3,32 | 9,953 |
| | | | (Liu et al., 2013) | F (n = 82) | Greek | 3D Stereophotogrammetry | 46,14 ± 3,40 | 31,447 |
| | | | (Liu et al., 2014) | F (n = 60) | African-American | 3D Stereophotogrammetry | 35,18 ± 3,44 | 14,442 |
| | | | (Menéndez López-Mateos et al., 2019) | F (n = 50) | Spanish | 3D Stereophotogrammetry | 47,56 ± 2,97 | 37,479 |
| | | | (Ozdemir et al., 2015) | F (n = 59) | Turkish | Direct | 47,81 ± 4,60 | 31,712 |
| | | | (Ridel et al., 2018) | F (n = 28) | White SA | CBCT | 39,87 ± 3,72 | -1,411 |
| | | | (Ridel et al., 2018) | F (n = 23) | Black SA | CBCT | 37,89 ± 3,63 | 0,197 |
| | | | (Weiliang et al., 2021) | F (n = 430) | Chinese | Direct | 43,30 ± 4,20 | 14,807 |
| | M (n = 64) | 42,14 ± 3,69 | (Bhandari et al., 2021) | M (n = 387) | Indian | Direct | 46,60 ± 3,93 | 33,135 |
| | | | (Celebi et al., 2017) | M (n = 44) | Mexican-American | 3D Stereophotogrammetry | 47,39 ± 4,14 | 16,225 |
| | | | (Celebi et al., 2017) | M (n = 63) | Columbian | 3D Stereophotogrammetry | 47,89 ± 3,04 | 31,248 |
| | | | (Farkas et al., 2007) | M (n = 50) | African-American | Direct | 45,60 ± 3,50 | 9,299 |
| | | | (Farkas et al., 2007) | M (n = 109) | North American White | Direct | 50,00 ± 3,60 | 59,333 |
| | | | (He et al., 2009) | M (n = 56) | Chinese | Direct | 51,80 ± 3,94 | 52,995 |
| | | | (Jayaratne et al., 2014) | M (n = 51) | Chinese | 3D Stereophotogrammetry | 42,50 ± 3,36 | -1,479 |
| | | | (Liu et al., 2014) | M (n = 32) | Chinese | 3D Stereophotogrammetry | 42,55 ± 3,22 | -1,350 |
| | | | (Liu et al., 2014) | M (n = 57) | African-American | 3D Stereophotogrammetry | 37,40 ± 3,17 | 20,614 |
| | | | (Menéndez López-Mateos et al., 2019) | M (n = 50) | Spanish | 3D Stereophotogrammetry | 48,35 ± 4,76 | 20,403 |
| | | | (Ozdemir et al., 2015) | M (n = 56) | Turkish | Direct | 52,95 ± 5,40 | 46,830 |
| | | | (Ridel et al., 2018) | M (n = 37) | Black SA | CBCT | 42,47 ± 4,84 | -1,472 |
| | | | (Ridel et al., 2018) | M (n = 32) | White SA | CBCT | 43,42 ± 5,27 | -0,826 |

| Facial Parameter | This study Sex (sample size) | Mean ± SD | Author | Sex (sample size) | Population | Modality | Mean ± SD | Bayes Factor log10 value* |
|---|---|---|---|---|---|---|---|---|
| | | | Other studies | | | | | |
| Nasal Height | F (n = 54) | 46,32 ± 3,57 | (Adekunle et al., 2022) | F (n = 198) | Nigerian | 3D Stereophotogrammetry | 49,30 ± 3,45 | 11,609 |
| | | | (Ahmed et al., 2016) | F (n = 120) | Sudanese | Direct | 55,46 ± 4,33 | 65,499 |
| | | | (Al-Sebaei, 2015) | F (n = 93) | Saudi Arabian | Direct | 53,19 ± 4,13 | 38,283 |
| | | | (Amini et al., 2014) | F (n = 50) | Iranian | Direct | 56,80 ± 3,40 | 57,122 |
| | | | (Antoun et al., 2014) | F (n = 15) | New Zealand European | 3D white light scanner | 51,90 ± 3,20 | 10,968 |
| | | | (Antoun et al., 2014) | F (n = 15) | Maori | 3D white light scanner | 55,70 ± 2,80 | 30,051 |
| | | | (Bayat et al., 2018) | F (n = 100) | Iranian | Direct | 46,09 ± 6,75 | -1,673 |
| | | | (Bhandari et al., 2021) | F (n = 113) | Indian | Direct | 50,06 ± 4,85 | 11,848 |
| | | | (Borman et al., 1999) | F (n = 525) | Turkish | Direct | 54,48 ± 4,03 | 99,601 |
| | | | (Budai et al., 2003) | F (n = 26) | Hungarian | Direct | 51,50 ± 3,50 | 12,730 |
| | | | (Celebi et al., 2017) | F (n = 68) | Columbian | 3D Stereophotogrammetry | 48,66 ± 2,93 | 4,929 |
| | | | (Celebi et al., 2017) | F (n = 48) | Mexican-American | 3D Stereophotogrammetry | 51,37 ± 3,55 | 17,791 |
| | | | (Farkas et al., 2007) | F (n = 50) | African-American | Direct | 48,80 ± 3,70 | 3,622 |
| | | | (Farkas et al., 2007) | F (n = 200) | North American White | Direct | 50,60 ± 3,10 | 25,699 |
| | | | (Galantucci et al., 2016) | F (n = 66) | Italian | 3D Stereophotogrammetry | 50,29 ± 2,43 | 17,471 |
| | | | (Galantucci et al., 2016) | F (n = 66) | Italian | 3D Stereophotogrammetry | 50,29 ± 2,43 | 17,471 |
| | | | (He et al., 2009) | F (n = 63) | Chinese | Direct | 58,23 ± 3,73 | 71,227 |
| | | | (Heidari et al., 2009) | F (n = 200) | Iranian Sistani | Direct | 46,50 ± 1,80 | -1,737 |
| | | | (Heidari et al., 2009) | F (n = 200) | Iranian Baluch | Direct | 53,00 ± 1,30 | 64,923 |
| | | | (Houlton et al., 2020) | F (n = 23) | Black SA | CBCT | 48,50 ± 3,70 | 1,014 |
| | | | (Houlton et al., 2020) | F (n = 20) | White SA | CBCT | 51,99 ± 2,61 | 17,607 |
| | | | (Jayaratne et al., 2014) | F (n = 52) | Chinese | 3D Stereophotogrammetry | 50,46 ± 3,18 | 14,153 |
| | | | (Lee et al., 2013) | F (n = 58) | Korean | 3D white light scanner | 51,10 ± 3,00 | 20,485 |
| | | | (Liu et al., 2014) | F (n = 60) | African-American | 3D Stereophotogrammetry | 47,01 ± 3,28 | -1,099 |
| | | | (Liu et al., 2014) | F (n = 40) | Chinese | 3D Stereophotogrammetry | 51,78 ± 3,37 | 19,330 |
| | | | (Menéndez López-Mateos et al., 2019) | F (n = 50) | Spanish | 3D Stereophotogrammetry | 56,17 ± 2,83 | 58,560 |
| | | | (Olusanya et al., 2018) | F (n = 51) | Nigerian | Direct | 58,80 ± 6,67 | 40,797 |
| | | | (Ouni et al., 2022) | F (n = 134) | Tunisian | Direct | 57,80 ± 4,43 | 93,377 |
| | | | (Ozdemir et al., 2015) | F (n = 59) | Turkish | Direct | 50,90 ± 4,20 | 14,100 |
| | | | (Rahimi Jaberi et al., 2019) | F (n = 100) | Iranian | Direct | 32,00 ± 2,00 | 130,207 |
| | | | (Ridel et al., 2018) | F (n = 23) | Black SA | CBCT | 49,51 ± 3,30 | 4,424 |

Supplementary table 2: Comparative analysis with the literature comparisons

50

| | This study | | Other studies | | | | | Bayes Factor |
|---|---|---|---|---|---|---|---|---|
| Facial Parameter | Sex (sample size) | Mean ± SD | Author | Sex (sample size) | Population | Modality | Mean ± SD | log10 value* |
| Nasal Height (continued) | F (n = 54) | 46,32 ± 3,57 | (Ridel et al., 2018) | F (n = 28) | White SA | CBCT | 55,54 ± 5,06 | 23,002 |
| | | | (Sarna et al., 2023a) | F (n = 50) | Chinese | Direct | 59,74 ± 3,89 | 70,076 |
| | | | (Sarna et al., 2023a) | F (n = 45) | Kenyan | Direct | 65,58 ± 5,75 | 73,333 |
| | | | (Sarna et al., 2023b) | F (n = 64) | Kenyan Indians | Direct | 59,54 ± 6,56 | 53,003 |
| | | | (Virdi et al., 2019) | F (n = 36) | Kenyan | Direct | 47,60 ± 3,10 | -0,078 |
| | | | (Weiliang et al., 2021) | F (n = 430) | Chinese | Direct | 48,90 ± 4,20 | 9,259 |
| | M (n = 64) | 48,31 ± 3,56 | (Adekunle et al., 2022) | M (n = 254) | Nigerian | 3D Stereophotogrammetry | 50,34 ± 3,58 | 5,772 |
| | | | (Ahmed et al., 2016) | M (n = 120) | Sudanese | Direct | 56,95 ± 4,71 | 62,560 |
| | | | (Al-Sebaei, 2015) | M (n = 75) | Saudi Arabian | Direct | 54,12 ± 4,34 | 26,876 |
| | | | (Amini et al., 2014) | M (n = 50) | Iranian | Direct | 58,40 ± 3,70 | 56,349 |
| | | | (Antoun et al., 2014) | M (n = 15) | New Zealand European | 3D white light scanner | 56,40 ± 4,90 | 12,089 |
| | | | (Antoun et al., 2014) | M (n = 15) | Maori | 3D white light scanner | 57,10 ± 3,80 | 20,737 |
| | | | (Bayat et al., 2018) | M (n = 100) | Iranian | Direct | 47,35 ± 9,77 | -1,389 |
| | | | (Bhandari et al., 2021) | M (n = 387) | Indian | Direct | 52,40 ± 3,64 | 30,324 |
| | | | (Borman et al., 1999) | M (n = 525) | Turkish | Direct | 55,15 ± 4,57 | 81,026 |
| | | | (Budai et al., 2003) | M (n = 25) | Hungarian | Direct | 53,80 ± 4,30 | 11,048 |
| | | | (Celebi et al., 2017) | M (n = 44) | Mexican-American | 3D Stereophotogrammetry | 53,24 ± 3,67 | 17,039 |
| | | | (Celebi et al., 2017) | M (n = 63) | Columbian | 3D Stereophotogrammetry | 52,39 ± 2,55 | 19,989 |
| | | | (Farkas et al., 2007) | M (n = 50) | African-American | Direct | 51,80 ± 3,10 | 11,213 |
| | | | (Farkas et al., 2007) | M (n = 109) | North American White | Direct | 54,80 ± 3,30 | 48,029 |
| | | | (He et al., 2009) | M (n = 56) | Chinese | Direct | 60,33 ± 4,25 | 67,434 |
| | | | (Houlton et al., 2020) | M (n = 42) | Black SA | CBCT | 51,80 ± 3,05 | 10,284 |
| | | | (Houlton et al., 2020) | M (n = 19) | White SA | CBCT | 55,49 ± 3,26 | 21,501 |
| | | | (Jayaratne et al., 2014) | M (n = 51) | Chinese | 3D Stereophotogrammetry | 53,05 ± 3,88 | 16,355 |
| | | | (Lee et al., 2013) | M (n = 278) | Korean | 3D white light scanner | 55,00 ± 3,10 | 72,498 |
| | | | (Liu et al., 2014) | M (n = 57) | African-American | 3D Stereophotogrammetry | 50,30 ± 3,13 | 3,069 |
| | | | (Liu et al., 2014) | M (n = 32) | Chinese | 3D Stereophotogrammetry | 53,54 ± 3,10 | 18,663 |
| | | | (Menéndez López-Mateos et al., 2019) | M (n = 50) | Spanish | 3D Stereophotogrammetry | 56,94 ± 4,45 | 38,621 |
| | | | (Olusanya et al., 2018) | M (n = 50) | Nigerian | Direct | 57,40 ± 8,73 | 17,149 |
| | | | (Ouni et al., 2022) | M (n = 67) | Tunisian | Direct | 60,75 ± 5,46 | 64,074 |
| | | | (Ozdemir et al., 2015) | M (n = 56) | Turkish | Direct | 54,38 ± 4,60 | 22,567 |

| Supplementary table 2: Comparative analysis with the literature comparisons | | | | | | | | |
|---|---|---|---|---|---|---|---|---|
| | **This study** | | **Other studies** | | | | | **Bayes Factor** |
| **Facial Parameter** | **Sex (sample size)** | **Mean ± SD** | **Author** | **Sex (sample size)** | **Population** | **Modality** | **Mean ± SD** | **log10 value*** |
| Nasal Height (continued) | M (n = 64) | 48,31 ± 3,56 | (Rahimi Jaberi et al., 2019) | M (n = 100) | Iranian | Direct | 32,00 ± 3,00 | 149,455 |
| | | | (Ridel et al., 2018) | M (n = 37) | Black SA | CBCT | 53,19 ± 5,06 | 9,365 |
| | | | (Ridel et al., 2018) | M (n = 32) | White SA | CBCT | 52,40 ± 3,59 | 9,683 |
| | | | (Sarna et al., 2023a) | M (n = 45) | Kenyan | Direct | 65,58 ± 5,75 | 69,977 |
| | | | (Sarna et al., 2023a) | M (n = 40) | Chinese | Direct | 63,25 ± 3,22 | 85,233 |
| | | | (Sarna et al., 2023b) | M (n = 66) | Kenyan Indians | Direct | 60,82 ± 7,13 | 48,676 |
| | | | (Virdi et al., 2019) | M (n = 36) | Kenyan | Direct | 51,00 ± 2,30 | 7,164 |
| Nasal Protrusion | F (n = 54) | 16,44 ± 1,81 | (Amini et al., 2014) | F (n = 50) | Iranian | Direct | 19,30 ± 2,20 | 18,120 |
| | | | (Bhandari et al., 2021) | F (n = 113) | Indian | Direct | 18,10 ± 1,91 | 11,102 |
| | | | (Celebi et al., 2017) | F (n = 48) | Mexican-American | 3D Stereophotogrammetry | 16,14 ± 1,96 | -1,279 |
| | | | (Celebi et al., 2017) | F (n = 68) | Columbian | 3D Stereophotogrammetry | 15,14 ± 1,92 | 4,761 |
| | | | (Farkas et al., 2007) | F (n = 50) | African-American | Direct | 16,10 ± 2,10 | -1,227 |
| | | | (Farkas et al., 2007) | F (n = 200) | North American White | Direct | 19,70 ± 1,60 | 53,594 |
| | | | (Galantucci et al., 2016) | F (n = 66) | Italian | 3D Stereophotogrammetry | 18,62 ± 1,84 | 15,395 |
| | | | (He et al., 2009) | F (n = 63) | Chinese | Direct | 16,54 ± 1,75 | -1,583 |
| | | | (Jayaratne et al., 2014) | F (n = 52) | Chinese | 3D Stereophotogrammetry | 17,74 ± 1,82 | 4,256 |
| | | | (Lee et al., 2013) | F (n = 58) | Korean | 3D white light scanner | 12,40 ± 1,50 | 46,606 |
| | | | (Ozdemir et al., 2015) | F (n = 59) | Turkish | Direct | 21,15 ± 2,56 | 39,379 |
| | | | (Rodríguez et al., 2022) | F (n = 229) | Chilean | Direct | 17,20 ± 2,40 | 1,296 |
| | | | (Weiliang et al., 2021) | F (n = 430) | Chinese | Direct | 21,10 ± 2,20 | 113,044 |
| | M (n = 64) | 17,11 ± 1,77 | (Amini et al., 2014) | M (n = 50) | Iranian | Direct | 20,00 ± 2,60 | 16,259 |
| | | | (Bhandari et al., 2021) | M (n = 387) | Indian | Direct | 19,02 ± 1,86 | 26,496 |
| | | | (Celebi et al., 2017) | M (n = 44) | Mexican-American | 3D Stereophotogrammetry | 17,50 ± 2,19 | -1,146 |
| | | | (Celebi et al., 2017) | M (n = 63) | Columbian | 3D Stereophotogrammetry | 17,86 ± 1,55 | 1,225 |
| | | | (Farkas et al., 2007) | M (n = 50) | African-American | Direct | 17,50 ± 2,10 | -1,111 |
| | | | (Farkas et al., 2007) | M (n = 109) | North American White | Direct | 19,50 ± 1,90 | 26,172 |
| | | | (He et al., 2009) | M (n = 56) | Chinese | Direct | 18,24 ± 2,33 | 2,231 |
| | | | (Jayaratne et al., 2014) | M (n = 51) | Chinese | 3D Stereophotogrammetry | 18,68 ± 2,27 | 5,452 |
| | | | (Lee et al., 2013) | M (n = 278) | Korean | 3D white light scanner | 14,40 ± 1,60 | 50,243 |
| | | | (Ozdemir et al., 2015) | M (n = 56) | Turkish | Direct | 22,81 ± 3,02 | 45,578 |
| | | | (Rodríguez et al., 2022) | M (n = 245) | Chilean | Direct | 19,10 ± 2,50 | 21,653 |

| Supplementary table 2: Comparative analysis with the literature comparisons | | | | | | | | |
|---|---|---|---|---|---|---|---|---|
| | **This study** | | **Other studies** | | | | | **Bayes Factor** |
| **Facial Parameter** | **Sex (sample size)** | **Mean ± SD** | **Author** | **Sex (sample size)** | **Population** | **Modality** | **Mean ± SD** | **log10 value*** |
| Alar Length Lt | F (n = 54) | 30,32 ± 2,51 | (Jayaratne et al., 2014) | F (n = 52) | Chinese | 3D Stereophotogrammetry | 26,24 ± 2,2 | 26,343 |
| | | | (He et al., 2009) | F (n = 63) | Chinese | Direct | 28,9 ± 2,28 | 2,820 |
| | | | (Ozdemir et al., 2015) | F (n = 59) | Turkish | Direct | 33,61 ± 2,98 | 14,560 |
| | M (n = 64) | 32,73 ± 2,57 | (Jayaratne et al., 2014) | M (n = 51) | Chinese | 3D Stereophotogrammetry | 29,34 ± 2,39 | 18,983 |
| | | | (He et al., 2009) | M (n = 56) | Chinese | Direct | 32,37 ± 1,48 | -1,225 |
| | | | (Ozdemir et al., 2015) | M (n = 56) | Turkish | Direct | 30,09 ± 2,92 | 9,797 |
| Alar Length Rt | F (n = 54) | 31,11 ± 2,75 | (Jayaratne et al., 2014) | F (n = 52) | Chinese | 3D Stereophotogrammetry | 27,19 ± 2,15 | 22,858 |
| | | | (He et al., 2009) | F (n = 63) | Chinese | Direct | 28,81 ± 2,17 | 8,738 |
| | | | (Ozdemir et al., 2015) | F (n = 59) | Turkish | Direct | 33,43 ± 2,89 | 6,528 |
| | M (n = 64) | 33,7 ± 2,73 | (Jayaratne et al., 2014) | M (n = 51) | Chinese | 3D Stereophotogrammetry | 29,71 ± 2,21 | 25,663 |
| | | | (He et al., 2009) | M (n = 56) | Chinese | Direct | 32,32 ± 1,48 | 3,720 |
| | | | (Ozdemir et al., 2015) | M (n = 56) | Turkish | Direct | 30,22 ± 2,82 | 16,935 |
| Columella Width | F (n = 54) | 9,4 ± 1,56 | (He et al., 2009) | F (n = 63) | Chinese | Direct | 8,07 ± 1 | 10,431 |
| | M (n = 64) | 9,2 ± 1,35 | (He et al., 2009) | M (n = 56) | Chinese | Direct | 8,9 ± 1,28 | -0,934 |
| Columella Length Lt | F (n = 54) | 8,17 ± 1,49 | (Jayaratne et al., 2014) | F (n = 52) | Chinese | 3D Stereophotogrammetry | 10,92 ± 1,31 | 32,241 |
| | M (n = 64) | 8,06 ± 1,49 | (Jayaratne et al., 2014) | M (n = 51) | Chinese | 3D Stereophotogrammetry | 11,71 ± 1,45 | 49,302 |
| Columella Length Rt | F (n = 54) | 8,3 ± 1,51 | (Jayaratne et al., 2014) | F (n = 52) | Chinese | 3D Stereophotogrammetry | 11,81 ± 1,23 | 47,246 |
| | M (n = 64) | 8,09 ± 1,48 | (Jayaratne et al., 2014) | M (n = 51) | Chinese | 3D Stereophotogrammetry | 12,92 ± 1,43 | 71,085 |
| Eye Fissure Length Lt | F (n = 25) | 26,58 ± 2,57 | (Amini et al., 2014) | F (n = 50) | Iranian | Direct | 31,00 ± 1,70 | 19,030 |
| | | | (Bayat et al., 2018) | F (n = 100) | Iranian | Direct | 28,93 ± 4,28 | 3,795 |
| | | | (Borman et al., 1999) | F (n = 525) | Turkish | Direct | 31,70 ± 1,34 | 41,482 |
| | | | (Celebi et al., 2017) | F (n = 68) | Columbian | 3D Stereophotogrammetry | 29,56 ± 2,12 | 9,263 |
| | | | (Celebi et al., 2017) | F (n = 48) | Mexican-American | 3D Stereophotogrammetry | 29,70 ± 1,79 | 9,742 |
| | | | (Farkas et al., 2007) | F (n = 200) | North American White | Direct | 30,70 ± 1,20 | 24,404 |
| | | | (Farkas et al., 2007) | F (n = 50) | African-American | Direct | 32,20 ± 2,00 | 26,387 |
| | | | (Galantucci et al., 2016) | F (n = 66) | Italian | 3D Stereophotogrammetry | 27,54 ± 1,31 | -0,063 |
| | | | (Ogawa et al., 2015) | F (n = 261) | Japanese | 3D Stereophotogrammetry | 27,40 ± 1,60 | -0,439 |
| | M (n = 33) | 27,59 ± 3,28 | (Amini et al., 2014) | M (n = 50) | Iranian | Direct | 31,60 ± 1,90 | 13,639 |
| | | | (Bayat et al., 2018) | M (n = 100) | Iranian | Direct | 28,93 ± 4,73 | -0,111 |
| | | | (Borman et al., 1999) | M (n = 525) | Turkish | Direct | 32,06 ± 1,51 | 25,603 |
| | | | (Celebi et al., 2017) | M (n = 44) | Mexican-American | 3D Stereophotogrammetry | 30,89 ± 2,17 | 8,400 |

| Supplementary table 2: Comparative analysis with the literature comparisons | | | | | | | | |
|---|---|---|---|---|---|---|---|---|
| | **This study** | | **Other studies** | | | | | **Bayes Factor** |
| **Facial Parameter** | **Sex (sample size)** | **Mean ± SD** | **Author** | **Sex (sample size)** | **Population** | **Modality** | **Mean ± SD** | **log10 value*** |
| Eye Fissure Length Lt (continued) | M (n = 33) | 27,59 ± 3,28 | (Celebi et al., 2017) | M (n = 63) | Columbian | 3D Stereophotogrammetry | 31,54 ± 1,79 | 14,392 |
| | | | (Farkas et al., 2007) | M (n = 109) | North American White | Direct | 31,30 ± 1,20 | 15,053 |
| | | | (Farkas et al., 2007) | M (n = 50) | African-American | Direct | 32,90 ± 1,60 | 23,329 |
| | | | (Ogawa et al., 2015) | M (n = 865) | Japanese | 3D Stereophotogrammetry | 28,10 ± 1,89 | -1,308 |
| | | | (Olusanya et al., 2018) | M (n = 50) | Nigerian | Direct | 36,30 ± 3,34 | 36,762 |
| Eye Fissure Length Rt | F (n = 25) | 26,97 ± 2,86 | (Adekunle et al., 2022) | F (n = 198) | Nigerian | 3D Stereophotogrammetry | 28,44 ± 2,51 | 1,132 |
| | | | (Al-Sebaei, 2015) | F (n = 93) | Saudi Arabian | Direct | 32,41 ± 3,44 | 22,707 |
| | | | (Bayat et al., 2018) | F (n = 100) | Iranian | Direct | 29,54 ± 3,90 | 4,390 |
| | | | (Bhandari et al., 2021) | F (n = 113) | Indian | Direct | 31,68 ± 2,06 | 22,034 |
| | | | (Farkas et al., 2007) | F (n = 200) | North American White | Direct | 30,70 ± 1,20 | 16,217 |
| | | | (Farkas et al., 2007) | F (n = 50) | African-American | Direct | 32,40 ± 2,40 | 20,564 |
| | | | (Galantucci et al., 2016) | F (n = 66) | Italian | 3D Stereophotogrammetry | 27,77 ± 1,46 | -0,656 |
| | | | (Guo et al., 2020) | F (n = 48) | European (German) | 3D Stereophotogrammetry | 30,11 ± 1,17 | 9,176 |
| | | | (Ogawa et al., 2015) | F (n = 261) | Japanese | 3D Stereophotogrammetry | 27,50 ± 1,68 | -1,152 |
| | | | (Oladipo et al., 2010) | F (n = 500) | Nigerian (Ijaw) | Direct | 36,00 ± 1,69 | 96,120 |
| | | | (Olusanya et al., 2018) | F (n = 51) | Nigerian | Direct | 33,50 ± 2,05 | 29,088 |
| | | | (Oztürk et al., 2006) | F (n = 177) | Turkish | Direct | 30,00 ± 2,50 | 9,413 |
| | | | (Sarna et al., 2023a) | F (n = 50) | Chinese | Direct | 27,42 ± 1,62 | -1,155 |
| | | | (Sarna et al., 2023a) | F (n = 45) | Kenyan | Direct | 34,49 ± 5,35 | 18,137 |
| | | | (Sarna et al., 2023b) | F (n = 64) | Kenyan Indians | Direct | 36,84 ± 6,02 | 31,879 |
| | | | (Virdi et al., 2019) | F (n = 36) | Kenyan | Direct | 33,70 ± 1,50 | 28,651 |
| | M (n = 33) | 28,33 ± 2,77 | (Adekunle et al., 2022) | M (n = 254) | Nigerian | 3D Stereophotogrammetry | 28,61 ± 5,29 | -1,523 |
| | | | (Al-Sebaei, 2015) | M (n = 75) | Saudi Arabian | Direct | 32,85 ± 2,73 | 21,239 |
| | | | (Bayat et al., 2018) | M (n = 100) | Iranian | Direct | 29,55 ± 4,69 | -0,101 |
| | | | (Bhandari et al., 2021) | M (n = 387) | Indian | Direct | 32,68 ± 2,21 | 32,139 |
| | | | (Farkas et al., 2007) | M (n = 109) | North American White | Direct | 31,30 ± 1,20 | 13,296 |
| | | | (Farkas et al., 2007) | M (n = 50) | African-American | Direct | 32,90 ± 1,70 | 22,617 |
| | | | (Guo et al., 2020) | M (n = 30) | European (German) | 3D Stereophotogrammetry | 32,14 ± 2,51 | 10,504 |
| | | | (Ogawa et al., 2015) | M (n = 865) | Japanese | 3D Stereophotogrammetry | 28,30 ± 1,95 | -1,662 |
| | | | (Oladipo et al., 2010) | M (n = 500) | Nigerian (Ijaw) | Direct | 38,10 ± 2,33 | 142,266 |
| | | | (Olusanya et al., 2018) | M (n = 50) | Nigerian | Direct | 36,00 ± 3,41 | 34,604 |

| Facial Parameter | This study Sex (sample size) | Mean ± SD | Author | Sex (sample size) | Population | Modality | Mean ± SD | Bayes Factor log10 value* |
|---|---|---|---|---|---|---|---|---|
| Eye Fissure Length Rt (continued) | M (n = 33) | 28,33 ± 2,77 | (Oztürk et al., 2006) | M (n = 176) | Turkish | Direct | 30,00 ± 2,90 | 2,822 |
| | | | (Sarna et al., 2023a) | M (n = 40) | Chinese | Direct | 28,91 ± 1,93 | -0,973 |
| | | | (Sarna et al., 2023a) | M (n = 45) | Kenyan | Direct | 34,93 ± 3,74 | 24,172 |
| | | | (Sarna et al., 2023b) | M (n = 66) | Kenyan Indians | Direct | 36,64 ± 4,75 | 35,631 |
| | | | (Virdi et al., 2019) | M (n = 36) | Kenyan | Direct | 34,00 ± 3,40 | 17,922 |
| Outer-canthal Width | F (n = 25) | 92,27 ± 3,94 | (Amini et al., 2014) | F (n = 50) | Iranian | Direct | 92,30 ± 3,60 | -1,382 |
| | | | (Antoun et al., 2014) | F (n = 15) | New Zealand European | 3D white light scanner | 91,10 ± 4,10 | -0,842 |
| | | | (Antoun et al., 2014) | F (n = 15) | Maori | 3D white light scanner | 94,70 ± 5,90 | -0,369 |
| | | | (Bayat et al., 2018) | F (n = 100) | Iranian | Direct | 80,19 ± 6,47 | 43,144 |
| | | | (Celebi et al., 2017) | F (n = 48) | Mexican-American | 3D Stereophotogrammetry | 92,54 ± 3,84 | -1,343 |
| | | | (Celebi et al., 2017) | F (n = 68) | Columbian | 3D Stereophotogrammetry | 90,43 ± 4,42 | 0,168 |
| | | | (Farkas et al., 2007) | F (n = 50) | African-American | Direct | 92,90 ± 5,30 | -1,239 |
| | | | (Farkas et al., 2007) | F (n = 200) | North American White | Direct | 87,80 ± 3,20 | 11,332 |
| | | | (Galantucci et al., 2016) | F (n = 66) | Italian | 3D Stereophotogrammetry | 84,01 ± 2,98 | 27,835 |
| | | | (Guo et al., 2020) | F (n = 48) | European (German) | 3D Stereophotogrammetry | 88,32 ± 2,99 | 6,247 |
| | | | (Liu et al., 2013) | F (n = 40) | Chinese | 3D Stereophotogrammetry | 93,02 ± 4,15 | -1,123 |
| | | | (Liu et al., 2013) | F (n = 82) | Greek | 3D Stereophotogrammetry | 94,29 ± 3,70 | 0,775 |
| | | | (Liu et al., 2014) | F (n = 60) | African-American | 3D Stereophotogrammetry | 95,05 ± 4,27 | 2,089 |
| | | | (Menéndez López-Mateos et al., 2019) | F (n = 50) | Spanish | 3D Stereophotogrammetry | 86,58 ± 3,20 | 12,936 |
| | | | (Ogawa et al., 2015) | F (n = 261) | Japanese | 3D Stereophotogrammetry | 90,90 ± 4,06 | -0,312 |
| | | | (Oladipo et al., 2010) | F (n = 500) | Nigerian (Ijaw) | Direct | 104,50 ± 3,22 | 92,094 |
| | | | (Oztürk et al., 2006) | F (n = 177) | Turkish | Direct | 90,10 ± 6,20 | 0,957 |
| | | | (Virdi et al., 2019) | F (n = 36) | Kenyan | Direct | 94,40 ± 4,90 | 0,126 |
| | M (n = 33) | 94,1 ± 5,56 | (Amini et al., 2014) | M (n = 50) | Iranian | Direct | 94,70 ± 4,20 | -1,336 |
| | | | (Antoun et al., 2014) | M (n = 15) | New Zealand European | 3D white light scanner | 93,80 ± 4,90 | -1,173 |
| | | | (Antoun et al., 2014) | M (n = 15) | Maori | 3D white light scanner | 101,00 ± 5,50 | 4,700 |
| | | | (Bayat et al., 2018) | M (n = 100) | Iranian | Direct | 92,59 ± 4,80 | -0,689 |
| | | | (Celebi et al., 2017) | M (n = 63) | Columbian | 3D Stereophotogrammetry | 94,58 ± 4,31 | -1,412 |
| | | | (Celebi et al., 2017) | M (n = 44) | Mexican-American | 3D Stereophotogrammetry | 96,32 ± 4,00 | 0,183 |
| | | | (Farkas et al., 2007) | M (n = 50) | African-American | Direct | 96,80 ± 4,50 | 0,863 |
| | | | (Farkas et al., 2007) | M (n = 109) | North American White | Direct | 91,20 ± 3,00 | 2,058 |

Supplementary table 2: Comparative analysis with the literature comparisons

| Supplementary table 2: Comparative analysis with the literature comparisons | | | | | | | | |
|---|---|---|---|---|---|---|---|---|
| | **This study** | | **Other studies** | | | | | **Bayes Factor** |
| **Facial Parameter** | **Sex (sample size)** | **Mean ± SD** | **Author** | **Sex (sample size)** | **Population** | **Modality** | **Mean ± SD** | **log10 value*** |
| Outer-canthal Width (continued) | M (n = 33) | 94,1 ± 5,56 | (Guo et al., 2020) | M (n = 30) | European (German) | 3D Stereophotogrammetry | 94,62 ± 4,84 | -1,291 |
| | | | (Liu et al., 2014) | M (n = 32) | Chinese | 3D Stereophotogrammetry | 95,90 ± 4,23 | -0,458 |
| | | | (Liu et al., 2014) | M (n = 57) | African-American | 3D Stereophotogrammetry | 98,04 ± 3,63 | 4,086 |
| | | | (Menéndez López-Mateos et al., 2019) | M (n = 50) | Spanish | 3D Stereophotogrammetry | 90,40 ± 4,68 | 2,725 |
| | | | (Ogawa et al., 2015) | M (n = 865) | Japanese | 3D Stereophotogrammetry | 94,00 ± 4,68 | -1,659 |
| | | | (Oladipo et al., 2010) | M (n = 500) | Nigerian (Ijaw) | Direct | 107,60 ± 3,78 | 76,756 |
| | | | (Oztürk et al., 2006) | M (n = 176) | Turkish | Direct | 91,30 ± 6,90 | 1,293 |
| | | | (Virdi et al., 2019) | M (n = 36) | Kenyan | Direct | 98,20 ± 3,50 | 3,928 |
| Mouth Width | F (n = 54) | 52,63 ± 4,7 | (Adekunle et al., 2022) | F (n = 198) | Nigerian | 3D Stereophotogrammetry | 51,26 ± 4,35 | -0,079 |
| | | | (Amini et al., 2014) | F (n = 50) | Iranian | Direct | 47,00 ± 3,10 | 18,366 |
| | | | (Bayat et al., 2018) | F (n = 100) | Iranian | Direct | 49,12 ± 16,67 | 0,047 |
| | | | (Bhandari et al., 2021) | F (n = 113) | Indian | Direct | 48,37 ± 3,49 | 13,293 |
| | | | (Borman et al., 1999) | F (n = 525) | Turkish | Direct | 50,67 ± 5,24 | 2,021 |
| | | | (Celebi et al., 2017) | F (n = 48) | Mexican-American | 3D Stereophotogrammetry | 49,32 ± 3,83 | 4,952 |
| | | | (Celebi et al., 2017) | F (n = 68) | Columbian | 3D Stereophotogrammetry | 47,76 ± 3,48 | 14,705 |
| | | | (Farkas et al., 2007) | F (n = 50) | African-American | Direct | 53,60 ± 4,00 | -0,999 |
| | | | (Farkas et al., 2007) | F (n = 200) | North American White | Direct | 50,20 ± 3,50 | 3,943 |
| | | | (Galantucci et al., 2016) | F (n = 66) | Italian | 3D Stereophotogrammetry | 45,70 ± 2,77 | 30,618 |
| | | | (Houlton et al., 2019) | F (n = 52) | Black SA | CBCT | 53,01 ± 3,99 | -1,492 |
| | | | (Houlton et al., 2019) | F (n = 20) | White SA | CBCT | 50,46 ± 2,67 | 1,201 |
| | | | (Houlton et al., 2022) | F (n = 41) | Black SA | CBCT | 53,70 ± 4,60 | -0,981 |
| | | | (Lee et al., 2013) | F (n = 58) | Korean | 3D white light scanner | 45,40 ± 3,20 | 29,460 |
| | | | (Liu et al., 2013) | F (n = 82) | Greek | 3D Stereophotogrammetry | 49,67 ± 3,19 | 5,517 |
| | | | (Liu et al., 2013) | F (n = 40) | Chinese | 3D Stereophotogrammetry | 46,64 ± 3,05 | 18,907 |
| | | | (Liu et al., 2014) | F (n = 60) | African-American | 3D Stereophotogrammetry | 51,75 ± 3,80 | -1,079 |
| | | | (Menéndez López-Mateos et al., 2019) | F (n = 50) | Spanish | 3D Stereophotogrammetry | 47,34 ± 3,65 | 14,655 |
| | | | (Ogawa et al., 2015) | F (n = 261) | Japanese | 3D Stereophotogrammetry | 47,90 ± 3,51 | 19,934 |
| | | | (Olusanya et al., 2018) | F (n = 51) | Nigerian | Direct | 54,70 ± 3,75 | 1,169 |
| | | | (Ouni et al., 2022) | F (n = 134) | Tunisian | Direct | 47,25 ± 3,15 | 23,017 |
| | | | (Rodríguez et al., 2022) | F (n = 229) | Chilean | Direct | 52,80 ± 3,80 | -1,781 |
| | | | (Sarna et al., 2023a) | F (n = 45) | Kenyan | Direct | 66,24 ± 10,89 | 20,632 |

| | | | | | | | | |
|---|---|---|---|---|---|---|---|---|
| **Supplementary table 2: Comparative analysis with the literature comparisons** |

| Facial Parameter | This study | | Other studies | | | | | Bayes Factor |
|---|---|---|---|---|---|---|---|---|
| | Sex (sample size) | Mean ± SD | Author | Sex (sample size) | Population | Modality | Mean ± SD | log10 value* |
| Mouth Width (continued) | F (n = 54) | 52,63 ± 4,7 | (Sarna et al., 2023a) | F (n = 50) | Chinese | Direct | 44,97 ± 3,46 | 29,151 |
| | | | (Sarna et al., 2023b) | F (n = 64) | Kenyan Indians | Direct | 54,22 ± 6,53 | -0,572 |
| | | | (Virdi et al., 2019) | F (n = 36) | Kenyan | Direct | 52,00 ± 4,00 | -1,289 |
| | M (n = 64) | 55,44 ± 3,63 | (Adekunle et al., 2022) | M (n = 254) | Nigerian | 3D Stereophotogrammetry | 53,37 ± 4,88 | 4,733 |
| | | | (Amini et al., 2014) | M (n = 50) | Iranian | Direct | 50,50 ± 3,50 | 19,184 |
| | | | (Bayat et al., 2018) | M (n = 100) | Iranian | Direct | 44,31 ± 11,33 | 30,421 |
| | | | (Bhandari et al., 2021) | M (n = 387) | Indian | Direct | 51,17 ± 3,78 | 31,614 |
| | | | (Borman et al., 1999) | M (n = 525) | Turkish | Direct | 51,34 ± 4,80 | 28,818 |
| | | | (Celebi et al., 2017) | M (n = 44) | Mexican-American | 3D Stereophotogrammetry | 51,12 ± 4,21 | 10,916 |
| | | | (Celebi et al., 2017) | M (n = 63) | Columbian | 3D Stereophotogrammetry | 50,82 ± 3,69 | 18,399 |
| | | | (Farkas et al., 2007) | M (n = 50) | African-American | Direct | 54,60 ± 4,20 | -1,042 |
| | | | (Farkas et al., 2007) | M (n = 109) | North American White | Direct | 54,50 ± 3,00 | -0,364 |
| | | | (Houlton et al., 2019) | M (n = 68) | Black SA | CBCT | 55,37 ± 4,34 | -1,676 |
| | | | (Houlton et al., 2019) | M (n = 19) | White SA | CBCT | 58,80 ± 5,41 | 1,337 |
| | | | (Houlton et al., 2022) | M (n = 67) | Black SA | CBCT | 56,20 ± 4,80 | -1,200 |
| | | | (Lee et al., 2013) | M (n = 278) | Korean | 3D white light scanner | 49,90 ± 3,40 | 49,432 |
| | | | (Liu et al., 2014) | M (n = 57) | African-American | 3D Stereophotogrammetry | 52,06 ± 3,33 | 10,288 |
| | | | (Liu et al., 2014) | M (n = 32) | Chinese | 3D Stereophotogrammetry | 49,15 ± 3,62 | 21,435 |
| | | | (Menéndez López-Mateos et al., 2019) | M (n = 50) | Spanish | 3D Stereophotogrammetry | 51,11 ± 4,77 | 10,144 |
| | | | (Ogawa et al., 2015) | M (n = 865) | Japanese | 3D Stereophotogrammetry | 50,70 ± 3,71 | 44,731 |
| | | | (Olusanya et al., 2018) | M (n = 50) | Nigerian | Direct | 59,10 ± 4,57 | 7,477 |
| | | | (Ouni et al., 2022) | M (n = 67) | Tunisian | Direct | 48,18 ± 3,25 | 45,072 |
| | | | (Rodríguez et al., 2022) | M (n = 245) | Chilean | Direct | 55,80 ± 4,10 | -1,658 |
| | | | (Sarna et al., 2023a) | M (n = 45) | Kenyan | Direct | 68,27 ± 12,18 | 16,668 |
| | | | (Sarna et al., 2023a) | M (n = 40) | Chinese | Direct | 47,73 ± 3,24 | 37,755 |
| | | | (Sarna et al., 2023b) | M (n = 66) | Kenyan Indians | Direct | 54,38 ± 7,90 | -1,231 |
| | | | (Virdi et al., 2019) | M (n = 36) | Kenyan | Direct | 55,90 ± 3,30 | -1,337 |
| | | | (Yokota, 2005) | M (n = 26) | Mixed race American | Direct | 56,30 ± 3,10 | -0,874 |
| | | | (Yokota, 2005) | M (n = 820) | North American White | Direct | 54,40 ± 3,70 | 0,340 |
| | | | (Yokota, 2005) | M (n = 1189) | African-American | Direct | 59,00 ± 3,80 | 25,447 |

| Supplementary table 2: Comparative analysis with the literature comparisons | | | | | | | | |
|---|---|---|---|---|---|---|---|---|
| | **This study** | | **Other studies** | | | | | **Bayes Factor** |
| **Facial Parameter** | **Sex (sample size)** | **Mean ± SD** | **Author** | **Sex (sample size)** | **Population** | **Modality** | **Mean ± SD** | **log10 value*** |
| Philtrum Width | F (n = 54) | 13,67 ± 2,23 | (Houlton et al., 2019) | F (n = 20) | White SA | CBCT | 13,29 ± 1,54 | -1,040 |
| | | | (Houlton et al., 2019) | F (n = 52) | Black SA | CBCT | 14,99 ± 1,65 | 3,625 |
| | | | (Houlton et al., 2022) | F (n = 41) | Black SA | CBCT | 14,60 ± 1,90 | 0,566 |
| | | | (Liu et al., 2013) | F (n = 40) | Chinese | 3D Stereophotogrammetry | 12,30 ± 1,45 | 3,972 |
| | | | (Liu et al., 2013) | F (n = 82) | Greek | 3D Stereophotogrammetry | 11,22 ± 1,94 | 16,089 |
| | | | (Liu et al., 2014) | F (n = 60) | African-American | 3D Stereophotogrammetry | 12,76 ± 1,38 | 1,343 |
| | | | (Menéndez López-Mateos et al., 2019) | F (n = 50) | Spanish | 3D Stereophotogrammetry | 9,29 ± 1,95 | 34,903 |
| | M (n = 64) | 15,15 ± 1,94 | (Houlton et al., 2019) | M (n = 19) | White SA | CBCT | 14,83 ± 1,45 | -1,076 |
| | | | (Houlton et al., 2019) | M (n = 68) | Black SA | CBCT | 16,20 ± 1,71 | 3,124 |
| | | | (Houlton et al., 2022) | M (n = 67) | Black SA | CBCT | 16,00 ± 2,00 | 1,059 |
| | | | (Liu et al., 2014) | M (n = 57) | African-American | 3D Stereophotogrammetry | 14,74 ± 1,96 | -1,039 |
| | | | (Liu et al., 2014) | M (n = 32) | Chinese | 3D Stereophotogrammetry | 13,77 ± 1,61 | 4,241 |
| | | | (Menéndez López-Mateos et al., 2019) | M (n = 50) | Spanish | 3D Stereophotogrammetry | 10,62 ± 2,43 | 36,417 |
| Upper Lip Height | F (n = 54) | 25,09 ± 2,71 | (Amini et al., 2014) | F (n = 50) | Iranian | Direct | 20,10 ± 2,20 | 33,232 |
| | | | (Budai et al., 2003) | F (n = 26) | Hungarian | Direct | 25,40 ± 2,70 | -1,305 |
| | | | (Celebi et al., 2017) | F (n = 48) | Mexican-American | 3D Stereophotogrammetry | 21,86 ± 2,12 | 15,938 |
| | | | (Celebi et al., 2017) | F (n = 68) | Columbian | 3D Stereophotogrammetry | 21,24 ± 2,22 | 24,856 |
| | | | (Farkas et al., 2007) | F (n = 50) | African-American | Direct | 24,50 ± 3,00 | -1,083 |
| | | | (Farkas et al., 2007) | F (n = 200) | North American White | Direct | 21,10 ± 2,00 | 39,520 |
| | | | (Liu et al., 2014) | F (n = 60) | African-American | 3D Stereophotogrammetry | 24,34 ± 2,20 | -0,453 |
| | | | (Liu et al., 2014) | F (n = 40) | Chinese | 3D Stereophotogrammetry | 21,43 ± 1,83 | 20,394 |
| | | | (Ogawa et al., 2015) | F (n = 261) | Japanese | 3D Stereophotogrammetry | 24,30 ± 1,97 | 0,096 |
| | | | (Ouni et al., 2022) | F (n = 134) | Tunisian | Direct | 22,59 ± 18,21 | -0,652 |
| | | | (Virdi et al., 2019) | F (n = 36) | Kenyan | Direct | 24,00 ± 2,50 | 0,171 |
| | M (n = 64) | 25,48 ± 3,43 | (Amini et al., 2014) | M (n = 50) | Iranian | Direct | 22,10 ± 2,60 | 12,901 |
| | | | (Budai et al., 2003) | M (n = 25) | Hungarian | Direct | 26,50 ± 3,20 | -0,664 |
| | | | (Celebi et al., 2017) | M (n = 63) | Columbian | 3D Stereophotogrammetry | 24,24 ± 2,40 | 0,840 |
| | | | (Celebi et al., 2017) | M (n = 44) | Mexican-American | 3D Stereophotogrammetry | 23,97 ± 2,46 | 1,533 |
| | | | (Farkas et al., 2007) | M (n = 50) | African-American | Direct | 26,10 ± 2,50 | -1,050 |
| | | | (Farkas et al., 2007) | M (n = 109) | North American White | Direct | 22,30 ± 2,10 | 17,252 |
| | | | (Liu et al., 2014) | M (n = 57) | African-American | 3D Stereophotogrammetry | 25,44 ± 7,47 | -1,640 |

| Supplementary table 2: Comparative analysis with the literature comparisons | | | | | | | | |
|---|---|---|---|---|---|---|---|---|
| | This study | | Other studies | | | | | Bayes Factor |
| Facial Parameter | Sex (sample size) | Mean ± SD | Author | Sex (sample size) | Population | Modality | Mean ± SD | log10 value* |
| Upper Lip Height (continued) | M (n = 64) | 25,48 ± 3,43 | (Liu et al., 2014) | M (n = 32) | Chinese | 3D Stereophotogrammetry | 23,24 ± 2,05 | 5,158 |
| | | | (Ogawa et al., 2015) | M (n = 865) | Japanese | 3D Stereophotogrammetry | 25,80 ± 2,51 | -1,701 |
| | | | (Ouni et al., 2022) | M (n = 67) | Tunisian | Direct | 21,12 ± 2,14 | 26,594 |
| | | | (Virdi et al., 2019) | M (n = 36) | Kenyan | Direct | 25,50 ± 1,30 | -1,520 |
| Upper Vermillion Height | F (n = 54) | 11,51 ± 2,65 | (Amini et al., 2014) | F (n = 50) | Iranian | Direct | 7,60 ± 1,50 | 28,335 |
| | | | (Celebi et al., 2017) | F (n = 68) | Columbian | 3D Stereophotogrammetry | 9,57 ± 1,42 | 8,361 |
| | | | (Celebi et al., 2017) | F (n = 48) | Mexican-American | 3D Stereophotogrammetry | 8,34 ± 1,47 | 19,742 |
| | | | (Houlton et al., 2020) | F (n = 52) | Black SA | CBCT | 12,78 ± 2,26 | 1,516 |
| | | | (Houlton et al., 2020) | F (n = 20) | White SA | CBCT | 8,51 ± 1,23 | 14,224 |
| | | | (Houlton et al., 2022) | F (n = 41) | Black SA | CBCT | 12,50 ± 2,20 | 0,200 |
| | | | (Ogawa et al., 2015) | F (n = 261) | Japanese | 3D Stereophotogrammetry | 9,00 ± 1,36 | 18,631 |
| | | | (Virdi et al., 2019) | F (n = 36) | Kenyan | Direct | 13,40 ± 0,90 | 7,983 |
| | M (n = 64) | 12,37 ± 2,7 | (Amini et al., 2014) | M (n = 50) | Iranian | Direct | 7,00 ± 1,70 | 47,672 |
| | | | (Celebi et al., 2017) | M (n = 63) | Columbian | 3D Stereophotogrammetry | 9,86 ± 1,96 | 13,197 |
| | | | (Celebi et al., 2017) | M (n = 44) | Mexican-American | 3D Stereophotogrammetry | 8,89 ± 1,99 | 20,614 |
| | | | (Houlton et al., 2020) | M (n = 72) | Black SA | CBCT | 13,77 ± 2,21 | 3,106 |
| | | | (Houlton et al., 2020) | M (n = 19) | White SA | CBCT | 7,87 ± 1,93 | 20,779 |
| | | | (Houlton et al., 2022) | M (n = 67) | Black SA | CBCT | 13,30 ± 2,30 | 0,344 |
| | | | (Ogawa et al., 2015) | M (n = 865) | Japanese | 3D Stereophotogrammetry | 9,00 ± 1,61 | 42,888 |
| | | | (Virdi et al., 2019) | M (n = 36) | Kenyan | Direct | 13,70 ± 1,30 | 3,181 |
| Lower Lip Height | F (n = 54) | 19,56 ± 2,79 | (Amini et al., 2014) | F (n = 50) | Iranian | Direct | 17,40 ± 2,00 | 7,141 |
| | | | (Farkas et al., 2007) | F (n = 50) | African-American | Direct | 20,20 ± 2,40 | -0,871 |
| | | | (Farkas et al., 2007) | F (n = 200) | North American White | Direct | 17,80 ± 4,70 | 3,768 |
| | | | (Virdi et al., 2019) | F (n = 36) | Kenyan | Direct | 20,70 ± 1,10 | 1,640 |
| | M (n = 64) | 22,08 ± 3,26 | (Amini et al., 2014) | M (n = 50) | Iranian | Direct | 18,70 ± 2,10 | 16,115 |
| | | | (Farkas et al., 2007) | M (n = 50) | African-American | Direct | 22,10 ± 2,40 | -1,608 |
| | | | (Farkas et al., 2007) | M (n = 109) | North American White | Direct | 19,70 ± 2,10 | 10,234 |
| | | | (Virdi et al., 2019) | M (n = 36) | Kenyan | Direct | 22,50 ± 1,90 | -1,229 |

| Supplementary table 2: Comparative analysis with the literature comparisons | | | | | | | | |
|---|---|---|---|---|---|---|---|---|
| | **This study** | | **Other studies** | | | | | **Bayes Factor** |
| **Facial Parameter** | **Sex (sample size)** | **Mean ± SD** | **Author** | **Sex (sample size)** | **Population** | **Modality** | **Mean ± SD** | **log10 value*** |
| Lower Vermillion Height | F (n = 54) | 11,71 ± 2,38 | (Amini et al., 2014) | F (n = 50) | Iranian | Direct | 10,00 ± 1,50 | 6,629 |
| | | | (Celebi et al., 2017) | F (n = 48) | Mexican-American | 3D Stereophotogrammetry | 8,92 ± 1,48 | 17,969 |
| | | | (Celebi et al., 2017) | F (n = 68) | Columbian | 3D Stereophotogrammetry | 8,67 ± 1,41 | 24,182 |
| | | | (Houlton et al., 2020) | F (n = 52) | Black SA | CBCT | 12,13 ± 2,30 | -1,201 |
| | | | (Houlton et al., 2020) | F (n = 20) | White SA | CBCT | 7,84 ± 1,76 | 18,115 |
| | | | (Houlton et al., 2022) | F (n = 41) | Black SA | CBCT | 12,40 ± 2,30 | -0,631 |
| | | | (Ogawa et al., 2015) | F (n = 261) | Japanese | 3D Stereophotogrammetry | 9,40 ± 1,81 | 18,416 |
| | | | (Virdi et al., 2019) | F (n = 36) | Kenyan | Direct | 13,60 ± 1,00 | 9,264 |
| | M (n = 64) | 12,74 ± 2,25 | (Amini et al., 2014) | M (n = 50) | Iranian | Direct | 9,90 ± 1,60 | 21,659 |
| | | | (Celebi et al., 2017) | M (n = 63) | Columbian | 3D Stereophotogrammetry | 9,65 ± 2,21 | 21,872 |
| | | | (Celebi et al., 2017) | M (n = 44) | Mexican-American | 3D Stereophotogrammetry | 8,93 ± 1,77 | 31,043 |
| | | | (Houlton et al., 2020) | M (n = 72) | Black SA | CBCT | 12,99 ± 2,07 | -1,487 |
| | | | (Houlton et al., 2020) | M (n = 19) | White SA | CBCT | 7,72 ± 2,38 | 21,169 |
| | | | (Houlton et al., 2022) | M (n = 67) | Black SA | CBCT | 12,90 ± 2,10 | -1,597 |
| | | | (Ogawa et al., 2015) | M (n = 865) | Japanese | 3D Stereophotogrammetry | 9,20 ± 2,27 | 64,747 |
| | | | (Virdi et al., 2019) | M (n = 36) | Kenyan | Direct | 13,80 ± 0,90 | 3,206 |

* Note: Interpretation of Bayes Factor is done according to Jeffreys' (1961) scale of the base 10 logarithmic Bayes Factor (logBF) where the logBF provides evidence for the alternative hypothesis which posits that there is a differences between population means. In this context, the following colours is interpreted:

| | | | |
|---|---|---|---|
| ▨ | Weak evidence that there is no difference between population means | ▨ | Weak evidence that there is a difference between population means |
| ▨ | Substantial evidence that there is no difference between population means | ▨ | Substantial evidence that there is a difference between population means |
| ▨ | Strong evidence that there is no difference between population means | ▨ | Strong evidence that there is a difference between population means |
| ▨ | Very strong evidence that there is no difference between population means | ▨ | Very strong evidence that there is a difference between population means |
| | | ▨ | Decisive evidence that there is a difference between population means |

| Facial Parameter | Count of comparisons with African groups where population means are similar | Count of comparisons with African groups where population means NOT similar | Count of comparisons with other groups where population means are similar | Count of comparisons with other groups where population means NOT similar |
|---|---|---|---|---|
| Midfacial Height | 1 | 1 | 1 | 3 |
| Nasofrontal Angle | 0 | 4 | 2 | 4 |
| Nasolabial Angle | 0 | 4 | 0 | 10 |
| Alar Base Width | 5 | 12 | 1 | 52 |
| Alar Length Lt | 0 | 0 | 1 | 5 |
| Alar Length Rt | 0 | 0 | 0 | 6 |
| Columella Length Lt | 0 | 0 | 0 | 2 |
| Columella Length Rt | 0 | 0 | 0 | 2 |
| Columella Width | 0 | 0 | 1 | 1 |
| Nasal Height | 2 | 16 | 3 | 48 |
| Nasal Length | 1 | 5 | 4 | 21 |
| Nasal Protrusion | 2 | 0 | 3 | 19 |
| Eye Fissure Length Lt | 0 | 4 | 4 | 11 |
| Eye Fissure Length Rt | 1 | 11 | 6 | 13 |
| Intercanthal Width | 1 | 13 | 0 | 35 |
| Outer-canthal Width | 1 | 7 | 13 | 13 |
| Mouth Width | 10 | 7 | 6 | 30 |
| Philtrum Width | 1 | 5 | 2 | 5 |
| Upper Lip Height | 5 | 1 | 4 | 12 |
| Upper Vermillion Height | 0 | 6 | 0 | 10 |
| Lower Lip Height | 3 | 1 | 0 | 4 |
| Lower Vermillion Height | 4 | 2 | 0 | 10 |
| **Total (n = 502)** | 37 | 99 | 51 | 316 |

Table caption: Supplementary table 3: Summary of individual facial parameter comparisons with other African and non-African populations

| Supplementary table 4: Summary of feature group comparisons with other African and non-African populations | | | | | | |
|---|---|---|---|---|---|---|
| Feature Group | Count of comparisons with African groups where population means are similar | Count of comparisons with African groups where population means NOT similar | Count of comparisons with other groups where population means are similar | Count of comparisons with other groups where population means NOT similar | Percentage of different population means (African groups) | Percentage of different population means (other groups) |
| Nasal Features | 11 | 42 | 16 | 173 | 79% | 92% |
| Ocular Features | 3 | 35 | 23 | 72 | 92% | 76% |
| Oral Features | 23 | 22 | 12 | 71 | 49% | 86% |

## Supplementary References

Adekunle, A.A., Olowo, A.Y., James, O., Adamson, O.O., Alade, A.A., Agbogidi, F.O., et al. 2022. Facial Anthropometry Measurements Using Three-Dimensional Stereophotogrammetry Analysis Among Nigerians. J Craniofac Surg. 33:(4):1178-81.

Ahmed, A.A., Taha, S. 2016. Cephalo-facial analysis to estimate stature in a Sudanese population. Leg Med (Tokyo). 20:80-6.

Al-Sebaei, M.O. 2015. The validity of three neo-classical facial canons in young adults originating from the Arabian Peninsula. Head Face Med. 11:4.

Amini, F., Mashayekhi, Z., Rahimi, H., Morad, G. 2014. Craniofacial morphologic parameters in a Persian population: an anthropometric study. J Craniofac Surg. 25:(5):1874-81.

Antoun, J.S., Lawrence, C., Leow, A., Rongo, R., Dias, G., Farella, M. 2014. A three-dimensional evaluation of Māori and New Zealand European faces. Australasian Orthodontic Journal. 30:(2):169-75.

Bayat, M., Shariati, M., Rajaeirad, F., Yekaninejad, M.S., Momen-Heravi, F., Davoudmanesh, Z. 2018. Facial Anthropometric Norms of the Young Iranian Population. J Maxillofac Oral Surg. 17:(2):150-7.

Bhandari, P.S., Dhar, S., Gulati, A. 2021. Anthropometric analysis of linear parameters of the Indian nose: A cross-sectional study and comparison with literature. J Plast Reconstr Aesthet Surg. 74:(12):3421-30.

Borman, H., Ozgür, F., Gürsu, G. 1999. Evaluation of soft-tissue morphology of the face in 1,050 young adults. Ann Plast Surg. 42:(3):280-8.

Budai, M., Farkas, L.G., Tompson, B., Katic, M., Forrest, C.R. 2003. Relation between anthropometric and cephalometric measurements and proportions of the face of healthy young white adult men and women. J Craniofac Surg. 14:(2):154-61.

Celebi, A.A., Kau, C.H., Ozaydin, B. 2017. Three-Dimensional Anthropometric Evaluation of Facial Morphology. J Craniofac Surg. 28:(5):e470-e4.

Farkas, L.G., Katic, M.J., Forrest, C.R. 2007. Comparison of craniofacial measurements of young adult African-American and North American white males and females. Ann Plast Surg. 59:(6):692-8.

Galantucci, L.M., Deli, R., Laino, A., Di Gioia, E., D'Alessio, R., Lavecchia, F., et al. 2016. Three-Dimensional Anthropometric Database of Attractive Caucasian Women: Standards and Comparisons. J Craniofac Surg. 27:(7):1884-95.

Guo, Y., Schaub, F., Mor, J.M., Jia, R., Koch, K.R., Heindl, L.M. 2020. A Simple Standardized Three-Dimensional Anthropometry for the Periocular Region in a European Population. Plast Reconstr Surg. 145:(3):514e-23e.

He, Z.-j., Jian, X.-c., Wu, X.-s., Gao, X., Zhou, S.-h., Zhong, X.-h. 2009. Anthropometric measurement and analysis of the external nasal soft tissue in 119 young Han Chinese adults. J Craniofac Surg. 20:(5)**:**1347-51.

Heidari, Z., Mahmoudzadeh-Sagheb, H., Khammar, T., Khammar, M. 2009. Anthropometric measurements of the external nose in 18–25-year-old Sistani and Baluch aborigine women in the southeast of Iran. Folia morphologica. 68:(2)**:**88-92.

Houlton, T.M., Jooste, N., Uys, A., Steyn, M. 2020. Lip height estimation in a southern African sample. SADJ. 75:415-24.

Houlton, T.M., Jooste, N., Steyn, M., Hemingway, J. 2022. Visualising trends in dentition to lip mouth morphology using geometric morphometrics. PloS one. 17:(9)**:**e0274127.

Houlton, T.M.R., Jooste, N., Steyn, M. 2019. Mouth Width and Cupid's Bow Estimation in a Southern African Population. J Forensic Sci. 65:(2)**:**372-9.

Jayaratne, Y.S., Deutsch, C.K., Zwahlen, R.A. 2014. Nasal morphology of the Chinese: three-dimensional reference values for rhinoplasty. Otolaryngol Head Neck Surg. 150:(6)**:**956-61.

Lee, W., Jeong, J., Park, J., Jeon, E., Kim, H., Jung, D., et al. 2013. Analysis of the facial measurements of Korean Air Force pilots for oxygen mask design. Ergonomics. 56:(9)**:**1451-64.

Liu, Y., Kau, C.H., Talbert, L., Pan, F. 2014. Three-dimensional analysis of facial morphology. J Craniofac Surg. 25:(5)**:**1890-4.

Liu, Y., Kau, C.H., Pan, F., Zhou, H., Zhang, Q., Zacharopoulos, G.V. 2013. A 3-dimensional anthropometric evaluation of facial morphology among Chinese and Greek population. J Craniofac Surg. 24:(4)**:**e353-e8.

Menéndez López-Mateos, M.L., Carreño-Carreño, J., Palma, J.C., Alarcón, J.A., Menéndez López-Mateos, C., Menéndez-Núñez, M. 2019. Three-dimensional photographic analysis of the face in European adults from southern Spain with normal occlusion: reference anthropometric measurements. BMC Oral Health. 19:1-8.

Ogawa, Y., Wada, B., Taniguchi, K., Miyasaka, S., Imaizumi, K. 2015. Photo anthropometric variations in Japanese facial features: Establishment of large-sample standard reference data for personal identification using a three-dimensional capture system. Forensic Sci Int. 257:511.e1-.e9.

Oladipo, G., Okoh, P., Hart, J. 2010. Anthropometric study of ocular dimensions in adult ijaws of Nigeria. Res J Med Med Sci. 5:121-4.

Olusanya, A.A., Aladelusi, T.O., Adedokun, B. 2018. Anthropometric Analysis of the Nigerian Face: Any Conformity to the Neoclassical Canons? J Craniofac Surg. 29:(7)**:**1978-82.

Ouni, I., Jebali, R., Amar, S., Mansour, L. 2022. Correlation between facial measurements and vertical dimension of occlusion among Tunisian populations: An anthropometric study. J Dent Res Dent Clin Dent Prospects. 16:(2)**:87-90.**

Ozdemir, F., Uzun, A. 2015. Anthropometric analysis of the nose in young Turkish men and women. J Craniomaxillofac Surg. 43:(7)**:1244-7.**

Oztürk, F., Yavas, G., Inan, U.U. 2006. Normal periocular anthropometric measurements in the Turkish population. Ophthalmic Epidemiol. 13:(2)**:145-9.**

Rahimi Jaberi, K., Kavakebian, F., Mojaverrostami, S., Najibi, A., Safari, M., Hassanzadeh, G., et al. 2019. Nasofacial Anthropometric Study Among Students of Shiraz University of Medical Sciences, Iran: A Population Based Study. Indian J Otolaryngol Head Neck Surg. 71:(2)**:206-11.**

Ridel, A.F., Demeter, F., Liebenberg, J., L'Abbe, E.N., Vandermeulen, D., Oettle, A.C. 2018. Skeletal dimensions as predictors for the shape of the nose in a South African sample: A cone-beam computed tomography (CBCT) study. Forensic Sci Int. 289:18-26.

Rodríguez, A.A., Escanilla, D.E., Caroca, L.A., Albornoz, C.E., Marshall, P.A., Molenbroek, J.F.M., et al. 2022. Head and facial dimensions of Chilean workers for design purposes and the differences with other populations. Work. 71:(4)**:1073-85.**

Sarna, K., Sonigra, K.J., Ngeow, W.C. 2023a. A Cross-Sectional Study to Determine and Compare the Craniofacial Anthropometric Norms in a Selected Kenyan and Chinese Population. Plast Surg (Oakv). 31:(1)**:84-90.**

Sarna, K., Osundwa, T.M., Kamau, M., Sonigra, K.J. 2023b. Analysis of Neoclassical Canons in Adult Kenyans of Indian Descent. Craniomaxillofac Trauma Reconstr. 16:(1)**:55-61.**

Virdi, S.S., Wertheim, D., Naini, F.B. 2019. Normative anthropometry and proportions of the Kenyan-African face and comparative anthropometry in relation to African Americans and North American Whites. Maxillofac Plast Reconstr Surg. 41:(1)**:9.**

Weiliang, Z., Wei, W., Lili, G. 2021. Comparative Study of Anthropometric Nasal Anslysis Based on Han Nationality Young Female Adults in Central China. J Craniofac Surg. 32:(4)**:1455-8.**

Yokota, M. 2005. Head and facial anthropometry of mixed-race US Army male soldiers for military design and sizing: a pilot study. Appl Ergon. 36:(3)**:379-83.**

# Bridge between Chapter 3 and 4

The research encapsulated in the paper "Normative Facial Capulometric Measurements in a Black South African Population", currently under review at *Journal of Plastic, Reconstructive & Aesthetic Surgery*, laid the foundational work of establishing normative facial measurements through precise landmarks on the face. The simplest representation of facial form is through linear distances, angles, and ratios between these landmarks. These geometric descriptors are invaluable for facial analyses, allowing for nuanced comparisons across populations, sexes, and individuals. The normative values reported in this paper have broad applications, from guiding clinical interventions to serving as a reference in forensic reconstructions.

Statistical shape models are sophisticated dense landmark-based models that use a training set of instances of shape (e.g., a face), to derive the mean shape as well as a model of variation in shape, providing a comprehensive description of facial morphology. The SSM reported in the next paper, "A Statistical Shape Model for Estimating Missing Soft Tissues of the Face in a Black South African Population" published in the *Journal of Prosthodontics*, offers a more comprehensive description of 3D facial variation. This is then exploited to specifically addresses the nuanced challenges of prosthetic design, offering a tailored solution that can significantly improve the quality of life for individuals with facial disfigurements, within the context of the population's norm.

Both of these studies cater to the unique facial features of the black South African population and not only fill a gap in the existing literature but also lay the groundwork for future research that could extend these methodologies to other ethnic groups in South Africa and beyond, with the ultimate goal of improving patient outcomes and gaining a more thorough understanding of the rich tapestry of human diversity.

# Chapter 4: Aim 2

This chapter presents the research methods and results of the second aim of this thesis as a manuscript published in the *Journal of Prosthodontics* titled "A statistical shape model for estimating missing soft tissues of the face in a black South African population".

This is the accepted version of the following article:

AMERICAN COLLEGE OF
# PROSTHODONTISTS
*Your smile. Our specialty.™*

# A statistical shape model for estimating missing soft tissues of the face

| | |
|---|---|
| Journal: | *Journal of Prosthodontics* |
| Manuscript ID | JOPR-23-023 |
| Wiley - Manuscript type: | Original Article |
| Manuscript Categories: | |
| Index Words: | statistical shape model, facial prostheses, facial variation, facial defects |
| Abstract: | Purpose:<br>Facial disfigurement may affect the quality of life of southern African patients. Facial prosthetics are often used as an adjuvant to surgical intervention and may sometimes be the only viable treatment option. As traditional methods for designing soft-tissue facial prostheses are time-consuming and subject to the clinician's artistic skill, we aim to support the objective design of facial prostheses by developing and validating a statistical shape model (SSM) for estimating the shape of missing facial soft tissue segments.<br><br>Materials & Methods:<br>An SSM of 3D facial variations was built from meshes extracted from computed tomography and cone beam computed tomography images of a black South African sample (n = 235) without facial disfigurement. The SSM was evaluated in terms of model generalisation and specificity. Various types of facial defects were simulated, and the missing parts were estimated automatically by a weighted fit of each mesh to the SSM. The estimated regions were compared to the original regions using colour maps and root-mean-square (RMS) distances.<br><br>Results:<br>The SSM had mean generalisation and specificity errors of 1.09 and 2.75 mm respectively. RMSE for defect imputations of one orbit, partial nose, cheek, and lip were all below 1.71 mm. Errors for the full nose, bi-orbital defects and composites 1 and 2 were between 2.10 and 2.58 mm. Statistically significant associations of age and type of defect with RMSE were observed, but not with sex or imaging modality.<br>Conclusion:<br>This method can support the objective and automated design of facial prostheses by replacing time-consuming and skill-dependent aspects of prosthesis design. |
| | |
| Note: The following files were submitted by the author for peer review, but cannot be converted to PDF. You must view these files (e.g. movies) online. | |
| Mode1.mp4<br>Mode2.mp4 | |

1
2
3
4
5
6
7
8
9
10
11
12
13
14
15
16
17
18
19
20
21
22
23
24
25
26
27
28
29
30
31
32
33
34
35
36
37
38
39
40
41
42
43
44
45
46
47
48
49
50
51
52
53
54
55
56
57
58
59
60

Mode3.mp4
Mode4.mp4
Mode5.mp4

SCHOLARONE™
Manuscripts

## ABSTRACT

**Purpose:** Facial disfigurement may affect the quality of life of southern African patients. Facial prosthetics are often used as an adjuvant to surgical intervention and may sometimes be the only viable treatment option. As traditional methods for designing soft-tissue facial prostheses are time-consuming and subject to the clinician's artistic skill, we aim to support the objective design of facial prostheses by developing and validating a statistical shape model (SSM) for estimating the shape of missing facial soft tissue segments.

**Materials & Methods:** An SSM of 3D facial variations was built from meshes extracted from computed tomography and cone beam computed tomography images of a black South African sample (n = 235) without facial disfigurement. The SSM was evaluated in terms of model generalisation and specificity. Various types of facial defects were simulated, and the missing parts were estimated automatically by a weighted fit of each mesh to the SSM. The estimated regions were compared to the original regions using colour maps and root-mean-square (RMS) distances.

**Results:** The SSM had mean generalisation and specificity errors of 1.09 and 2.75 mm respectively. RMSE for defect imputations of one orbit, partial nose, cheek, and lip were all below 1.71 mm. Errors for the full nose, bi-orbital defects and composites 1 and 2 were between 2.10 and 2.58 mm. Statistically significant associations of age and type of defect with RMSE were observed, but not with sex or imaging modality.

**Conclusion:** This method can support the objective and automated design of facial prostheses by replacing time-consuming and skill-dependent aspects of prosthesis design.

1

The face is fundamental to human social interaction, among other functions. Even seemingly minor facial disfigurement may result in social anxiety, depression, and poor self-esteem, ultimately lowering quality of life.[1-4] Disfigurement may be the result of congenital deformities, infectious lesions, trauma, both human immunodeficiency virus (HIV)-related lesions like Kaposi's sarcoma and non-Hodgkin's lymphoma, [5] and non-HIV-related cancerous lesions, as well as conditions with complex pathology such as noma.[5-8] Facial disfigurement is a prevalent issue in southern African populations due to the high prevalence of HIV, [9] poverty [6,8] and facial trauma. [10] Furthermore, head and neck cancers account for approximately 18% of all cancer diagnoses in South Africa. [11]

Facial defects are classified according to location as intra-oral, extra-oral or a combination of both.[12] Intraoral defects comprise maxillary, mandibular, or velopharyngeal, and rehabilitation usually requires intra-oral devices such as implants or obturators which fall outside the scope of this study. Extraoral defects typically relate to the various facial features, including auricular, ocular, orbital, nasal as well as lip and cheek defects and generally require an aesthetic prosthesis. Some defects may include more than one feature, for example, the mouth, nose, and cheek. Lastly, defects involving both intra-oral aspects as well as extra-oral features typically require surgical and prosthetic intervention, with implants providing the underlying framework for an outer aesthetic prosthesis. [12]

The rehabilitation of facial defects continues to need complex interventions. Despite advances in surgical rehabilitation techniques, limiting factors include inadequate residual soft and hard tissue, and vascular compromise after radiation.[13] When the functional and aesthetic requirements are beyond the capacity of local reconstructive efforts, aesthetic prosthetics are an alternative or adjunct rehabilitation option, especially for elderly patients or those with significant comorbidities.[13-15] The principal goal of an external aesthetic prosthesis is to restore a missing body part with a life-like substitute, which often has no other functional role.[16]

2

Attempts to design partial facial prostheses are less than satisfactory in the South African context.[17] As standard guidelines are based on individuals of European descent[18] and not applicable to black South Africans, a combination of artistic methods is used in the design and manufacturing of facial prostheses for this population. Artistic methods are naturally time- and energy -intensive and rely heavily on the artistic skills of the clinician.  As there is a lack of both training facilities and trained clinicians capable of performing these skills, producing facial prostheses in South Africa[19] is delayed resulting in an extensive waiting list for patients in need of rehabilitation.

Objective and automated methods for designing facial prostheses could substantially reduce the time cost and waiting times. For unilateral defects, computerised methods based on mirroring the intact half of the face about the midline could be used in the design of prostheses.[20] The mirroring approach, while ideal for unilateral defects is not as effective and often cannot be applied at all to defects that cross the facial midline. In contrast, SSMs model shape variation based on homologous landmarks within a training sample of shapes and by using an SSM, missing parts of a shape can be inferred from any available intact parts, not only regions bilaterally paired with the defect. SSMs have been applied for the reconstruction of pelvic defects,[21] mandibular defects,[22] orbital floor defects,[23] and reconstructions of cranial vault and midfacial (skeletal) defects.[24,25]

In this study, we model facial variation among black South Africans by means of an SSM and evaluate the use of this SSM to estimate missing soft tissue parts for a sample of artificially defective faces. This tool can contribute to the design and manufacturing of aesthetic prostheses by establishing a more objective and automated approach to estimating missing soft tissue segments of the face.

3

## Materials and Methods

Ethical approval for this study was obtained from the Faculty of Health Sciences Ethics Committee at the University ████████ (Ref# 58/2020). A sample of cone beam computed tomography (CBCT) and computed tomography (CT) scans of adult black South African patients were retrospectively collected from the University ████████████████ ███████████████████████████████████████████████ South Africa. All identifying metadata was removed, with only age and sex recorded. Scans were excluded if the face showed any underlying pathology, evidence of current orthodontic treatment or visible facial interventions. The sample comprised 118 CBCT (age range: 18 - 87) and 119 CT (age range: 18 - 85) scans. The demographic characteristics of the sample are shown in Table 1.

An overview of the entire process of imputing missing soft tissue segments of the face is illustrated in Figure 1, including the creation of the SSM and how it is used to impute defected regions of the face.

Threshold segmentation of all CT and CBCT scans were performed to segment the soft tissue and support structures from the background of the image. The resulting iso-surface was tessellated into a mesh (Figure 1A). Twenty anatomical landmarks *(Supplementary figure 1)* were placed on the sample meshes and used to initialise a non-rigid registration (mapping) of a template mesh onto all the meshes in the training sample (Figure 1B; Supplementary methods 1.1.1) using MeshMonk [26] (https://gitlab.kuleuven.be/mirc/meshmonk). The standard template mesh was generated using a bootstrapping approach (see Supplementary methods 1.1.2). Registration brings all meshes into correspondence by gradually deforming a standard template into the shape of each target mesh. For samples where the chin was missing or the eyes were closed, these regions were deterministically flagged as outliers and ignored when estimating

4

the deformation during registration (Figure 1B). Each face was then represented in the topology of the template mesh comprising approximately 20 000 dense quasi-landmarks.

The SSM was built iteratively (Supplementary methods 1.1.3). In each iteration, all training faces were aligned to the sample mean and scaled to unit size by generalized Procrustes analysis and the modes of variation were calculated (through Principal Component Analysis) by a singular value decomposition of the n (observations) by 3k(k landmarks) matrix. Firstly, only samples with complete chin morphology were included to build the first version of the SSM. This model was used to impute the chins of samples where these features were missing or unusable (Figure 1C). A second version of the SSM was then generated including all the complete and imputed chins, as well as all samples with open eyes, and used to impute the eyes of the samples with closed eyes (Figure 1D). Subsequent calculation of the final SSM included samples with imputed chins and eyes and again aligning all the samples to the mean and re-calculating SSM (Figure 1E). The SSM represents facial variation in this population as modes of variation, each of which corresponds to a linear transformation of facial shape, and the normal-range variance along each mode.

The ability of the model to represent the population in question was evaluated by computing its generalisation and specificity (Supplementary methods 1.1.4). Both properties contribute in principle to the ability of the model to realistically impute missing parts of the face. Generalisation relates to how well the model can represent faces not used in training and is the mean of the average out-of-sample reconstruction error of the training data. Reconstruction error was the difference between the face and the reconstruction of that face from their projections onto the modes of variation. This was computed in a leave-one-out set-up where all but one sample was used to learn the modes of variation and the reconstruction error was calculated for the held-out sample. The generalisation was also evaluated with different training sample sizes. Model in-sample accuracy is the reconstruction error of the training data when

5

74

1
2
3
4
5
6
7
8
9
10
11
12
13
14
15
16
17
18
19
20
21
22
23
24
25
26
27
28
29
30
31
32
33
34
35
36
37
38
39
40
41
42
43
44
45
46
47
48
49
50
51
52
53
54
55
56
57
58
59
60

samples are not held out. This was calculated as a function of the number of modes of variation to illustrate their individual contribution to the model. The in-sample accuracy for a given number of modes constitutes the lower bound of what is the possible generalisation error and calibrates the interpretation of the generalisation. Model specificity concerns the ability of the SSM to represent only realistic or valid faces and is the average difference, computed over 1000 faces, between a face randomly sampled from the multivariate Gaussian distribution of the SSM and the most similar training face. Generalisation, specificity, and in-sample accuracy are expressed in RMSE in mm units accomplished by scaling the model-based faces (e.g., reconstructions or simulated faces) to the size of the real face to which they are compared prior to calculating the error. This is weighted to ignore imputed areas such as the chin and eyes where applicable.

The defect sample was processed to simulate 240 defects (Figure 1F, Supplementary methods 1.2) on 30 faces with open eyes, according to 6 classes (Supplementary Table 1). Class 1 to 5 were individual feature defects of the orbital region, cheek and upper lip, lips or isolated lower lip, full nasal region, and partial nasal region, respectively. Class 6 defects involved more than one facial feature in assorted combinations. Large (composite 1) defects involved three features, e.g., orbital, cheek and full nose defects; small (composite 2) defects involved two features e.g., partial nose and lips. and bi-orbital defects included defects in both eyes. The defect faces were then segmented and tessellated into a mesh (Figure 1G). Correspondence with the standard facial template was established (Figure 1I) for each original non-defective face, along with its defective copies, as described in the supplementary methods section 1.1.1, however, landmarks that could not be placed on the defect mesh (due to the anatomical region being removed, (for example endo -and exocanthion where the defect involved regions of the eye) were excluded and ignored in the initialisation (Figure 1H). The region of interest was identified on the unprocessed defective scan by manual selection (Supplementary methods 1.3)

6

and then transferred onto the topology of the template and the statistical shape model by finding

any points on its registered counterpart whose closest point on the defective scan was part of

the defective region. The final SSM was used to estimate the linear combination of the modes

of variation that most closely approximates the intact regions of each face and imputes the

missing regions using a weighted projection onto the modes of variation (Supplementary

methods 1.1.3 and 1.3). The face reconstructed from these projections was blended with the

mapped version of the defective face. This result is the mapped version of the defective face

with vertices of the defective region substituted with those of the weighted fit face. The

interpolated region is then visualised and interpreted in the context of the of the original

unprocessed defective mesh (Figure 1J).

The error for each defected scan was quantified as the RMS distance between the original

mapped scan without the defect and its interpolation, computed over the interpolated region. A

linear mixed model assessed the contributions of demographic and imaging factors as well as

the type of defect to the RMSE. Demographic and imaging factors all varied between subjects

and included age, imaging modality (CT/CBCT) and sex (male/female). Defect type varied

within subjects (orbital, cheek, lip, full nasal, partial nasal, bi-orbital, composite 1 and

composite 2). The mixed model comprised fixed main effects of each factor and intercepts for

each participant and was fitted using lmerTest package [27] in R. [28] Residuals were plotted against

the fitted values and evaluated for heteroscedasticity, skewness, and kurtosis.

**Results**

Forty-three modes of variation were required to model 96% of the shape variation and were

retained. The first 5 modes of variation are visualised in Figure 2a. Video representations of

the first 5 modes of variation can be viewed in the Supplementary Materials (supplementary

video files 1 to 5). The first mode of variation, responsible for the most variation,

7

predominantly represents total facial height and width, with changes in the length of the maxillary alveolar processes, mode 2 relates to midfacial projection with changes in the zygomatic breadth, mode 3 represents primarily variability in upper facial height and nose height. In mode 4, the depth of the eyes is influenced by the zygomatic width and frontal area bossing and mode 5 relates to maxillary and mandibular protrusion.

The distributions of out-of-sample reconstruction errors with different training sample sizes are shown in Figure 2c. As the model generalisation error decreases with an increasing sample size, the model better represents the population. As the curve is reaching a plateau, the errors as a function of the sample size are decreasing very slowly. This indicates that beyond the current sample size a large number of additional participants would result in only an incremental improvement to the model. No difference in out-of-sample reconstruction error was observed between imaging modality (Figure 2d) or sex (Figure 2e) and age (Figure 2f). In Figure 2 g and h, the weighted RMS per point is also visualised as a colour map for mean generalisation and specificity. The mean generalisation error was 1.09 mm (Figure 2g). Specificity, the model's ability to represent only valid or realistic faces, resulted in a mean error of 2.75 mm (Figure 2h). Regions of slightly higher errors include the eyelids, nose bridge, and lips (Figure 2 g and h).

Figure 3 shows the distribution of errors plotted by defect type, sex, imaging modality and age. Means and standard deviations of the errors by defect type are also reported in Table 2. Errors for unilateral orbital defects, the partial nose, cheek and lip were all below 1.71 mm. Errors for the full nose, composite 1 (combination of three features) and composite 2 (combination of two features) and bi-orbital defects were between 2.10 and 2.58 mm.

The linear mixed model showed main effects of age ($F(1,26) = 16.949$, $p < 0.001$) and defect type ($F(7,203) = 27.030$, $p < 0.001$) on RMSE were significant, all others were not ($p > 0.050$, Supplementary Table 2). Residuals were plotted against the fitted values, and we found no

8

evidence of heteroscedasticity. Residuals were normally distributed with low skewness (0.52) and kurtosis close to three (3.25). Homogeneity of variance was satisfied among levels of each between-subjects factor (p-value of Levene's tests all $> 0.05$). The unstandardized regression coefficient for age showed the effect is a small decrease in error of -0.015 mm (SE = 0.003) per year. The expected values and 95% confidence intervals of the expectation for each defect type are shown in (Supplementary figure 2). From this and the boxplots in Figure 3 we see that the full nose and larger defects including bi-orbital and composites 1 and 2 are the most difficult to reconstruct.

An example of defect imputations (a – h) for one sample is shown in Figure 4. Imputations of all defects are shown in the Supplementary information (Supplementary figures 3 - 32). These were assessed visually by author HFS. In approximately 38% of cases, the defect was smoothly blended with the surrounding tissue. Cheek and full nose defects performed the best, with respectively 63 % and 60% of instances smoothly blending. Non-smooth blending (e.g., Figure 5) was most frequent for bi-orbital defects (87 %), followed by composite 1 (80 %), and, composite 2 and lip (both at 67%).  The majority of these issues were due to the region selected for imputation being sub-optimal. Figure 5b shows the weightings used for one case. Deep blue regions were 100% imputed whereas yellow regions were 100% not imputed and are expected to match the target face perfectly. For areas coloured in-between yellow and deep blue, the shape is a weighted combination of the face estimated from the SSM and the target face and as such may not match the target face perfectly. Essentially the mismatch between the two surfaces is because the region selected for imputation extends beyond the true defective region. The scope of the imputed region is determined by both the manual selection of points to define initial binary weights and the number of smoothing passes applied to these initial weights. This smoothing is necessary for even blending, but it also blurs, and effectively extends, the boundary of the selected region (Supplementary methods 1.3). Thirteen cases of poor defect

9

imputations were because of failed non-rigid registration. In 10 cases, the defects extended beyond the anatomical region covered by the facial template (Figure 6) and thus were only partially imputed.

**Discussion**

Automated and objective techniques to aid in the design of facial prosthetics are urgently needed, especially in South Africa. Towards this end, we evaluated a statistical shape model-based approach for estimating missing soft tissue parts in a black South African sample. In contrast to commonly employed artistic methods, the approach is objective, being derived from a statistical model of real facial variation. In contrast to mirroring approaches, it can be easily applied to bilateral defects. This approach can help reduce the burden on rehabilitation clinics by assisting in faster and less laborious design and manufacture of aesthetic facial prostheses.

While computer-aided design can currently address unilateral defects employing mirroring techniques,[29-36] midline and bilateral defects present challenges. The perception of perfect facial symmetry, such as seen in mirror images, is considered disconcerting and unattractive.[37] Addressing midline defects currently mostly relies on the use of templates, or archetypes.[32,38-41] Using an archetype is a good solution at least in terms of reducing the treatment period and the intensity of the work required by the technicians,[39] however, it requires access to a digital library of facial features which is not readily available and is furthermore time-consuming in that the operator has to try a variety of templates to find the one that is most in harmony or aesthetically appealing.[40] In this study, we evaluate the use of a statistical shape model to infer the most statistically plausible missing regions based on a model of real facial variation. As a region can be inferred from any intact parts, defects crossing the midline e.g., the nose and mouth, as well as bi-lateral defects can be easily inferred. Overall, the statistical shape model showed good generalization and specificity. No statistically significant differences in the

10

accuracy of estimation of the simulated defects were observed between sexes or imaging modalities. A slight decrease in error with age was observed as well as differences between defect types. This is expected as the mean accuracy of the reconstruction of any given defective region depends on the degree of statistical dependence (covariation) between the defective region and the remaining intact regions. As such not all regions are equally well predicted. For example, whereas the partial nose and the unilateral orbital defect show relatively low errors, the full nose and bi-orbital defect show higher errors most likely because of the strong statistical dependence between a part of the nose and the whole nose and between one orbit and its bilateral counterpart.

A recent review (2019) [42] on the current state of maxillofacial rehabilitation in resource-limited nations like South Africa indicates that the majority of issues stem from high costs, time constraints, technical difficulties, specific material-related shortcomings, and the lack of skilled maxillofacial prosthetists and technicians. Along with the lack of expertise in fabricating facial prosthetics, [19] conventional methods are time-intensive for both the patient and clinician. [42] The conventional manufacturing process chain for external facial prostheses involves three main phases: 1) obtaining an impression of the face model, 2) designing the prosthesis model and 3) manufacturing the prosthesis model.[43] The specific steps forming part of the process chain include: a) taking a cast of the region of interest of the facial anatomy; b) creating a positive model of the face; c) designing and sculpting the prosthesis model out of wax; d) creating a negative mould of the prosthesis model; e) casting the final prosthesis into the negative mould using medical grade silicone and f) finishing the prosthesis.[43] Computerised methods may be used to expedite the entire process by replacing steps (a) to (c) and pose several advantages. For example, patient involvement is drastically reduced due to capturing the facial anatomy through CT/CBCT/laser scanner, resulting in a less traumatic experience. The time-consuming and artistic skill-dependent process of sculpting the missing feature from wax is replaced by

11

1
2
3
4
5
6
7
8
9
10
11
12
13
14
15
16
17
18
19
20
21
22
23
24
25
26
27
28
29
30
31
32
33
34
35
36
37
38
39
40
41
42
43
44
45
46
47
48
49
50
51
52
53
54
55
56
57
58
59
60

assorted techniques to reconstruct the missing soft tissue. Furthermore, computerised methods also allow for the manufacturing of a more realistic and complex medical model with the ability to digitally store the information for future use.[43] At this stage in South Africa, the design and manufacturing of unilateral maxillofacial prostheses are based on a combination of artistic methods and digital processing. Moreover, there is a lack of both training facilities and trained clinicians capable of manufacturing maxillofacial prostheses in South Africa.[19] Employing digital techniques like this SSM may eliminate some of the artistic skills needed for the design and manufacture of facial prosthetics, ultimately making it more widely available and relieving the burden on rehabilitation clinics. It is the first step in developing an end-user tool for 3D printing of an automated and objective prosthetic model to fit the patient before moulding and curing of the final silicone prosthesis. [44] Indeed, with advances in 3D printing technology, the ability to directly print the 3D prosthesis using silicone is rapidly becoming more likely.[45,46]

In some cases, the imputed region did not blend seamlessly with the adjacent soft tissue. While this is not optimal, the final imputation is still a realistic and accurate representation of the missing area as indicated by acceptable RMS errors. In most cases this was caused by sub-optimal selection of the imputation region. The manual selection of points as well as the number of smoothing passes to smooth the transition from imputed to non-imputed region both affect this selection, and both are difficult to optimise across a large sample of scans. However, when proceeding case by case, as a clinician would, more energy can be devoted to optimising for a single scan. This can be facilitated in future by the development of a graphical user interface where points can be selected and the selection edited, and the imputation updated in real time. Additionally, small discrepancies may be addressed when manufacturing the final prosthesis by blending to the surrounding areas for seamless borders at the edges of the prosthesis. One other limitation of the proposed method in this study is that only the outer surface of the face is considered. This necessitates further post-processing in software like Mimics (Materialise,

12

Leuven, Belgium) or Zbrush (Maxon, Los Angeles CA) [47] to create a virtual prosthesis, by positioning the prosthesis onto the face and merging the peripheries with the scanned healthy tissue and fitting to the internal surface.

**Conclusion**

The use of this statistical shape model has advantages over artistic and other computerised approaches for estimating missing soft tissue parts. This approach assists in addressing the need for an automated and objective method for designing facial prostheses, can lower the burden on rehabilitation clinics and ultimately aid in improving the quality of life of patients with facial defects.

**References**

1.      Bradbury E: Meeting the psychological needs of patients with facial disfigurement. Br J Oral Maxillofac Surg 2012;50:193-196

2.      Callahan C: Facial disfigurement and sense of self in head and neck cancer. Soc Work Health Care 2005;40:73-87

3.      Clarke A: 'What happened to your face?'Managing facial disfigurement. Br J Community Nurs 1998;3:13-16

4.      De Sousa A: Psychological issues in acquired facial trauma. Indian J Plast Surg 2010;43:200

5.      Zwane NB, Mohangi GU, Shangase SL: Head and neck cancers among HIV-positive patients: A five year retrospective study from a Johannesburg hospital, South Africa. SADJ 2018;73:121-126

6.      Feller L, Altini M, Chandran R, et al: Noma (cancrum oris) in the South A frican context. J Oral Pathol Med 2014;43:1-6

13

7.    Sykes LM, Essop RM: Combination intraoral and extraoral prosthesis used for rehabilitation of a patient treated for cancrum oris: a clinical report. J Prosthet Dent 2000;83:613-616

8.    Pedro K, Smit DA, Morkel JA: Cancrum Oris (noma) in an HIV-positive adult: A case report and literature review. SADJ 2016;71:248-252

9.    HIV prevalence: http://aidsinfo.unaids.org/. Accessed 29 April 2020

10.   Omar M: The incidence and management of traumatic facial injury: 854 patients in 4 months in Charlotte Maxeke Johannesburg Academic Hospital (CMJA), South Africa. *3rd Online Edition of European Conference on Otolaryngology and ENT*. Webinar, Journal of Otology & Rhinology, 2020.

11.   Adeola H, Afrogheh A, Hille J: The burden of head and neck cancer in Africa: the status quo and research prospects. SADJ 2018;73:477-488

12.   Hovhannisyan SR, Mashinyan KA, Zopunyan VR: Maxillofacial defects. Yerevan State University, Department of Prosthodontics, 2009.

13.   Scolozzi P, Jaques B: Treatment of Midfacial Defects Using Prostheses Supported by ITI Dental Implants. Plast Reconstr Surg 2004;114:1395-1404

14.   Federspil P, Federspil P: Prosthetic management of craniofacial defects. HNO 1998;46:569-578

15.   Klimczak J, Helman S, Kadakia S, et al: Prosthetics in Facial Reconstruction. Craniomaxillofac Trauma Reconstr 2018;11:006-014

16.   Cosmetic    Prostheses:    https://www.aopa.org.au/publications/cosmetic-prostheses. Accessed 7 July 2022

17.   Van den Heever J, Sykes LM, Du Plessis F: The scope of maxillofacial prosthodontics: clinical review. SADJ 2012;67:593-595

18.   Naini FB: Facial aesthetics: concepts and clinical diagnosis, John Wiley & Sons, 2011

14

19.     Tsĭtã KPM, Owen CP: Analysis of the need for, and scope of training in, maxillo-facial prosthodontics in the South African dental technology programme. SADJ 2017;72:16-21

20.     Din TNDT, Jamayet N, Rajion ZA, et al: Design and fabrication of facial prostheses for cancer patient applying computer aided method and manufacturing (CADCAM). *AIP Conference Proceedings*. AIP Publishing LLC, 2016.

21.     Meynen A, Matthews H, Nauwelaers N, et al: Accurate reconstructions of pelvic defects and discontinuities using statistical shape models. Comput Methods Biomech Biomed Engin 2020;23:1026-1033

22.     Raith S, Wolff S, Steiner T, et al: Planning of mandibular reconstructions based on statistical shape models. Int J Comput Assist Radiol Surg 2017;12:99-112

23.     Gass M, Füßinger MA, Metzger MC, et al: Virtual reconstruction of orbital floor defects using a statistical shape model. J Anat 2022;240:323-329

24.     Fuessinger MA, Schwarz S, Metzger MC, et al: Planning of skull reconstruction based on a statistical shape model combined with geometric morphometrics. Int J Comput Assist Radiol Surg 2017:1-11

25.     Fuessinger MA, Schwarz S, Neubauer J, et al: Virtual reconstruction of bilateral midfacial defects by using statistical shape modeling. J Craniomaxillofac Surg 2019;47:1054-1059

26.     White JD, Ortega-Castrillón A, Matthews H, et al: MeshMonk: Open-source large-scale intensive 3D phenotyping. Sci Rep 2019;9:6085

27.     Kuznetsova A, Brockhoff P, Christensen R: lmerTest package: tests in linear mixed effect models. J Stat Softw 2017;82:1-26

28.     R Core Team: R: A Language and Environment for Statistical Computing. Vienna, Austria, R Foundation for Statistical Computing, 2022.

15

29.     Verdonck HW, Poukens J, Overveld HV, et al: Computer-assisted maxillofacial prosthodontics: a new treatment protocol. Int J Prosthodont 2003;16

30.     Jiao T, Zhang F, Huang X, et al: Design and fabrication of auricular prostheses by CAD/CAM system. Int J Prosthodont 2004;17

31.     Subburaj K, Nair C, Rajesh S, et al: Rapid development of auricular prosthesis using CAD and rapid prototyping technologies. Int J Oral Maxillofac Surg 2007;36:938-943

32.     Sun J, Xi J, Chen X, et al: A CAD/CAM system for fabrication of facial prostheses. Rapid Prototyp J 2011

33.     Sun M-H, Yen C-H, Tsai Y-J, et al: Fabrication of a facial prosthesis for a 13-year-old child by using a point-and-shoot three-dimensional scanner and CAD/CAM technology. Taiwan J Ophthalmol 2022;12:219-222

34.     Miechowicz S, Wojnarowska W, Majkut S, et al: Method of designing and manufacturing craniofacial soft tissue prostheses using Additive Manufacturing: A case study. Biocybern Biomed Eng 2021;41:854-865

35.     Sherwood RG, Murphy N, Kearns G, et al: The use of 3D printing technology in the creation of patient-specific facial prostheses. Ir J Med Sci 2020;189:1215-1221

36.     Chiu M, Hong SC, Wilson G: Digital fabrication of orbital prosthesis mold using 3D photography and computer-aided design. Graefes Arch Clin Exp Ophthalmol 2017;255:425-426

37.     Zaidel DW, Cohen JA: The face, beauty, and symmetry: perceiving asymmetry in beautiful faces. Int J Neurosci 2005;115:1165-1173

38.     Bi Y, Wei H: Fully digital workflow for the rehabilitation of a total nasal defect with a prosthesis. J Prosthet Dent 2022

39.     Sun J, Chen X, Liao H, et al: Template-based framework for nasal prosthesis fabrication. Rapid Prototyp J 2013

16

40.    Abdulameer HM, Tukmachi M: Nasal prosthesis fabrication using rapid prototyping and 3D printing (A case study). Int J Innov Res Sci Eng Technol 2016;6

41.    Palousek D, Rosicky J, Koutny D: Use of digital technologies for nasal prosthesis manufacturing. Prosthet Orthot Int 2014;38:171-175

42.    Tetteh S, Bibb RJ, Martin SJ: Maxillofacial prostheses challenges in resource constrained regions. Disabil Rehabil 2019;41:348-356

43.    Van Heerden I, Fossay A: Changing world of external maxillofacial prosthesis manufacturing. *20th Annual International RAPDASA Conference*. Bloemfontein, 2019.

44.    He Y, Xue G-h, Fu J-z: Fabrication of low cost soft tissue prostheses with the desktop 3D printer. Sci Rep 2014;4:6973

45.    Fay CD, Jeiranikhameneh A, Sayyar S, et al: Development of a customised 3D printer as a potential tool for direct printing of patient-specific facial prosthesis. Int J Adv Manuf Technol 2022;120:7143-7155

46.    Unkovskiy A, Spintzyk S, Brom J, et al: Direct 3D printing of silicone facial prostheses: A preliminary experience in digital workflow. J Prosthet Dent 2018;120:303-308

47.    Farook T, Jamayet N, Abdullah J, et al: A systematic review of the computerized tools and digital techniques applied to fabricate nasal, auricular, orbital and ocular prostheses for facial defect rehabilitation. J Stomatol Oral Maxillofac Surg 2019

17

Table 1: Demographics of the sample

| Age (years old) | | CBCT (n = 118) | | | | | | | | | | CT (n = 119) | | | | | | | | | |
| --- | --- | --- | --- | --- | --- | --- | --- | --- | --- | --- | --- | --- | --- | --- | --- | --- | --- | --- | --- | --- | --- |
| | | Male | | | | | Female | | | | | Male | | | | | Female | | | | |
| | | Total (n=64) | With Chins* (n=0) | Open Eyes (n=44) | Incl. in Model Training Dataset | Incl. in Defect Dataset (n=8) | Total (n=54) | With Chins* (n=1) | Open Eyes (n=29) | Incl. in Model Training Dataset | Incl. in Defect Dataset (n=7) | Total (n=67) | With Chins* (n=59) | Open Eyes (n=35) | Incl. in Model Training Dataset | Incl. in Defect Dataset (n=7) | Total (n=50) | With Chins* (n=42) | Open Eyes (n=18) | Incl. in Model Training Dataset | Incl. in Defect Dataset (n=8) |
| | 18-30 | 27 | 0 | 18 | 16 | 3 | 15 | 0 | 9 | 11 | 1 | 22 | 19 | 10 | 16 | 2 | 16 | 13 | 7 | 13 | 1 |
| | 31-40 | 19 | 0 | 13 | 10 | 2 | 12 | 0 | 5 | 8 | 1 | 18 | 16 | 9 | 15 | 1 | 18 | 16 | 7 | 10 | 3 |
| | 41-50 | 5 | 0 | 4 | 3 | 1 | 9 | 0 | 7 | 5 | 1 | 7 | 7 | 4 | 4 | 1 | 5 | 5 | 1 | 0 | 1 |
| | 51-60 | 9 | 0 | 6 | 7 | 0 | 9 | 0 | 4 | 4 | 2 | 6 | 6 | 6 | 2 | 1 | 5 | 4 | 1 | 4 | 1 |
| | 60+ | 4 | 0 | 3 | 1 | 2 | 9 | 1 | 4 | 5 | 2 | 4 | 2 | 1 | 1 | 2 | 5 | 4 | 2 | 2 | 2 |
| | Unknown | 0 | 0 | 0 | 0 | 0 | 0 | 0 | 0 | 0 | 0 | 10 | 9 | 5 | 10 | 0 | 1 | 0 | 0 | 1 | 0 |

*Complete morphology of the chin is available, i.e., a chin strut, as usually seen in CBCT, was not present

18

Table 2 RMS error for defect types in millimetres

| Defect type | Orbital | Cheek | Lip | FN | PN | Bi-orbital | Composite1 | Composite2 |
|---|---|---|---|---|---|---|---|---|
| Mean | 1.71 | 1.43 | 1.54 | 2.10 | 1.63 | 2.58 | 2.48 | 2.14 |
| SD | 0.51 | 0.51 | 0.65 | 0.59 | 0.47 | 0.76 | 0.69 | 0.59 |

19

88

1
2
3
4
5
6
7
8
9
10
11
12
13
14
15
16
17
18
19
20
21
22
23
24
25
26
27
28
29
30
31
32
33
34
35
36
37
38
39
40
41
42
43
44
45
46
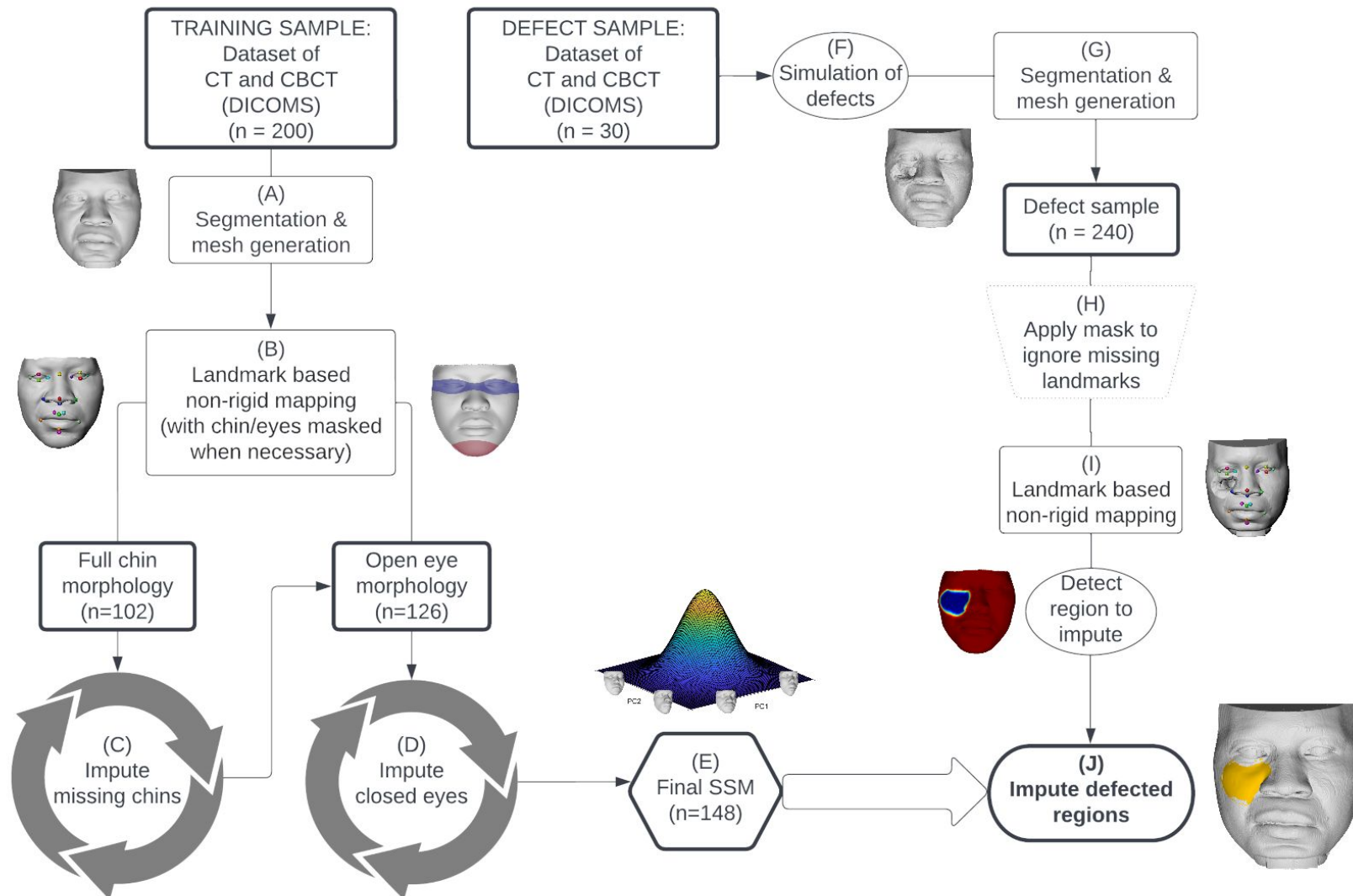
Figure 1: Methodology overview. The left side of the figure shows the steps involved in generating the statistical shape model used to impute missing regions of the defective face. The right side of the figure shows the steps involved in creating a sample of simulated defects, mapping the defective sample, and using the SSM to impute the defective regions. A more detailed description of each step can be found in the Supplementary Materials.

21

90

1
2
3
4
5
6
7
8
9
10
11
12
13
14
15
16
17
18
19
20
21
22
23
24
25
26
27
28
29
30
31
32
33
34
35
36
37
38
39
40
41
42
43
44
45
46
47
48
49
50
51
52
53
54
55
56
57
58
59
60
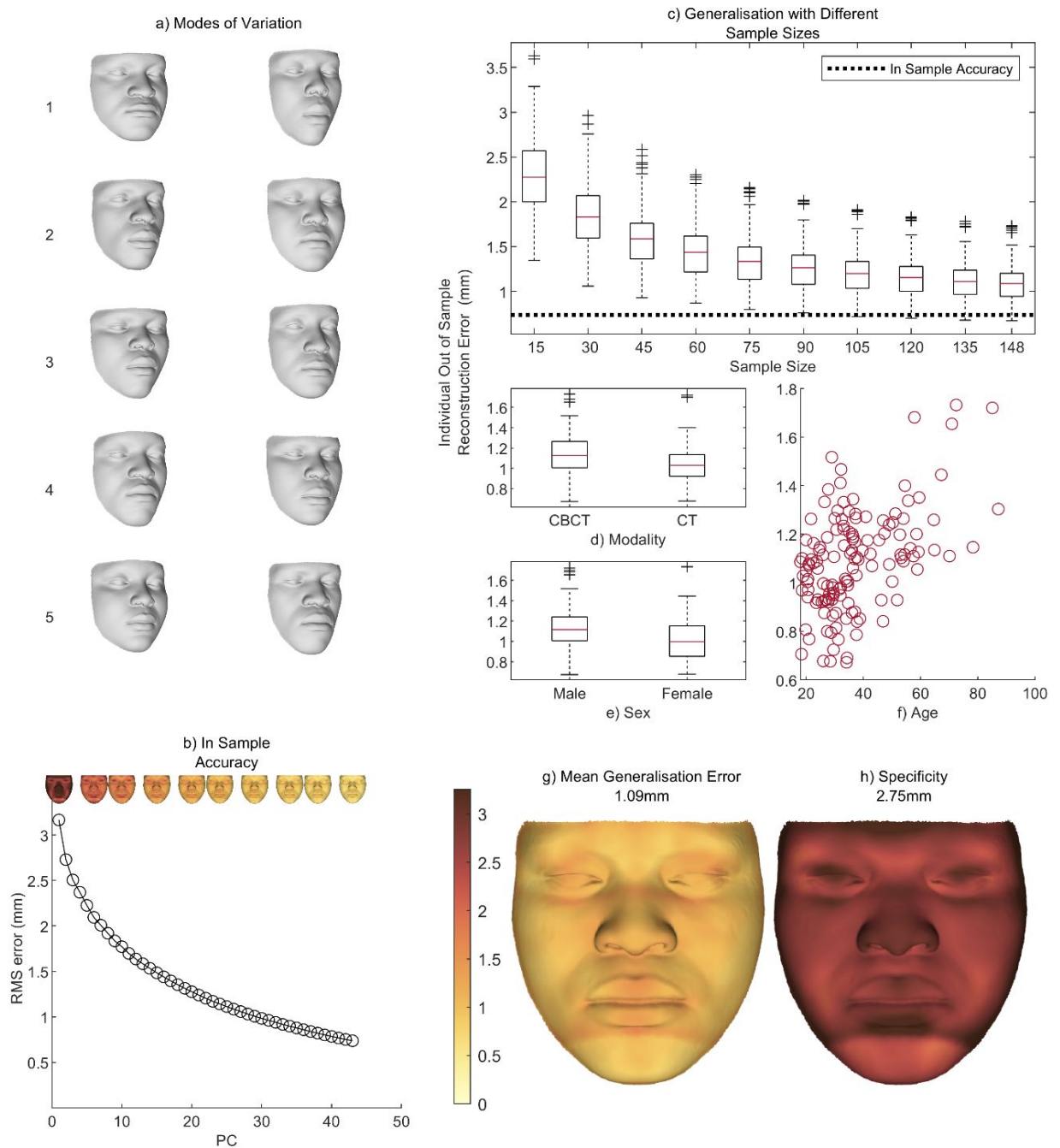


Figure 2: Statistical shape model evaluation. a) The first 5 modes of variation are visualised. b) the In Sample accuracy in terms of the RMSE. c) The individual Out of Sample error for different sample sizes (generalisation). d) e) and f) indicate the Out of Sample error for modality, sex and age. g) The mean generalisation error and h) specificity of the model.

22
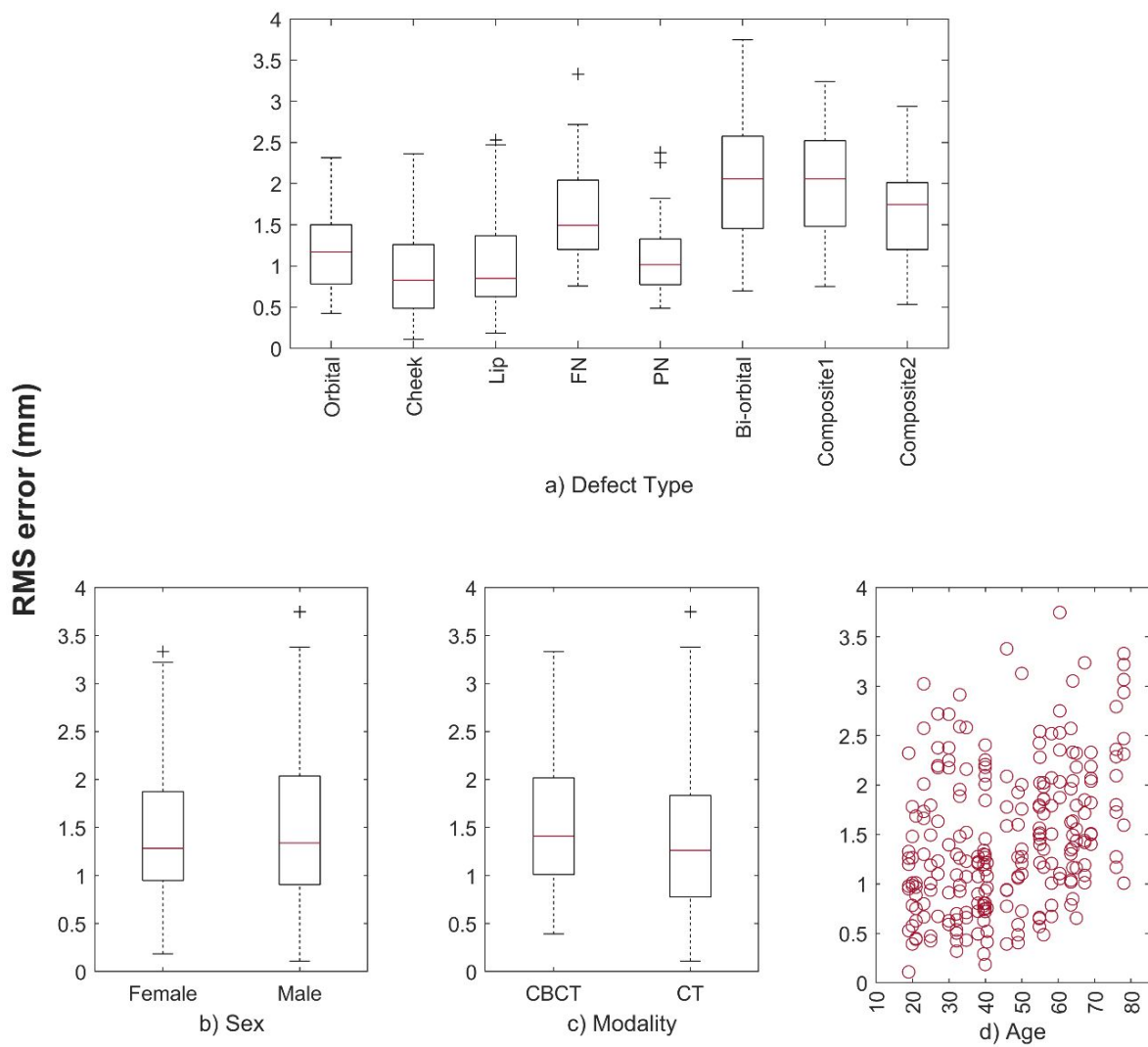
Figure 3: Accuracy of defect reconstructions. a) RMSE for the different classes of defect, b) RMSE according to sex, c) RMSE according to modality and d) RMSE according to age.

23

1
2
3
4
5
6
7
8
9
10
11
12
13
14
15
16
17
18
19
20
21
22
23
24
25
26
27
28
29
30
31
32
33
34
35
36
37
38
39
40
41
42
43
44
45
46
47
48
49
50
51
52
53
54
55
56
57
58
59
60
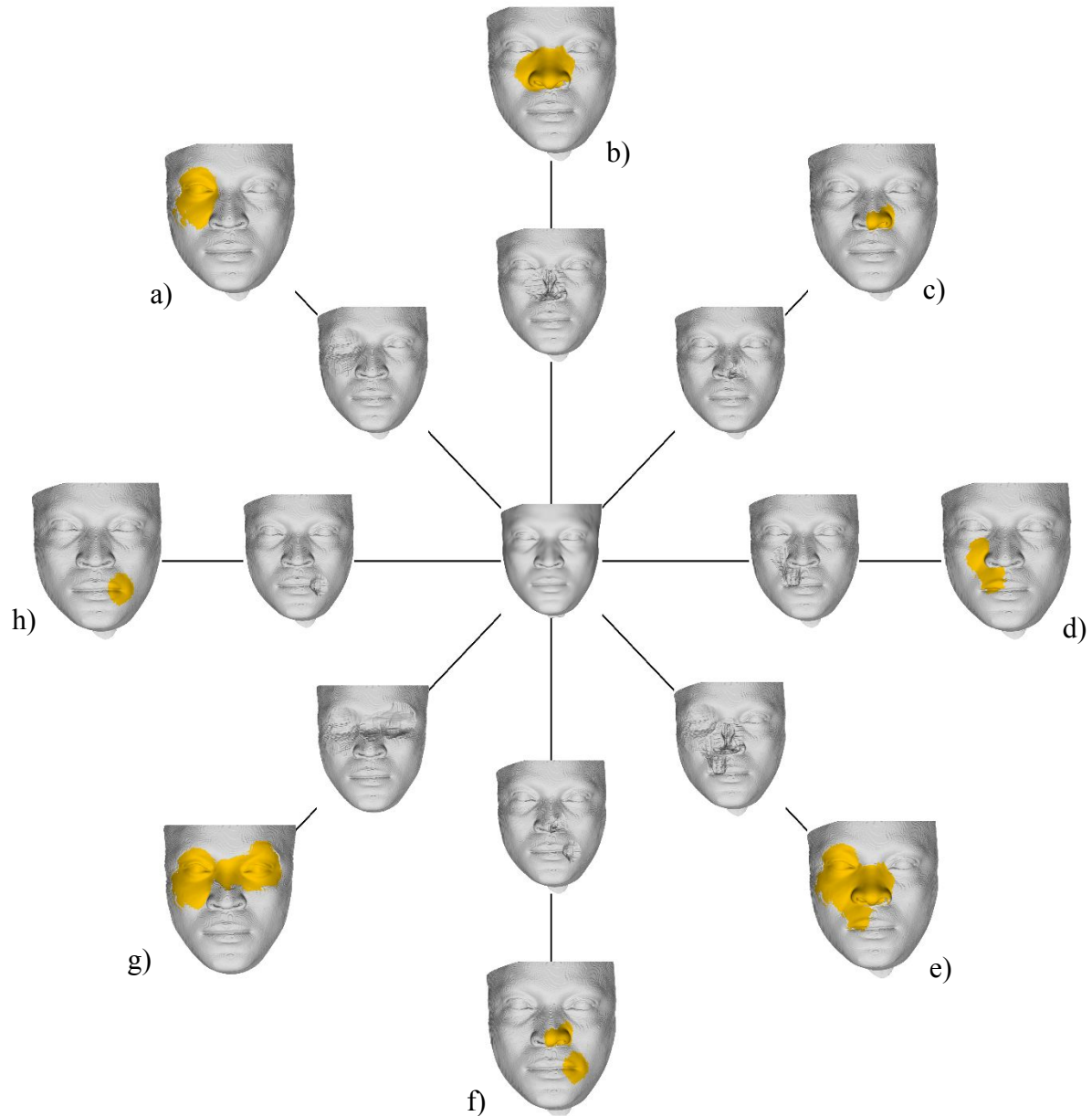


Figure 4: Example of one Individual's defect imputations. The central image is the original non-defective face; the inner ring represents the different defect simulations; the outer ring visualises in orange the defect imputation superimposed onto the defective face. a) Orbital defect, b) Full nose defect, c) Partial nose defect, d) Cheek defect, e) Large (composite 1) defect, f) Small (composite 2) defect, g) Bi-orbital defect and h) Lip defect.

24
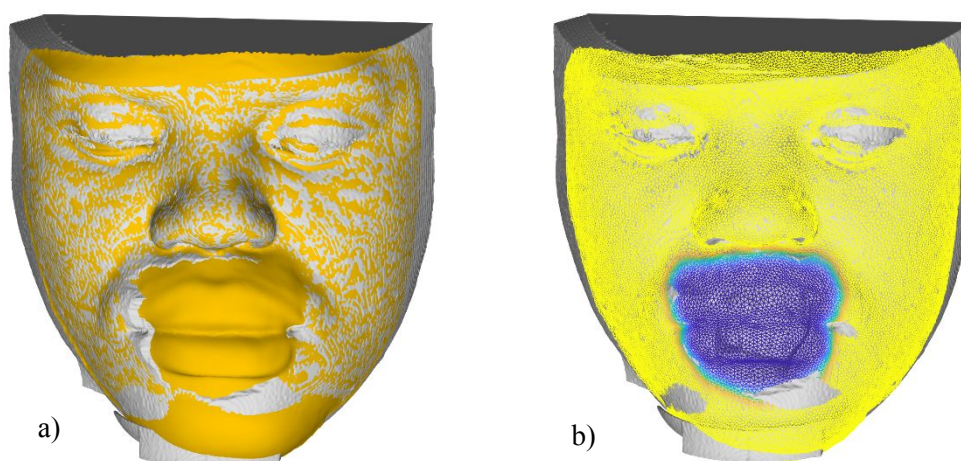
Figure 5: Example of a poor defect imputation of the lips. a) The corners of the mouth and parts of the chin (in grey) are cut off due to defect flags seen in blue in b) being too small.
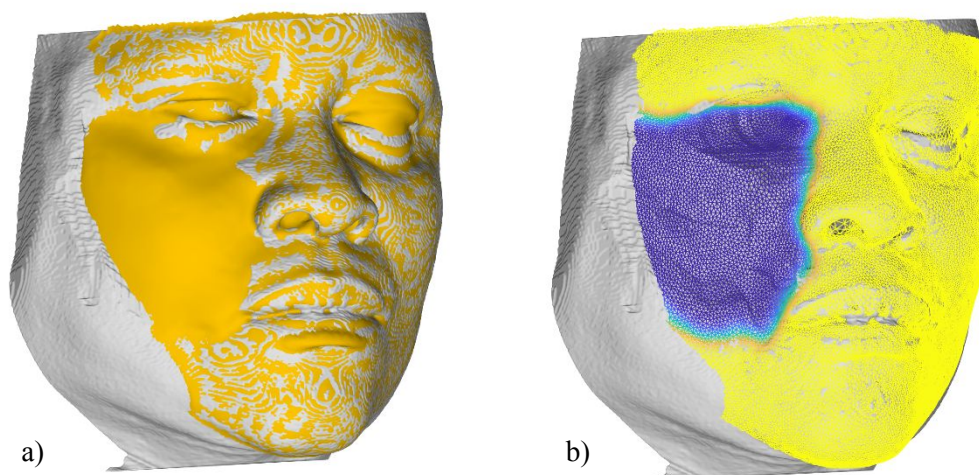


Figure 6: Example of mismatch between the defect imputation region and the original defective face due to the defect extending beyond the borders of the template. a) The imputation (in orange) does not cover the defective region. b) Mapping of the defective scan shows that the template does not capture the entire surface of the face, with the flagged defective region in blue.

25

# Supplementary Information: A statistical shape model for estimating missing soft tissues of the face in a black South African population

**Helene F Swanepoel, MSc** [1] / **Harold Matthews, PhD** [2,3,4] /, **Peter Claes, PhD** [2,3,4,5] / **Dirk Vandermeulen, PhD** [3,5] / **Anna C Oettlé, MD, PhD** [1,6]

## 1. SUPPLEMENTARY METHODS

### 1.1. Statistical shape modelling

#### 1.1.1. Establishing correspondence among facial meshes.

The CBCT and CT scans were collected as Digital Imaging and Communications in Medicine (DICOM) files. These were first transformed into mesh representations of the facial images by importing the volume into MeVisLab,[1] and applying threshold segmentation to segment the soft tissue surface of the face only. In this way, an iso-surface is generated which is then tessellated to create the triangular mesh and exported as a wavefront object (Supplementary text Fig. 2A). Constructing an SSM and imputing missing parts of a shape from it requires that each face be represented by the same number of vertices and that these vertices should correspond across all instances of the shapes. This can be accomplished via a non-rigid registration of a template face onto each mesh. A standard template face (section 1.1.2) is gradually deformed into the shape of the target, imposing onto the target shape its vertices and topology comprising approximately 20 000 dense quasi-landmarks. In general, we use a non-rigid iterative closest point (ICP) framework,[2] which, over multiple iterations, updates both the estimated corresponding (closest) points on the target to the template as well as the non-rigid deformation from the template to the target. Combined with the gradual relaxation

95

of a regularization parameter on the deformation field, this allows the template to gradually become more flexible in its approach to the target. We employ the non-parametric non-rigid ICP registration implemented in the MeshMonk toolbox,[3] (https://gitlab.kuleuven.be/mirc/meshmonk) in MATLAB version R2021b.[4] The approach is non-parametric in that it incorporates no prior model of allowable deformations. In theory, this allows it to deform to any shape, but another impact is that, if the target is too dissimilar from the template, it can run to anatomically implausible solutions and correspondence is then incorrectly established.

To improve the precision of the final registration, the non-rigid ICP was initialized with a landmark-guided non-rigid deformation. Twenty landmarks (Supplementary text Fig. 1) were carefully placed on each target mesh and the template mesh (Supplementary text Fig. 2B). This initial non-rigid deformation was modelled as three thin-plate spline interpolants each predicting the scalar x, y, or z coordinates of the landmarks on the target, from the x, y and z coordinates of the landmarks on the template. Evaluating the interpolants for all points on the template yielded their deformed coordinates. For registration of the defect scans not all landmarks could be placed so the full set of 20 landmarks was reduced to only those that were not on a defective region.

Following initialization, the non-rigid ICP was performed. The MeshMonk framework allows for user-specified regions of the face to be ignored while computing the deformation towards the target. For those participants where the chin was supported by a chin strut or had closed eyes, these regions were ignored in the calculation of the deformation field. Any participants that still failed the registration were excluded and a total of 148 samples were included in the final model.

96
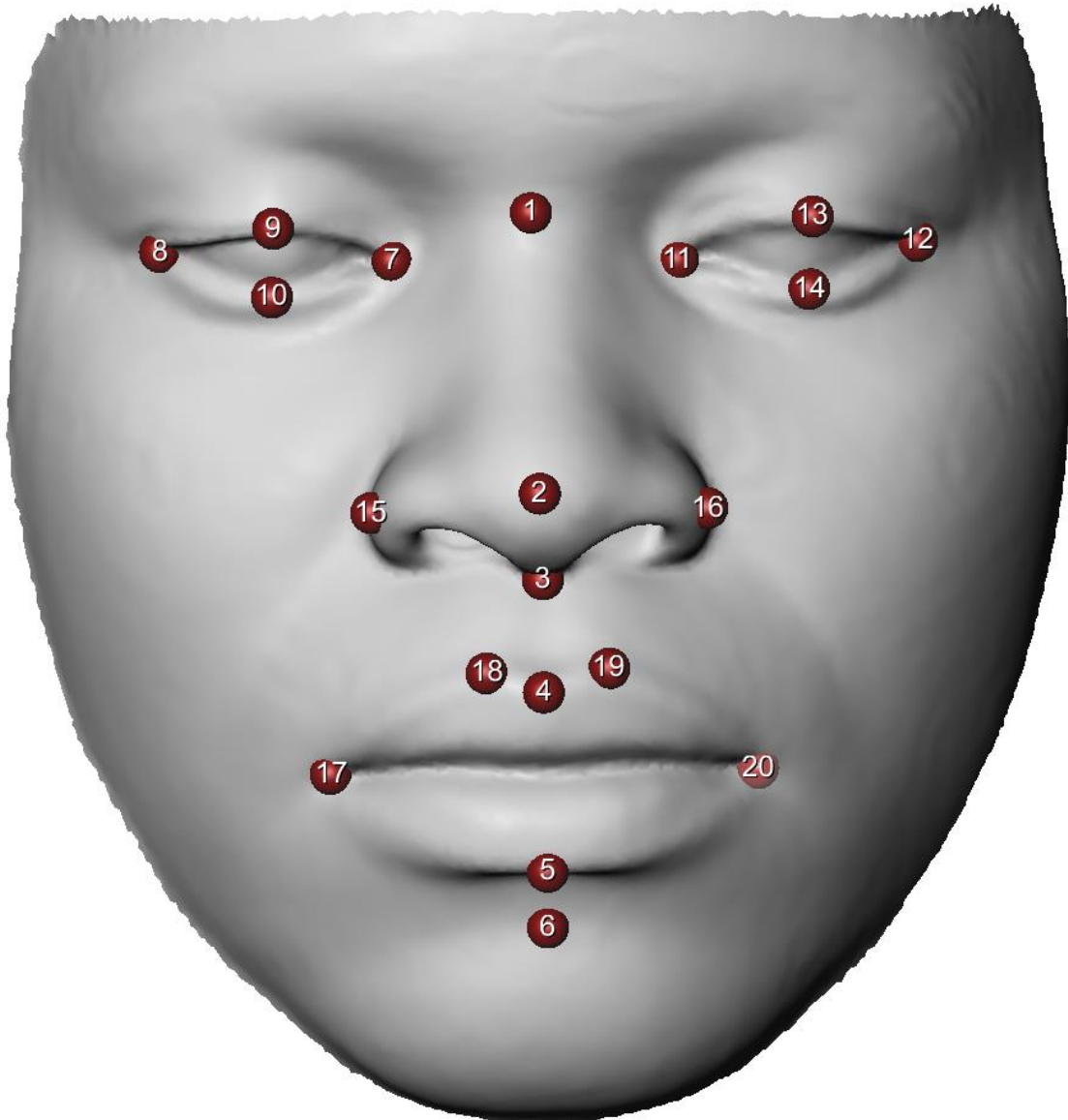
*Supplementary text figure 1: Anatomical landmarks used for initialization during mapping.*

*1. Nasion 2. Pronasale 3. Subnasale 4. Labiale superius 5. Labiale inferius 6. Sublabiale 7.*

*Endocanthion (right) 8. Exocanthion (right) 9. Upper lid (right) 10. Lower lid (right) 11.*

*Endocanthion (left) 12. Exocanthion (left) 13. Upper lid (left) 14. Lower lid (left) 15. Alare (right)*

*16. Alare (left) 17. Cheilion (right) 18. Christa philtre (right) 19. Christa philtre (left) 20. Cheilion*
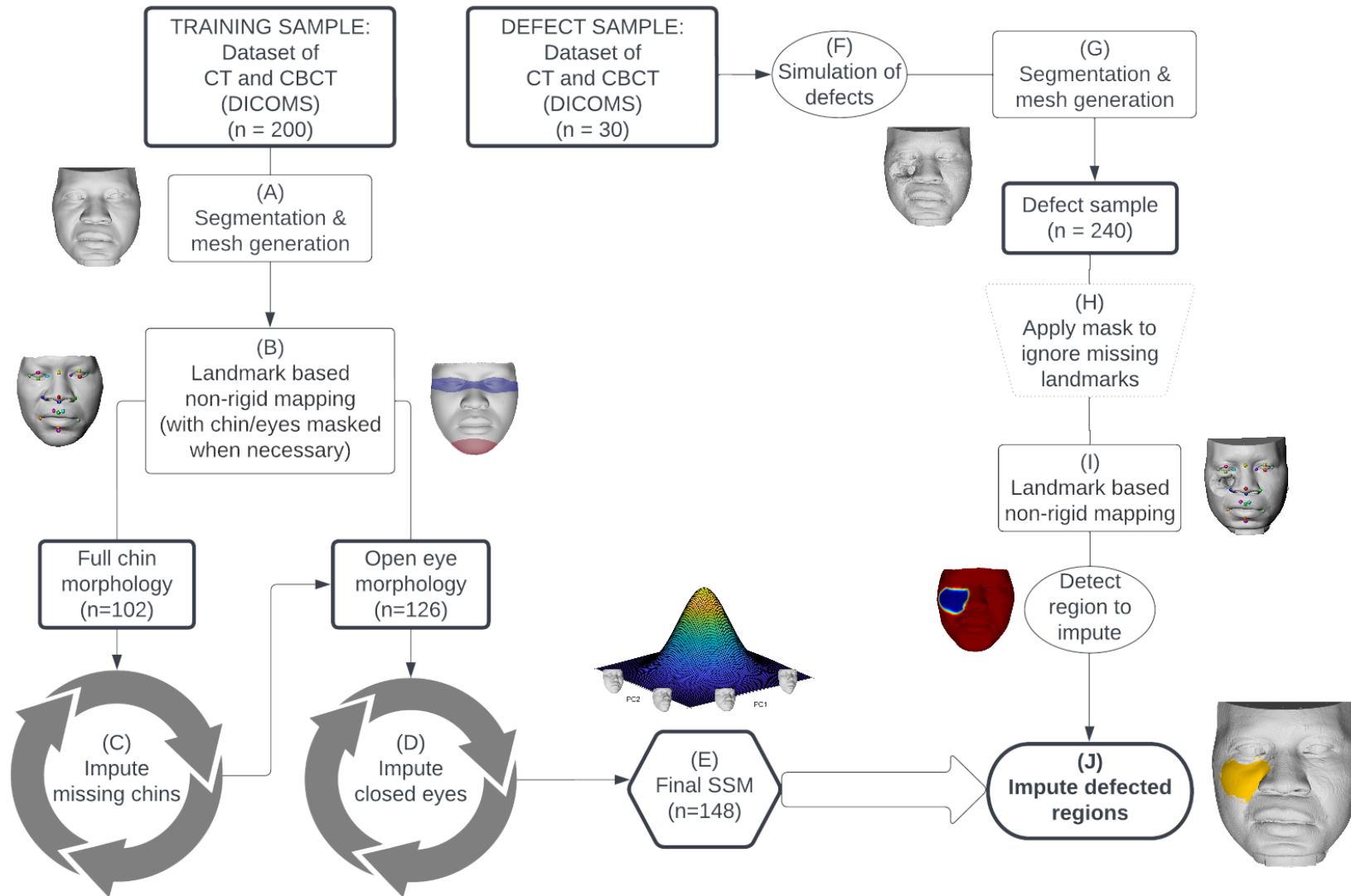
*(left)*

*Supplementary text figure 2: Methodology overview. The left side of the figure shows the steps involved in generating the statistical shape model used to estimate missing regions of the defective face. The right side of the figure shows the steps involved in creating a sample of simulated defects, mapping the defective sample, and using the SSM to estimate the defective regions. (A) A training set of DICOMS was segmented and the resulting iso-surface of the soft tissue face was tessellated into meshes for further processing. (B) To achieve correspondence, a set of 20 landmarks was placed on the meshes and a standard facial template. Non-rigid mapping was conducted in the MeshMonk toolbox to ensure a standardized topology across all meshes. (C) and (D) An iterative bootstrapping approach was followed to estimate chins and eyes for samples without complete chin morphology or with closed eyes and sequentially added to the SSM. (E) The final SSM was generated by calculating the modes of variation (through Principal Component Analysis) for the total sample including open-eye and chin estimations. (F) Six classes of facial defects were simulated using the Avizo software. (G) Defect faces were segmented and tessellated into meshes for further processing. (H) Missing landmarks due to defect regions were masked from the subsequent mapping during (I) by assigning 'target flags'. (J) The defect regions were estimated using the SSM by the same process used to estimate the chins and eyes in (C) and (D) and visualized in the context of the original unprocessed defective mesh.*

### 1.1.2. Construction of the standard template

One of the sample meshes was selected that showed clear and crisp details and had open eyes and full chin morphology. The mesh was trimmed to shape and resampled to ensure an even distribution of vertices using the isotropic explicit re-meshing tool in Meshlab.[5] Each mesh in the training sample was brought into correspondence with the resampled template mesh using the same method described in section 1.1.1 above. Once correspondence was achieved, the average face of an SSM was generated as described in section 1.1.3 below. Three iterations of mapping for each of the faces in the training sample with complete chin morphology and open eyes (n = 41) were completed using the average face as template, with the template being updated continuously. The final average face was used as the standard template for all further steps. Figure 3 shows the final standard template used in this study.



*Supplementary text figure 3: Standard facial template obtained by using a bootstrapping approach and used for correspondence throughout the study.*

### 1.1.3. Model building

The mixed nature of the data (i.e., some with complete chin morphology, some with chin struts, some with open eyes and some with closed eyes) presented a particular challenge.

100

This was addressed by following a bootstrapping approach in which those with incomplete morphology were first estimated and added to the model sequentially. Given a sample of shapes represented by the same landmarks, the SSM was built as follows. Firstly, only samples with complete chin morphology were included to generate the first version of the SSM. Non-shape-related variation is removed by generalized Procrustes analysis (GPA) which aligns all landmark configurations onto the sample mean and scales all configurations to unit size. Over multiple iterations, each face is aligned to the mean configuration via a rigid scaled least-squares Procrustes alignment. Following this, the mean configuration is re-calculated. To minimize the influence of the chin region for those scans including the chin support we used a weighted least-squares Procrustes superimposition with weights of zero assigned to the chin region and ones assigned to all other points. Similarly, the mean configuration is the weighted mean configuration, employing the same weights. The first version of the model was used to estimate (see next paragraph below) the chins of samples where these features were missing or unusable (Supplementary text Fig. 2C). A second version of the SSM was then generated including all the complete and estimated chins, as well as all samples with open eyes (Supplementary text Fig. 2D). We again used a weighted least-squares Procrustes superimposition, this time with weights of zero assigned to the eye region and ones assigned to all other points. This version of the SSM was used to estimate the eyes of the samples with closed eyes. Finally, the SSM was updated to include all samples (Supplementary text Fig. 2E). Each SSM was created by principal components analysis (PCA) of the GPA-aligned landmarks. An SSM comprises modes of variation or PCs, which each correspond to a linear transformation of facial shape, as well as the normal range variance along each mode together defining multinormal parameterization of shape variation. The modes of variation

101

were calculated (through Principal Component Analysis) by a singular value decomposition of the n (observations) by 3k(k landmarks) matrix.

To estimate user-identified missing parts of the face, the vertices to be estimated are assigned weights of zeros and those to remain unchanged are assigned a value of one. To avoid discontinuities in the final result the weights are smoothed with 10 iterations of Laplacian smoothing. Alignment and scaling to the model average, followed by a weighted fit to the SSM is accomplished as described by Matthews et al.[6] to estimate the linear combination of the modes of variation that most closely approximates the face in a weighted least-squares sense. In essence, the linear combination is such that it aims to correctly reconstruct the parts of the face with high weighting while ignoring the regions of low weighting, as a result, the regions of low weighting are simply filled in with the most likely shape given the regions of high weighting. The estimated 'weighted fit face' can then be reconstructed by evaluating the linear combination. The weighted fit face is then returned to the coordinate system and the size of the face prior to the estimation. The final estimated face is created by blending the face before estimation with the weighted fit face as the weighted sum of the two landmark configurations, with the original face weighted according to the weights described above and the weighted fit face weighted according to 1 minus the weights.

### 1.1.4. Model evaluation

We evaluated the model's representation of the target population by calculating its generalization and specificity. In principle, both of these properties contribute to the ability of the model to realistically estimate missing parts of the face. All these computations require the calculation of inter-shape distances. To avoid the chin and eye regions influencing these

102

calculations where it is not informative, weights of zero were assigned to these regions. The inter-shape distance was then calculated as the weighted root mean squared (RMS) distance between the two shapes. Generalization represents how well the model can represent realistic faces not used in training and can also be interpreted as the mean of the average reconstruction error between the model and an unseen shape,[7] or the out-of-sample reconstruction error of the training data. The reconstruction error is calculated as the difference between the face and the reconstruction of that face from their projections onto the modes of variation. It was calculated by sequentially holding each face out of the training of the SSM and then estimating their 'weighted fit face' from the model and calculating the inter-shape distance between the two. The average of all these inter-shape distances is the model generalization. In-sample accuracy is computed identically to the generalization, except that the face is not held out from training the model. The in-sample accuracy for a given number of modes constitutes the lower bound of what is the possible generalization error and calibrates the interpretation of the generalization.

Model specificity concerns the ability of the SSM to represent only realistic or valid faces. This is calculated by randomly simulating 1000 faces by randomly sampling linear combination coefficients from their multivariate Gaussian distribution and reconstructing the corresponding faces. The verisimilitude of each simulated face is calculated as the inter-shape distance to the most similarly shaped face from the training sample. Both generalization and specificity were calculated using SSMs trimmed to only the modes of variation that explained up to 96% of the variation in the sample. To express model specificity, generalization and in-sample accuracy in mm units, before calculating the inter-shape distance, the simulated shapes and weighted fit shapes were scaled to the size of the face to which they were being

103

compared. This is weighted to ignore estimated areas such as the chin and eyes where applicable.

Whether the model could be improved by collecting further data was assessed by evaluating how generalization evolves when gradually more and more data are added up to the available amount. Specifically for 10 repetitions, 15 samples were randomly chosen to train an SSM and iteratively 15 subjects are randomly selected and added to the model training data up to the total sample size. At each iteration, the distribution of the average error values over the 10 repetitions was plotted as boxplots (Supplementary text Fig. 6c).

### 1.2. Simulation of facial defects

Facial defects included only extra-oral defects. These were classed into six groups and simulated on a sample of 30 open-eyed faces using the Avizo® v. 8.0.0 software.[8] A total of 240 defect instances were simulated (30 faces x 8 simulations per face). The classes and their descriptions are represented in *Supplementary Table 1.*

Sample volumes were imported into the Avizo and visualized in three planes. Essentially, the voxels corresponding to each defect must be deselected (Supplementary text Fig. 2F). Firstly, the entire head was selected by thresholding and exported as a DICOM stack. The labels were then edited manually in Avizo to deselect the defective regions to be removed (Supplementary text Fig. 4 a) and each set of labels, corresponding to each defect class 1-5 was again exported as a DICOM stack. For class 1-5 defects, the labelled DICOM stacks were each individually imported into MeVisLab, an iso-surface was generated, tessellated into a mesh and exported as a wavefront object (Supplementary text Fig. 2G) (Supplementary text Fig. 4 b). For class 6 combination defects, we imported labels for the entire head and for all

104

class 1-5 defects into MeVisLab at the same time. Defects were combined for an individual by taking the intersection of labels from a selection of class 1-5 defects and tessellating the resulting isosurface of the intersection. Three selections were done per individual. The first selection simulated bi-orbital defects, where both the right and left orbits were involved, the second selection (composite 1) simulated a large defect involving three facial features (e.g., orbital, cheek, and lips etc.), while the third selection (composite 2) simulated smaller defects only involving two features (e.g., orbital & full nasal, or partial nasal and cheek etc.).

To establish correspondence for the meshes in the defect sample a modification of the process as described in section 1.1.1 above was used. Landmarks that could not be placed on the defect scan were not used to estimate the landmark-guided non-rigid initialization (Supplementary text Fig. 2I). Points corresponding to the defect region of the scan (section 1.3) were ignored by assigning 'target flags' to MeshMonk's ShapeMapper (Supplementary text Fig. 2H).

105
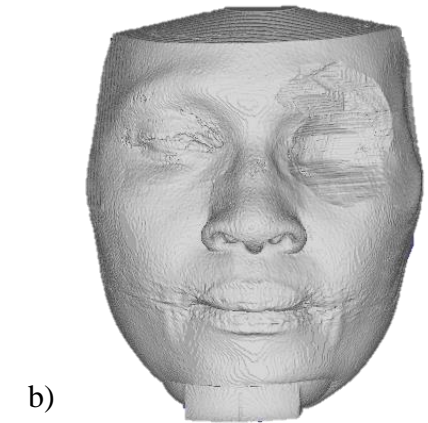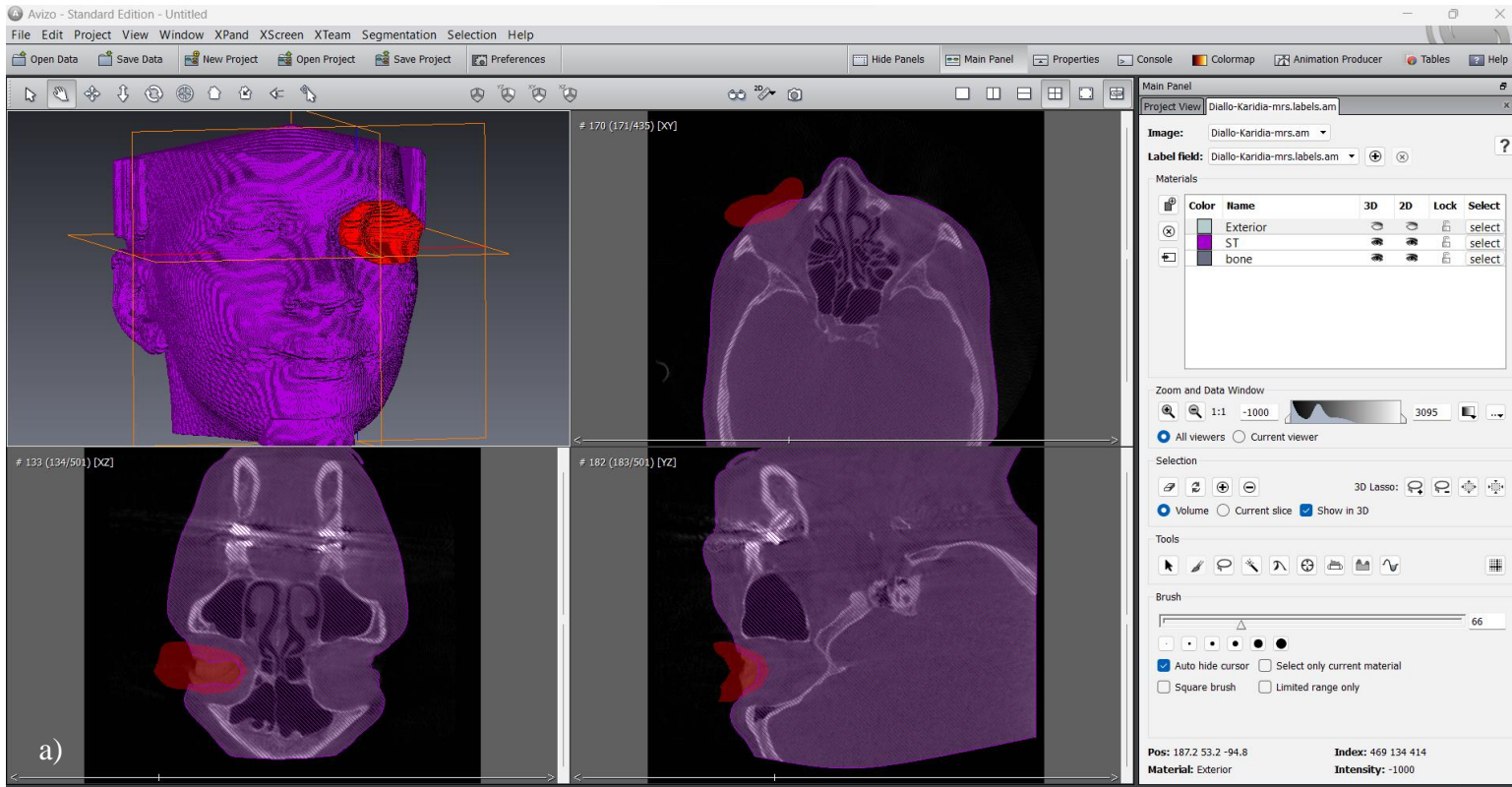
*Supplementary text figure 4: Simulating the defective region on Avizo 8.0.0. a) A label field was created from which voxels corresponding to a defect were deselected and the remainder exported as a DICOM stack, which was then b) imported into MeVisLab to visualize the isosurface of the defective face.*

### 1.3. Estimation of facial defects

The same process to estimate defects was followed as described above for imputing the chins and eyes used in the SSMs, the only difference being that the weights were applied to the defective region, instead of the chin or eye regions. Supplementary text Fig. 5 shows how the defective regions were identified by isolating the vertices corresponding to the defect on the unmapped isosurface of the defective face using MeVisLab. The defective regions were then transferred onto the registered version of the face by flagging the closest points on the mapped mesh that corresponds to the defective region. The final SSM was used to estimate the linear combination of the modes of variation that most closely approximates the intact regions of each face and estimated the missing regions using a weighted projection onto the modes of variation (section 1.1.3). The face reconstructed from these projections was blended with the mapped version of the defective face by smoothing the flagged points to blend in with the surrounding areas. This result is the mapped version of the defective face with vertices of the defective region substituted with those of the weighted fit face. The estimated region was then visualized and interpreted in the context of the original unprocessed defective mesh (Supplementary text Fig. 2J).

In the future, the manual selection of points to be estimated can be executed via several methods, for example, using an interactive brush tool to select points (https://github.com/harrymatthews50/MeshEditor).
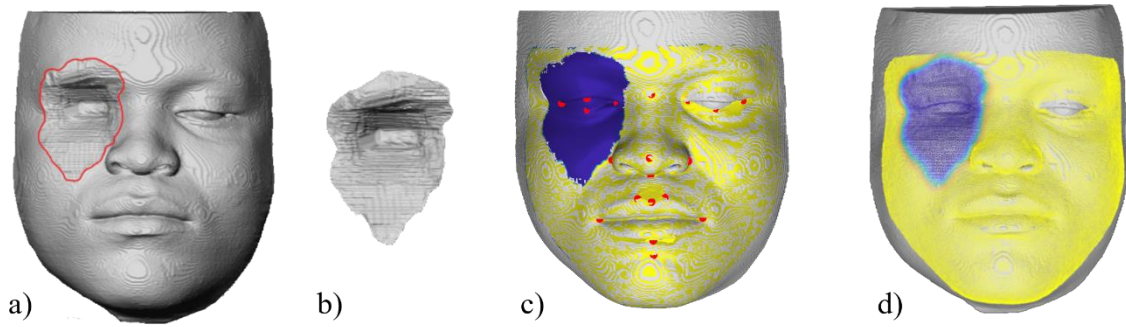
*Supplementary text figure 5: a) Identifying the defective region. b) The vertices corresponding to the defective region were isolated by removing the rest of the isosurface (areas not part of the defective region) in MeVisLab. c) The closest points corresponding to the defective region are transferred onto the mapped version of the face and weighted 0 during the estimation (dark blue). d) Selected points are smoothed to blend in with the surrounding area.*

## 2.1. Model evaluation

Forty-three modes of variation were required to model 96% of the shape variation and were retained. The first 5 modes of variation are shown in Supplementary text Fig. 6 a. Video representations of the first 5 modes of variation can be viewed in the Supplementary Materials (supplementary video files 1 to 5). The first mode of variation, responsible for the most variation, predominantly represents total facial height and width, with changes in the length of the maxillary alveolar processes, mode 2 relates to midfacial projection with changes in the zygomatic width, mode 3 represents primarily variability in upper facial height and nose height. In mode 4, the depth of the eyes is influenced by the zygomatic width and frontal area bossing and mode 5 relates to maxillary and mandibular protrusion.

Supplementary text Fig. 6 c displays the distributions of out-of-sample reconstruction errors corresponding to various training sample sizes. As the model generalization error decreases with increasing sample size, the model better represents the population. As the curve is reaching a plateau, the errors as a function of the sample size are decreasing very slowly. This indicates that beyond the current sample size, a large number of additional participants would result in only an incremental improvement to the model. No difference in out-of-sample reconstruction error was observed between imaging modality (Supplementary text Fig. 6 d) or sex (Supplementary text Fig. 6 e) and age (Supplementary text Fig. 6 f). In Supplementary text Fig. 6 g and h, the weighted RMS per point is also shown as a color map for mean generalization and specificity. The mean generalization error was 1.09 mm (Supplementary text Fig. 6 g). Specificity, the model's ability to represent only valid or realistic faces, resulted in a mean error of 2.75 mm (Supplementary text Fig. 6 h). Regions of slightly higher errors include the eyelids, nose bridge, and lips (Supplementary text Fig. 6 g and h).
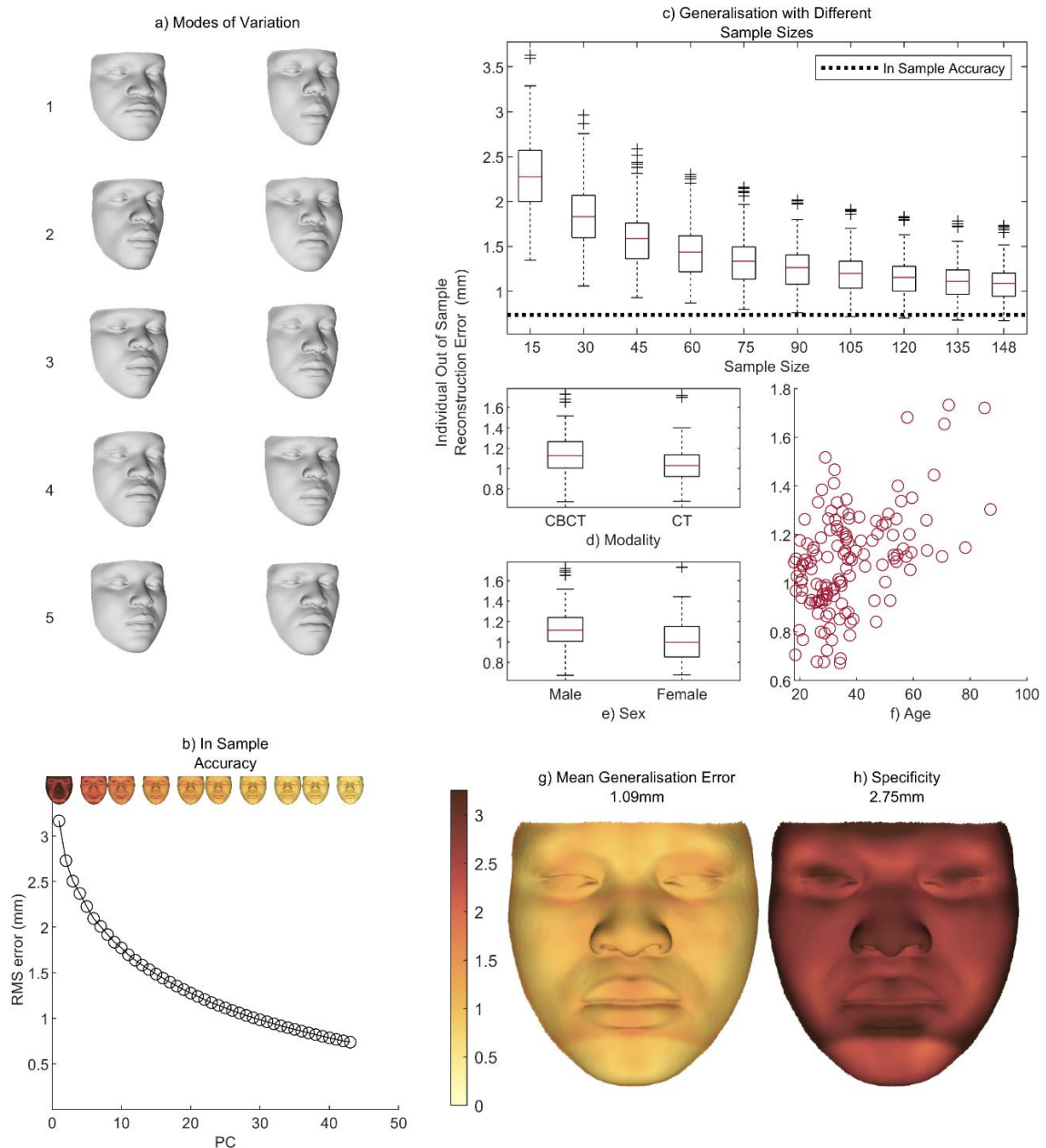
*Supplementary text figure 6: Statistical shape model evaluation. a) The first 5 modes of variation are shown. b) The In-sample accuracy in terms of the RMSE shows the lower bound of the possible generalization error and calibrates the interpretation of the generalization for a given number of modes. c) The individual Out of Sample error for different sample sizes (generalization) indicates that beyond the current sample size, a large number of additional participants would result in only an incremental improvement to the model. d) e) and f)*

*indicate the Out of Sample error for modality, sex and age and showed no differences in the reconstruction error. g) A color map of the mean generalization error shows an acceptable error of 1.09 mm and h) a color map of the specificity of the model indicates a mean error of 2.75 mm.*

### 2.2. Qualitative defect evaluation

In approximately 38% of cases, visual inspection of the defect estimations showed that the defect was not smoothly blended with the surrounding tissue. Supplementary text Fig. 7 b shows the weightings used in one case for blending the weighted-fit face to the defective face. Deep blue regions were completely estimated whereas yellow regions were not, and are expected to match the target face perfectly. For areas colored in-between yellow and deep blue, the shape is a weighted combination of the face estimated from the SSM and the target face and as such may not match the target face perfectly. Essentially the mismatch between the two surfaces is because the region selected for estimation extends beyond the true defective region. The scope of the estimated region is determined by both the manual selection of points to define initial binary weights and the number of smoothing passes applied to these initial weights. This smoothing is necessary for even blending, but it also blurs and effectively extends, the boundary of the selected region (section 1.3).
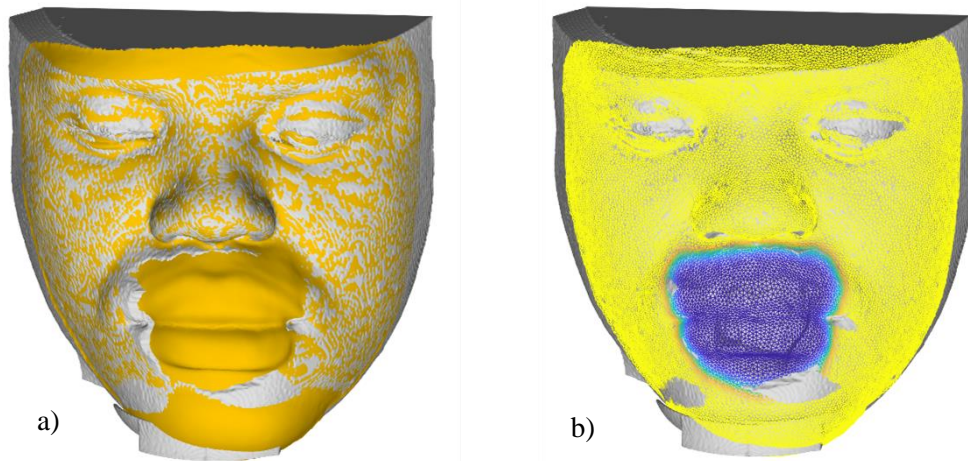
*Supplementary text figure 7: Example of a poor defect estimation of the lips. a) The corners of the mouth and parts of the chin (in grey) are cut off due to the flagged defective region seen in blue in b) being too small.*

## 3. SUPPLEMENTARY TABLES

*Supplementary Table 1: Classification of facial defects according to facial feature involvement*

| Class | Description |
|---|---|
| 1. Orbital | Defects of the eye and orbit: including the globe, extraocular muscles, eyelashes, and at least part of the eyelids, orbital fat, and periorbita as seen in orbital exenteration |
| 2. Cheek and upper lip | Defects of the soft tissue and bony tissue, or soft tissue only, of maxillary and zygomatic regions, including the upper lip. May extend into the maxillary sinuses. |
| 3. Lips or isolated lower lip | Defects of the soft tissue and bony tissue, or soft tissue only, of mental and mandibular regions, involving the lower lip alone, or both upper and lower lips |
| 4. Full nasal | Defects of the entire soft tissue (and cartilaginous) nose |
| 5. Partial nasal | Defects involving only parts of the soft tissue (and cartilaginous) nose e.g., ala and columella only |
| 6. Combined | Defects involving more than one facial feature in 3 assorted combinations (bi-orbital, large and small), e.g., both eyes; orbital, cheek, and full nose; partial nose and lips etc. |

*Supplementary Table 2: ANOVA for the effects of defect type, imaging modality, sex and age on the RMSE*

| | Sumsq | Meansq | NumDF | DenDF | Statistic | p-value |
|---|---|---|---|---|---|---|
| Defect type | 40.194 | 5.742 | 7 | 203 | 27.030 | <0.001 |
| Modality | 0.433 | 0.433 | 1 | 26 | 2.036 | 0.165 |
| Sex | 0.200 | 0.200 | 1 | 26 | 0.942 | 0.341 |
| Age | 3.601 | 3.601 | 1 | 26 | 16.950 | <0.001 |

113

## 4. SUPPLEMENTARY FIGURES
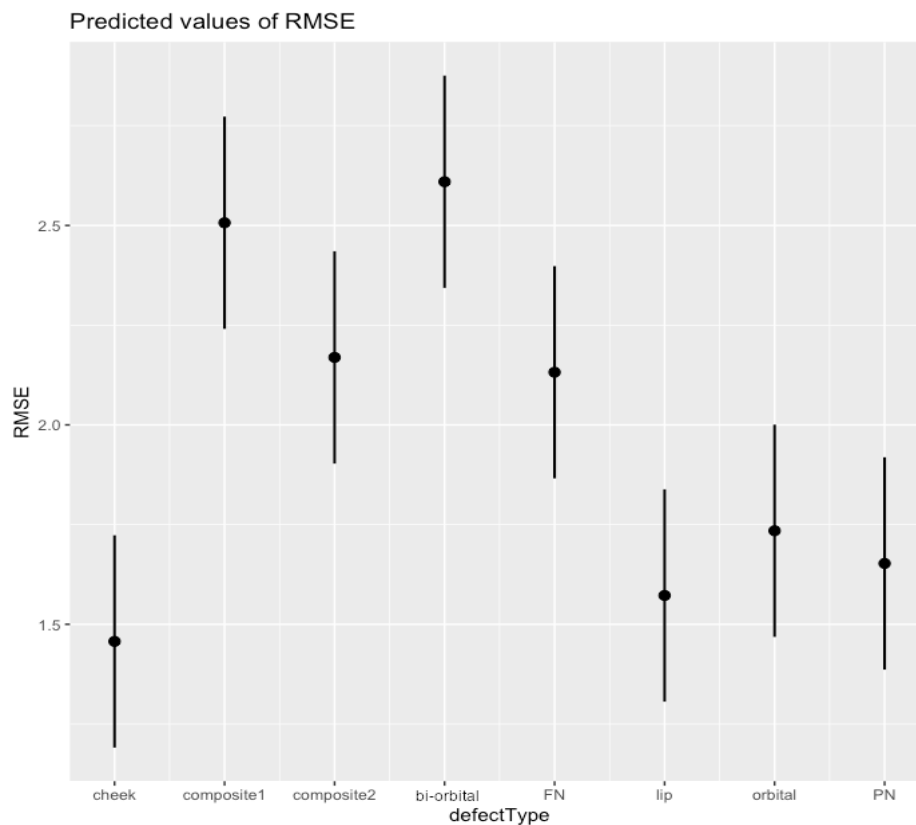


*Supplementary figure 1: The expected RMSE values and 95% confidence intervals of the expectation for each defect type. As can be seen, these can be grouped into two distinct groups: composite, bi-orbital and full nose defects; and individual feature defects (cheek, lip, orbital and partial nose defects).*
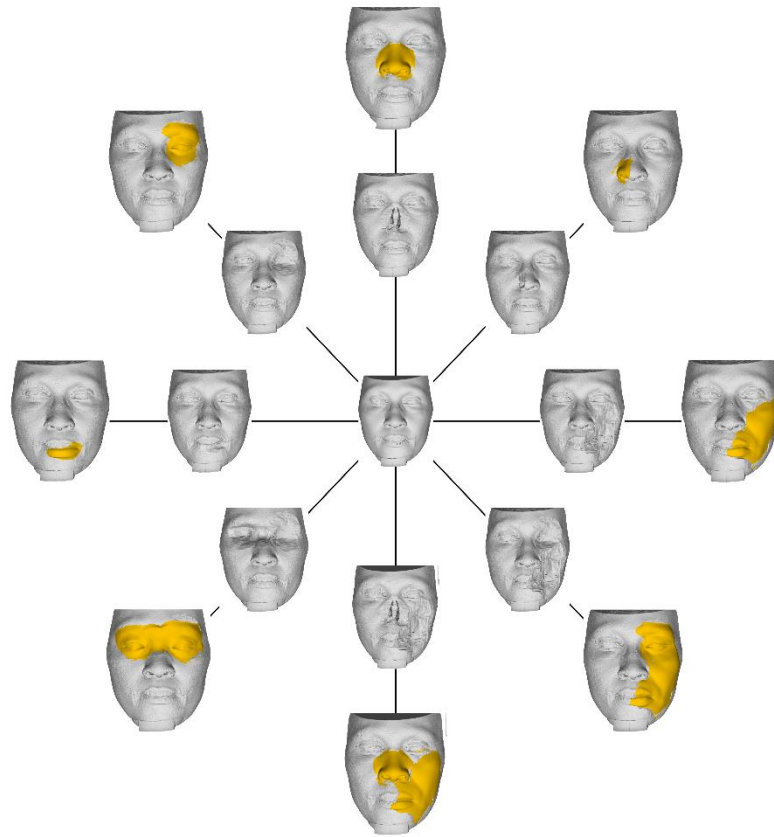
*Supplementary figure 2: Individual 1 defect estimations. The central image is the original non-defective face; the inner ring represents the different defect simulations; the outer ring shows in orange the defect estimation superimposed onto the defective face, from the top in a clockwise direction: Full nose defect, partial nose defect, cheek defect, large (composite 1) defect, small (composite 2) defect, bi-orbital defect, lip defect and orbital defect.*
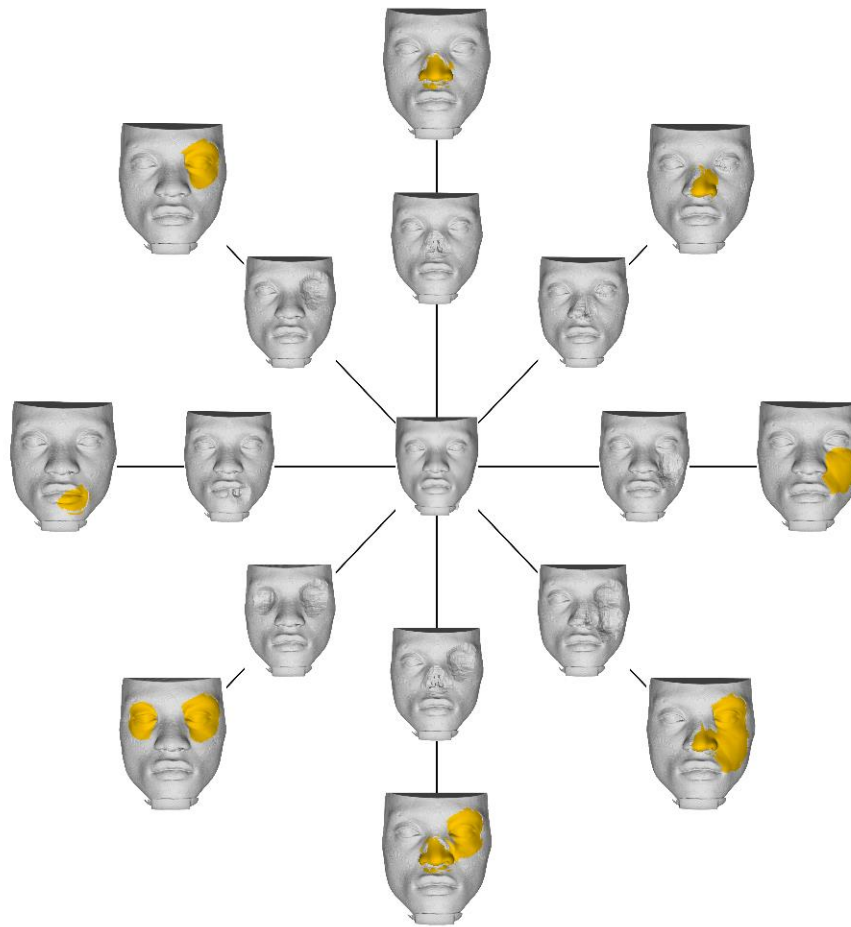
*Supplementary figure 3: Individual 2 defect estimations. The central image is the original non-defective face; the inner ring represents the different defect simulations; the outer ring shows in orange the defect estimation superimposed onto the defective face, from the top in a clockwise direction: Full nose defect, partial nose defect, cheek defect, large (composite 1) defect, small (composite 2) defect, bi-orbital defect, lip defect and orbital defect.*
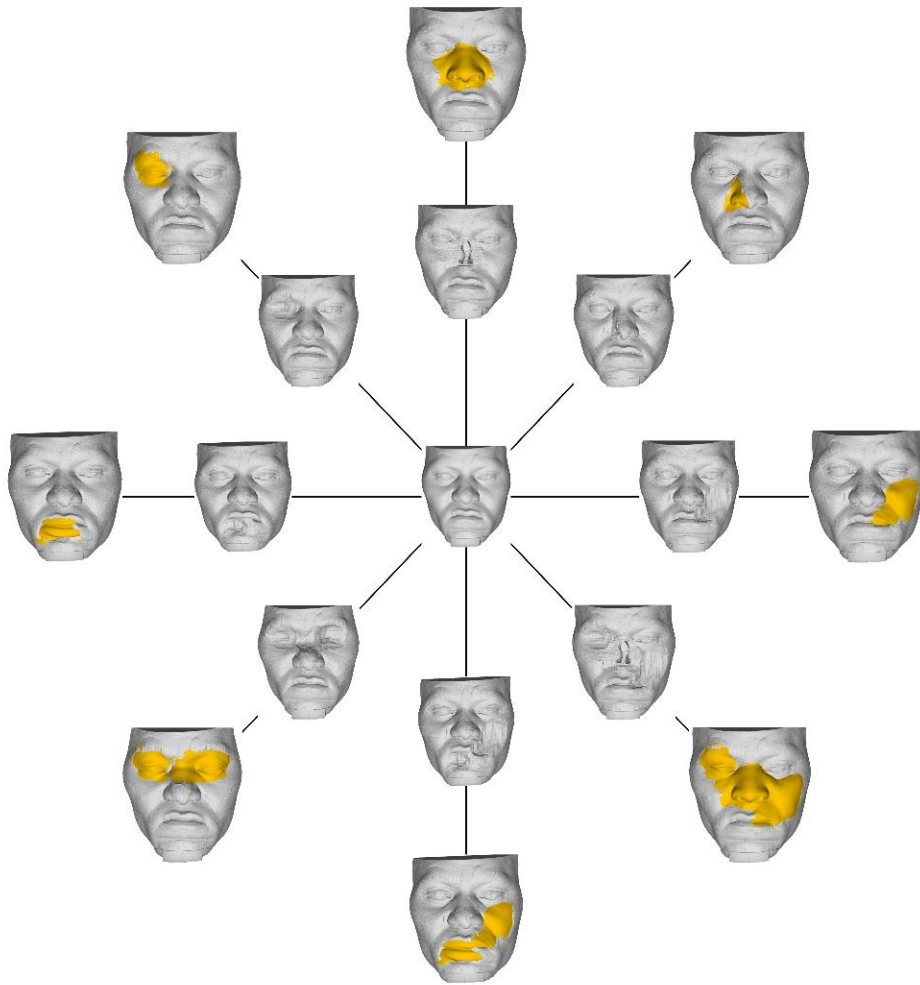
*Supplementary figure 4: Individual 3 defect estimations. The central image is the original non-defective face; the inner ring represents the different defect simulations; the outer ring shows in orange the defect estimation superimposed onto the defective face, from the top in a clockwise direction: Full nose defect, partial nose defect, cheek defect, large (composite 1) defect, small (composite 2) defect, bi-orbital defect, lip defect and orbital defect.*
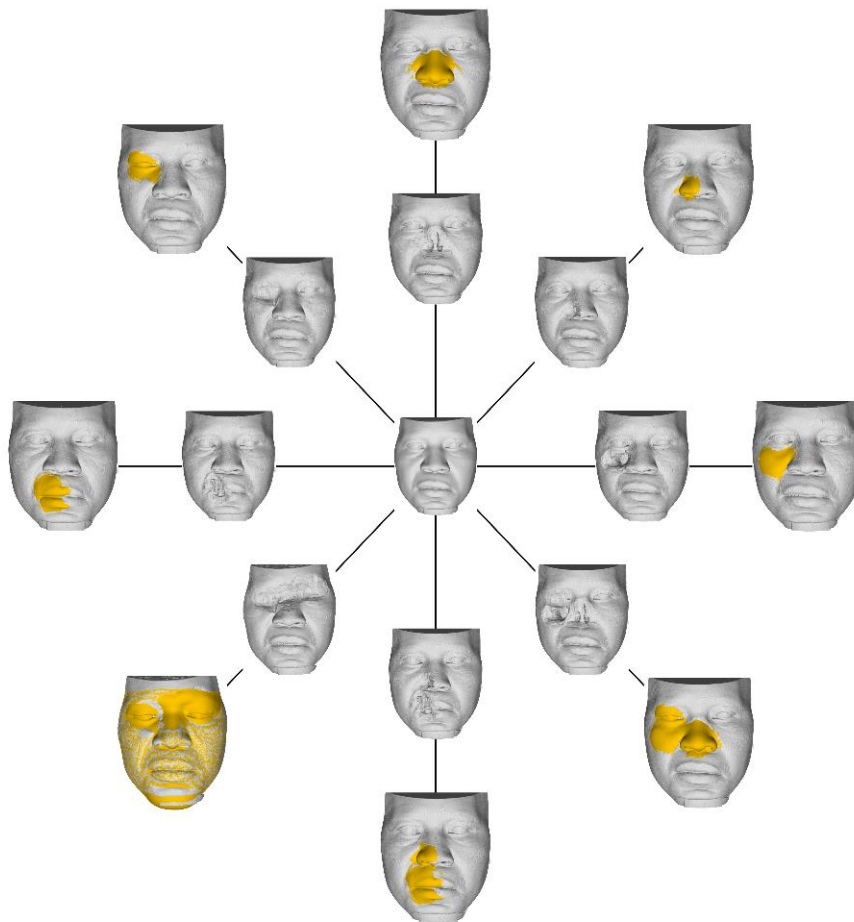
*Supplementary figure 5: Individual 4 defect estimations. The central image is the original non-defective face; the inner ring represents the different defect simulations; the outer ring shows in orange the defect estimation superimposed onto the defective face, from the top in a clockwise direction: Full nose defect, partial nose defect, cheek defect, large (composite 1) defect, small (composite 2) defect, bi-orbital defect, lip defect and orbital defect.*
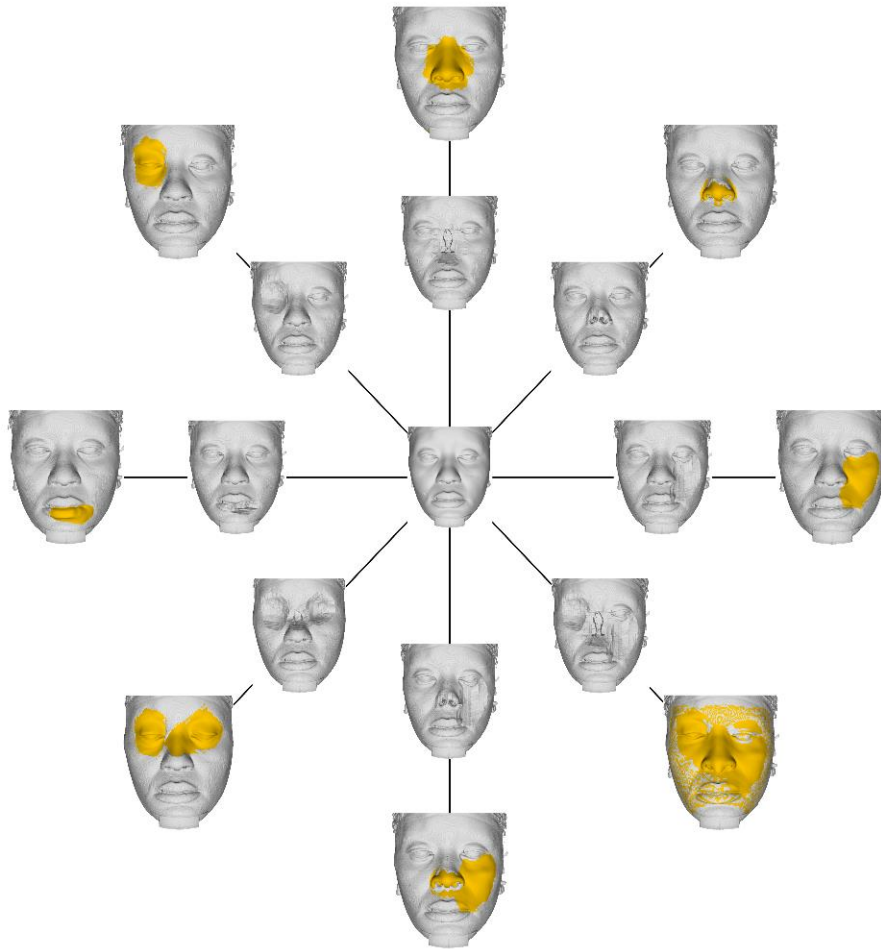
*Supplementary figure 6: Individual 5 defect estimations. The central image is the original non-defective face; the inner ring represents the different defect simulations; the outer ring shows in orange the defect estimation superimposed onto the defective face, from the top in a clockwise direction: Full nose defect, partial nose defect, cheek defect, large (composite 1) defect, small (composite 2) defect, bi-orbital defect, lip defect and orbital defect.*
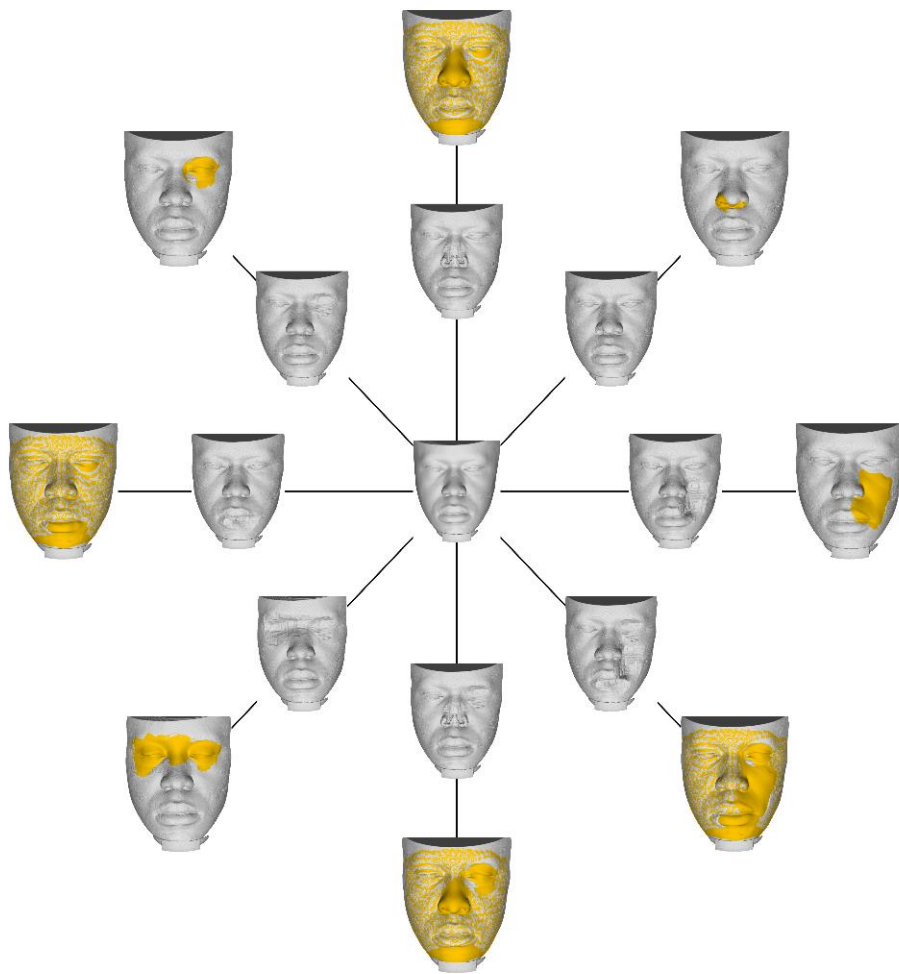
*Supplementary figure 7: Individual 6 defect estimations. The central image is the original non-defective face; the inner ring represents the different defect simulations; the outer ring shows in orange the defect estimation superimposed onto the defective face, from the top in a clockwise direction: Full nose defect, partial nose defect, cheek defect, large (composite 1) defect, small (composite 2) defect, bi-orbital defect, lip defect and orbital defect.*
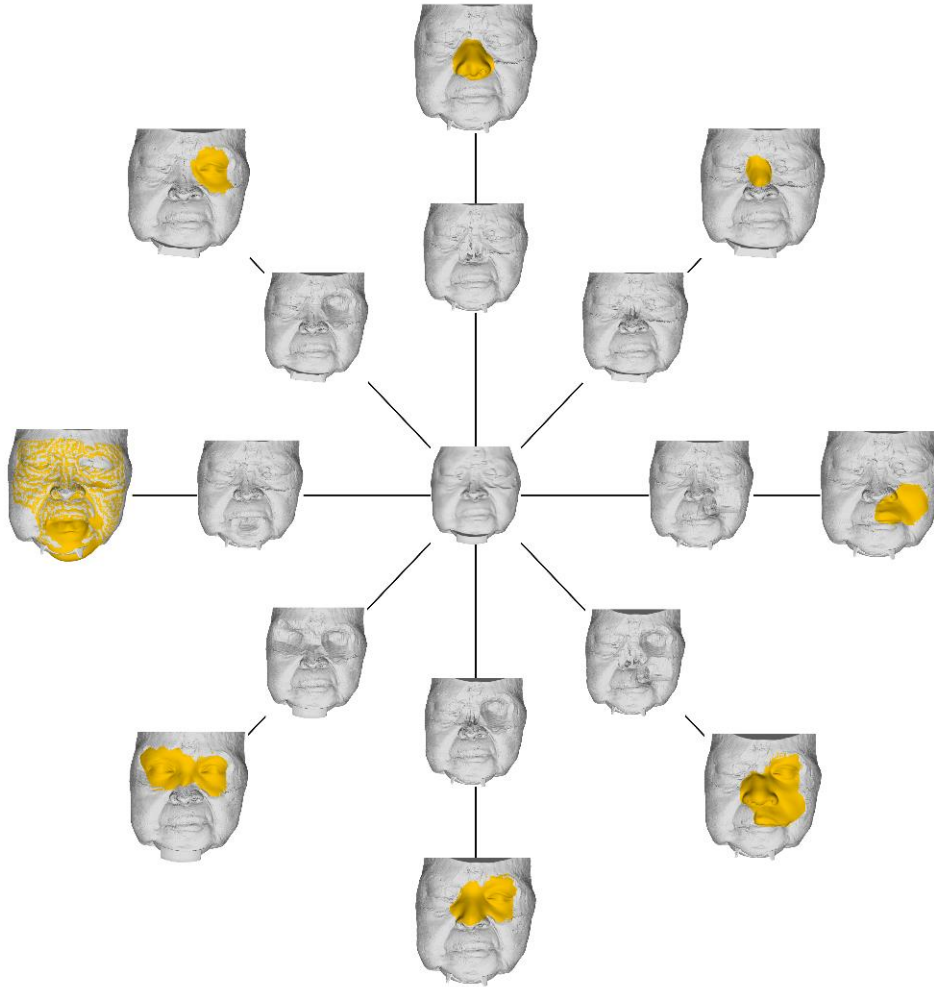
*Supplementary figure 8: Individual 7 defect estimations. The central image is the original non-defective face; the inner ring represents the different defect simulations; the outer ring shows in orange the defect estimation superimposed onto the defective face, from the top in a clockwise direction: Full nose defect, partial nose defect, cheek defect, large (composite 1) defect, small (composite 2) defect, bi-orbital defect, lip defect and orbital defect.*
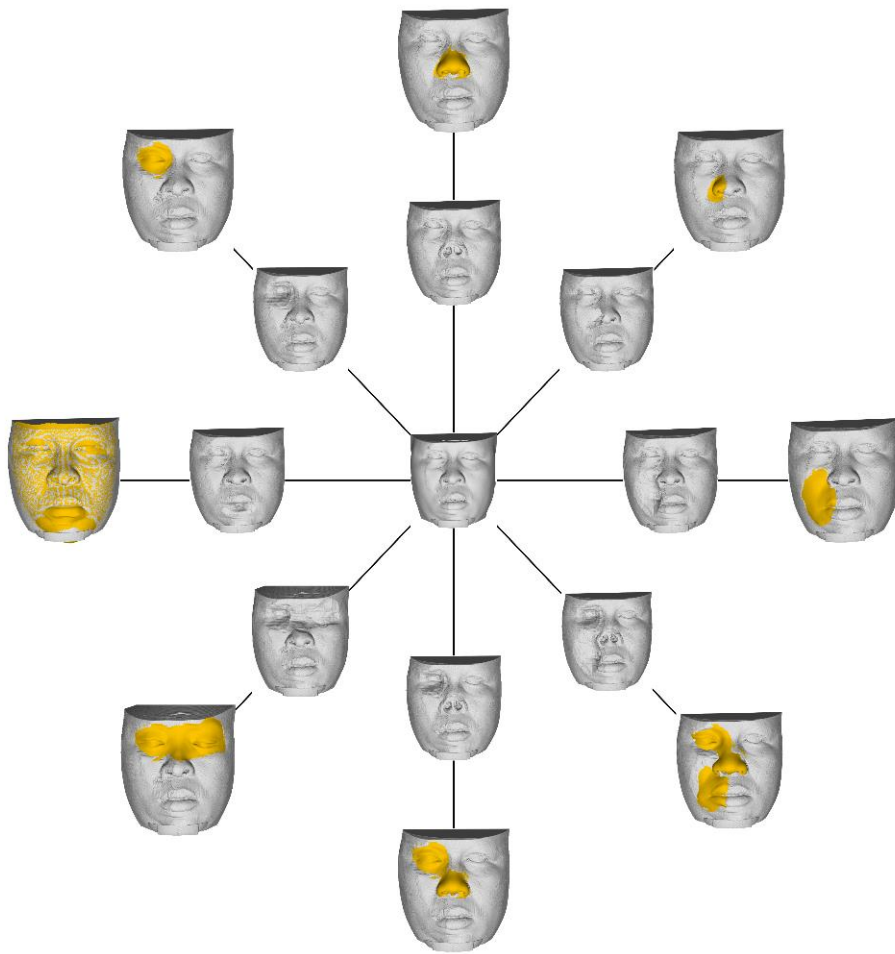
*Supplementary figure 9: Individual 8 defect estimations. The central image is the original non-defective face; the inner ring represents the different defect simulations; the outer ring shows in orange the defect estimation superimposed onto the defective face, from the top in a clockwise direction: Full nose defect, partial nose defect, cheek defect, large (composite 1) defect, small (composite 2) defect, bi-orbital defect, lip defect and orbital defect.*
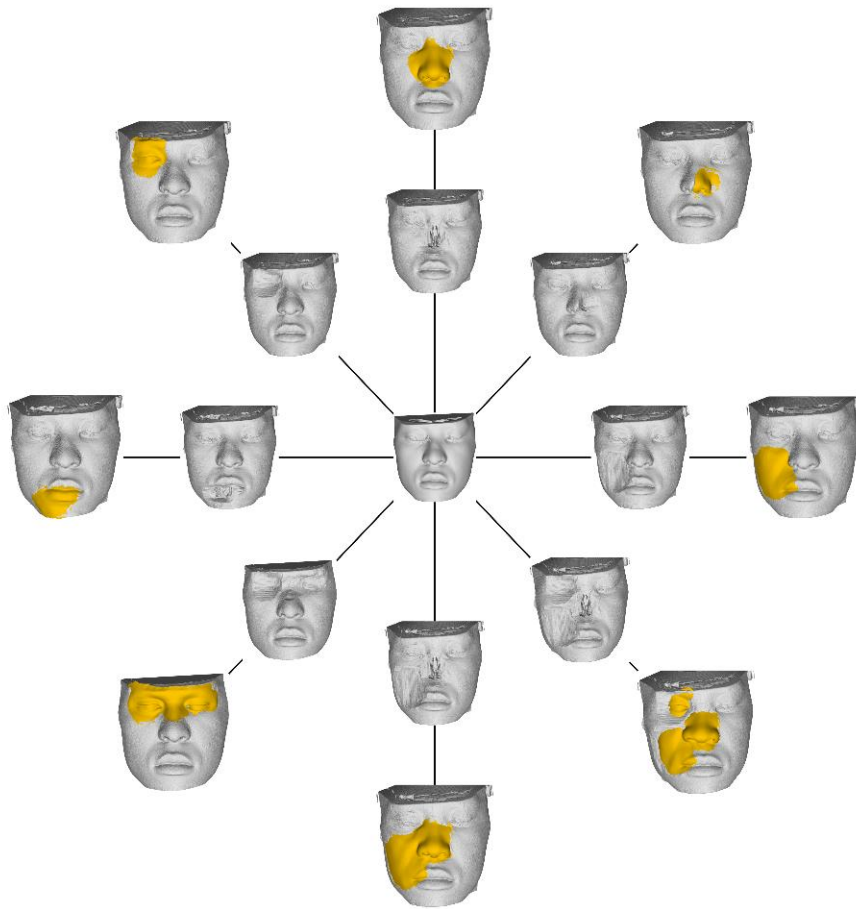
*Supplementary figure 10: Individual 9 defect estimations. The central image is the original non-defective face; the inner ring represents the different defect simulations; the outer ring shows in orange the defect estimation superimposed onto the defective face, from the top in a clockwise direction: Full nose defect, partial nose defect, cheek defect, large (composite 1) defect, small (composite 2) defect, bi-orbital defect, lip defect and orbital defect.*
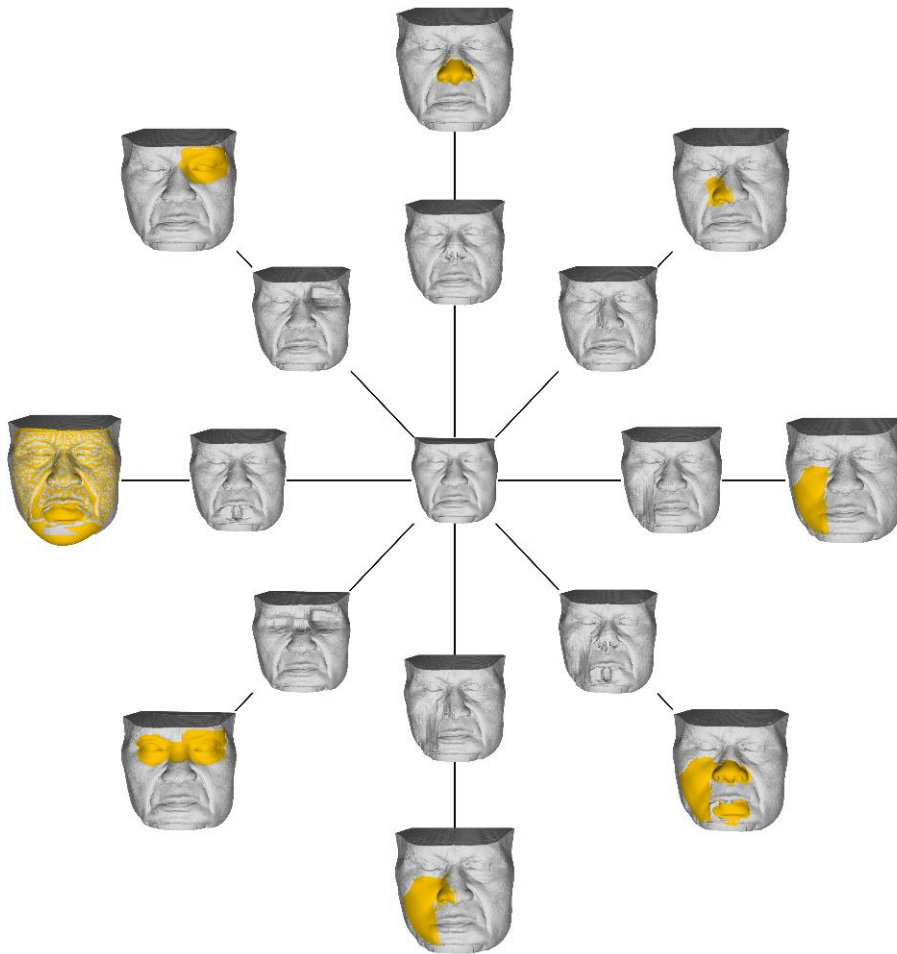
*Supplementary figure 11: Individual 10 defect estimations. The central image is the original non-defective face; the inner ring represents the different defect simulations; the outer ring shows in orange the defect estimation superimposed onto the defective face. (a) Orbital defect, (b) Full nose defect, (c) Partial nose defect, (d) Cheek defect, (e) Large (composite 1) defect, (f) Small (composite 2) defect, (g) Bi-orbital defect, and (h) Lip defect.*
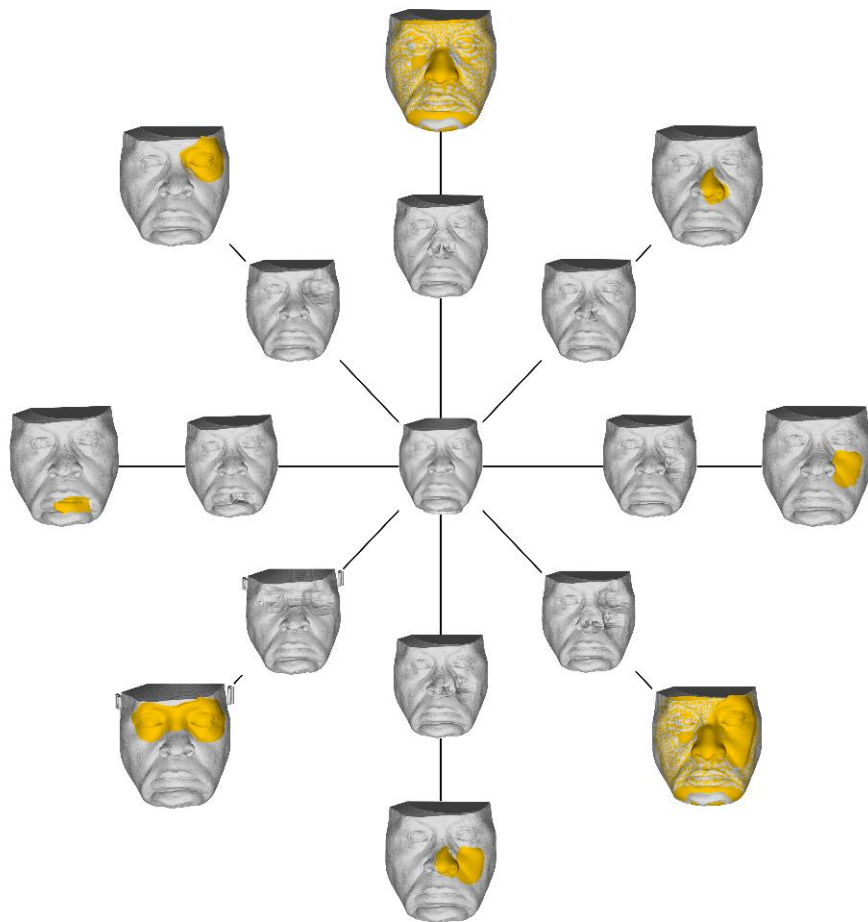
*Supplementary figure 12: Individual 11 defect estimations. The central image is the original non-defective face; the inner ring represents the different defect simulations; the outer ring shows in orange the defect estimation superimposed onto the defective face, from the top in a clockwise direction: Full nose defect, partial nose defect, cheek defect, large (composite 1) defect, small (composite 2) defect, bi-orbital defect, lip defect and orbital defect.*
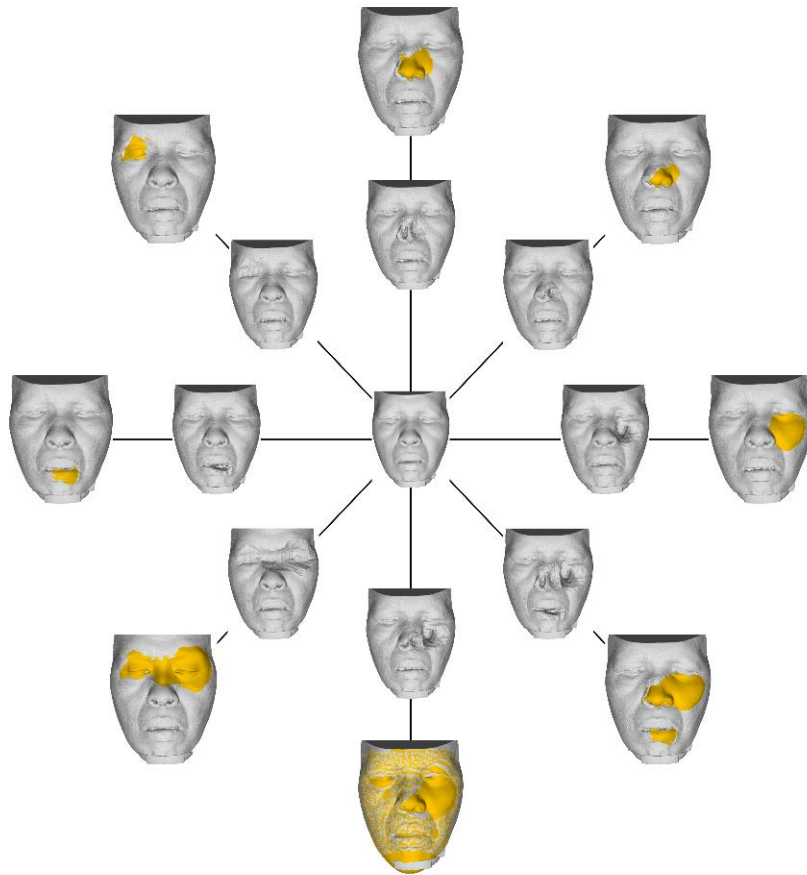
*Supplementary figure 13: Individual 12 defect estimations. The central image is the original non-defective face; the inner ring represents the different defect simulations; the outer ring shows in orange the defect estimation superimposed onto the defective face, from the top in a clockwise direction: Full nose defect, partial nose defect, cheek defect, large (composite 1) defect, small (composite 2) defect, bi-orbital defect, lip defect and orbital defect.*
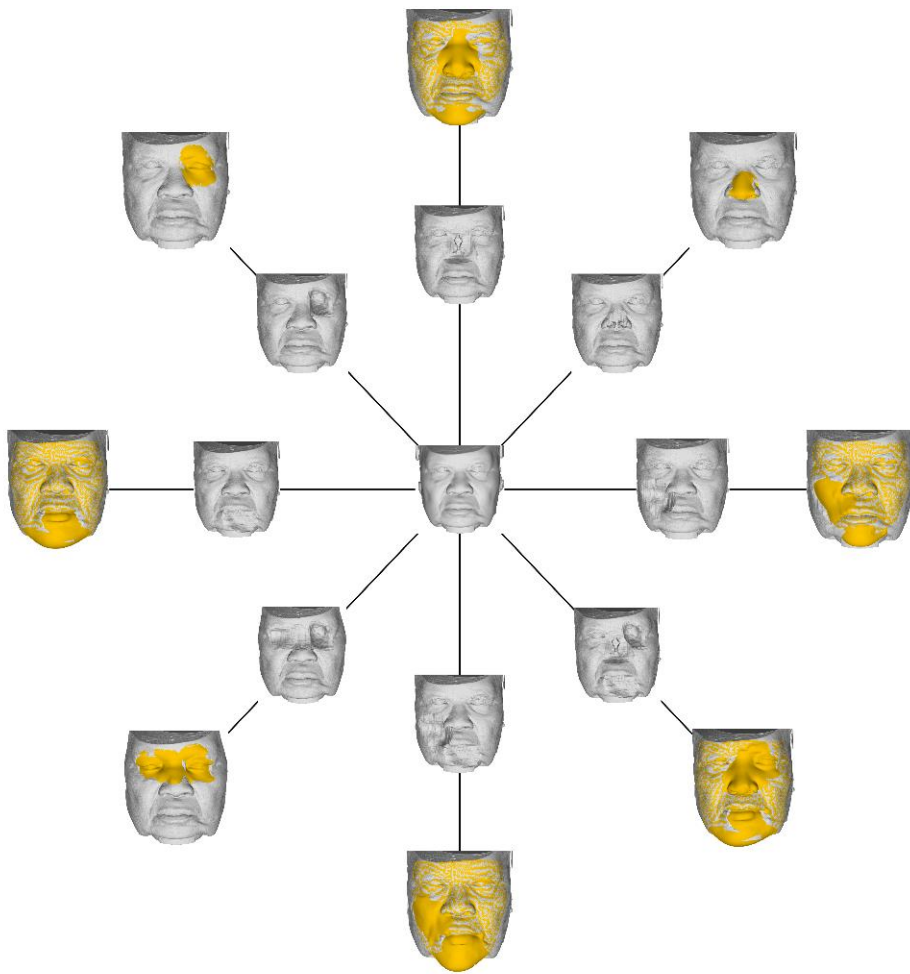
*Supplementary figure 14: Individual 13 defect estimations. The central image is the original non-defective face; the inner ring represents the different defect simulations; the outer ring shows in orange the defect estimation superimposed onto the defective face, from the top in a clockwise direction: Full nose defect, partial nose defect, cheek defect, large (composite 1) defect, small (composite 2) defect, bi-orbital defect, lip defect and orbital defect.*
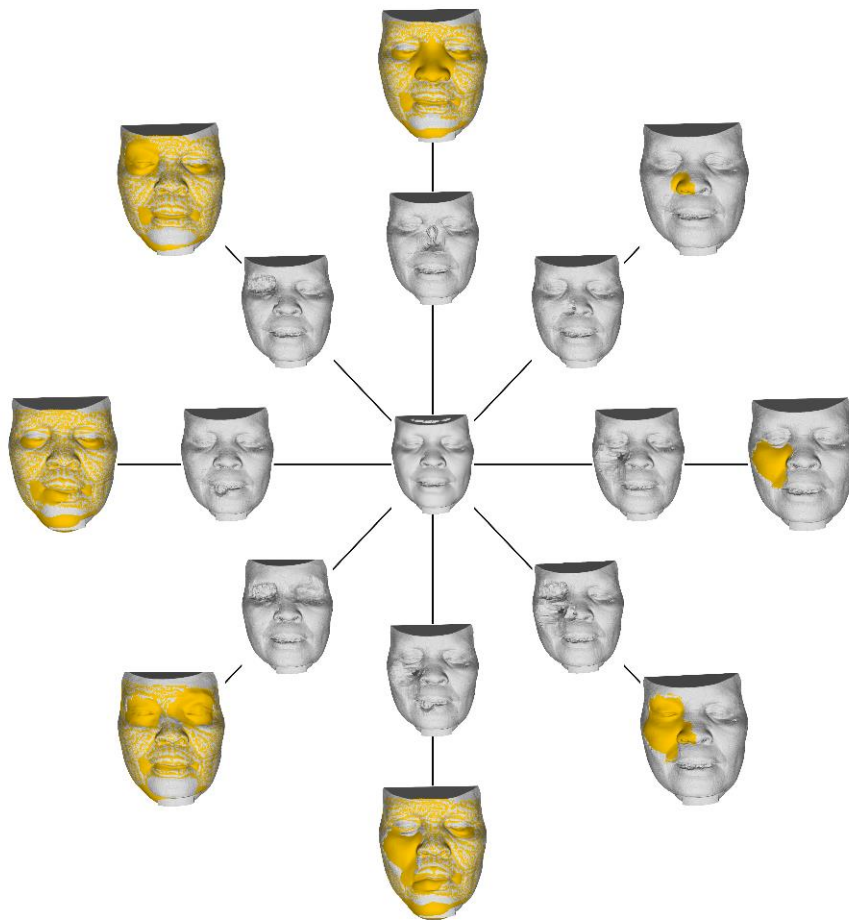
*Supplementary figure 15: Individual 14 defect estimations. The central image is the original non-defective face; the inner ring represents the different defect simulations; the outer ring shows in orange the defect estimation superimposed onto the defective face, from the top in a clockwise direction: Full nose defect, partial nose defect, cheek defect, large (composite 1) defect, small (composite 2) defect, bi-orbital defect, lip defect and orbital defect.*
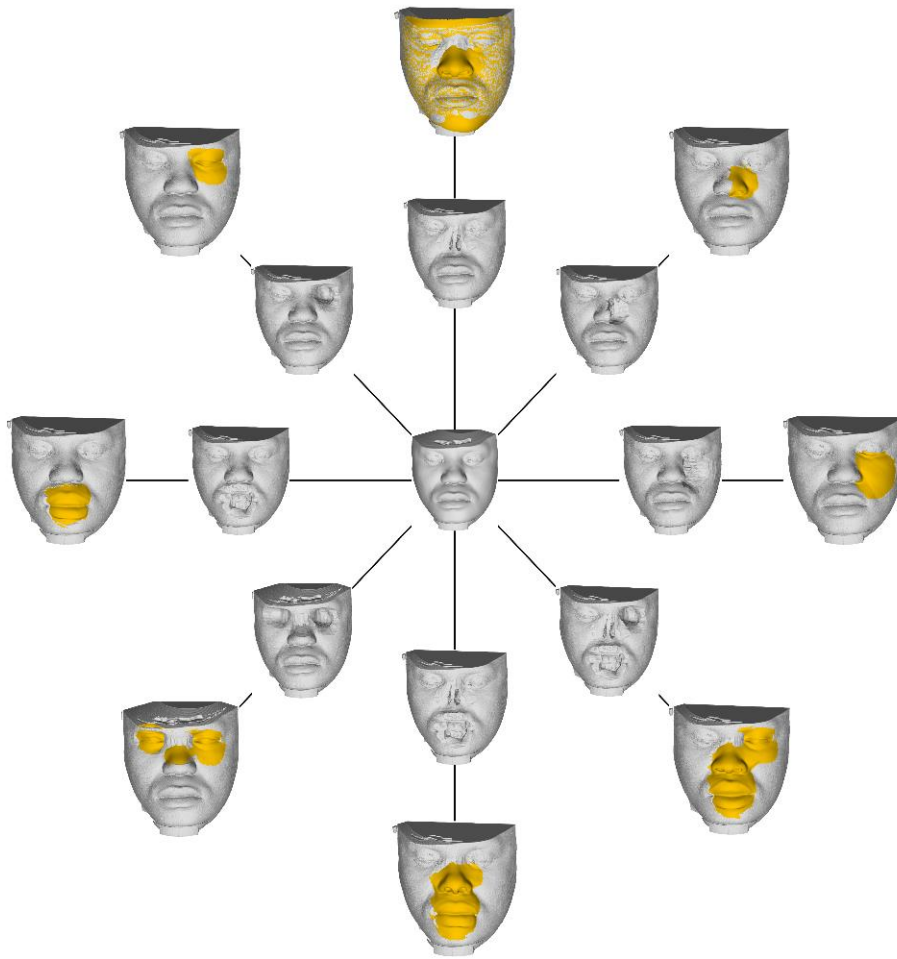
*Supplementary figure 16: Individual 15 defect estimations. The central image is the original non-defective face; the inner ring represents the different defect simulations; the outer ring shows in orange the defect estimation superimposed onto the defective face, from the top in a clockwise direction: Full nose defect, partial nose defect, cheek defect, large (composite 1) defect, small (composite 2) defect, bi-orbital defect, lip defect and orbital defect.*

## 5. References

1.      MeVisLab. (ed 2.7.1). Bremen, Germany, MeVis Medical Solutions AG, 2015.

2.      Amberg B, Romdhani S, Vetter T. Optimal step nonrigid ICP algorithms for surface registration. 2007 IEEE conference on Computer Vision and Pattern Recognition. 2007 17-22 June. Minneapolis, USA.

3.      White JD, Ortega-Castrillon A, Matthews H, et al. MeshMonk: Open-source large-scale intensive 3D phenotyping. Sci Rep. 2019;9(1):6085

4.      MATLAB. (ed 9.11.0.1837725 (2021b)). Natick, Massachusetts, The Mathworks, Inc., 2021.

5.      Cignoni P, Callieri M, Corsini M, et al. Meshlab: an open-source mesh processing tool. Eurographics Italian chapter conference. 2008

6.      Matthews HS, Palmer RL, Baynam GS, et al. Large-scale open-source three-dimensional growth curves for clinical facial assessment and objective description of facial dysmorphism. Sci Rep. 2021;11(1):12175

7.      Marzola A, Robilotta C, Volpe Y, et al. Statistical Shape Model: comparison between ICP and CPD algorithms on medical applications. Int J Interact Des Manuf. 2021;15:85-89

8.      Amira-Avizo. (ed 8.0.0), Thermo Fisher Scientific, 2013.

# General discussion and conclusion

The primary objective of this work was to address the significant gap in population-specific data on facial soft tissue variation, particularly for black South Africans, a demographic that not only constitutes the majority in the country but also represents a substantial proportion of forensic cases (L'Abbé, Van Rooyen, Nawrocki and Becker, 2011) and instances of head and neck cancer that led to facial disfigurement (Zwane, Mohangi and Shangase, 2018). The research outlined has successfully generated normative facial capulometric measurements from a CT and CBCT scan database, as detailed in Chapter 3. These measurements are essential for a wide range of applications, from forensic craniofacial approximations to reconstructive and aesthetic surgery. Moreover, Chapter 4 introduces an innovative statistical shape model derived from the same database and presents a method for estimating missing soft tissue segments, the accuracy of which is assessed using simulated defective faces. This discussion will explore the significance of these findings and methods within the context of existing literature, their practical applications in medical and forensic sciences, limitations, and their potential for future technological advancements in facial reconstruction and related fields. To facilitate the discussion, these points will be discussed separately for Chapter 3 and 4 respectively.

## Chapter 3: Normative facial capulometric measurements in a black South African population.

Chapter 3 presented normative facial measurements for the black South African population and assessed differences between this group and various other populations. Significant differences between groups were observed in most facial parameters, with more similarities observed between the South African black population and other global African populations. Pronounced differences were particularly evident in the orbital and nasal anatomy, while the data showed stronger evidence that there was no difference between population means for the oral parameters when compared to other non-African groups. This finding adds a crucial dimension to the existing body of literature, highlighting the importance of considering population specific variations in facial anatomy, especially in medical and forensic applications.

In the context of aesthetic and reconstructive surgery, the classical facial canons traditionally described by Da Vinci, more recently updated by Leslie Farkas and based on European standards, have been a guiding force. Initially, aesthetic surgery was primarily requested by white individuals, and those of different ethnicities sought to efface rather than celebrate their features (Gupta, 2015).

However, for example in the United States of America, many surgeons now report a trend towards the preservation of ethnic features, which necessitates re-evaluating prevailing aesthetic standards and establishing new, diverse surgical guidelines. The traditional neoclassic canons are not suitable for classifying facial characteristics in ethnic groups due to drastic differences in measurements and proportions, especially in the orbital and nasal regions (McKnight, Momoh Ao Fau - Bullocks and Bullocks, 2009)

Craniofacial approximation (CFA) in the forensic context, pertains to the interpretation of skeletal remains with the aim of recreating the probable living appearance of the deceased (Wilkinson and Tillotson, 2012). Importantly, it is not a standalone identification method, but rather a tool to assist in the identification process. The accuracy of CFA is dependent on the relationships among the facial features, subcutaneous soft tissues and the underlying bony structure of the skull (Cavanagh and Steyn, 2011). The primary objectives of CFA are twofold: to amplify public awareness about a particular case, thereby maximising leads and aiding in case resolution, and to directly facilitate potential recognition of the deceased. (Stephan, 2013) Non-natural deaths accounted for 11.9% (n = 54,161) of deaths in South Africa in 2018 (Statistics South Africa, 2021). High rates of violent deaths, illegal immigration, and internal migration, compounded by a shortage of identification documents, result in a high incidence of unidentified deceased in the South African medico-legal system. Limited dental and DNA records are available for comparison, leading the South African Police Service (SAPS) to rely on CFA and cranio-facial superimposition to assist in identifying possible matches (Houlton, Jooste, Uys and Steyn, 2020). Previous reports on current techniques for CFA indicated that the non-consideration of South African standards in the approximation of specific facial features, such as the nose, limits the objectivity and the accuracy of the approximation, and by extension, the success of the recognition (Ridel, Demeter, L'abbe, Vandermeulen and Oettle, 2020) Before attempting CFA, a biological profile of the deceased must be completed. Much research has been conducted in South Africa to improve methods for creating this profile, including studies on sexual dimorphism, ancestry estimations, and age-at-death estimations from skeletal remains (Bacci, Nchabeleng and Billings, 2018; Jooste, L'Abbé, Pretorius and Steyn, 2016; Krüger, L'Abbé, Stull and Kenyhercz, 2015; Krüger, Liebenberg, Myburgh, Meyer, Oettlé, Botha et al., 2018; Oettle, Becker, De Villiers and Steyn, 2009). Recently, more population-specific research on soft tissue facial thickness and estimations of the mouth and nose has been conducted (Briers, Briers, Becker and Steyn, 2015; Cavanagh et al., 2011; Houlton et al., 2020; Houlton, Jooste and Steyn, 2019; Meiring, 2019; Ridel et al., 2020; Ridel, Demeter, Liebenberg, L'Abbe, Vandermeulen and Oettle, 2018). The results of the study discussed in Chapter 3 further expanded the existing body of literature and may contribute to more accurate productions of

CFA's. However, in South African forensic investigations, the population is broadly classified into three main groups: black, "coloured", or white South Africans (Krüger et al., 2018), with the majority (81.4 %) of the population being black. While there are similarities among different black South African populations, the results of this study may not be optimally applicable to the entirety of this group due to its diverse ethnic composition. The study was conducted in the Tshwane Metropolitan area of Gauteng province, where 75 % of this population is black. Notably, within this demographic, languages such as Sepedi and Setswana predominate, which may be indicative of specific ethnicities in this region and is not necessarily representative of the entire black South African population. While there is value in utilising the broadly classified black South African data for population specific applications, future research could benefit from more refined classifications, investigating specific ethnic groups within the black South African population and perhaps as a function of continuous genomic ancestry.

A limitation is that the effect of gravity on soft tissues presents differently in CT compared to CBCT images due to the patients being imaged in a supine compared to an upright position. This variation which may lead to discrepancies in soft tissue representation, (Iblher, Gladilin and Stark, 2013) was noted as statistically significant differences in columella lengths and width, mouth width, lower lip, and vermillion heights. Additionally, the use of retrospective CBCT scans, primarily intended for dental purposes, often excluded areas such as the forehead, chin, or ears. This limitation restricted the collection of measurements involving these features including certain important facial ratios such as total face height, lower face height, bizygomatic width etc. The presence of chin struts in the CBCT scans may also distort the soft tissues of the chin and mouth areas, potentially impacting the accuracy of measurements in these regions. Furthermore, while the effect of age on facial parameters was found to be a significant factor, this was not further investigated due to skewed age groupings, and should be considered in future research, as it may have an impact on the applications of these measurements in both aesthetic and reconstructive surgery, and in the forensic context.

## Chapter 4: A statistical shape model for estimating missing soft tissues of the face in a black South African population.

Prosthetic rehabilitation for facial defects is often used as adjuvant or alternative therapy when the functional and aesthetic requirements are beyond the capacity of local reconstructive efforts. Prostheses are known to provide aesthetically pleasing outcomes for large facial defects involving multiple subunits and are especially useful in oncologic cases as they facilitate visually accessible surveillance (Le, Ying, Kase and Morlandt, 2022). As extensively discussed in the literature, the design and manufacture of facial prosthetics typically consists of three phases. (Van Heerden and Fossay,

2019) The first phase is to obtain an imprint of the facial anatomy and defect, either by traditional casting, or digital image acquisition. Secondly, the prosthetic model is designed by modelling the missing parts onto the face. This has traditionally been done by wax sculpting (Le et al., 2022), or more recently by the use of digital libraries (Bi and Wei, 2022; Palousek, Rosicky and Koutny, 2014) or digital sculpting methods (Abdulameer and Tukmachi, 2016; Nuseir, Hatamleh, Alnazzawi, Al-Rabab'ah, Kamel and Jaradat, 2019; Unkovskiy, Spintzyk, Brom, Huettig and Keutel, 2018), including mirror imaging in digital modelling (Ballo, Nguyen and Lee, 2019; Liu, Bai, Yu and Zhao, 2019). Finally, the prosthesis is created from the modelled area, by casting a negative mould from the model and casting with silicone, or by 3D printing a mould to cast with silicone.

The use of a statistical shape model (SSM) for designing the prosthetic model, as presented in Chapter 4, represents a novel approach in the field of facial prosthetics. One report of using SSMs for soft tissue estimations of the face was found in the literature (Jablonski, Malhotra, Coward, Shaw, Bojke, Pavitt et al., 2023). The University of Leeds developed an open-access digital database of nose models that has been generated based upon a 3D Morphable Face Model (SSM) approach. This database comprises 44 simple nose meshes with standardised alignment that are ideal for computer-aided design. Unlike mirror-imaging techniques, which are limited to midline or bilateral defects, or the Leeds database of noses, the SSM developed in this study is capable of addressing any type of defect by inferring missing soft tissue from any intact parts of the face, not just regions bilaterally paired with the defect. Furthermore, while access to a digital library of features are effective in reducing the treatment period and the intensity of work required by technicians (Jablonski et al., 2023; Sun, Chen, Liao and Xi, 2013) this solution remains time-consuming, as the operator needs to experiment with a variety of models to find the most aesthetically pleasing one. Since the study presented in Chapter 4 elucidated an experimental method, unfortunately quantitative comparison with traditional methods could not be conducted. However, the semi-automated nature of the SSM approach significantly reduces subjectivity and the need for artistic skill in modelling facial features, while providing a patient specific model.

Statistical shape models can potentially in future be applied in clinical settings as part of streamlined digital workflows. Generally, the integration of 3D technologies in prosthetic design can aid in defect and data acquisition (the imprint of the facial anatomy and defect needed for prosthesis design), as well as data manipulation for pre-surgical and prosthesis planning. Furthermore, tangible physical models for the visualisation of the prosthesis post-treatment can easily be created, which can aid in managing patient expectations by showing them what the prosthesis will look like before production.

Such technologies enhance the ability to deliver complex, reproducible, high-quality facial prosthetic treatments at affordable costs. (Hatamleh, Hatamlah and Nuseir, 2023) Understandably, the shift towards digital techniques is not without its challenges. The learning curve for technicians, especially in the absence of standardised workflows, and the requirement for significant upfront investment, pose hurdles.

Designing the ideal workflow for improved patient outcomes in the South African context is a significant challenge. This requires an interdisciplinary approach, and the integration of current methods and experimental technologies like the population specific SSM presented in Chapter 4. Starting at the presurgical planning phase of patient rehabilitation, effective interdisciplinary communication and involvement is pivotal. The optimal method for retaining a prosthesis should already be a topic of discussion during the pre-surgery stage. Typical methods encompass adhesive applications like glue or tape, mechanical attachment to eyeglass frames, and the surgical insertion of osseointegrated posts designed for magnetic or clip-on attachments. (Diken Türksayar, Saglam and Bulut, 2019) The suitability of each method depends heavily on clinical circumstances (Powell, Cruz, Ross and Woodruff, 2020) and influences the prosthetic design and manufacturing. Although the combination of facial prosthetics with osseointegrated implants for retention offers higher prosthetic success rates by providing better stability and retention without the reliance on adhesives, it may not be viable for every patient (Vincent, Kohlert, Kadakia, Sawhney and Ducic, 2019). Ideally, the implant placement should be incorporated into presurgical planning and placed at the time of the tumour removal to mitigate the negative side effects following radiation such as fibrosis, osteonecrosis and impaired wound healing. (Le et al., 2022).

Following the selection of the appropriate retention method, the next step is digital data acquisition. In the context of South Africa, there are specific challenges and opportunities. For instance, the inconsistent availability and/or reliability of CBCT machines necessitates exploring alternative methods for image acquisition, such as intraoral scanners and 3D photography. Intraoral scanners like the TRIOS systems can capture detailed surface data including pores and wrinkles (Liu et al., 2019), while more cost-effective options like using a smart device with specialised apps may offer potential alternatives in future, although the technology is not as accurate as 3D traditional photogrammetry systems. (Bartella, Laser, Kamal, Krause, Neuhaus, Pausch et al., 2023). Once the image data has been obtained, the SSM may be used to estimate the prosthetic model for any missing regions from the rest of the intact face. Ideally, this would be implemented in a streamlined and user-friendly software such as proposed in Chapter 1 and is currently under development.

Following the prosthesis design, the prosthesis model (Abdulameer et al., 2016; Mohammed, Cadd, Peart and Gibson, 2018; Sun et al., 2013) must be 3D printed and fitted to the patient to check for modifications, alterations made and the final silicone prosthesis manufactured and coloured. Alternatively, the negative prosthesis mould (Bi et al., 2022; Bi, Wu, Zhao and Bai, 2013) may be 3D printed and directly used to manufacture the final prosthesis. Advancements in 3D printing like direct silicone printing are already being investigated, and becoming more viable (Fay, Jeiranikhameneh, Sayyar, Talebian, Nagle, Cheng et al., 2022; Unkovskiy et al., 2018). Another option is using alternative flexible materials like TangoPlus (Stratasys Ltd) combined with 3D digital colouring such as the Spectromatch digital colour system to print the final prosthesis. (Nuseir et al., 2019). The Spectromatch colour system can record the patient's skin tones and used to digitally colour 3D reconstructions, leading to more personalized and aesthetically appealing outcomes.

The accuracy and applicability of the SSM-based estimation pipeline, as detailed in Chapter 4, are influenced by various factors. The most notable limitation of the SSM-based estimation pipeline is the cumbersome procedure for selecting the region to be estimated. However, by using a specially designed graphical interface, this may be easily overcome. Furthermore, the model is tailored for South African black adults, limiting its use for other groups like children or people of different ethnicities. Additionally, the focus on extra-oral defects overlooks the potential impact of intra-oral issues, like those arising from maxillectomies, on facial prosthetic needs, pointing to a significant area for future exploration. Furthermore, like the limitations relating to Chapter 3, the model doesn't include the forehead, ears, and occipital regions, as these are often not captured in CBCT scans, affecting its completeness, and the presence of chin struts, which may affect the accuracy of surrounding soft tissue structures. Our statistical analysis revealed a moderate but significant correlation (R = 0.5423; p < 0.001) between defect size and estimation error, indicating that larger defects pose greater challenges in accurate estimation, yet the relationship is not sufficiently strong to predict accuracy linearly across all defect sizes and types. As discussed in Chapter 4, notably, regions like the full nose and bi-orbital areas are particularly challenging, underscoring the need for an in-depth analysis of the SSMs performance across different facial regions and defect complexities. Future research must therefore not only aim to enhance the model's demographic inclusivity and address intra-oral defect estimation but also develop a more comprehensive dataset that captures the diversity in face shapes, defect types, and locations to truly refine the SSM's clinical efficacy and broaden its application. Moreover, the enhancement of user-friendly tools, such as the graphical interface we mentioned, will be paramount. This tool should not only ease the selection and modification of regions of interest for clinicians but also incorporate functionalities that allow for

iterative adjustments and re-estimations based on specific clinical considerations, such as scarring or radiation changes.

Building on the innovative approaches and technologies discussed in Chapter 4, the integration of a the SSM in the design of facial prosthetics represents a significant advancement in personalised medical care. This method promises to revolutionise the way facial defects are addressed in the South African context and enhance the quality of prosthetic rehabilitation. Together with cutting-edge digital technologies including 3D printing, the potential for delivering more accurate, efficient, and patient-tailored prosthetic solutions is immense. This shift towards digitalisation in prosthetic design, not only aligns with global trends in medical technology but also addresses specific local needs and challenges. The promising results of this study underscore the importance of continued research and development in this field, paving the way for more refined, accessible, and effective solutions in facial rehabilitation, especially considering the diverse population and unique healthcare challenges in South Africa.

## Conclusion

This thesis contributes significantly to our understanding of facial soft tissue variation in the black South African population, filling a noteworthy gap in both forensic and medical sciences. The normative facial capulometric measurements elucidated in Chapter 3 provide an essential reference for forensic craniofacial approximations and aesthetic as well as reconstructive surgery, challenging traditional Eurocentric standards and advocating for a more inclusive approach. Chapter 4's development of a statistical shape model for estimating missing soft tissue segments is an innovation in digital reconstruction methodologies, offering a more objective, patient-specific approach in prosthetic design. Whilst the study acknowledges its limitations, such as variations in imaging modalities and the need for more refined classifications within the black South African population, its findings pave the way for future research. Other key areas requiring exploration to fully realise the benefits of digital technologies in clinical settings include the integration of direct silicone 3D printing and digital colour matching technologies that holds the potential to streamline the prosthetic manufacturing process, making it more accessible and patient-specific. The most significant barriers to implementation are primarily access to technology and resource constraints. Challenges such as the steep learning curve for new digital techniques, the need for substantial initial investment, and the development of user-friendly software interfaces must be addressed. The transformative potential of digital technologies in enhancing facial prosthetic rehabilitation advocates for continued interdisciplinary research, and the adoption of digital workflows to improve patient outcomes in

diverse healthcare landscapes like South Africa. Addressing these challenges is not just a matter of logistical and technical refinement. Overcoming these barriers is crucial for translating the theoretical advancements into tangible benefits in facial reconstruction and prosthetic rehabilitation. This thesis stands to significantly improve outcomes in both forensic and medical applications. More broadly, the work demonstrates the importance of population-specific research and its role in fostering a more diverse and culturally sensitive practice in related fields.

## References

Abdulameer, H.M., Tukmachi, M. 2016. Nasal prosthesis fabrication using rapid prototyping and 3D printing (A case study). Int J Innov Res Sci Eng Technol. 6:(8):15520-6.

Bacci, N., Nchabeleng, E.K., Billings, B.K. 2018. Forensic age-at-death estimation from the sternum in a black South African population. Forensic Sci Int. 282:233.e1-.e7.

Ballo, A.M., Nguyen, C.T., Lee, V.S. 2019. Digital workflow of auricular rehabilitation: a technical report using an intraoral scanner. J Prosthodont. 28:(5):596-600.

Bartella, A.K., Laser, J., Kamal, M., Krause, M., Neuhaus, M., Pausch, N.C., et al. 2023. Accuracy of low-cost alternative facial scanners: a prospective cohort study. Oral Maxillofac Surg. 27:(1):33-41.

Bi, Y., Wei, H. 2022. Fully digital workflow for the rehabilitation of a total nasal defect with a prosthesis. J Prosthet Dent.

Bi, Y., Wu, S., Zhao, Y., Bai, S. 2013. A new method for fabricating orbital prosthesis with a CAD/CAM negative mold. J Prosthet Dent. 110:(5):424-8.

Briers, N., Briers, T., Becker, P.J., Steyn, M. 2015. Soft tissue thickness values for black and coloured South African children aged 6–13 years. Forensic Sci Int. 252:188. e1-. e10.

Cavanagh, D., Steyn, M. 2011. Facial reconstruction: soft tissue thickness values for South African black females. Forensic Sci Int. 206:(1-3):215. e1-. e7.

Diken Türksayar, A., Saglam, S., Bulut, A. 2019. Retention Systems Used in Maxillofacial Prostheses: A Review. Niger J Clin Pract. 22:(12):1629-34.

Fay, C.D., Jeiranikhameneh, A., Sayyar, S., Talebian, S., Nagle, A., Cheng, K., et al. 2022. Development of a customised 3D printer as a potential tool for direct printing of patient-specific facial prosthesis. Int J Adv Manuf Technol. 120:(11-12):7143-55.

Gupta, S. 2015. Surgery: Diverse interventions. Nature. 526:(7572):S6-S7.

Hatamleh, M.M.d., Hatamlah, H.M., Nuseir, A. 2023. Maxillofacial prosthetics and digital technologies: Cross-sectional study of healthcare service provision, patient attitudes, and opinions. J Prosthodont. https://doi.org/10.1111/jopr.13718.

Houlton, T.M., Jooste, N., Uys, A., Steyn, M. 2020. Lip height estimation in a southern African sample. SADJ. 75:415-24.

Houlton, T.M.R., Jooste, N., Steyn, M. 2019. Mouth Width and Cupid's Bow Estimation in a Southern African Population. J Forensic Sci. 65:(2):372-9.

Iblher, N., Gladilin, E., Stark, B.G. 2013. Soft-Tissue Mobility of the Lower Face Depending on Positional Changes and Age: A Three-Dimensional Morphometric Surface Analysis. Plast Reconstr Surg. 131:(2):372-81.

Jablonski, R.Y., Malhotra, T., Coward, T.J., Shaw, D., Bojke, C., Pavitt, S.H., et al. 2023. Digital database for nasal prosthesis design with a 3D morphable face model approach. J Prosthet Dent. 10.1016/j.prosdent.2023.02.019.

Jooste, N., L'Abbé, E.N., Pretorius, S., Steyn, M. 2016. Validation of transition analysis as a method of adult age estimation in a modern South African sample. Forensic Sci Int. 266:580.e1-.e7.

Krüger, G.C., L'Abbé, E.N., Stull, K.E., Kenyhercz, M.W. 2015. Sexual dimorphism in cranial morphology among modern South Africans. Int J Legal Med. 129:869-75.

Krüger, G.C., Liebenberg, L., Myburgh, J., Meyer, A., Oettlé, A.C., Botha, D., et al. 2018. Forensic anthropology and the biological profile in South Africa. New Perspectives in Forensic Human Skeletal Identification. Elsevier.

L'Abbé, E.N., Van Rooyen, C., Nawrocki, S.P., Becker, P.J. 2011. An evaluation of non-metric cranial traits used to estimate ancestry in a South African sample. Forensic Sci Int. 209:(1-3):195. e1-. e7.

Le, J.M., Ying, Y.P., Kase, M.T., Morlandt, A.B. 2022. Surgical reconstruction and rehabilitation of midface defects using osseointegrated implant-supported maxillofacial prosthetics. J Diagn Treat Oral Maxillofac Pathol. 6:(1):9-25.

Liu, H., Bai, S., Yu, X., Zhao, Y. 2019. Combined use of a facial scanner and an intraoral scanner to acquire a digital scan for the fabrication of an orbital prosthesis. J Prosthet Dent. 121:(3):531-4.

McKnight, A., Momoh Ao Fau - Bullocks, J.M., Bullocks, J.M. 2009. Variations of structural components: specific intercultural differences in facial morphology, skin type, and structures. Seminars in plastic surgery. 23:(3):163-7.

Meiring, K.O. 2019. Facial Soft Tissue Thickness and Facial Recognition of Black South African Adults. Master of Science in Medicine, University of the Witwatersrand.

Mohammed, M.I., Cadd, B., Peart, G., Gibson, I. 2018. Augmented patient-specific facial prosthesis production using medical imaging modelling and 3D printing technologies for improved patient outcomes. Virtual Phys Prototyp. 13:(3):164-76.

Nuseir, A., Hatamleh, M.M.d., Alnazzawi, A., Al-Rabab'ah, M., Kamel, B., Jaradat, E. 2019. Direct 3D Printing of Flexible Nasal Prosthesis: Optimized Digital Workflow from Scan to Fit. J Prosthodont. 28:(1)**:**10-4.

Oettle, A.C., Becker, P.J., De Villiers, E., Steyn, M. 2009. The influence of age, sex, population group, and dentition on the mandibular angle as measured on a South African sample. Am J Phys Anthropol. 139:(4)**:**505-11.

Palousek, D., Rosicky, J., Koutny, D. 2014. Use of digital technologies for nasal prosthesis manufacturing. Prosthet Orthot Int. 38:(2)**:**171-5.

Powell, S.K., Cruz, R.L., Ross, M.T., Woodruff, M.A. 2020. Past, present, and future of soft-tissue prosthetics: advanced polymers and advanced manufacturing. Adv Mater. 32:(42)**:**2001122.

Ridel, A.F., Demeter, F., L'abbe, E.N., Vandermeulen, D., Oettle, A.C. 2020. Nose approximation among South African groups from cone-beam computed tomography (CBCT) using a new computer-assisted method based on automatic landmarking. Forensic Sci Int. 313:110357.

Ridel, A.F., Demeter, F., Liebenberg, J., L'Abbe, E.N., Vandermeulen, D., Oettle, A.C. 2018. Skeletal dimensions as predictors for the shape of the nose in a South African sample: A cone-beam computed tomography (CBCT) study. Forensic Sci Int. 289:18-26.

Statistics South Africa 2021. Mortality and causes of death in South Africa: findings from death notification, 2018 (Statistical release no: P0309.3. South Africa.

Stephan, C.N. 2013. Facial approximation. In: Siegel, J.Saukko, P. (eds.) Encyclopedia of Forensic Sciences. 2nd edn. USA: Elsevier.

Sun, J., Chen, X., Liao, H., Xi, J. 2013. Template-based framework for nasal prosthesis fabrication. Rapid Prototyp J. 19:(2)**:**68-76.

Unkovskiy, A., Spintzyk, S., Brom, J., Huettig, F., Keutel, C. 2018. Direct 3D printing of silicone facial prostheses: A preliminary experience in digital workflow. J Prosthet Dent. 120:(2)**:**303-8.

Van Heerden, I., Fossay, A. 2019. Changing world of external maxillofacial prosthesis manufacturing. 20th Annual International RAPDASA Conference, 6-8 November 2019 2019 Bloemfontein, South Africa. 362-70.

Vincent, A., Kohlert, S., Kadakia, S., Sawhney, R., Ducic, Y. 2019. Prosthetic Reconstruction of Orbital Defects. Seminars in plastic surgery. 33:(2)**:**132-7.

Wilkinson, C., Tillotson, A. 2012. Post-mortem prediction of facial appearance. In: Wilkinson, C.Rynn, C. (eds.) Craniofacial identification. New York, USA: Cambridge University Press.

Zwane, N.B., Mohangi, G.U., Shangase, S.L. 2018. Head and neck cancers among HIV-positive patients: A five year retrospective study from a Johannesburg hospital, South Africa. SADJ. 73:(3)**:**121-6.

# Appendices

## Appendix A: Ethics approval

**UNIVERSITEIT VAN PRETORIA**
**UNIVERSITY OF PRETORIA**
**YUNIBESITHI YA PRETORIA**

**Faculty of Health Sciences**

Faculty of Health Sciences **Research Ethics Committee**

14 April 2023

**Approval Certificate**
**Annual Renewal**

Dear Mrs HF Swanepoel,

**Ethics Reference No.: 58/2020 – Line 4**
**Title: Creating a statistical shape model to aid in the estimation of incomplete soft tissue segments of the surface of South African faces**

The **Annual Renewal** as supported by documents received between 2023-03-15 and 2023-04-12 for your research, was approved by the Faculty of Health Sciences Research Ethics Committee on 2023-04-12 as resolved by its quorate meeting.

Please note the following about your ethics approval:
- Renewal of ethics approval is valid for 1 year, subsequent annual renewal will become due on 2024-04-14.
- Please remember to use your protocol number (58/2020) on any documents or correspondence with the Research Ethics Committee regarding your research.
- Please note that the Research Ethics Committee may ask further questions, seek additional information, require further modification, monitor the conduct of your research, or suspend or withdraw ethics approval.

**Ethics approval is subject to the following:**
- The ethics approval is conditional on the research being conducted as stipulated by the details of all documents submitted to the Committee. In the event that a further need arises to change who the investigators are, the methods or any other aspect, such changes must be submitted as an Amendment for approval by the Committee.

We wish you the best with your research.

**Yours sincerely**

**On behalf of the FHS REC, Dr R Sommers**
MBChB, MMed (Int), MPharmMed, PhD
*Deputy Chairperson of the Faculty of Health Sciences Research Ethics Committee, University of Pretoria*

*The Faculty of Health Sciences Research Ethics Committee complies with the SA National Act 61 of 2003 as it pertains to health research and the United States Code of Federal Regulations Title 45 and 46. This committee abides by the ethical norms and principles for research, established by the Declaration of Helsinki, the South African Medical Research Council Guidelines as well as the Guidelines for Ethical Research: Principles Structures and Processes, Second Edition 2016 (Department of Health)*

# Appendix B: Proof of submission to South African Dental Journal

## Manuscript submission: Recent developments in methodologies for extra-oral facial prostheses in South Africa

Franci Swanepoel <franci.dorfling@gmail.com>                                   Wed, Dec 6, 2023 at 2:21 PM
To: ngoeped@sada.co.za, bill.evans@wits.ac.za, nmojela@sada.co.za
Cc: sadj@sada.co.za

Dear Editorial Team of the SADJ,

I hope this email finds you well.

I am writing to submit our manuscript titled "Recent Developments in Methodologies for Extra-Oral Facial Prostheses in South Africa" for consideration in the South African Dental Journal. This manuscript delves into the advancements and innovations in extra-oral facial prosthesis, with a specific focus on practices and developments within the South African context.

Enclosed with this email are the following documents for your review:

1. Cover Letter
2. Manuscript
3. Figures
4. Signed Author Declaration Form

We believe that our manuscript makes a significant contribution to the field and would be of interest to the readership of SADJ. We have adhered to all the guidelines provided for submission and have ensured that the manuscript and accompanying documents meet the high standards of your journal.

We appreciate your consideration of our work and look forward to the opportunity to contribute to the South African Dental Journal. Please feel free to contact me if you require any further information or clarification.

Thank you for your time and consideration.

Best regards,

Helene Francia Swanepoel
University of Pretoria

4 attachments


Figure 1.jpg
144K

cover letter.pdf
188K

facial prostheses in SA_manuscript_SADJ.docx
1059K

Author Declaration_signed.pdf
656K

franci swanepoel <franci.dorfling@gmail.com>

## Submission Confirmation

Journal of Plastic, Reconstructive & Aesthetic Surgery <em@editorialmanager.com>    Wed, Dec 6, 2023 at 10:32 AM
Reply-To: "Journal of Plastic, Reconstructive & Aesthetic Surgery" <jpras@elsevier.com>
To: Helene Francia Swanepoel <franci.dorfling@gmail.com>

Dear Franci,

Thank you for your submission entitled "Normative Facial Capulometric Measurements in a Black South African Population" which has been received by the Journal of Plastic, Reconstructive & Aesthetic Surgery.

The full list of authors for this paper is Ms Helene Francia Swanepoel,
Harold Matthews, BA, PhD; Peter Claes, ME, PhD; Dirk Vandermeulen, PhD; Ericka Noelle L'Abbé, BA, MA, PhD; Anna Catharina Oettlé, MBChB, MSc, PhD, DTE

If you are not an author of this paper and should not have been included in the list of authors during the submission then please email jpras@elsevier.com.

The corresponding author will be able to check on the progress of your paper by logging on to Editorial Managers as an author, the URL is https://www.editorialmanager.com/jpras/.

Your username is: SwanepoelHF

If you need to retrieve password details please go to: https://www.editorialmanager.com/jpras/l.asp?i=563562&l=WSCTPFTE

Your manuscript will be given a reference number once an Editor has been assigned.

Thank you for submitting your work to this journal.

Kind regards,


Editorial Manager
Journal of Plastic, Reconstructive & Aesthetic Surgery

At Elsevier, we want to help all our authors to stay safe when publishing. Please be aware of fraudulent messages requesting money in return for the publication of your paper. If you are publishing open access with Elsevier, bear in mind that we will never request payment before the paper has been accepted. We have prepared some guidelines (https://www.elsevier.com/connect/authors-update/seven-top-tips-on-stopping-apc-scams ) that you may find helpful, including a short video on Identifying fake acceptance letters (https://www.youtube.com/watch?v=o5l8thD9XtE ). Please remember that you can contact Elsevier?s Researcher Support team (https://service.elsevier.com/app/home/supporthub/publishing/) at any time if you have questions about your manuscript, and you can log into Editorial Manager to check the status of your manuscript (https://service.elsevier.com/app/answers/detail/a_id/29155/c/10530/supporthub/publishing/kw/status/).

_____
In compliance with data protection regulations, you may request that we remove your personal registration details at any time. (Use the following URL: https://www.editorialmanager.com/jpras/login.asp?a=r). Please contact the publication office if you have any questions.

# Journal of Plastic, Reconstructive & Aesthetic Surgery
## Normative Facial Capulometric Measurements in a Black South African Population
### --Manuscript Draft--

| | |
|---|---|
| **Corresponding Author:** | Helene Francia Swanepoel, MSc<br>University of Pretoria Faculty of Health Sciences<br>Pretoria, Gauteng SOUTH AFRICA |
| **First Author:** | Helene Francia Swanepoel, BSc (Hons), MSc |
| **Order of Authors:** | Helene Francia Swanepoel, BSc (Hons), MSc |
| | Harold Matthews, BA, PhD |
| | Peter Claes, ME, PhD |
| | Dirk Vandermeulen, PhD |
| | Ericka Noelle L'Abbé, BA, MA, PhD |
| | Anna Catharina Oettlé, MBChB, MSc, PhD, DTE |

**Abstract:**

Facial analysis serves as the foundation for surgical planning and is vital for devising suitable treatment strategies in cosmetic and reconstructive surgeries. The aim of this study was to establish normative capulometric values for facial measurements specific to the black South African population. This study reports normative capulometric values of 22 clinically relevant inter-landmark distances for the black South African population. These were derived from 235 computed tomography (CT) and cone beam computed tomography (CBCT) scans of adults aged 18-87 years.

Significant sex-differences were found in nasal parameters, with males generally having larger measurements. Few significant differences were found between sexes for ocular parameters, challenging existing literature that suggests sexual dimorphism in these features. Oral parameters showed significant sex differences, with no notable disparities between modalities (CT and CBCT), except for lower lip and vermillion heights.

The study's results were benchmarked against similar studies of different populations, revealing that while the black South African population is in general similar to other African population groups, particularly in oral features, significant differences exist across all facial parameters when compared to non-African populations. The research highlights the unique facial characteristics of the black South African population, providing valuable data for forensic anthropology, prosthodontics, and reconstructive and aesthetic surgery. It emphasises the importance of recognising population-specific features to ensure optimal clinical interventions and contributes to the broader understanding of human facial diversity.

144

# Facial approximations: Characteristics of the eye in a South African sample

Heléne F. Dorfling[a,*], Zarina Lockhat[b], Samantha Pretorius[c], Maryna Steyn[d], Anna C. Oettlé[a,e]

[a] *Department of Anatomy, Faculty of Health Sciences, University of Pretoria, Pretoria, South Africa*
[b] *Department of Radiology, Faculty of Health Sciences, University of Pretoria, South Africa*
[c] *Department Actuarial Science, Faculty of Natural and Agricultural Sciences, University of Pretoria, South Africa*
[d] *Human Variation and Identification Research Unit, School of Anatomical Sciences, Faculty of Health Sciences, University of the Witwatersrand, South Africa*
[e] *Department of Anatomy and Histology, School of Medicine, Sefako Makgatho Health Sciences University, Ga-Rankuwa, Pretoria, South Africa*

## ARTICLE INFO

## ABSTRACT

Although guidelines for facial approximations, including those for the eye, are in use in South Africa, limited data on African populations exist to confirm its validity. As precise placement of the eyes in facial approximations is of importance for facial recognition, this study tested established guidelines by measuring specific instrumental dimensions. Forty-nine cadavers from the Sefako Makgatho Health Sciences University and the University of Pretoria were dissected to determine the position of the canthi and the size and position of the eyeball in the orbit. Thirty cone beam computer tomography scans and 30 computer tomography scans from the Oral and Dental and Steve Biko Hospitals respectively were used to determine the size of the eyeball. Results from this study were compared to the published guidelines. The most prominent discrepancies included a more rectangular shape of the orbit, an oval shaped eyeball and a different position of the canthi. In African faces, the medial canthus was found to be located higher than the lateral canthus. The distance between the endocanthion and superior orbital margin was 17.7 mm and the exocanthion and superior orbital margin 19.5 mm. Inter-population differences may have an effect on facial approximations and its accuracy as is often demonstrated in practice. The findings of this study should be taken into consideration when designing population specific guidelines for reconstruction of the eye in South Africans of African ancestry.

## 1. Introduction

Identification of unknown individuals is a challenge in the South African context. In cases where there is a strong suspicion regarding the identity of the unknown individual and a close relative is available, methods such as DNA comparison and dental record comparison are useful. However, because of socio-economic and other reasons in the South African context, unidentified individuals without known relationships are commonplace [1]. In these cases, it is not possible to identify unknown individuals with primary identifiers and therefore forensic facial reconstruction/approximation is often used to obtain information on a case [1,2].

The facial reconstruction/approximation process always begins with the placement of the eyes. Facial recognition (especially of familiar individuals) is dependent on the morphology of the orbital area [3–7], therefore it is important to be precise and correct in placing the eyes [8] and associated features. The eyes are to be positioned supero-laterally in the orbit according to guidelines established by expert studies [8–15]. Although conflicting findings on the position of the eyes have been reported [16], several studies [8,14,15] provide strong evidence of a more superior and lateral placement of the eyeball in the orbit. Specific distances of this position have been established for some populations [8,14], but it is uncertain how applicable these absolute values are in the South African context.

Variations in the position of the endocanthion and exocanthion are also reported in the literature. Although all researchers did not use directly comparable landmarks to define the position of the endocanthion and the exocanthion, the general trend indicates that the endocanthion is positioned lower than the exocanthion

* Corresponding author.
*E-mail addresses:* u27089691@tuks.co.za (H.F. Dorfling),
zarina.lockhat@up.ac.za (Z. Lockhat), Samantha.Pretorius@up.ac.za (S. Pretorius),
maryna.steyn@wits.ac.za (M. Steyn), anna.oettle@smu.ac.za (A.C. Oettlé).

[8,16]. A study by Stewart [17], however, found the endocanthion and exocanthion to be on the same level. It would therefore be of value to determine the position of these landmarks in South African groups.

Similarly, variations have been reported in the dimensions of the eyeball. Although the eyeball is often considered as almost spherical [15], slight elongation in certain axes has been reported in the literature [15,18]. The medio-lateral axis was found to often be longer than the supero-inferior axis [18].

In South Africa, guidelines created for and based on other populations are often applied in facial approximations (Capt. T.M. Briers, personal communication, 2014). However, these guidelines may not necessarily be applicable in the South African context as a degree of inter-population variation exists in facial features. It is postulated that these inter-population differences may have an effect on facial approximations and its accuracy, as is often demonstrated in practice. The less accurate a facial representation, the smaller the likelihood of an unknown individual being recognised and identified.

The purpose of this study was to assess specific features related to the eye in South Africans and compare it to established guidelines commonly used in the facial approximation process. The features assessed included the position of the eyeball within the orbit, the size of the eyeball and the position of the canthi.

## 2. Materials & methods

A total of 49 adult cadavers (38 males and 11 females, age range 22–73 years, mean age 47 years) from the dissection halls of two South African universities, namely Sefako Makgatho Health Sciences University (SMU) and the University of Pretoria (UP), were used in this study. Bodies at UP generally had their origins from local hospitals in Pretoria [1], while those at SMU originated from a wider area of the Gauteng Province and some areas in the North West Province. Samples demonstrating damage, distortion, or any effects of desiccation due to embalming were excluded.

A total of 30 computer tomography (CT) scans (23 males, 7 females, age range 21–84 years, mean age 42 years) from Steve Biko Academic Hospital affiliated with UP and 30 cone beam computer tomography (CBCT) scans (17 males and 13 females, age range 18–64 years, mean age 33) from the Oral and Dental Hospital, UP, were also used for measurement and analyses. These hospitals service the greater Gauteng area, as well as parts of the Limpopo and North West provinces. Patients' heads were orientated in the standard natural head position for scanning — supine in the case of CT and sitting in the case of CBCT. The CT scans slices taken by a Siemens SOMATOM Sensation 64 scanner were 2 mm thick. CBCT scans were obtained using a Planmeca ProMax 3D scanner with a voxel size of 0.4 mm. Scans were retrospectively analysed and excluded if not orientated in the desired plane, the implicated structures could not be clearly identified or injury to the orbital area was present. All cadavers and scans were of South Africans of African ancestry (hereafter referred to as South Africans (SA)).

Ethics clearance was obtained from the Main Ethics and Research Committee, Faculty of Health Science, University of Pretoria (Cadaver sample: 8/2016; Scan sample: 183/2016) prior to commencement of this study. The Faculty of Health Sciences Research Ethics Committee complies with the SA National Act no. 61 of 2003 as it pertains to health research.

The orbital regions of 49 cadavers were dissected and measured to determine the position of the canthi, the position of the eyeball in the orbit and the diameters of the eyeball. A non-parametric Wilcoxon Rank Sum test (2-sided) was used to investigate whether differences occurred between sexes. As the p values for all individual measurements were non-significant (p > 0.05), male and female samples were pooled for the remainder of the analyses.

The position of the canthi was determined on cadavers by pinning the Frankfort Horizontal Plane (FHP) from porion to orbitale and marking a reference plane parallel to the FHP and tangent to the most superior point on the superior orbital margin (SOM). This is similar to the methodology followed by Stephan & Davidson [8] and Stephan et al. [14]. The endo- and exocanthion were identified and pinned and four distances were measured namely (1) between the endocanthion and medial orbital margin (MOM) (en-MOM), (2) between the endocanthion and SOM (en-SOM), (3) between the exocanthion and lateral orbital margin (LOM) (ex-LOM) and (4) between the exocanthion and SOM (ex-SOM) (Fig. 1a).

To determine the position of the eyeball in the orbit of each cadaver, a circular cut was made approximately 5 mm outside of the orbital margin. The skin and orbicularis oculi muscle were removed, and the entire eyeball exposed by careful blunt dissection and removal of peri-orbital fat and tissue. Pins were placed perpendicular to the surface of the bone at the most extreme points on the LOM, MOM, IOM and SOM. Another set of four pins were placed at the shortest distances respectively from the LOM, MOM, IOM and SOM on the equator of the eyeball (an imaginary line encircling the globe of the eye equidistant from the anterior and posterior poles) [19]. Four distances were measured between the pins, namely (1) inferior equator to IOM (iIeq-IOM), (2) superior equator to SOM (Seq-SOM), (3) lateral equator to LOM (Leq-LOM) and (4) medial equator to MOM (Meq-MOM) (Fig. 1b).

Two measurements were taken on the cadavers to determine the diameters of the eyeball, namely (1) medio-lateral diameter (distance between pins at medial and lateral equators i.e. Meq-Leq) and (2) supero-inferior diameter (distance between pins at superior and inferior equators i.e. Seq-Ieq) (Fig. 1c). Individual measurements (as shown in Fig. 1b and c) were used to obtain the horizontal and vertical diameters of the orbit. For the horizontal diameter, the distances considered were Meq-MOM (Fig. 1b (4)); Meq-Leq (Fig. 1c (1)); and Leq-LOM (Fig. 1b (3)). To obtain the vertical diameter of the orbit, the distances added together were the Seq-SOM (Fig. 1b (2)); Seq-Ieq (Fig. 1c (2)); and Ieq-IOM (Fig. 1b (1))

CBCT and CT scans were imported into MevisLab [20] as Digital Imaging and Communications in Medicine (DICOM) files for measurements regarding the diameter of the eyeball. The ExaminerViewer function in MevisLab was used to visualise the 3D reconstruction of the files to ensure the correct voxel size and reconstruction. Region of Interest (ROI) Select was used to select a specific region of interest, enlarging the relevant areas, in this case the orbital area (Fig. 2). The OrthoView2D function was then used to visualise the region of interest and identify two points corresponding in all three planes (coronal, sagittal and transverse). The relevant points to determine the diameter of the eyeball were the most inferior, superior, medial, lateral, anterior and posterior points on the equator of the eyeball. Lastly, the function XMarkerListMaxDistance was used to measure the distance between the identified points. Scans were orientated, points identified and measurements taken on a multiplanar level as the relevant landmarks and distances were not necessarily visible on a single plane simultaneously. The points, however, retained their respective three-dimensional (3D) positions regardless of scrolling through the slices. The dimensions reflecting the size and shape of the eyeball included the antero-posterior diameter (Aeq-Peq) (Fig. 3a), the medio-lateral diameter (Meq-Leq) (Fig. 3b) and the supero-inferior diameter (Seq-Ieq) (Fig. 3c). Although visualisation of the eyeball on the 2D figure is not that clear, by scrolling up and down on the 3D image, the borders of the eyeball could be more readily identified thus enabling measurements. Non-parametric Wilcoxon Rank Sum tests (2-sided) once again determined non-significant variations (p > 0.05) between male and female, thus samples were pooled.
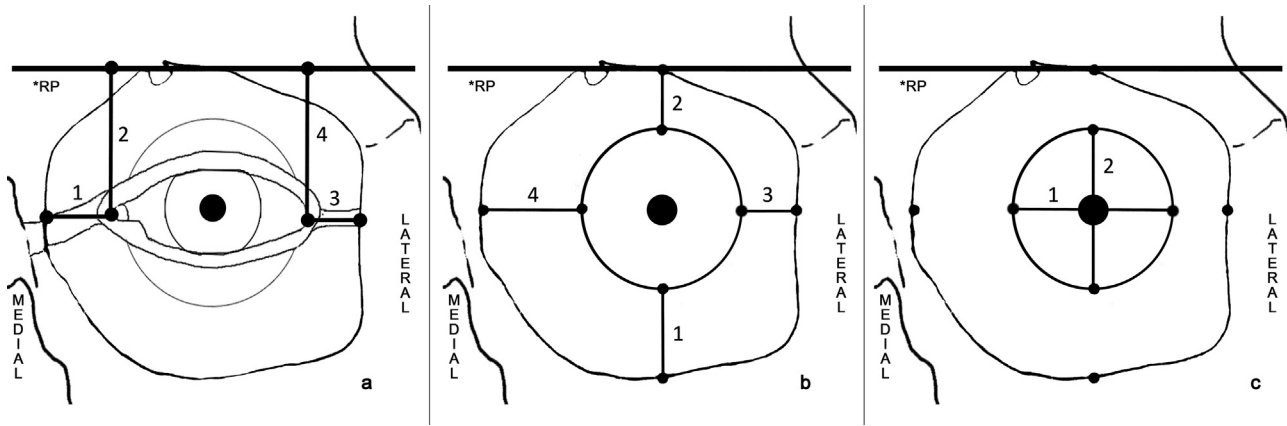
**Fig. 1.** Orbital and optic measurements. *RP: Reference plane parallel to FHP.
(a) Position of the canthi
1: distance between the medial canthus and MOM
2: distance between the medial canthus and SOM reference plane
3: distance between the lateral canthus and LOM
4: distance between the lateral canthus and the SOM reference plane.
(b) Position of the eyeball in the orbit
1: distance between the inferior equator and the IOM
2: distance between the superior equator and SOM
3: distance between the lateral equator and LOM
4: distance between the medial equator and MOM.
(c) Size of the eyeball
1: medio-lateral diameter (distance from the medial equator to the lateral equator)
2: supero-inferior diameter (distance from the superior to inferior equator).

The data were tested for variations between the sexes by means of a non-parametric Wilcoxon Rank Sum test (2-sided). Male and female samples were pooled together as there were no statistical differences between the sexes (except CBCT Meq-Leq where $p < 0.05$).

Comparisons were conducted between the measurements of the eyeball for all three modalities (dissection, CT and CBCT) utilising the Kruskal–Wallis test. The Kruskal–Wallis test is a non-parametric version of the classical one-way ANOVA, and an extension of the Wilcoxon Rank Sum test to more than two groups. Further comparisons on the medio-lateral and supero-inferior diameters were done between two modalities at a time by means of the non-parametric Wilcoxon Rank Sum test, i.e. CT vs CBCT; CT vs dissection and dissections vs CBCT.

Intra-observer repeatability was assured for all measurements by obtaining three measurements for each dimension and calculating

the technical error of measurement (TEM). Inter-observer repeatability testing was performed by obtaining measurements from one other observer. A total of 38 cadavers as well as all CT and CBCT scans were re-measured for all parameters. Interclass Correlation Coefficient A-1 (ICC) testing was done to compare measurements obtained by the two different observers.

## 3. Results

TEM results for cadaver measurements were all very low, with the mean reported as <0.02 mm. CT scan TEM results were all calculated as <0.2 mm. CBCT scan results however, were less accurate with TEM results for Meq-Leq calculated at 0.88 mm, Seq-leq at 0.81 mm and Aeq-Peq at 1.31 mm. The accuracy of the measurements, when repeated by the same researcher, was
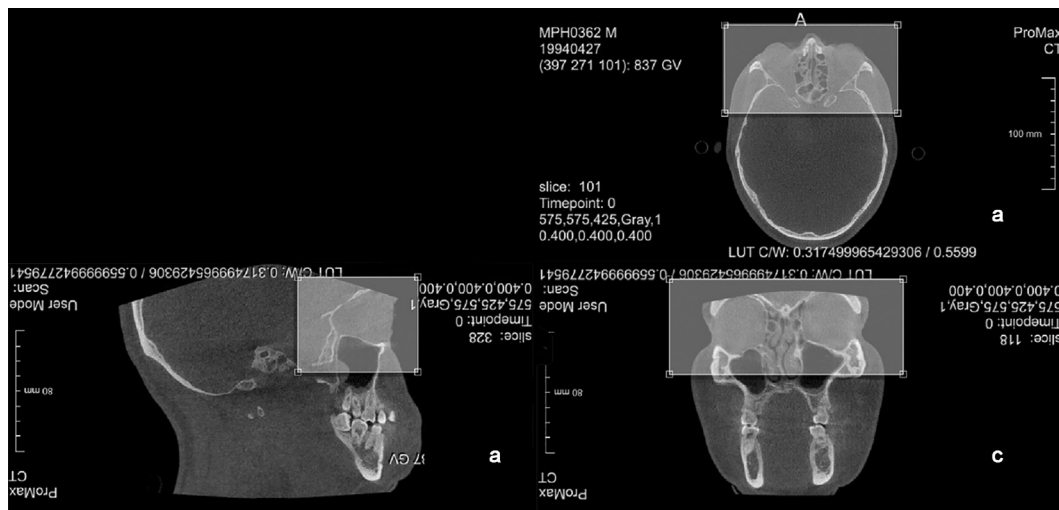


**Fig. 2.** Selecting the region of interest on MevisLab.
(a) Transvers plane; (b) sagittal plane and (c) coronal plane.
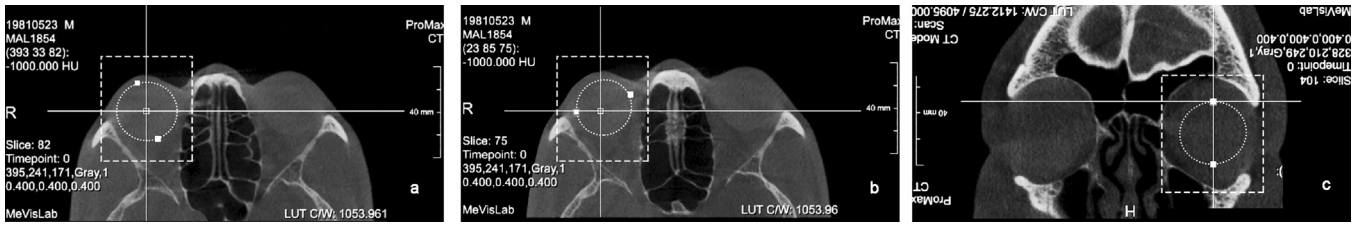
**Fig. 3.** Measuring the diameters of the eyeball between white squares.
(a) Antero-posterior diameter; (b) medio-lateral diameter; (c) supero-inferior diameter.

considered higher the closer the TEM was to zero. Therefore, due to such small TEM's, the average measurement for each parameter was used for all further statistical analyses.

Descriptive statistics of the dimensions describing specific features of the eye including the position of the canthi, the position of the eyeball and the size of the eyeball were calculated and are summarised in Figs. 4–6, respectively.

Regarding the position of the canthi (Fig. 4), the endocanthion was found to be located higher and closer to the orbital margin than the exocanthion. Distances between ex-SOM (4) were found to be greater than the en-SOM (2) ($p < 0.01$), indicating that the exocanthion is located lower than the endocanthion in relation to the SOM reference plane.

From Fig. 5 it can be noted that the eyeball is positioned supero-laterally within the orbit. A statistically significant difference between the distances of the Seq-SOM and Ieq-IOM ($p < 0.01$) and the Meq-MOM and Leq-LOM ($p < 0.01$) was found. Fig. 5 illustrates that the distances between Seq-SOM (2) and Leq-LOM (3) were smaller than the distances between Ieq-IOM (1) and Meq-MOM (4), indicating that the eyeball is located more supero-laterally within the orbit. The dimensions of the eyeball with all modalities demonstrated a transverse elongation. The diameter of the eyeball (Fig. 6) as measured on cadavers (1), indicated that the medio-lateral diameter was greater at statistically significantly levels than the supero-inferior diameter ($p < 0.01$). Similar results were found with CT (2) ($p < 0.01$) and CBCT (3).

Calculations show that the width of the orbit is consistently greater that the height of the orbit, ($p < 0.01$) indicating a more rectangular shaped orbit. The shape of the eyeball thus reflects the shape of the orbits.
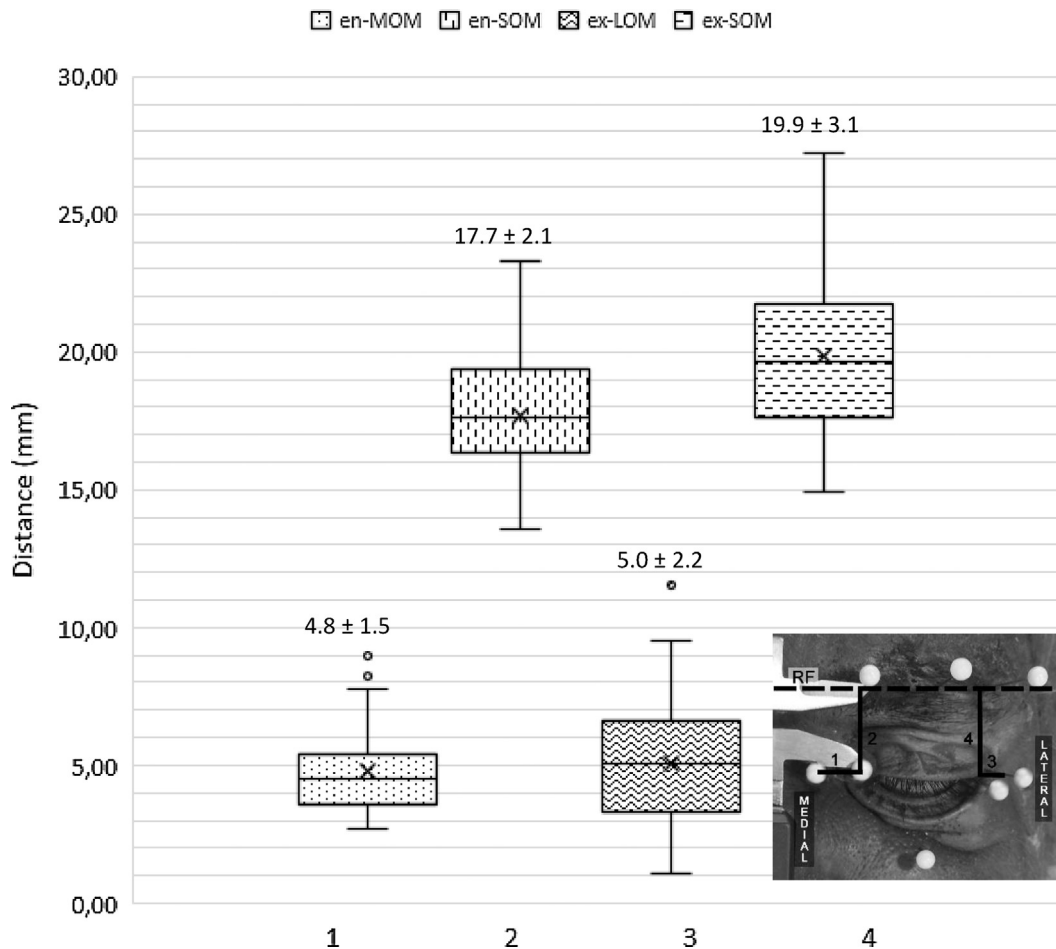


**Fig. 4.** Basic descriptive statistics for the measurements pertaining to the position of the canthi. (1) Distance between endocanthion and MOM, (2) distance between endocanthion and SOM, (3) distance between exocanthion and LOM and (4) distances between exocanthion and SOM.
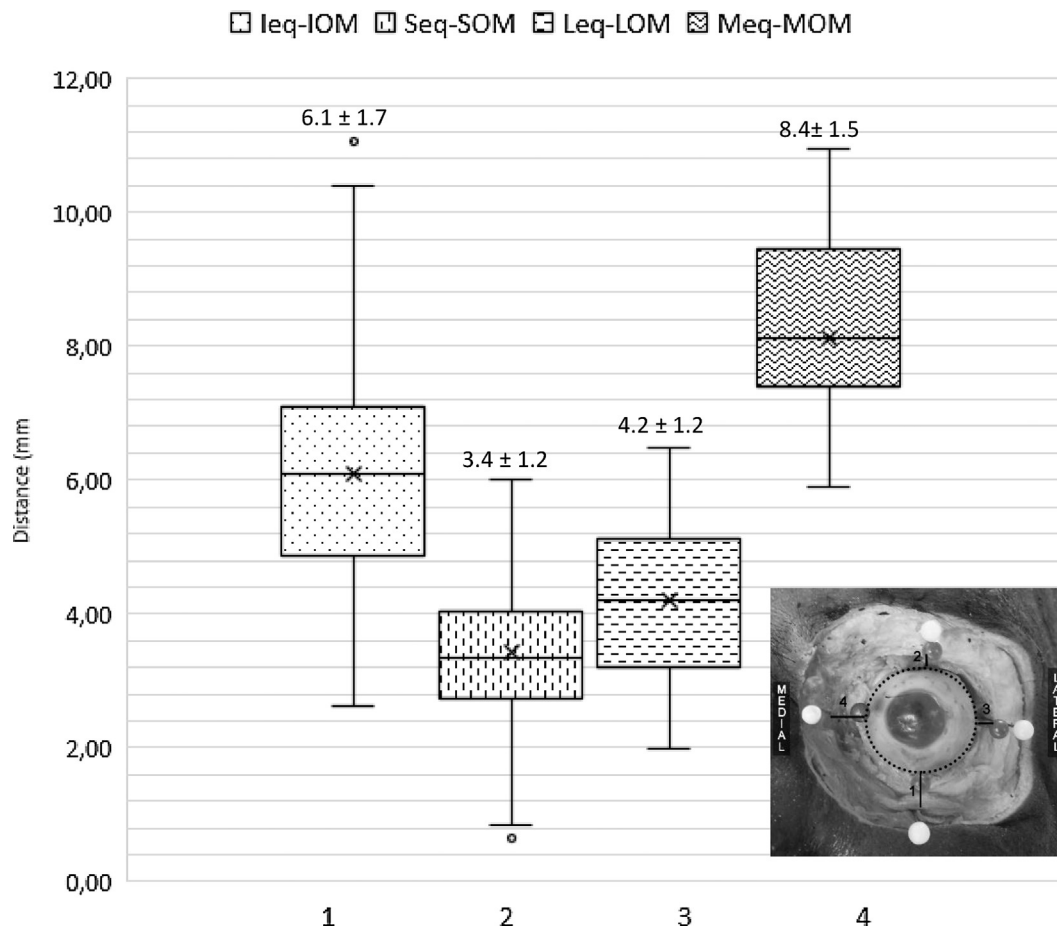
**Fig. 5.** Basic descriptive statistics for measurements pertaining to the position of the eyeball in the orbit in dissections. (1) Distances between the inferior equator and the IOM, (2) distances between the superior equator and the SOM, (3) distances between the lateral equator and the LOM and (4) distances between the medial equator and the MOM.

### 3.1. Statistical comparisons between modalities

Comparisons between two modalities were performed by utilising a Wilcoxon Rank Sum test for each of the three diameters (medio-lateral, supero-inferior and antero-posterior) of the eyeball. Box-and-whisker plots illustrate the variations in measurements obtained by using the different modalities (Fig. 6).

The dissection and CBCT measurements of the medio-lateral and supero-inferior dimensions of the eyeball showed a greater agreement than did CT measurements vs. CBCT measurements. This is demonstrated in the non-statistically significant differences demonstrated in the CBCT vs dissection derived means ($p = 0.39$), while the variation between CT vs dissection measurements concerning the medio-lateral diameter was statistically significant ($p < 0.01$) and so was CBCT vs CT ($p < 0.01$). When considering the supero-inferior diameter, a statistically significant difference existed when comparing CBCT and CT ($p < 0.01$); however, this difference was less significant when comparing CBCT to cadaver measurements ($p = 0.02$). The variation in the supero-inferior diameters when comparing CT to dissection measurements was not statistically significant ($p = 0.05$). CBCT data had the highest mean values, followed by the dissection data and then the CT data. Dissection data, however, had the greatest range, followed by CT data and lastly CBCT data. When comparing CBCT to CT measurements for the antero-posterior diameter, a statistically significant difference was observed ($p < 0.01$).

Table 1 summarises the descriptive relationships for measurements performed on dissections, CBCT and CT scans. From the relationship between measurements, it can be seen that the distance from the exocanthion to SOM was greater than the distance from the endocanthion to the SOM, indicating that the exocanthion was on average located lower than the endocanthion. The width of the orbit was greater than the height, indicating that the orbit was more rectangular shaped. It can also be seen that the distance of the medial equator to the MOM and the distance of the inferior equator to the IOM was greater than the distance between the lateral equator to LOM and superior equator to SOM, demonstrating a more supero-laterally positioned eyeball. The medio-lateral diameter was also greater than the supero-inferior diameter, indicating that the eyeball is elongated or oval shaped in the transverse axis.

ICC tests for cadaver measurements performed consistently, with excellent agreement (ICC > 0.90) between observers for ex-SOM, Meq-MOM, Leq-LOM, Ieq-IOM, and Leq-Meq. Good agreement (ICC > 0.85) was found between observers for en-SOM, Seq-SOM, Seq-Ieq, however the ex-LOM showed only moderate agreement (ICC = 0.68) and the en-MOM dimension displayed poor inter-observer repeatability (ICC = 0.04). Inter-observer repeatability tests for all CT and CBCT scan measurements were reported as less than 0.21.

### 4. Discussion and conclusions

In this study, specific dimensions (absolute measurements and relationships between measurements) of the eye and orbit in South Africans were determined. Fig. 7 summarises the findings recorded in the literature and mean dimensions observed in this
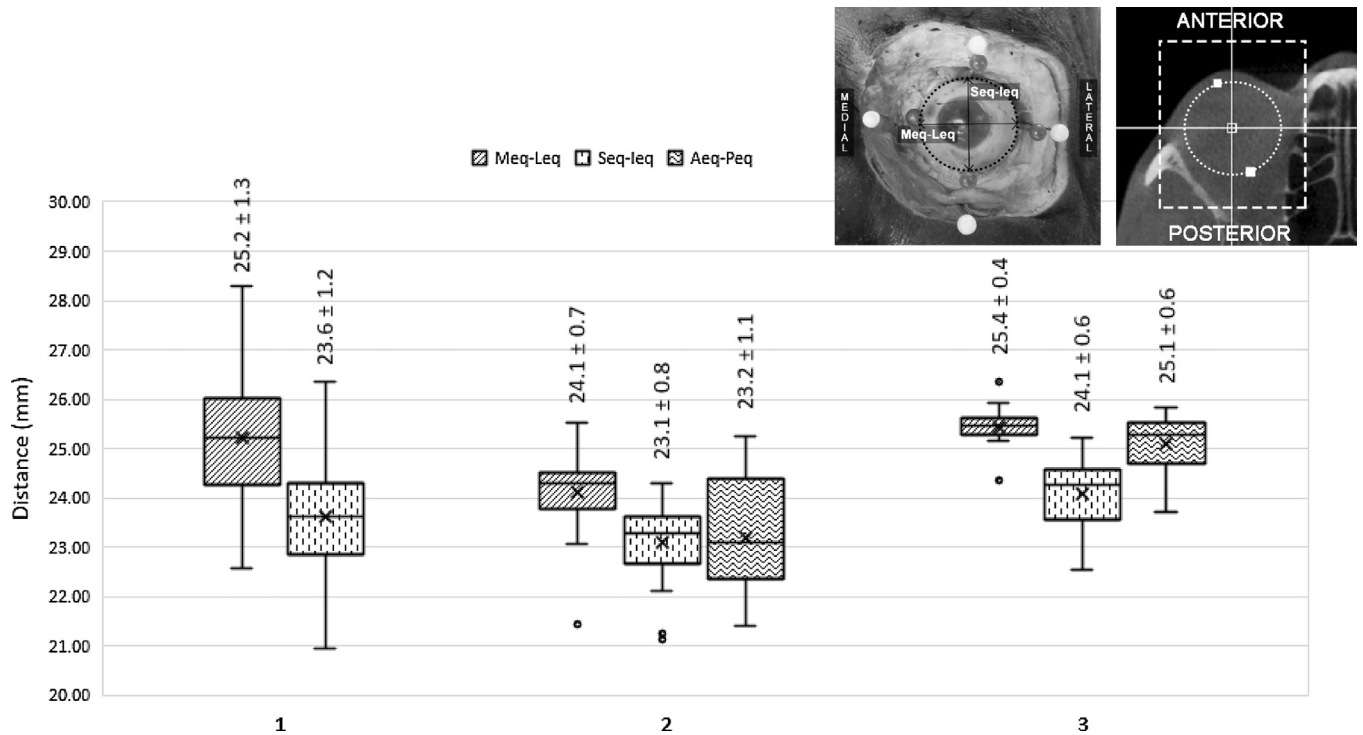
Fig. 6. Basic descriptive statistics for measurements pertaining to the size of the eyeball in all three modalities: (1) dissections, (2) CT scans and (3) CBCT scans.
Kruskal–Wallis test (dissections vs CT vs CBCT) for medio-lateral diameter p-value <0.01.
Kruskal–Wallis test (dissections vs CT vs CBCT) for supero-inferior diameter p-value <0.01.
Wilcoxon Rank Sum test (CT vs CBCT) for antero-posterior diameter p-value <0.01.

**Table 1**
Descriptive relationships between measurements.

| Measurements compared | Description | Result | Dissections (Wilcoxon Rank Sum test) | | CBCT (Signed Rank Test) | | CT (Signed Rank Test) | |
|---|---|---|---|---|---|---|---|---|
| | | | Ratio | p-Value | Ratio | p-Value | Ratio | p-Value |
| en-SOM vs ex-SOM | Vertical position of the canthi | ex-SOM > en-SOM | 1.12 | <0.01 | | | | |
| Width of orbit vs Height of orbit | Orbital shape | Width > Height | 1.14 | <0.01 | | | | |
| Meq–MOM vs Leq–LOM | Horizontal position of eyeball in the orbit | Meq–MOM > Leq–LOM | 1.98 | <0.01 | | | | |
| Seq–SOM vs Ieq–IOM | Vertical position of eyeball in the orbit | Ieq–IOM > Seq–SOM | 1.79 | <0.01 | | | | |
| Medial–lateral equators vs superior–inferior equators | Shape of eyeball | Meq-Leq > Seq-Ieq | 1.07 | <0.01 | 1.05 | <0.01 | 1.04 | <0.01 |

study. Integration of the measurements obtained from the three modalities used (cadaver dissections, CT and CBCT) demonstrates that the exocanthion was positioned lower than the endocanthion, the orbit was rectangular-shaped and the oval shaped eyeball was situated in the superolateral aspect of the orbit. Findings regarding the shape of the orbit were in agreement with Krogman (1955) and others stating that the orbits of skulls of Africans are more rectangular than those from other populations.

While most of the cadaver measurements had good inter-observer repeatability, the en-MOM dimension displayed poorly (ICC = 0.04). This observation might be explained by the exact placement of the MOM that is not clearly defined. Unlike the lateral orbital margin, the MOM is less well defined, rounded and irregular. Inter-observer repeatability tests on CBCT and CT scan measurements had a similar performance but were less well than expected (All ICC < 0.21) as compared to intra-observer tests. Mean values of most measurements, however, differed with less than 2 mm in general, which may be considered acceptable [21].

Variations in the exact position of the endocanthion and exocanthion are reported in the literature. In most research done previously, the endocanthion was reported to be situated *lower* than the exocanthion. According to Stephan and Davidson [8], the endocanthion in an Australian population lies lower than the exocanthion, with the endocanthion approximately 19.5 mm below the SOM reference plane and the exocanthion 18.5 mm below the SOM reference plane. Kim et al. [16] similarly reported that in their sample of Korean individuals, the endocanthion is found lower than the exocanthion, at 22.8 mm and 20.2 mm respectively below the SOM. However, although specific distances are quite similar, especially to Ref. [8], in contrast to these studies reporting on the position of the canthi, the current study found the endocanthion to be positioned *higher* than the exocanthion. The endocanthion was located 17.7 mm below the SOM reference plane and the exocanthion was situated 19.5 mm below the SOM reference plane. It is reasonable to postulate that the differences in position observed in this population may be related to the
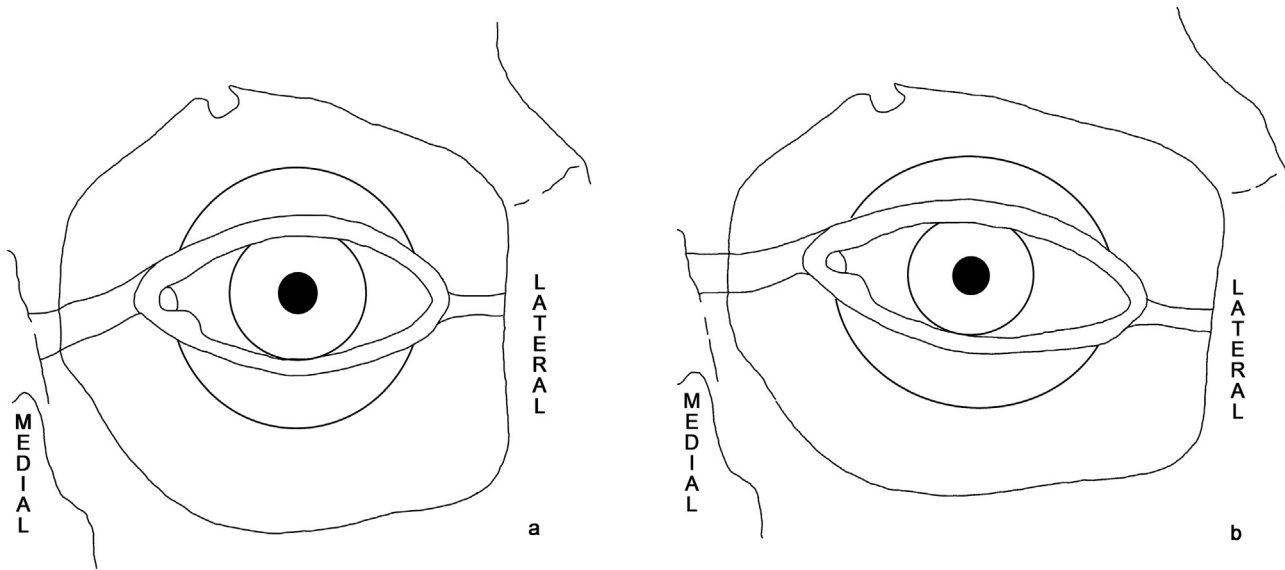
**Fig. 7.** Graphic illustration of (a) the expected findings and (b) the mean dimensions of this study sample.

population specific variation in the morphology of the zygomatic bone as well as the zygomatic processes of the frontal and maxillary bones contributing to the margins of the orbit resulting in variations in the shape of the orbital border [22].

Reports regarding the distance of the exocanthion from the lateral orbital margin are remarkably similar at 4.5 mm [8], 4.7 mm [16] and 5 mm medial to the malar tubercle [23], and are comparable to our findings (5.0 mm). The distance from the medial orbital margin to the endocanthion is more variable: 4.8 mm [8], 9.8 mm [16], approximately 2 mm lateral to the MOM [23] and 4.8 mm (current study). The variation noted in the Korean sample [16] might be due to the presence of epicanthal folds in people of Asian descent. Epicanthal folds that cover the endocanthion may influence the inclination of the eye fissure's in the longitudinal axis, by shifting the medial point of the axis from the endocanthion to a lower positioned point at the crossing of the epicanthus with the rim of the lower eyelid [24]. It may also be influenced by the size and shape of the nasal root [24].

Considering the position of the eyeball in the orbit, measurements found in this study are consistent with many previous studies, indicating a more supero-laterally placed eyeball [8–11,13,14]. Distances observed in this population group were measured as 3.4 mm from the SOM, 6.1 mm from the IOM, 8.3 mm from the MOM and 4.2 mm from the LOM. Distances reported by other authors [8,9,11,14] ranged between 4.0–5.0 mm from the SOM; 6.8–7.8 mm from the IOM; 6.5–8.0 mm from the MOM and 3.9–4.5 mm from the LOM. Although some

measurements obtained in this study are similar to the other studies (e.g., Refs. [8,9,11,14]), small differences are observed cumulatively in the transverse axis (i.e. the medial equator to MOM plus lateral equator to LOM), as compared to the longitudinal axis (i.e. the superior equator to SOM plus inferior equator to IOM). This is indicative of a greater periorbital space transversely compared to a smaller periorbital space observed longitudinally. These greater distances in the transverse axis in the African group is probably related to the more rectangular shape of the orbit in this group.

Evaluation of the diameters of the eyeball (summarised in Table 2) indicate an oval shape (elongation in the transverse axis) which has also been observed by clinicians [18,25]. The medio-lateral diameter of the eye in Africans is slightly greater than the supero-inferior diameter, but also to a small extent (approximately 1 mm) greater than in other population groups [15,18]. All diameters were marginally greater on CBCT than reported on other modalities and other groups while the CT findings were more in agreement with previous findings [15,18,25,26].

In conclusion, it was found that dimensions of the eye itself and its relative position in the orbit in South Africans varied minimally from the established guidelines. However, the more rectangular orbit resulted in a more transversely elongated eyeball which was located supero-laterally within the orbit. The exocanthion in this group was situated lower than the endocanthion, in contrast to what was found in other studies. These variations can have a significant impact on the approximation of this pivotal feature. The combined effect of these variations can influence the likelihood of

**Table 2**
Summary of variations in eyeball diameters.

| Author(s) | Year | Modality | n | Ancestry | Antero-posterior diameter | SD | Medio-lateral diameter | SD | Supero-inferior diameter | SD |
|---|---|---|---|---|---|---|---|---|---|---|
| Wilkinson & Mautner | 2003 | MRI | 39 | European | 23.28 | 1.66 | – | – | – | – |
| Guyomarc'h et al. | 2012 | CT | 375 | French | 23.7 | – | 24.3 | – | 24.6 | – |
| Bekerman et al. | 2014 | CT | 500 | Mixed ancestral groups | 22.1–24.9 | – | 24.1–24.3 | – | 23.7– 23.8 | – |
| Özer et al. | 2016 | CT | 198 | Turkish | 22.7 (females) | 6.38 (females) | – | – | – | – |
| | | | | | 23.3 (males) | 0.88 (males) | | | | |
| This study | 2017 | Dissections | 36 | SA | – | – | 25.2 | 1.42 | 23.6 | 1.29 |
| This study | 2017 | CT | 30 | SA | 23.2 | 1.07 | 24.1 | 0.73 | 23.1 | 0.75 |
| This study | 2017 | CBCT | 30 | SA | 25.1 | 0.56 | 25.4 | 0.38 | 24.1 | 0.64 |

an unknown individual being identified, and therefore population specific standards should be used in cases of facial approximation.

## Conflict of interest declaration

None.

## Acknowledgements

## References

[1] E.N. L'Abbé, M. Loots, J.H. Meiring, The Pretoria Bone Collection: a modern South African skeletal sample, HOMO — J. Comp. Hum. Biol. 56 (2005) 197–205.

[2] D. Cavanagh, M. Steyn, Facial reconstruction: soft tissue thickness values for South African black females, Forensic Sci. Int. 206 (2011) 215.e1–215.e7.

[3] E. Hjelmas, J. Wroldsen, Recognizing faces from the eyes only, Proceedings of the 11th Scandinavian Conference on Image Analysis, Citeseer, 1999.

[4] H.D. Ellis, J.W. Shepherd, G.M. Davies, Identification of familiar and unfamiliar faces from internal and external features: some implications for theories of face recognition, Perception 8 (1979) 431–439.

[5] S.J. McKelvie, The role of eyes and mouth in the memory of a face, Am. J. Psychol. (1976) 311–323.

[6] N.D. Haig, Exploring recognition with interchanged facial features, Perception 15 (1986) 235–247.

[7] N.D. Haig, The effect of feature displacement on face recognition, Perception 42 (1984) 1158–1165.

[8] C.N. Stephan, P.L. Davidson, The placement of the human eyeball and canthi in craniofacial identification, J. Forensic Sci. 53 (2008) 612–619.

[9] S.E. Whitnall, The Anatomy of the Human Orbit and Accessory Organs of Vision, Oxford Medical Publications, London, 1921.

[10] W.W. Goldnamer, The Anatomy of the Human Eye and Orbit, Professional Press, 1923.

[11] S.E. Whitnall, The Anatomy of the Human Orbit and Accessory Organs of Vision, Oxford University Press, London, 1932.

[12] E. Wolff, The Anatomy of the Eye and Orbit, Including the Central Connections, Development, and Comparative Anatomy of the Visual Apparatus, H.K. Lewis, London, 1933.

[13] A. Bron, R. Tripathi, B. Tripathi, Wolff's Anatomy of the Eye and Orbit, 8th ed., Chapman & Hall Medical, London, UK, 1997.

[14] C.N. Stephan, A.J.R. Haung, P.L. Davidson, Further evidence on the anatomical placement of the human eyeball for facial approximation and craniofacial superimposition, J. Forensic Sci. 54 (2009) 267–269.

[15] P. Guyomarc'h, B. Dutailly, C. Couture, H. Coqueugniot, Anatomical placement of the human eyeball in the orbit—validation using CT scans of living adults and prediction for facial approximation, J. Forensic Sci. 57 (2012) 1271–1275.

[16] S.-R. Kim, K.-M. Lee, J.-H. Cho, H.-S. Hwang, Three-dimensional prediction of the human eyeball and canthi for craniofacial reconstruction using cone-beam computed tomography, Forensic Sci. Int. 261 (2016) 164.e1–164.e8.

[17] T. Stewart, The points of attachment of the palpebral ligaments: their use in facial reconstructions on the skull, J. Forensic Sci. 28 (1983) 858–863.

[18] I. Bekerman, P. Gottlieb, M. Vaiman, Variations in eyeball diameters of the healthy adults, J. Ophthalmol. 2014 (2014) 5.

[19] mediLexicon, Equator of Eyeball, mediLexicon, 2017.

[20] MeVisLab. https://www.mevislab.de, MeVis Medical Solutions AG, Germany, 2016.

[21] P.Z. Mala, Pronasale position: an appraisal of two recently proposed methods for predicting nasal projection in facial reconstruction, J. Forensic Sci. 58 (4) (2013) 957–963.

[22] A.C. Oettlé, F.P. Demeter, E.N. L'abbé, Ancestral variations in the shape and size of the zygoma, Anat. Rec. 300 (2017) 196–208.

[23] T. Balueva, E. Veselovskaya, E. Kobyliansky, Craniofacial reconstruction by applying the ultrasound method in live human populations, Int. J. Anthropol. 24 (2009) 87–111.

[24] L. Farkas, Anthropometry of the Head & Face, 2nd ed., Raven Press, New York, 1994.

[25] C.M. Özer, I.I. Öz, I. Serifoglu, M.Ç. Büyükuysal, Ç. Barut, Evaluation of eyeball and orbit in relation to gender and age, J. Craniofac. Surg. 27 (2016) e793–e800.

[26] C.M. Wilkinson, S.A. Mautner, Measurement of eyeball protrusion and its application in facial reconstruction, J. Forensic Sci. 48 (2003) 12–16.

# Normative Facial Capulometric Measurements in a Black South African Population

H.F. SWANEPOEL,[1] H. MATTHEWS,[2] E.N. L'ABBÉ,[1] A.C. OETTLÉ,[1,3]

[1] Department of Anatomy, Faculty of Health Sciences, University of Pretoria
[2] Medical Image Research Centre, Katholieke Universiteit Leuven
3 Department of Anatomy and Histology, School of Medicine, Sefako Makgatho Health Sciences University

April 2022
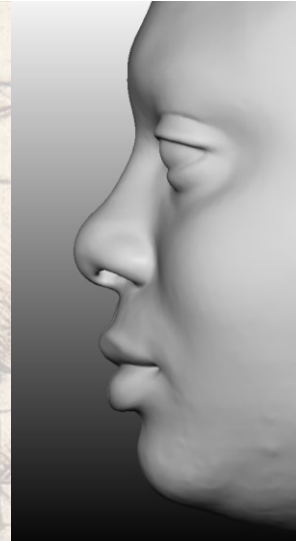
Co-funded by the Bakeng se Afrika
Erasmus+ Programme
of the European Union

UNIVERSITEIT VAN PRETORIA
UNIVERSITY OF PRETORIA
YUNIBESITHI YA PRETORIA

# Background

- The face is important for both functional aspects and fundamental social interactions, as well as being the means by which a person is recognised
- Ratios and absolute measurements based on capulometric landmarks are valuable
  - e.g. forensic approximations, reconstructive or aesthetic surgery, facial prosthetics (Sforza, de Menezes and Ferrario, 2013)

- Landmark identification on 3D surface renderings are more realistic and accurate than on 2D planes, and both CT and CBCT are appropriate modalities for 3D measurements (Ganguly *et al.*, 2011; Kim *et al.*, 2012; Ali, Chandna and Munjal, 2020)

# Aim

To generate population specific capulometric measurements for inter-landmark distances in a Black South African population from Computed Tomography and Cone Beam Computed Tomography scans

# Materials & Methods

- Ethics approval obtained from the Research Committee of the Faculty of Health Sciences of the University of Pretoria (58/2020)
- 117 Computed Tomography (CT) scans of black South African faces
  - 67 males and 50 females, age range 18 – 85; mean age 39 years
- 118 Cone Beam Computed Tomography (CBCT) scans of black South African faces
  - 64 males and 54 females, age range 19 – 87; mean age 40 years
1. UP Oral and Dental Hospital
2. Life Groenkloof Hospital
3. Cintocare Hospital

154

# Materials & Methods



1. Segmentation: visualise soft tissue meshes of the faces in Mevislab

2. Correspondence: geometrical relationship between two or more surfaces, or a one-to-one correspondence between landmarks on the various surfaces
   - Rigid initialisation (initial alignment) from 5 landmarks
   - Non-rigid and rigid scaled surface registration (mapping) or optimisation

3. Validation of automatic landmarks
   - Twenty-four anatomical landmarks were manually identified on each face using MevisLab 3.0.2 software
   - Mean Euclidean Distances (MED) calculated for intra-and interobserver sets on manually and automatically indicated landmarks

4. Inter-landmark distances were calculated from automatically indicated landmarks using Matlab and the Meshmonk toolbox
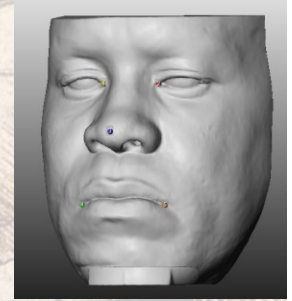


Scaled Rigid Registration
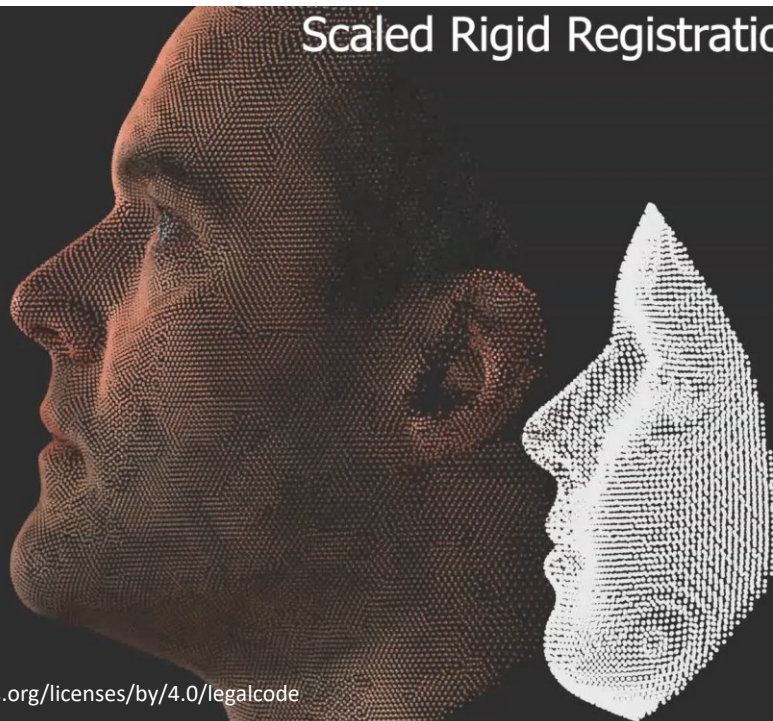
# Materials & Methods



1. Segmentation: visualise soft tissue meshes of the faces (Mevislab 3.0.2)
2. Correspondence: geometrical relationship between two or more surfaces, or a one-to-one correspondence between landmarks on the various surfaces (Matlab and the Meshmonk toolbox)
   - Rigid initialisation (initial alignment) from 5 landmarks
   - Non-rigid and rigid scaled surface registration (mapping) or optimisation
3. Validation of automatic landmarks
   - Twenty-four anatomical landmarks manually identified on each face (MevisLab 3.0.2)
   - Mean Euclidean Distances (MED) calculated for intra-and interobserver sets on manually and automatically indicated landmarks
4. Inter-landmark distances were calculated from automatically indicated landmarks (Matlab and the Meshmonk toolbox)
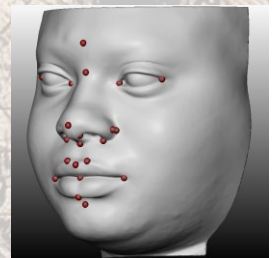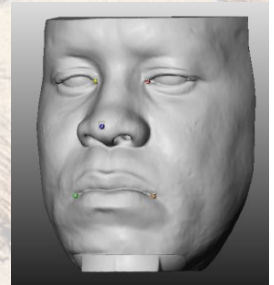
# Repeatability Results

- n = 40
- Dispersion errors: Mean Euclidean Distance (MED) calculated for each manual and automatic landmark indication for intra –and interobserver repeatability
- Distances under 2 mm is considered acceptable and reproductible (Ridel *et al.*, 2020)
- Automatic landmark indications performed better – used for calculation of inter-landmark distances and all further statistical analyses



Mean dispersion (measurement error) of landmark positions

|  | Manual | | Automatic | |
|---|---|---|---|---|
|  | Intra | Inter | Intra | Inter |
| Mean | 0,57 | 0,76 | **0,47** | 0,62 |
| SD | 0,41 | 0,55 | 0,10 | 0,12 |

1 vs 2 manual (intra)   1 vs 3 manual (inter)   1 vs 2 auto (intra)   1 vs 3 auto (inter)
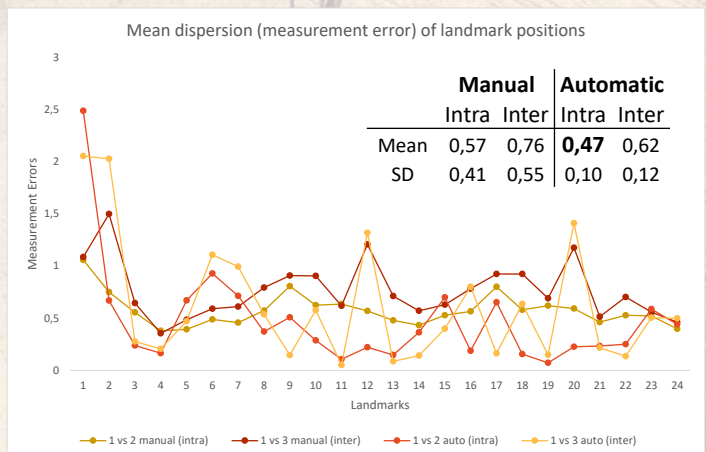
| Measurement (mm) | CBCT F (n=54) | CBCT M (n=64) | CT F (n=50) | CT M (n=67) |
|---|---|---|---|---|
| 1. Nasal Length | **39.62** ± 3.43 (32.66 - 47.71) | **42.06** ± 3.40 (35.33 - 49.32) | **39.20** ± 3.15 (33.54 - 45.79) | **40.59** ± 3.24 (34.15 - 48.93) |
| 2. Nasal Height | **46.49** ± 3.17 (40.32 - 56.37) | **48.79** ± 3.33 (42.62 - 56.21) | **46.86** ± 3.12 (40.86 - 54.45) | **48.58** ± 3.14 (42.37 - 56.30) |
| 3. Nasal Protrusion | **16.20** ± 1.53 (12.92 - 20.34) | **16.96** ± 1.48 (14.17 - 22.03) | **16.29** ± 1.44 (13.25 - 20.47) | **17.02** ± 1.82 (12.57 - 22.35) |
| 4. Nasal Width | **41.84** ± 3.74 (35.05 - 50.62) | **45.22** ± 4.31 (36.39 - 53.53) | **41.64** ± 3.18 (37.02 - 51.97) | **45.56** ± 3.44 (35.02 - 53.78) |
| 5. Alar Length Lt | **30.37** ± 2.56 (24.25 - 36.74) | **32.97** ± 2.69 (25.99 - 38.28) | **30.15** ± 1.94 (26.82 - 34.89) | **33.15** ± 2.46 (27.37 - 39.14) |
| 6. Alar Length Rt | **30.69** ± 2.71 (25.59 - 39.25) | **33.84** ± 2.77 (26.58 - 41.21) | **30.50** ± 1.92 (26.31 - 35.82) | **33.76** ± 2.29 (27.69 - 38.90) |
| 7. Columella Width | **9.81** ± 1.43 (6.65 - 13.01) | **10.57** ± 1.12 (8.41 - 12.99) | **10.01** ± 1.25 (6.59 - 12.94) | **10.78** ± 1.22 (7.614 - 13.18) |
| 8. Columella Length Lt | **7.79 ± 1.21** (5.83 - 11.72) | **8.58 ± 1.45** (5.80 - 12.61) | **8.12 ± 1.13** (5.93 - 11.22) | **8.74 ± 1.26** (6.07 - 11.89) |
| 9. Columella Length Rt | **7.91 ± 1.27** (5.47 - 10.87) | **8.38 ± 1.27** (6.02 - 11.83) | **8.03 ± 1.22** (5.93 - 11.66) | **8.65 ± 1.30** (6.46 - 13.00) |
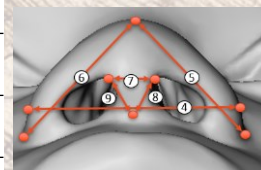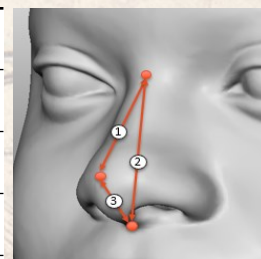
South African black and white: (Ridel, Demeter, Liebenberg, L'Abbé, Vandermeulen and Oettlé, 2018)
Nigerian: (Jimoh, Alabi, Kayode, Salihu and Ogidi, 2011)
Kenyan: (Virdi, Wertheim and Naini, 2019)
Iranian: (Heidari, Mahmoudzadeh-Sagheb, Khammar and Khammar, 2009)

# Statistical Significant Variations: Nasal parameters

| | | Nasal length | Nasal height | Nasal protrusion | Nasal width | Alar length Lt | Alar length Rt | Columella width | Columella length Lt | Columella length Rt |
|---|---|---|---|---|---|---|---|---|---|---|
| **Between sexes:** | CBCT F vs M | 0.0005 | 0.0008 | 0.0048 | < 0.0001 | < 0.0001 | < 0.0001 | 0.0061 | 0.0019 | 0.0471 |
| | CT F vs M | x | 0.0228 | 0.0401 | < 0.0001 | < 0.0001 | < 0.0001 | 0.0065 | 0.0091 | 0.0058 |
| **Between modalities:** | CBCT vs CT F | x | x | x | x | x | x | x | x | x |
| | CBCT vs CT M | x | x | x | x | x | x | x | x | x |
| | CBCT F | Weak - | Weak - | Weak + | Weak + | Weak + | Weak + | Weak + | Weak - | Mild + |
| | CBCT M | Weak + | Weak + | Weak + | Weak + | Weak - | Weak + | Mild + | Mild + | Mild + |
| | CT F | Weak + | Weak + | Weak + | Weak + | Weak + | Weak + | Mild + | Weak + | Mild + |
| **Age correlation** | CT M | Weak - | Weak + | Weak + | Mod + | Weak + | Weak + | Mild + | Weak + | Weak + |

South African study: (Schmidlin *et al.,* 2018)

| Measurement (mm) | CBCT F (n=29) | CBCT M (n=44) | CT F (n=18) | CT M (n=35) |
|---|---|---|---|---|
| 1. Palpebral Fissure Width Lt | **26.90** ± 1.60 (24.04 - 30.56) | **27.55** ± 1.63 (23.05 - 30.61) | **27.17** ± 2.22 (23.91 - 32.31) | **27.57** ± 1.89 (24.90 - 32.05) |
| 2. Palpebral Fissure Width Rt | **27.20** ± 2.18 (24.06 - 31.97) | **27.73** ± 1.77 (24.40 - 31.80) | **27.01** ± 2.23 (23.69 - 31.82) | **27.71** ± 1.43 (25.04 - 30.41) |
| 3. Inter-Canthal Width | **42.08** ± 2.75 (35.97 - 47.65) | **43.04** ± 3.35 (33.94 - 48.32) | **41.04** ± 2.97 (33.66 - 45.28) | **42.86** ± 3.77 (34.90 - 50.07) |
| 4. Outer-Canthal Width | **93.73** ± 4.49 (84.79 - 103.29) | **96.21** ± 3.33 (88.22 - 103.54) | **93.66** ± 4.39 (87.79 - 99.85) | **96.86** ± 4.27 (88.19 - 110.22) |
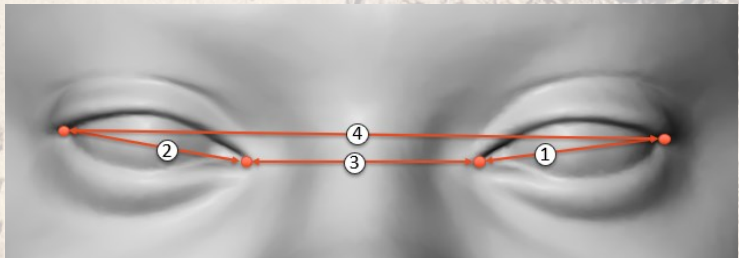


Kenyan: Virdi, Wertheim and Naini, 2019
American white: Price, Gupta, Woodward, Stinnett and Murchison, 2009
European white: Guo, Schaub, Mor, Jia, Koch and Heindl, 2020

# Statistical Significant Variations: Ocular parameters

| | | Palpebral fissure width Lt | Palpebral fissure width Rt | Inter-canthal width | Outer-canthal width |
|---|---|---|---|---|---|
| **Between sexes:** | CBCT F vs M | x | x | x | 0.0161 |
| | CT F vs M | x | x | x | 0.0315 |
| **Between modalities:** | CBCT vs CT F | x | x | x | x |
| | CBCT vs CT M | x | x | x | x |
| **Age correlation:** | CBCT F | Weak + | Weak + | Weak - | Weak - |
| | CBCT M | Weak + | Weak + | Weak - | Weak - |
| | CT F | Weak + | Weak + | Weak - | Weak + |
| | CT M | Weak + | Weak + | Weak - | Weak + |

Nigerian: (Oladipo, Okoh and Hart, 2010)
Egyptian: (Abdel-Rahman, Amr and Khalil, 2019)
Oriental: (Takahagi, Schellini, Padovani, Ideta, Katori and Nakamura, 2008)
European white: (Sforza et al., 2009); (Guo *et al.,* 2020)
American white: Price *et al.,* 2009)

| Measurement (mm) | CBCT F (n=54) | CBCT M (n=64) | CT F (n=50) | CT M (n=67) |
|---|---|---|---|---|
| 1. Mouth Width | **54.63** ± 3.26 (48.73 - 62.40) | **56.49** ± 3.42 (46.95 - 62.62) | **54.44** ± 3.63 (46.80 - 63.78) | **56.39** ± 3.44 (49.55 - 66.25) |
| 2. Philtrum Width | **13.58** ± 1.09 (11.77 - 16.69) | **14.57** ± 1.14 (11.53 - 17.42) | **13.83** ± 0.94 (12.08 - 15.99) | **14.56** ± 1.16 (11.69 - 17.92) |
| 3. Upper Lip Height | **24.12** ± 5.32 (11.92 - 33.59) | **27.02** ± 3.72 (18.45 - 34.08) | **25.22** ± 3.02 (18.55 - 30.74) | **25.96** ± 4.09 (14.26 - 34.54) |
| 4. Upper Vermilion Height | **10.37** ± 2.90 (3.73 - 16.04) | **12.24** ± 2.73 (5.19 - 22.23) | **11.97** ± 2.20 (5.29 - 15.51) | **12.22** ± 2.78 (5.06 - 17.18) |
| 5. Lower Lip Height | **19.69** ± 3.48 (11.78 - 33.79) | **21.64** ± 2.70 (14.29 - 26.67) | **22.23** ± 2.45 (15.39 - 27.32) | **23.22** ± 2.97 (12.48 - 26.96) |
| 6. Lower Vermilion Height | **10.8** ± 2.22 (5.72 - 15.93) | **11.88** ± 1.95 (5.71 - 17.87) | **12.24** ± 1.90 (6.67 - 15.74) | **12.44** ± 2.08 (5.29 - 16.16) |

South African black and white: (Houlton *et al.,* 2020)
Kenyan: (Virdi, Wertheim and Naini, 2019)
North American white: (Farkas, Katic and Forrest, 2007)
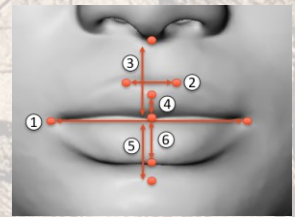
# Statistical Significant Variations: Oral parameters

| | | Mouth width | Philtrum width | Upper lip height | Upper vermilion height | Lower lip height | Lower vermilion height |
|---|---|---|---|---|---|---|---|
| **Within modalities:** | CBCT F vs M | 0.0191 | < 0.0001 | 0.0046 | 0.0006 | < 0.0001 | 0.0083 |
| | CT F vs M | 0.0138 | 0.0028 | x | x | 0.0063 | x |
| **Between modalities:** | CBCT vs CT F | x | x | x | 0.0019 | < 0.0001 | 0.0002 |
| | CBCT vs CT M | x | x | x | X | 0.0001 | 0.0332 |
| **Age correlations:** | CBCT F | Mild + | Weak + | Weak - | Mild - | Weak - | Weak - |
| | CBCT M | Weak - | Weak - | Weak - | Mild - | Weak - | Mild - |
| | CT F | Weak + | Weak + | Weak - | Mild - | Weak - | Mild - |
| | CT M | Mild + | Weak + | Weak + | Mild - | Weak - | Weak - |

## Statistical Significant Variations: Oral parameters

| | | Mouth width | Philtrum width | Upper li height |
|---|---|---|---|---|
| **Within modalities:** | CBCT F vs M | 0.0191 | < 0.0001 | 0.0046 |
| | CT F vs M | 0.0138 | 0.0028 | x |
| **Between modalities:** | CBCT vs CT F | x | x | x |
| | CBCT vs CT M | x | x | x |
| **Age correlations:** | CBCT F | Mild + | Weak + | Weak - |
| | CBCT M | Weak - | Weak - | Weak - |
| | CT F | Weak + | Weak + | Weak - |
| | CT M | Mild + | Weak + | Weak + |
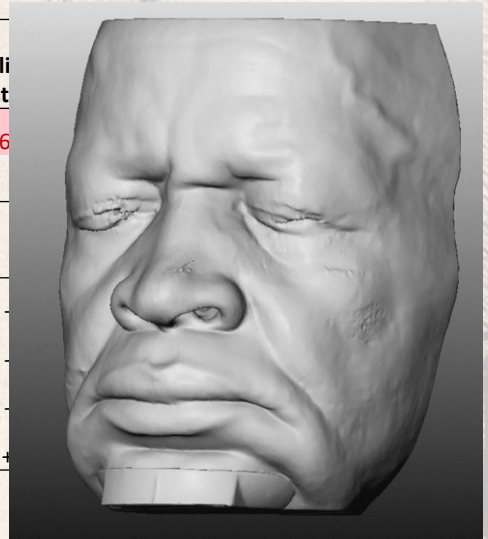
South African studies:
(Schmidlin *et al.,* 2018); (Houlton *et al.,* 2020)

---

# Conclusion

- Important to consider sexual dimorphism and population differences
- Analyses relating to the soft tissues of the chin region may be affected by
  1. The supportive struts of the CBCT machine
     - Consider CT measurements as an alternative
  2. Aging
     - Distinguish age groups when developing normative values

# Acknowledgements

- UP Postgraduate Bursary
- Bakeng se Afrika EU funding for mobilities to KUL
- Dr Alison Ridel for assistance with repeatability analyses

# References

- Abdel-Rahman, R.H., Amr, S.G., Khalil, A.A. 2019. Sexual dimorphism of anthropometric measurements of periorbital soft tissues in a sample of egyptian adults. Mansoura Journal of Forensic Medicine and Clinical Toxicology. 27:(1):13-25.

- Ali, A., Chandna, A.K., Munjal, A. 2020. Accuracy and reliability of soft tissue landmarks using three-dimensional imaging in comparison with two-dimensional cephalometrics: A systematic review. Journal of Indian Orthodontic Society. 54(4):289-96.

- Farkas, L.G., Katic, M.J., Forrest, C.R. 2007. Comparison of craniofacial measurements of young adult african-american and north american white males and females. Annals of plastic surgery. 59:(6):692-8.

- Franklin, D., Freedman, L., Milne, N., Oxnard, C. 2006. A geometric morphometric study of sexual dimorphism in the crania of indigenous southern africans. South African Journal of Science. 102(5):229-38.

- Ganguly, R., Ruprecht, A., Vincent, S., Hellstein, J., Timmons, S., Qian, F. 2011. Accuracy of linear measurement in the Galileos cone beam computed tomography under simulated clinical conditions. Dentomaxillofacial Radiology. 40(5):299-305.

- Guo, Y., Schaub, F., Mor, J.M., Jia, R., Koch, K.R., Heindl, L.M. 2020. A simple standardized three-dimensional anthropometry for the periocular region in a european population. Plastic and reconstructive surgery. 145:(3):514e-23e.

- Heidari, Z., Mahmoudzadeh-Sagheb, H., Khammar, T., Khammar, M. 2009. Anthropometric measurements of the external nose in 18–25-year-old sistani and baluch aborigine women in the southeast of iran. Folia morphologica. 68:(2):88-92.

- Houlton, T.M., Jooste, N., Steyn, M. 2020. Mouth width and cupid's bow estimation in a southern african population. Journal of Forensic Sciences. 65:(2):372-9.

- Jimoh, R.O., Alabi, S.B., Kayode, A.S., Salihu, A.M., Ogidi, O.D. 2011. Rhinometry: Spectrum of nasal profile among nigerian africans. Brazilian Journal of Otorhinolaryngology. 77:589-93.

- Kim, M., Huh, K.-H., Yi, W.-J., Heo, M.-S., Lee, S.-S., Choi, S.-C. 2012. Evaluation of accuracy of 3D reconstruction images using multi-detector CT and cone-beam CT. Imaging Science in Dentistry. 42(1):25-33.

- Oladipo, G., Okoh, P., Hart, J. 2010. Anthropometric study of ocular dimensions in adult ijaws of nigeria. Res J Med Med Sci. 5:121-4.

- Price, K.M., Gupta, P.K., Woodward, J.A., Stinnett, S.S., Murchison, A.P. 2009. Eyebrow and eyelid dimensions: An anthropometric analysis of african americans and caucasians. Plastic and reconstructive surgery. 124:(2):615-23.

- Ridel, A.F., Demeter, F., Liebenberg, J., L'abbé, E.N., Vandermeulen, D., Oettlé, A.C. 2018. Skeletal dimensions as predictors for the shape of the nose in a South African sample: A cone-beam computed tomography (CBCT) study. Forensic Science International. 289:18-26.

- Ridel, A., Demeter, F., L'abbé, E., Oettlé, A. 2020. Nose approximation among South African groups from cone-beam computed tomography (CBCT) using a new computer-assisted method based on automatic landmarking. Forensic Science International. 313110357.

- Roelofse, M.M., Steyn, M., Becker, P.J. 2008. Photo identification: Facial metrical and morphological features in south african males. Forensic science international. 177(2):168-75.

- Schmidlin, E.J., Steyn, M., Houlton, T.M., Briers, N. 2018. Facial ageing in south african adult males. Forensic science international. 289:277-86.

- Sforza, C., Grandi, G., Catti, F., Tommasi, D., Ugolini, A., Ferrario, V. 2009. Age- and sex-related changes in the soft tissues of the orbital region. Forensic science international. 185:115.e1-8.

- Sforza, C., De Menezes, M., Ferrario, V.F. 2013. Soft-and hard-tissue facial anthropometry in three dimensions: What's new. Journal of Anthropological Sciences. 91:159-84.

- Sjerobabski-Masnec, I., Šitum, M. 2010. Skin aging. Acta Clinica Croatica. 49:(4):515-8.

- Takahagi, R.U., Schellini, S.A., Padovani, C.R., Ideta, S., Katori, N., Nakamura, Y. 2008. Oriental oculopalpebral dimensions: Quantitative comparison between orientals from japan and brazil. Clinical ophthalmology (Auckland, N.Z.). 2:(3):563-7.

- Virdi, S.S., Wertheim, D., Naini, F.B. 2019. Normative anthropometry and proportions of the kenyan-african face and comparative anthropometry in relation to african americans and north american whites. Maxillofacial plastic and reconstructive surgery. 41:(1):1-14.

- White, J.D., Ortega-Castrillón, A., Matthews, H., Zaidi, A.A., Ekrami, O., Snyders, J., et al. 2019. Meshmonk: Open-source large-scale intensive 3D phenotyping. Scientific reports. 9:(1):1-11.

# The Scope of the Problem

- Facial disfigurement is a prevalent concern in South Africa resulting in decreased quality of life
- Surgical reconstruction is not always an option (Scolozzi & Jaques, 2004; Klimczak, Helman, Kadakia, Sawhney, Abraham, Vest & Ducic, 2018)



(Van den Heever, Sykes & Du Plessis, 2012)

# The Scope of the Problem

- European guidelines (Van den Heever, Sykes & Du Plessis, 2012)
- Current methods are time consuming, energy intensive and rely heavily on the clinician's artistic skills
- Lack of training facilities & trained clinicians (Tsïtä & Owen, 2017)



(Tatjana, Jiri, Milan, Jiri, Pavel, Jakub & Michaela, 2011)

(Wright, Minsley & Bak, n.d.)

(Center for Custom Prosthetics, 2020)

# The Scope of the Problem

- Advances in technology
  - Mirroring approach
  - Library of features
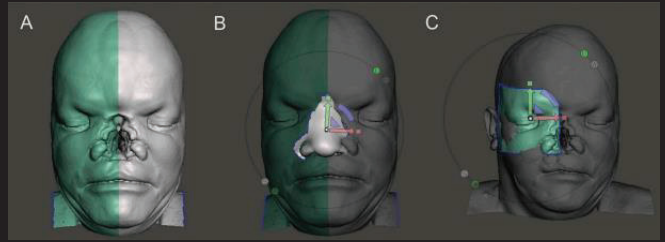


(Farook, Jamayet, Abdullah, Asif, Rajion & Alam, 2020)
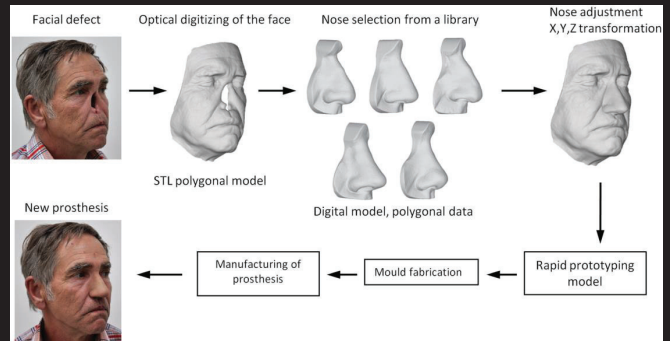


(Palousek, Rosicky & Koutny, 2014)

---

# Statistical Shape Modelling (SSM)

Objective and automated method to estimate missing parts

→

## Aim of the study:

**01**

Model facial variation of black South Africans

**02**

Estimating missing soft tissue segments of the face using an SSM

# 02

# SAMPLE

118 Cone-beam computed tomography (CBCT)
119 Computed tomography (CT)

Training Sample

Defect Sample

CBCT
M = 37
F = 33

CT
M = 48
F = 30

CBCT
M = 8
F = 7

Full chin = 1
Open eyes = 63

Full chin = 77
Open eyes = 48

CT
M = 7
F = 8
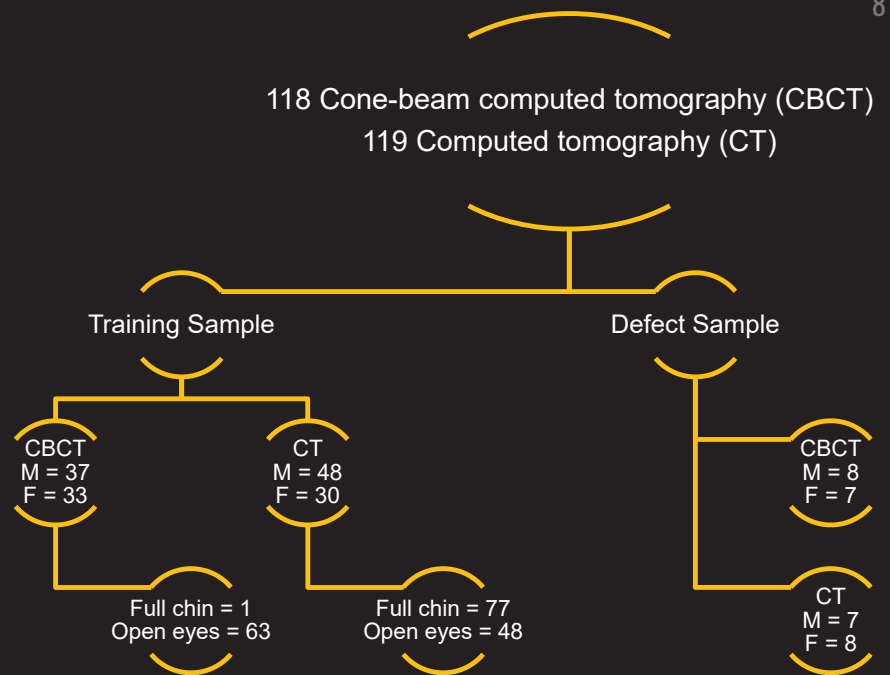
# 03

# METHODS

I. Overview

II. Landmarking (MeVisLab v3.0.2)

III. Registration (MeshMonk toolbox – MATLAB R2021b)

IV. Building the SSM (MeshMonk toolbox – MATLAB R2021b)

V. Defect simulation (Avizo Standard Edition 8.0.0 & MeVisLab v3.0.2)

VI. Defect imputation (MeshMonk toolbox – MATLAB R2021b)
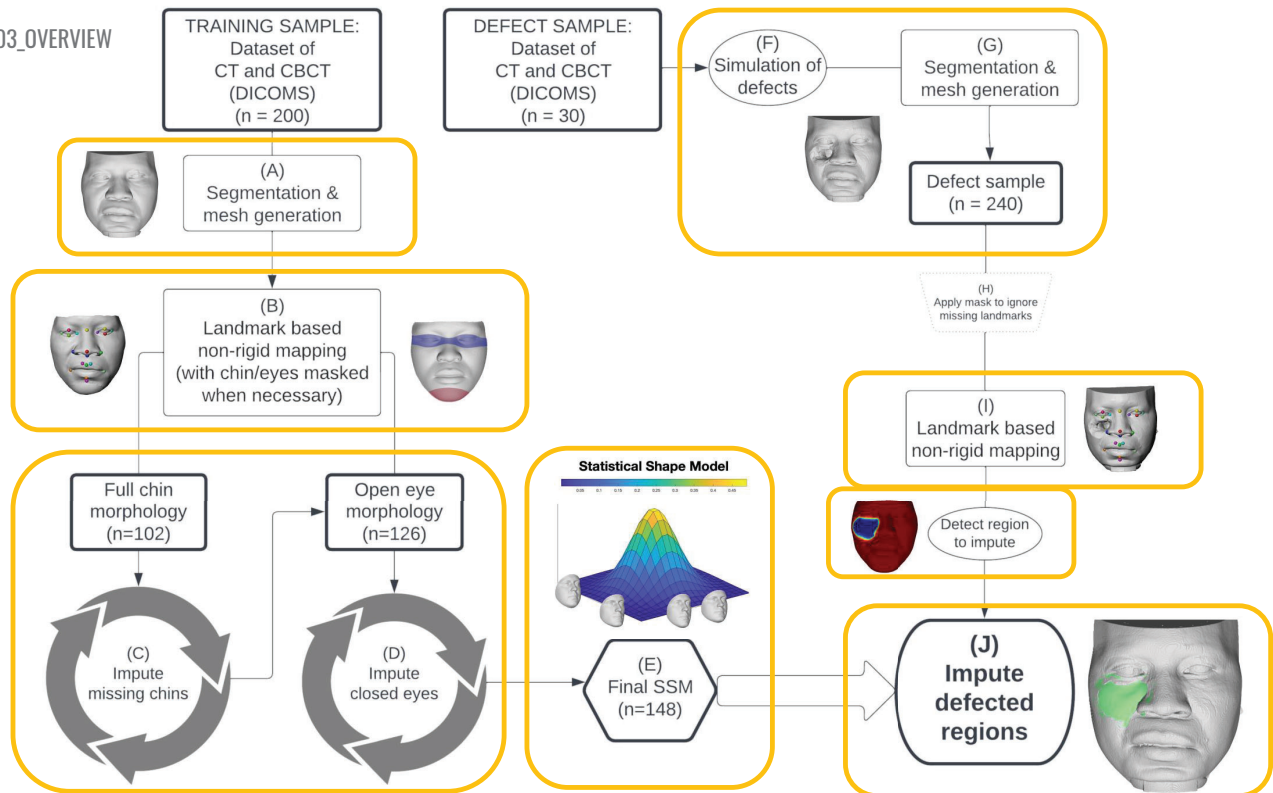
## 03_LANDMARKING AND REGISTRATION

1. Nasion
2. Pronasale
3. Subnasale
4. Labiale superius
5. Labiale inferius
6. Sublabiale
7. Endocanthion (right)
8. Exocanthion (right)
9. Upper lid (right)
10. Lower lid (right)

11. Endocanthion (left)
12. Exocanthion (left)
13. Upper lid (left)
14. Lower lid (left)
15. Alare (right)
16. Alare (left)
17. Cheilion (right)
18. Christa philtre (right)
19. Christa philtre (left)
20. Cheilion (left)

**20**
anatomical landmarks
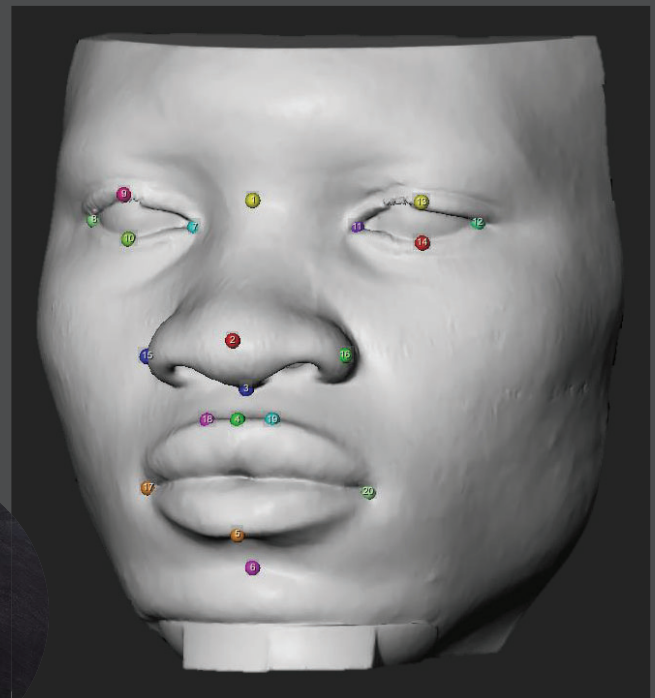
# Part 1



**01**

Generalised Procrustes Analysis (GPA)

**(a) Unaligned meshes (superimposed)** **(b) Aligned meshes (superimposed)**

**02**

Principal components analysis (PCA) of the GPA aligned landmarks

(Abedini, Elkenawy, Kim & Moon, 2018)

# Part 2

# Part **2**

**Mode 2**

**Mode 1**
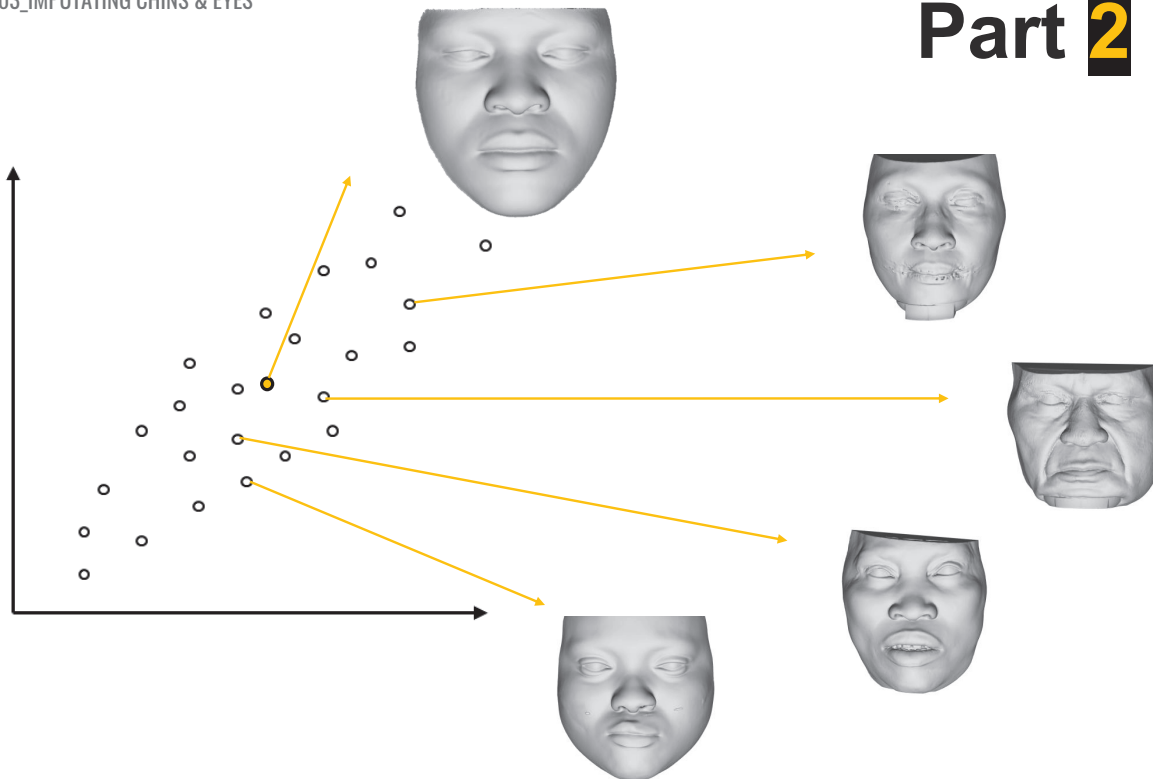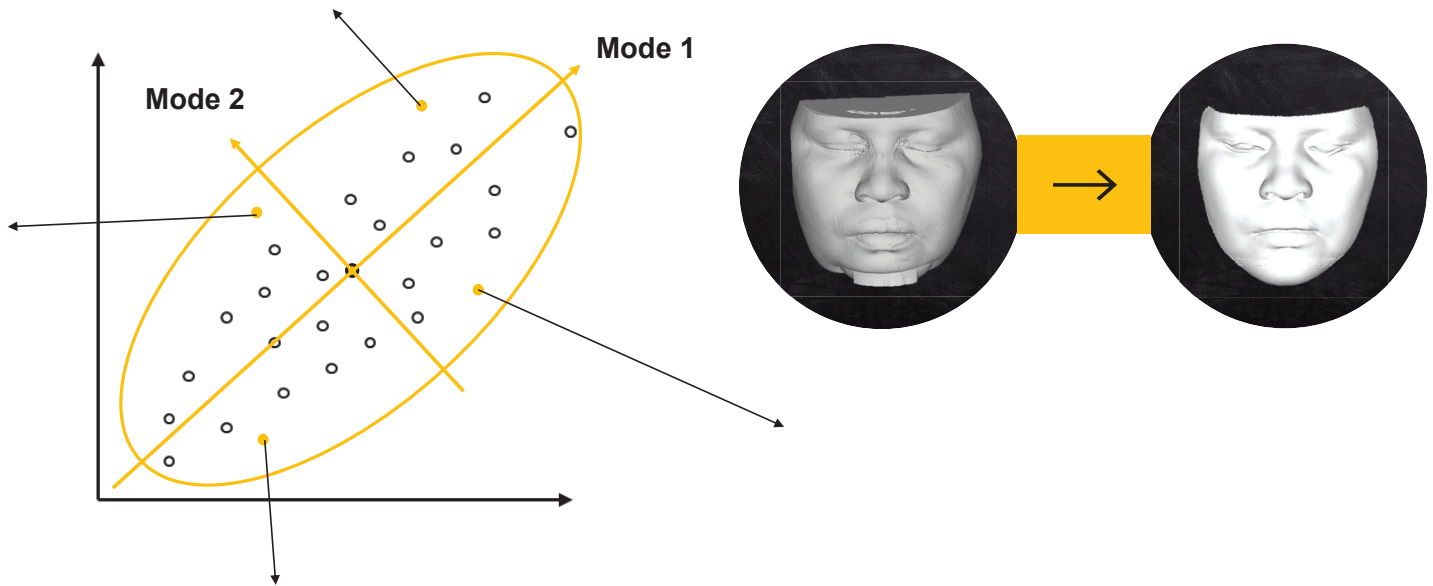
# Part **2** (Chin & Eye Imputation)

**06**

Define region to be imputed by assigning and smoothing weights

**07**

Align and scale to model average, weighted-fit to SSM

**08**

Estimate linear combination of modes of variation according to weights

**09**

Returned 'weighted-fit' face to the coordinate system and size of the face prior to the imputation

**10**

Blend original face with weighted fit face, add to SSM

03_DEFECT SIMULATION



Jackson, Low, Nguyen & Kent, 2018

Class 1

Class 2

Adaki, Raikar, Shigli & Gali, 2017

Class 3

(Alqarni, Montgomery, Aponte-Wesson, Won, Hofstede & Chambers, 2021)

Class 4

Javanmard, Mohammadi & Mojtahedi, 2020

DEFECT CLASSIFICATION

Malard, Lanhouet, Michel, Dreno, Espitalier & Rio, 2015

Class 5

Class 6 A

Shrivastava, Shrivastava, Agarwal & Bhoyar, 2015

Class 6 B

Nilanonth, Shakya, Chotprasert & Srithavaj, 2017

Class 6 C

Furdova, Kapitanova, Kollarova & Sekáč, 2020

03_DEFECT SIMULATION



169

# Defect Imputation



---

# Defect Imputation

**01**

Define region to be imputed by assigning and smoothing weights

**02**

Align and scale to model average, weighted-fit to SSM

**03**

Estimate linear combination of modes of variation according to weights

**04**

Returned 'weighted-fit' face to the coordinate system and size of the face prior to the imputation

**05**

Blend original face with weighted fit face

# 04

## RESULTS

I. Model Evaluation

II. Defect Evaluation



**Statistical Shape Model**

---
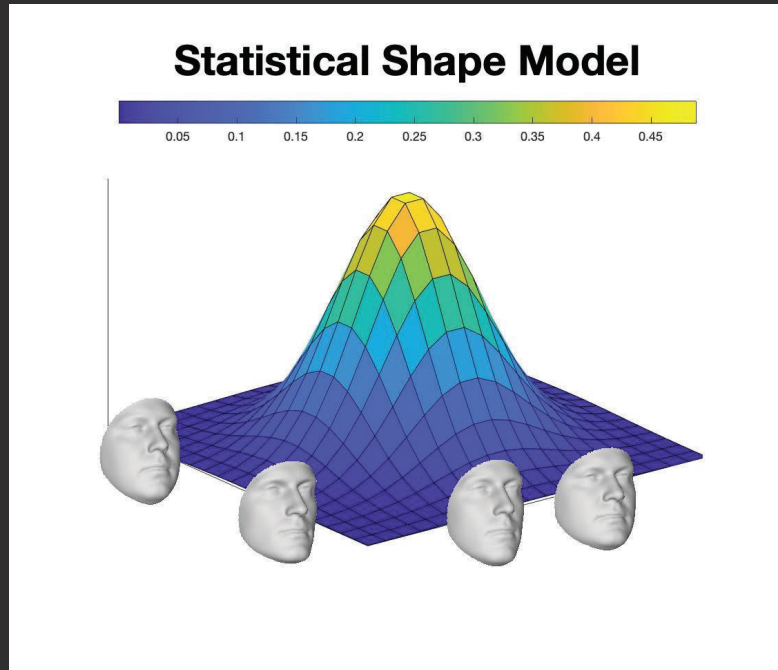
04_MODEL EVALUATION



**01**

**02**

**03**

**04**

**05**

**Modes of Variation**

04_MODEL EVALUATION

# Model
# accuracy

✓ **Generalisation**

✓ **Specificity**



Mean Generalization Error
1.09mm

Specificity
2.75mm
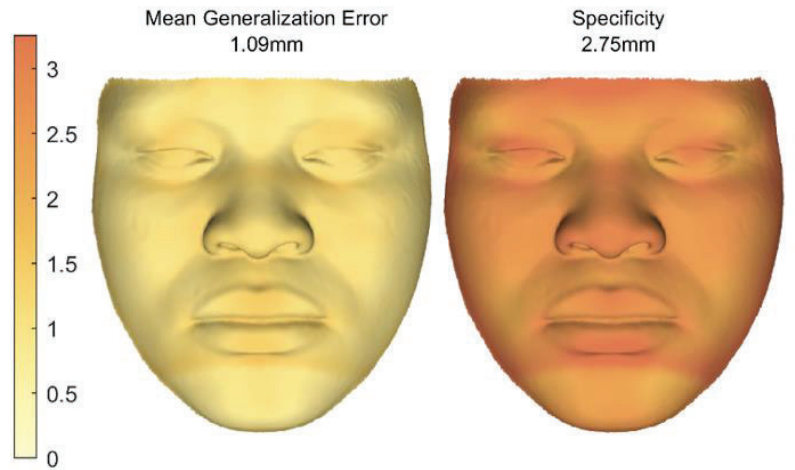
04_DEFECT EVALUATION

# Quantitative evaluation
# of defect imputation

## Defect type

Class 1, 2, 3 & 5: RMSE < 1.80 mm

Class 4, 6A, 6B & 6C: RMSE between 2.22 and 2.83 mm

## Sex & Modality

No statistically significant differences
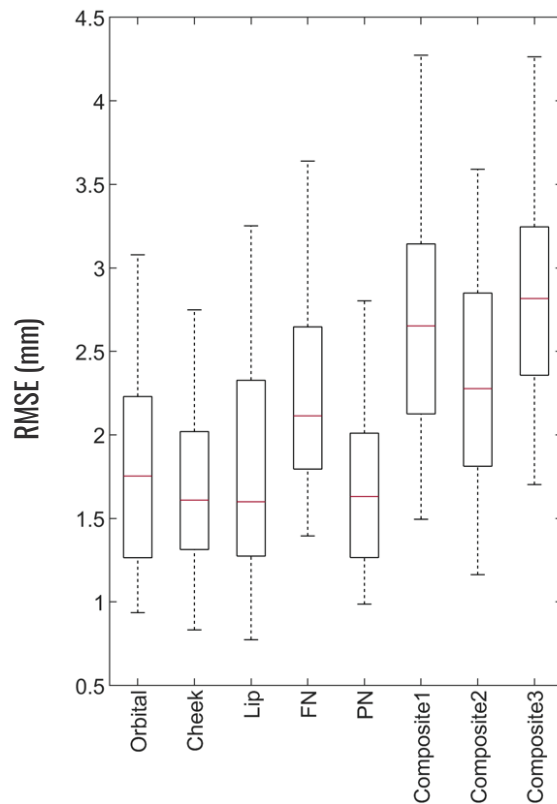
# Qualitative inspection of defect imputation

a) Cheek
b) Orbital
c) Lip
d) Partial nose
e) Full nose
f) Large composite 1
g) Small composite 2
h) Bi-orbital

# 05
# CONCLUSION
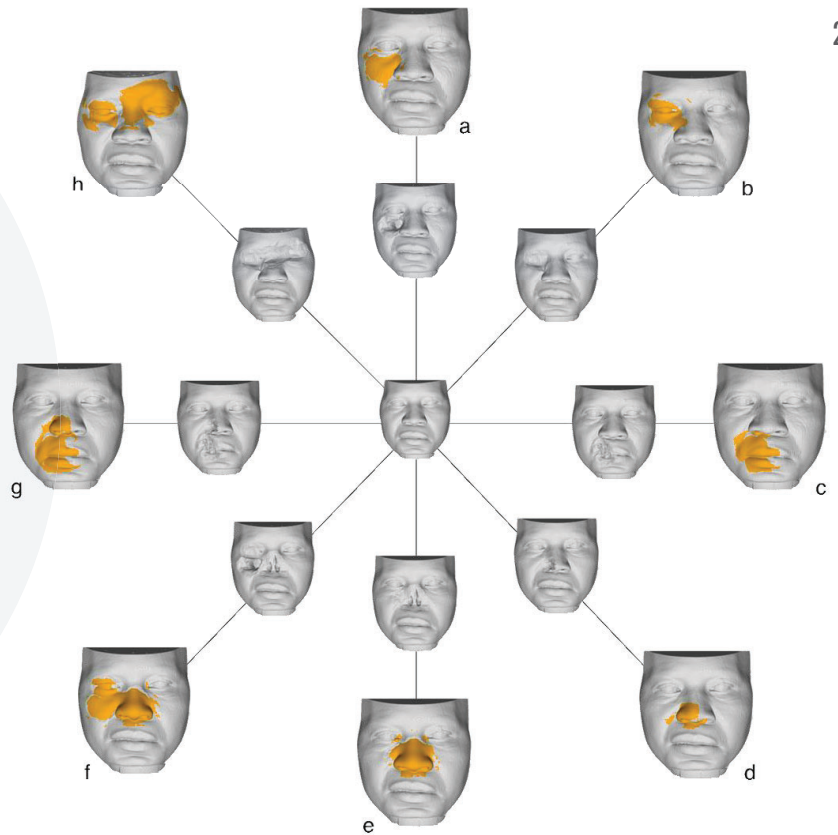
## 05_CONCLUSION
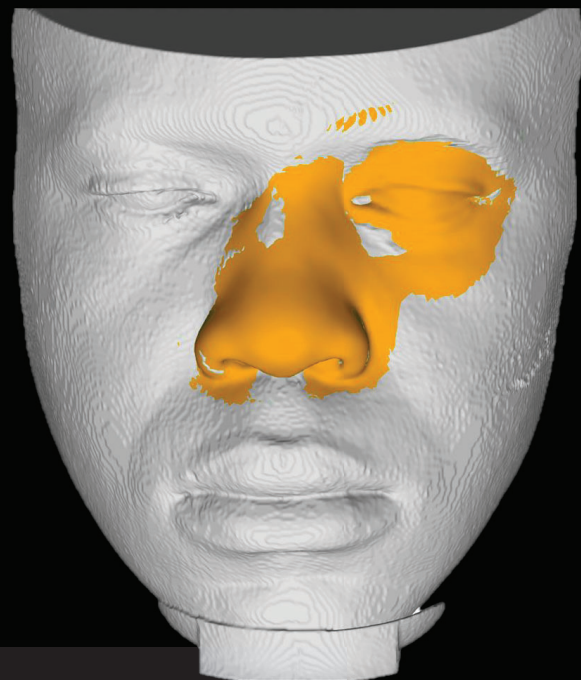
# Conventional approach

1) Obtain an impression of the face model
2) Design the prosthesis model
3) Manufacture the prosthesis model

(Van Heerden & Fossay, 2019)

Expensive

Time intensive

Skill intensive

(Tetteh, Bibb & Martin, 2019)

---

## 05_CONCLUSION

# Novel approach

Modelling facial variation in the black South African population has never been approached using SSMs before

## Statistical Shape Model

0.05  0.1  0.15  0.2  0.25  0.3  0.35  0.4  0.45
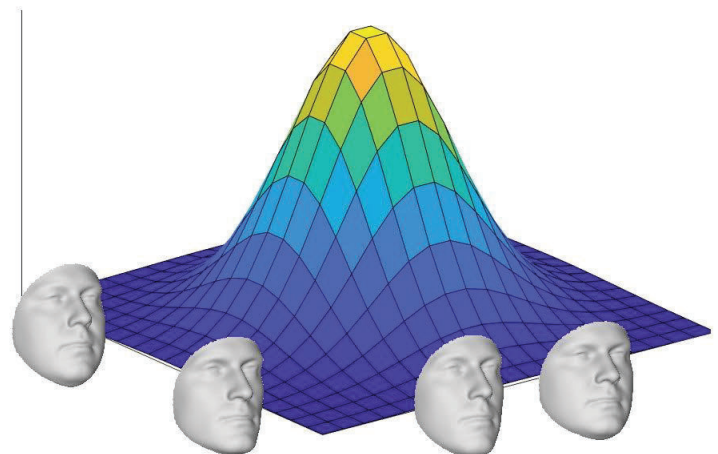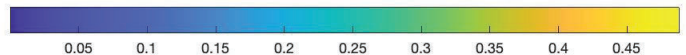
# 05_CONCLUSION



## 01 REALISTIC ESTIMATIONS

SSM limits
estimations to
within the normal
range of variance

## 02 WIDELY APPLICABLE

Any sex
Any modality
Population specific
Patient specific
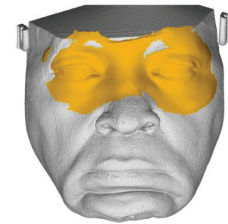
## 03 BILATERAL & MIDLINE DEFECTS

No need for
mirroring approach
or access to feature
library

# 08 REFERENCE LIST

1. ABEDINI, S., ELKENAWY, I., KIM, E. & MOON, W. 2018. Three-dimensional soft tissue analysis of the face following micro-implant-supported maxillary skeletal expansion. *Progress in Orthodontics,* 1912/01.

2. VAN DEN HEEVER, J., SYKES, L.M. & DU PLESSIS, F. 2012. The scope of maxillofacial prosthodontics: clinical review. *South African Dental Journal,* 67(10):593-595.

3. CENTER FOR CUSTOM PROSTHETICS. 2020. Prosthetic Orbitals with Custom Eyes. [Online]. Available from: https://www.bestprosthetics.com/prosthetic-eyes-orbital/. [Accessed: 3 November 2022].

4. TATJANA, D., JIRI, K., MILAN, H., JIRI, H., PAVEL, K.I.Z., JAKUB, S. & MICHAELA, S. 2011. Facial Prosthesis. In: Ilser, T. (ed.). *Implant Dentistry*. Rijeka: IntechOpen:Ch. 19.

5. WRIGHT, R., MINSLEY, G. & BAK, S. n.d. Implant-Retained Restoration of the Craniofacial Patient. [Online]. Available from: https://pocketdentistry.com/22-implant%E2%80%90retained-restoration-of-the-craniofacial-patient/#c22-fig-0019. [Accessed: 3 November 2022].

6. FAROOK, T.H., JAMAYET, N.B., ABDULLAH, J.Y., ASIF, J.A., RAJION, Z.A. & ALAM, M.K. 2020. Designing 3D prosthetic templates for maxillofacial defect rehabilitation: A comparative analysis of different virtual workflows. *omputers in Biology and Medicine,* 118:103646.

7. PALOUSEK, D., ROSICKY, J. & KOUTNY, D. 2014. Use of digital technologies for nasal prosthesis manufacturing. *Prosthetics and orthotics international,* 38(2):171-175.

8. FURDOVA, A., KAPITANOVA, K., KOLLAROVA, A. & SEKÁČ, J. 2020. Periocular basal cell carcinoma - clinical perspectives. *Oncology Reviews,* 1404/30.

9. ALQARNI, H., MONTGOMERY, P., APONTE-WESSON, R., WON, A.M., HOFSTEDE, T.M. & CHAMBERS, M.S. 2021. Combined rehabilitation of a lower lip defect after resection of floor of mouth cancer: A clinical report. *Journal of Prosthetic Dentistry..*

10. NILANONTH, S., SHAKYA, P., CHOTPRASERT, N. & SRITHAVAJ, T. 2017. Combination prosthetic design providing a superior retention for mid-facial defect rehabilitation: A Case Report. *Journal of Clinical and Experimental Dentistry,* 904/01.

11. JACKSON, O.A., LOW, D.W., NGUYEN, P.D. & KENT, K. 2018. Advanced Plastic Surgical Techniques: Facial Prosthetic Considerations, Periorbital Free Flaps, Reanimation, and Corneal Sensory Restoration. In: Katowitz, J.A. & Katowitz, W.R. (eds.). *Pediatric Oculoplastic Surgery*. Cham: Springer International Publishing:145-167.

12. ADAKI, R., RAIKAR, S., SHIGLI, K. & GALI, S. 2017. Prosthetic rehabilitation of a geriatric patient with squamous cell carcinoma of the buccal mucosa: A report of clinical challenges. *International Journal of Pharmaceutical Investigation,* 7(2):107.

13. JAVANMARD, A., MOHAMMADI, F. & MOJTAHEDI, H. 2020. Reconstruction of a total rhinectomy defect by implant-retained nasal prosthesis: A clinical report. *Oral and Maxillofacial Surgery Cases,* 6(1), 2020/03/01/:100141.

14. MALARD, O., LANHOUET, J., MICHEL, G., DRENO, B., ESPITALIER, F. & RIO, E. 2015. Full-thickness nasal defect: Place of prosthetic reconstruction. *European Annals of Otorhinolaryngology, Head and Neck Diseases,* 132(2), 2015/04/01/:85-89.

15. SHRIVASTAVA, K., SHRIVASTAVA, S., AGARWAL, S. & BHOYAR, A. 2015. Prosthetic rehabilitation of large mid-facial defect with magnet-retained silicone prosthesis. *The Journal of Indian Prosthodontic Society,* 15(3), July 1, 2015:276-280.

16. KLIMCZAK, J., HELMAN, S., KADAKIA, S., SAWHNEY, R., ABRAHAM, M., VEST, A.K. & DUCIC, Y. 2018. Prosthetics in Facial Reconstruction. *Craniomaxillofacial Trauma & Reconstruction*, 11(01):006-014.

17. SCOLOZZI, P. & JAQUES, B. 2004. Treatment of Midfacial Defects Using Prostheses Supported by ITI Dental Implants. *Plastic and Reconstructive Surgery,* 114(6):1395-1404.

18. WHITE, J.D., ORTEGA-CASTRILLÓN, A., MATTHEWS, H., ZAIDI, A.A., EKRAMI, O., SNYDERS, J., FAN, Y., PENINGTON, T., VAN DONGEN, S. & SHRIVER, M.D. 2019. MeshMonk: Open-source large-scale intensive 3D phenotyping. *Scientific reports,* 9(1):1-11.

# A statistical shape model for estimating missing soft tissues of the face

**Questions?**

**Heléne F Swanepoel,** Harold Matthews, Peter Claes, Dirk Vandermeulen and Anna C Oettlé